

Electronic Thesis and Dissertation Repository

4-22-2019 10:00 AM

Experimental Investigations on the Instantaneous Flow Structure in Circulating Fluidized Beds

Xiaoyang Wei
The University of Western Ontario

Supervisor
Zhu, Jingxu
The University of Western Ontario

Graduate Program in Chemical and Biochemical Engineering
A thesis submitted in partial fulfillment of the requirements for the degree in Doctor of Philosophy
© Xiaoyang Wei 2019

Follow this and additional works at: <https://ir.lib.uwo.ca/etd>

 Part of the [Catalysis and Reaction Engineering Commons](#)

Recommended Citation

Wei, Xiaoyang, "Experimental Investigations on the Instantaneous Flow Structure in Circulating Fluidized Beds" (2019). *Electronic Thesis and Dissertation Repository*. 6164.
<https://ir.lib.uwo.ca/etd/6164>

This Dissertation/Thesis is brought to you for free and open access by Scholarship@Western. It has been accepted for inclusion in Electronic Thesis and Dissertation Repository by an authorized administrator of Scholarship@Western. For more information, please contact wlsadmin@uwo.ca.

ABSTRACT

Knowing the instantaneous flow structure is of great importance for the understanding of gas-particle interaction and for the prediction of reactor performances. In this thesis, a systematic and comprehensive study has been conducted on the instantaneous flow structure in a narrow rectangular riser (19 mm in thickness, 114 mm in width and 7.6 m in height), in a cylindrical riser (76 mm in diameter, 10.2 m in height) and in a cylindrical downer (50 mm in diameter, 4.9 m in height). A wider range of operating conditions has been achieved in risers and downer with superficial gas velocity from 3.0 to 9.0 m/s and solids circulation rate from 50 to 700 kg/m²s.

With high-speed imaging and optical fiber sensing, it has been found that there are crest clusters, coalesced particles, trough clusters and dispersed particles in CFBs. Crest clusters are surrounded by a cloud of coalesced particles, while trough clusters are immersed in dispersed particles. Then, instantaneous flow dynamics are computed with the tracking of image blocks. The existence of aggregations influences both the particle velocity and the solids flux. After that, a physically meaningful threshold was proposed to characterize crest cluster and trough clusters in terms of solids holdup, size and shape.

As the optical fiber probe can be used in high-density conditions, a discrimination method was also proposed for probe signals using wavelet transform. A thorough characterization of crest clusters, coalesced particles, trough clusters and dispersed particles is conducted in the rectangular CFB and their properties are consistent with those originated from the images. Moreover, how particle properties influence phase characteristics was also investigated by comparing phase information formed by FCC and glass beads.

Finally, probe signals captured in the cylindrical riser and cylindrical downer are processed to investigate the phase properties in high-density conditions. Phases, including crest clusters, coalesced particles, trough clusters and dispersed particles, are characterized over the riser and downer in terms of length, frequency and time fraction. With the systematic comparison of flow information between the CFB riser and downer,

it has been found that aggregation in the CFB downer is less severe than that in the CFB riser.

Keywords: circulating fluidized bed; riser; downer; particle aggregation; cluster; instantaneous flow structure; aggregation mechanism.

CO-AUTHORSHIP

Chapter 2: Literature review

Authors: Xiaoyang Wei, Jesse Zhu

Under close supervision of Dr. J. Zhu, Xiaoyang Wei summarized the information in the literature, coded the MATLAB program, carried out an in-depth analysis of the details of cluster definitions and wrote this chapter. A concise version of this chapter has been submitted to “AICHE journal”.

Chapter 4: Capturing the instantaneous flow structure in gas-solid circulating fluidized bed using high-speed imaging and fiber optic sensing

Authors: Xiaoyang Wei, Jesse Zhu

This chapter has been submitted as a research paper to “Chemical Engineering Science”. The experimental data was collected by Jingsi Yang and Chengxiu Wang (previous PhDs in our group). Under close supervision of Dr. J. Zhu, Xiaoyang Wei coded the MATLAB program, carried out an extensive analysis of the instantaneous flow structure and wrote this chapter.

Chapter 5: Tracking the flow dynamics in gas-solid circulating fluidized bed through high-speed photographing

Authors: Xiaoyang Wei, Jesse Zhu

This chapter has been submitted as a research paper to “Industrial & Engineering Chemistry Research”. The experimental data was collected by Jingsi Yang (previous PhD in our group). Under close supervision of Dr. J. Zhu, Xiaoyang Wei coded the MATLAB program, carried out an extensive analysis of the flow dynamics and wrote this chapter.

Chapter 6: Analysis of phase segregation in gas-solid circulating fluidized bed with direct image calibration

Authors: Xiaoyang Wei, Jesse Zhu, Jingsi Yang

This chapter has been submitted as a research paper to “Chemical Engineering Journal”. The experimental data was collected by Jingsi Yang (previous PhD in our group). Under close supervision of Dr. J. Zhu, Xiaoyang Wei coded the MATLAB program, carried out an extensive characterization of clusters and wrote this chapter.

Chapter 7: A comprehensive characterization of aggregative flow in gas- solid circulating fluidized bed using wavelet analysis

Authors: Xiaoyang Wei, Jesse Zhu

The experiment data was collected by Jing Xu (previous PhD in our group). Under close supervision of Dr. J. Zhu, Xiaoyang Wei coded the MATLAB program, carried out an extensive phase characterization and wrote this chapter.

Chapter 8: A comprehensive characterization of aggregative flow in gas- solid circulating fluidized bed using wavelet analysis: high-density riser

Authors: Xiaoyang Wei, Jesse Zhu

The experiment data was collected by Chengxiu Wang (previous PhD in our group). Under close supervision of Dr. J. Zhu, Xiaoyang Wei coded the MATLAB program, carried out an extensive phase characterization and wrote this chapter.

Chapter 9: A comprehensive characterization of aggregative flow in gas- solid circulating fluidized bed using wavelet analysis: high-density downer

Authors: Xiaoyang Wei, Jesse Zhu

The experiment data was collected by Chengxiu Wang (previous PhD in our group). Under close supervision of Dr. J. Zhu, Xiaoyang Wei coded the MATLAB program, carried out an extensive phase characterization and wrote this chapter.

ACKNOWLEDGEMENT

In September 2014, I left my home country (China) for Canada alone. In the four years and a half, there are many frustrating moments and exciting moments for this project and for my life. Even though it is the time to say goodbye to my supervisor, to my colleagues, to my friends and to this project, all the memories in Western University shall never fade in my life.

First of all, I wish to express my sincere gratitude to my supervisor, Dr. Jesse Zhu, for his support, guidance and advices during my PhD program. His supervision brings me the idea of “how to conduct research” and contributed a lot on the successful fulfillment of this study.

Much appreciation is directed to previous students in our group. Jingsi Yang, Jing Xu, Chengxiu Wang and Jiangshan Liu contributed on the systematical experiments in the CFB risers and downer, which allows me to conduct the research more theoretically. Thank you all for the patient explanation and the

I would also thank my colleagues and visiting students. Zhijie Fu, Tian Nan, Zeneng Sun, Shan Gao, Mengqi Han, Haolong Wang and Lin Wang offered many valuable suggestions on this work and their encouragement took me through “the struggle time” of this research. Sizhe Wu, Haokai Huang, Siyuan Li and Tianzi Bai worked with me to analyze the data for chapter 4 and chapter 5.

Special appreciation to China Scholarship Council (CSC) providing me the financial support for my PhD study.

Finally, I would like to dedicate this work to my family and my girlfriend (Mengxing Lin). Without their consistent support and companion, I cannot accomplish this project. Mengxing, thanks for all the joys and happiness you brought to me. It is really an honor to have you in my life.

TABLE OF CONTENTS

ABSTRACT	ii
CO-AUTHORSHIP	iv
ACKNOWLEDGEMENT	vi
TABLE OF CONTENTS.....	vii
LIST OF FIGURES	xiii
LIST OF TABLES	xix
CHAPTER 1 General Introduction	1
1.1 Background.....	1
1.2 Research objectives.....	3
1.3 Thesis structure.....	3
References	6
CHAPTER 2 Literature Review	10
2.1 Introduction	10
2.2 Measurement techniques	11
2.2.1 High-speed camera	11
2.2.2 Needle-type probe	12
2.3 The evolving understanding of clusters	14
2.4 Cluster definitions.....	16
2.5 Cluster properties in the literature	20
2.6 Preliminary exploration.....	22
2.6.1 Analysis of example signal	23
2.6.2 Details of signal and thresholds	26
2.7 Conclusions	29
References	31

Chapter 3 Experimental Apparatuses and Measurement Methods	38
3.1 Circulating fluidized beds	38
3.1.1 Rectangular circulating fluidized bed.....	38
3.1.2 Cylindrical circulating fluidized beds.....	39
3.2 Particle properties	42
3.3 Measurement of superficial gas velocity and solids circulation rate	43
3.4 Visualization system	44
3.4.1 Measurement of solids holdup	46
3.4.2 Measurement of particle velocity and solids flux	47
3.5 Optical fiber probe	49
3.5.1 Measurement of solids holdup	50
3.5.2 Measurement of particle velocity	52
3.6 Summary	52
References	54
CHAPTER 4 Capturing the instantaneous flow structure in gas-solid circulating fluidized bed using high-speed imaging and fiber optic sensing.....	55
Abstract	55
4.1 Introduction	56
4.2 Experimental.....	57
4.2.1 Circulating fluidized bed	57
4.2.2 Visualization system.....	58
4.2.3 Optical fiber probe.....	60
4.3 Results and discussion.....	61
4.3.1 Overall flow structure.....	61
4.3.2 Clusters	63

4.3.3	Crest phase	67
4.3.4	Macroscopic fluctuation	73
4.4	Conclusions	75
	References	77
CHAPTER 5	Tracking the flow dynamics in gas-solid circulating fluidized bed through high-speed photographing	81
	Abstract	81
5.1	Introduction	82
5.2	Experimental.....	83
5.2.1	Circulating fluidized bed (rectangular riser).....	83
5.2.2	Visualization system.....	84
5.2.3	Data processing	86
5.3	Results and discussion.....	89
5.3.1	Time-average particle velocity.....	89
5.3.2	Time-average solids flux	90
5.3.3	Instantaneous information.....	91
5.3.4	Impact of macro fluctuation.....	96
5.4	Conclusions	99
	References	101
CHAPTER 6	Analysis of phase segregation in gas-solid circulating fluidized bed with direct image calibration	105
	Abstract	105
6.1	Introduction	106
6.2	Experimental.....	107
6.2.1	Circulating fluidized bed (rectangular riser).....	107
6.2.2	Visualization system.....	109

6.3 Results and discussion.....	110
6.3.1 Solids holdup gradient	110
6.3.2 Determination of cluster boundary.....	115
6.3.3 Cluster dimensions and shape	117
6.3.4 Cluster solids holdup	122
6.4 Conclusions	124
References	126
CHAPTER 7 A comprehensive characterization of aggregative flow in gas- solid circulating fluidized bed using wavelet analysis	129
Abstract	129
7.1 Introduction	130
7.2 Experimental.....	131
7.2.1 Circulating fluidized bed (rectangular riser).....	131
7.2.2 Optical fiber probe.....	133
7.2.3 Signal details	133
7.3 Results and discussion.....	140
7.3.1 Phase components	140
7.3.2 Crest phase	145
7.3.3 Validation using high-speed camera	146
7.3.4 Impact of the particle group.....	149
7.4 Conclusions	152
Nomenclature.....	154
References	155
CHAPTER 8 A comprehensive characterization of aggregative flow in gas- solid circulating fluidized bed using wavelet analysis: high-density riser	158
Abstract	158

8.1	Introduction	159
8.2	Experimental.....	160
8.2.1	Circulating fluidized bed (cylindrical riser).....	160
8.2.2	Optical fiber probe.....	161
8.2.3	Signal details	162
8.3	Results and discussion.....	164
8.3.1	Overall flow structure.....	164
8.3.2	Trough clusters and crest clusters	168
8.3.3	Crest phase	175
8.4	Conclusions	177
	Nomenclature.....	178
	References	179
CHAPTER 9	A comprehensive characterization of aggregative flow in gas- solid circulating fluidized bed using wavelet analysis: high-density downer	182
	Abstract	182
9.1	Introduction	183
9.2	Experimental.....	184
9.2.1	Circulating fluidized bed (cylindrical downer).....	184
9.2.2	Optical fiber probe.....	186
9.2.3	Signal details	187
9.3	Results and discussion.....	193
9.3.1	Overall flow structure.....	193
9.3.2	Trough clusters and crest clusters	195
9.3.3	Phase comparison with CFB riser	200
9.4	Conclusions	203

Nomenclature.....	204
References	205
CHAPTER 10 Conclusions and Recommendations.....	208
10.1 Conclusions	208
10.2 Recommendations.....	209
Appendix.....	211
Curriculum Vitae	226

LIST OF FIGURES

Figure 2-1 Number of publications for each cluster definition.....	20
Figure 2-2 Summarization of cluster voidage in the literature	21
Figure 2-3 Summarization of cluster size in the literature.....	22
Figure 2-4 Summarization of cluster frequency in the literature	22
Figure 2-5 Clusters properties versus cluster definitions (100kHz).....	25
Figure 2-6 Clusters properties versus cluster definitions (100Hz).....	26
Figure 2-7 Probe signal and thresholds originated from cluster definitions (a: whole picture, b: local details).....	28
Figure 2-8 Probe signals acquired using different sampling frequencies	29
Figure 3-1 Schematic diagram of the rectangular circulating fluidized bed.....	39
Figure 3-2 Schematic diagram of cylindrical circulating fluidized bed	41
Figure 3-3 Schematic diagram of the distributor at downer top	42
Figure 3-4 Schematic diagram of the visualization system	45
Figure 3-5 An image captured using the high-speed camera.....	46
Figure 3-6 Correlation between solids holdup and grayscale	47
Figure 3-7 Demonstration of the image tracking	48
Figure 3-8 Measurement system of optical fiber probe.....	50
Figure 3-9 Calibration system of the optical fiber probe.....	51
Figure 4-1 Schematic diagram of circulating fluidized bed.....	58

Figure 4-2 Schematic diagram of the visualization system	60
Figure 4-3 Schematic diagram of optical fiber probe.....	61
Figure 4-4 The instantaneous flow structure across riser (H=5.33 m, $U_g = 3$ m/s and $G_s=150$ kg/m ² s, a: the original image, b: the solids holdup map across riser, c: instantaneous radial distribution of solids holdup).....	62
Figure 4-5 Clusters captured using the high-speed camera	64
Figure 4-6 Solids holdup details of a typical cluster (H=5.33m, $U_g = 5$ m/s and $G_s=50$ kg/m ² s, a: the original image; b: the solids holdup map; c:the solids holdup contour)	65
Figure 4-7 Cluster details captured using optical fiber probe.....	67
Figure 4-8 Solids holdup details of a typical streamer (H=5.33 m, $U_g = 3$ m/s and $G_s=50$ kg/m ² s, a: the original image,; b: the solids holdup map; c:the solids holdup contour)	69
Figure 4-9 Formation of streamers	70
Figure 4-10 Solids holdup details of a typical chunk (H=5.33 m, $U_g = 5$ m/s and $G_s=100$ kg/m ² s, a: the image sequence with a chunk in the riser center; b: the solids holdup map;)	71
Figure 4-11 Trough phase and trough clusters.....	72
Figure 4-12 Phase details across riser captured using optical fiber probe.....	73
Figure 4-13 Macroscopic fluctuation of solids holdup.....	75
Figure 4-14 Histogram of solids holdup for dense moments and dilute moments (a: $U_g = 3$ m/s and $G_s=100$ kg/m ² s, b: $U_g = 5$ m/s and $G_s=100$ kg/m ² s).....	75
Figure 5-1 Schematic diagram of circulating fluidized bed.....	84
Figure 5-2 Schematic diagram of the visualization system	85

Figure 5-3 Demonstration of the image tracking	88
Figure 5-4 Probability density distribution of the cross-correlation coefficient	88
Figure 5-5 Radial distributions of the vertical velocity	89
Figure 5-6 Slip velocity versus superficial gas velocity	90
Figure 5-7 Radial distributions of the solids flux.....	91
Figure 5-8 Instantaneous particle velocity versus solids holdup	92
Figure 5-9 Instantaneous solids flux versus solids holdup	93
Figure 5-10 Radial distributions of instantaneous particle velocity (a: adjacent moments, b: distant moments)	94
Figure 5-11 Radial distributions of instantaneous solids flux.....	95
Figure 5-12 Periodical fluctuation of solids circulation rate	96
Figure 5-13 Radial distributions of the solids holdup for dense moments and dilute moments.....	97
Figure 5-14 Radial distributions of particle velocity for dense moments and dilute moments.....	98
Figure 5-15 Radial distributions of solids flux for dense moments and dilute moments ..	99
Figure 6-1 Schematic diagram of the circulating fluidized bed.....	108
Figure 6-2 Schematic diagram of the visualization system	110
Figure 6-3 Distribution of solids holdup gradient across riser (a: the original image, b: the map of solids holdup gradient)	113
Figure 6-4 Distribution of solids holdup gradient around clusters.....	114

Figure 6-5 Solids holdup slopes captured using optical fiber probe	115
Figure 6-6 Determination of cluster boundary.....	117
Figure 6-7 Radial distributions of cluster dimensions	118
Figure 6-8 Relationship between projected length/ width and equivalent diameter	119
Figure 6-9 Circularity versus equivalent diameter	120
Figure 6-10 cluster dimensions versus operating conditions	121
Figure 6-11 Probability density distribution of cluster size.....	122
Figure 6-12 Radial distributions of cluster solids holdup.....	123
Figure 6-13 Relationship between cluster solids holdup and cluster size	123
Figure 6-14 Cluster solids holdup versus operating conditions	124
Figure 7-1 Schematic diagram of the circulating fluidized bed.....	132
Figure 7-2 The instantaneous flow structure in the CFB (a: phase interpretation from signal captured by optical fiber probe, b: phase interpretation from the image captured by the high-speed camera).....	134
Figure 7-3 Demonstration of wavelet transform.....	135
Figure 7-4 Time lag versus wavelet scale.....	135
Figure 7-5 Probe signal and approximate signals	137
Figure 7-6 Correlation coefficient versus the wavelet scale	138
Figure 7-7 Probe signal and approximate signals (a10, a17).....	138
Figure 7-8 Phase properties versus local-mean solids holdup	142

Figure 7-9 Statistic properties of crest clusters and trough clusters versus operating conditions	144
Figure 7-10 Properties of crest phase versus operating conditions	146
Figure 7-11 Histogram of cluster length.....	147
Figure 7-12 Relationship between cluster solids holdup and cluster length.....	148
Figure 7-13 Comparison of cluster size between the optical fiber probe and high-speed camera.....	149
Figure 7-14 Comparison of crest clusters formed by FCC and glass beads	150
Figure 7-15 Comparison of trough clusters formed by FCC and glass beads	151
Figure 7-16 Comparison of crest phase formed by FCC and glass beads	152
Figure 8-1 Schematic diagram of the circulating fluidized bed	162
Figure 8-2 The instantaneous flow structure in the CFB (a: phase interpretation for signals captured by optical fiber probe, b: phase interpretation for images captured by the high-speed camera).....	163
Figure 8-3 Solids holdup signals captured in low density and high density conditions..	165
Figure 8-4 A transition signal from “dilute structure” and to “dense structure”	166
Figure 8-5 Distribution of particulate phase ($U_g = 7$ m/s and $G_s=700$ kg/m ² s).....	167
Figure 8-6 Radial distributions of phase solids holdup (a: 7 m/s-700 kg/m ² s, b:5 m/s-400 kg/m ² s).....	168
Figure 8-7 Properties of crest clusters and trough clusters versus radial positions.....	170
Figure 8-8 Properties of crest clusters and trough clusters versus axial positions	172
Figure 8-9 Statistic phase information versus operating conditions	174

Figure 8-10 Information of crest phase versus operating conditions (a: solids holdup, b: length)	176
Figure 9-1 Schematic diagram of the multifunctional circulating fluidized bed	185
Figure 9-2 Schematic diagram of downer inlet	186
Figure 9-3 Example signals across CFB downer	188
Figure 9-4 The instantaneous flow structure in the CFB (a: phase interpretation for signals captured by optical fiber probe, b: phase interpretation for images captured by the high-speed camera).....	189
Figure 9-5 Time lag versus wavelet scale	190
Figure 9-6 Correlation coefficient versus wavelet scale.....	191
Figure 9-7 Probe signal and approximate signals (a9 and a17)	191
Figure 9-8 Radial distributions of solids holdup in the CFB downer.....	193
Figure 9-9 Radial distribution of phase solids holdup (a: $U_g=5$ m/s, $G_s=100$ kg/m ² s; b: $U_g=5$ m/s, $G_s=700$ kg/m ² s).....	194
Figure 9-10 Properties of crest clusters and trough clusters versus radial positions	196
Figure 9-11 Properties of crest clusters and trough clusters versus axial positions	198
Figure 9-12 Statistic properties of crest clusters and trough clusters versus operating conditions	200
Figure 9-13 Comparison of crest clusters between riser and downer	201
Figure 9-14 Comparison of trough clusters between riser and downer.....	202
Figure 9-15 Comparison of crest phase between riser and downer	203

LIST OF TABLES

Table 2-1 Information of cluster bottom frequencies	19
Table 3-1 Information of particle properties	42
Table 7-1 Information of particle properties	132
Table 7-2 Phase classification using wavelet transform	140

CHAPTER 1

General Introduction

Studies on the instantaneous flow structure in circulating fluidized beds are reported in this dissertation. An introduction to research background, objectives and thesis structure is presented in this chapter.

1.1 Background

Gas-solid fluidization is a state where particles are suspended using flowing gas. According to the flow regime, there is particulate fluidization, bubbling fluidization, turbulent fluidization, fast fluidization and pneumatic transport for the gas-solid system. Particulate fluidization, bubbling fluidization and turbulent fluidization are considered as low velocity or conventional fluidization, since most particles remain in the fluidized bed. Fast fluidization and pneumatic transport belong to high-velocity fluidization, since significant amounts of particles are entrained out by gas. Comparing with other fluidization regimes, fast fluidization provides high gas productivity, enhanced mass and heat transfer between gas and particles, reduced back mixing of gas and particles, solids circulation, flexible control of gas and solids. Thus, fast fluidization has been widely used for petroleum refining, calcination, metallurgy, gasification and combustion (Berruti et al., 1995; Wang et al., 2014). In this work, our study focuses on fast fluidization (Yerushalmi et al., 1976).

To maintain fast fluidization, particles need to be fed in continuously. To achieve this, gas-solids circulating fluidized bed (CFB) was developed in the early 1940s (Lim et al., 1995). CFB mainly consists of a riser, cyclones at riser top and a solids-returning system. Particles are transported upward by high-velocity gas in the riser and are recovered from gas in the cyclones installed at the riser top. The collected particles are circulated to the riser bottom through a solids-returning system, which may be a standpipe or a regenerator. Normally, the solids-returning system and cyclones are considered as auxiliary devices, since the reactions happen in the riser. Hence, the performances of a CFB is highly related to the instantaneous flow structure in the riser.

In the CFB riser, the instantaneous flow structure is feathered with dispersed particles and aggregated clusters (Li et al., 1991; Cahyadi et al., 2017). Comparing with dispersed particles, clusters are much larger (Bi et al., 1993; Li et al., 1991), and much denser (Soong et al., 1994; Shi et al., 2008). As a result, gas has excellent contact with dispersed particles, but tends to bypass clusters (Li et al., 1998; Yunhau et al., 2006;). Besides that, a vast volume of the riser is occupied by clusters and a large proportion of particles is transported in cluster form (Cocco et al., 2010; Chew et al., 2011; 2012a; 2012b;). Thus, key parameters, like slip velocity (Yang et al., 1992), drag force (Yang et al., 2003), back mixing (Noymer and Glicksman, 1998;), heat transfer (Wu et al., 1991; Noymer and Glicksman, 1998;), mass transfer (Li et al., 1998; Yunhau et al., 2006;) and reactor scale-up (Cocco et al., 2017;) are affected inevitably by the existence of clusters.

However, the characterization of clusters in the CFB riser varies in an order of magnitude, even at the similar operating condition and with same detective technique. Cluster size is reported either in millimeters (Hatano et al., 1994; Xu and Zhu, 2011a; Xu and Zhu, 2011b; Firuzian et al., 2014;) or in centimeters (Li et al., 1995; Manyele et al., 2002; Guenther and Breault, 2007) and the difference is as high as one order of magnitude. Cluster time fraction is reported around 0.06 (Xu and Zhu, 2011a), around 0.10 (Manyele et al., 2002) or around 0.5 (Guenther and Breault, 2007; Afsahi et al., 2009; Firuzian et al., 2014; Chew et al., 2011; 2012a; 2012b;) and the difference is also found to be one order of magnitude. Moreover, almost all the studies have the solids circulation rate below $300 \text{ kg/m}^2 \text{ s}$ and cluster information is scarce in high-density conditions (Cahyadi et al., 2017).

Our group has focused on the experimental study of circulating fluidized beds since the early 1990s and accumulates abundant data. Particles, including FCC and Glass beads ($288 \mu\text{m}$), have been used as the fluidized medium (Xu and Zhu, 2011a; 2011b;). Various optical fiber probes (one-channel, dual channel and multi-channel) and high-speed camera have been employed to quantify the flow information in the CFB (Xu, 2010; Yang, 2013; Wang, 2013; Liu, 2016). Many large-scale CFB systems have been developed, including a rectangular CFB (Xu, 2010; Yang, 2013) and several cylindrical CFB (Wang, 2013;). The scale of the CFB riser and the CFB downer can be 76 mm i.d.

and 10 m in height, 50 mm i.d. and 4.9 m in height, respectively (Wang et al.,2014). The operating conditions for CFB systems are also wide enough for comprehensive studies. Superficial gas velocity spans from 3 to 9 m/s. Solids circulation rate ranges from 50 kg/m² s to 700 kg/m² s for the riser and from 100 kg/m² s to 700 kg/m² s for the downer, respectively (Wang et al., 2014; 2015;).

1.2 Research objectives

Characterization of clusters in the CFB has a severe discrepancy and it remains lacking in high-density conditions. Our group has abundant experimental data on the gas-solid flow in the CFBs. The task of this thesis is to extract reliable phase information from the experimental data.

Detailed objectives are:

1. to find out why key cluster properties vary in an order of magnitude in the literature,
2. to further analyze the flow details in the CFBs using high-speed camera and optical fiber probe,
3. to investigate how particle properties (FCC and glass beads) influence the instantaneous flow structure,
4. to characterize the instantaneous flow structure in high-density CFB riser,
5. to characterize the instantaneous flow structure in high-density CFB downer.

1.3 Thesis structure

This thesis follows the “Integrated-Article Format” as outlined in UWO Thesis Regulation.

Chapter 1 presents a general introduction of background, research objectives and thesis structure.

Chapter 2 presents a detailed literature review and a preliminary exploration of the cluster definitions.

Chapter 3 describes the apparatus, instruments and measuring principles.

Chapter 4 reports solids holdup mapping of the instantaneous flow structure in a CFB riser using high-speed camera and optical fiber probe. There are crest phase (high density) and trough phase (low density) in microscope. Within crest phase, there exists crest clusters and coalesced particles. Within trough phase, there exists trough clusters and dispersed particles.

Chapter 5 reports the particle velocity and solids flux in a rectangular CFB riser. The particle velocity and solids flux are computed based on two-dimensional cross-correlations. The time-average data is consistent with the literature and the influence of solids holdup fluctuation on velocity and flux has been analyzed systematically with the instantaneous flow dynamics.

Chapter 6 reports the cluster discrimination and characterization based on images in a rectangular CFB riser. A calibration method, proposed and validated by Yang (2013), is employed in this chapter to convert grayscale in images to solids holdup. The cluster boundary is determined with the sharp solids holdup increase around clusters. Then, detailed cluster information, such as cluster solids holdup, cluster length, cluster width, cluster equivalent diameter, are calculated and discussed.

Chapter 7 reports the phase discrimination and characterization in a rectangular CFB riser using optical fiber probe. A phase discrimination method applicable to an optical fiber probe has been proposed and the extracted phase information is validated using a high-speed camera. Moreover, how particle properties influence phase characteristics is also explored by comparing phase information formed by group A and group B powders.

Chapter 8 reports the phase characterization in a high-density cylindrical CFB riser using optical fiber probe. This riser is 10 m high and 76 mm i.d. and solids circulation rate is up to 700 kg/m² s in this chapter. The instantaneous flow structure in core and wall region, radial and axial distribution of phase properties, statistic phase characteristics in the fully developed region are reported and discussed in detail.

Chapter 9 reports the phase characterization in a high-density cylindrical CFB downer using optical fiber probe. This downer is 10 m high and 50 mm i.d. and solids circulation

rate is up to $700 \text{ kg/m}^2 \text{ s}$. Flow structure in core and wall region, radial and axial distribution of phase properties, statistic phase characteristics in the fully developed region are reported and discussed in detail. Besides, phase properties are compared between the CFB riser and the CFB downer in terms of solids holdup, length and time fraction.

Chapter 10 presents the conclusions and research recommendations for future work.

References

- Afsahi, F. A., Sotudeh - Gharebagh, R., & Mostoufi, N. (2009). Clusters identification and characterization in a gas - solid fluidized bed by the wavelet analysis. *The Canadian Journal of Chemical Engineering*, 87(3), 375-385.
- Berruti, F., Pugsley, T. S., Godfroy, L., Chaouki, J., & Patience, G. S. (1995). Hydrodynamics of circulating fluidized bed risers: a review. *The Canadian Journal of Chemical Engineering*, 73(5), 579-602.
- Bi, H. T., Zhu, J. X., Jin, Y., & Yu, Z. Q. (1993). Forms of particle aggregations in CFB. In *Proceedings of the Sixth Chinese Conference on Fluidization*, Wuhan, China (pp. 162-167).
- Cahyadi, A., Anantharaman, A., Yang, S., Karri, S. R., Findlay, J. G., Cocco, R. A., & Chew, J. W. (2017). Review of cluster characteristics in circulating fluidized bed (CFB) risers. *Chemical Engineering Science*, 158, 70-95.
- Chew, J. W., Hays, R., Findlay, J. G., Knowlton, T. M., Karri, S. R., Cocco, R. A., & Hrenya, C. M. (2012a). Cluster characteristics of Geldart Group B particles in a pilot-scale CFB riser. I. Monodisperse systems. *Chemical Engineering Science*, 68(1), 72-81.
- Chew, J. W., Hays, R., Findlay, J. G., Knowlton, T. M., Karri, S. R., Cocco, R. A., & Hrenya, C. M. (2012b). Cluster characteristics of Geldart group B particles in a pilot-scale CFB riser. II. Polydisperse systems. *Chemical Engineering Science*, 68(1), 82-93.
- Chew, J. W., Parker, D. M., Cocco, R. A., & Hrenya, C. M. (2011). Cluster characteristics of continuous size distributions and binary mixtures of Group B particles in dilute riser flow. *Chemical Engineering Journal*, 178, 348-358.
- Cocco, R., Issangya, A., SB, R. K., Freeman, T., Jaeger, H. M., & Knowlton, T. M. (2017). Small-Scale Particle Interactions Are Having Significant Effects on Global Fluidized Bed Behavior. *KONA Powder and Particle Journal*, 34, 155-167.

- Cocco, R., Shaffer, F., Hays, R., Karri, S. R., & Knowlton, T. (2010). Particle clusters in and above fluidized beds. *Powder Technology*, 203(1), 3-11.
- Firuzian, N., Sotudeh-Gharebagh, R., & Mostoufi, N. (2014). Experimental investigation of cluster properties in dense gas–solid fluidized beds of different diameters. *Particuology*, 16, 69-74.
- Guenther, C., & Breault, R. (2007). Wavelet analysis to characterize cluster dynamics in a circulating fluidized bed. *Powder Technology*, 173(3), 163-173.
- Hatano, H., Kido, N., & Takeuchi, H. (1994). Microscope visualization of solid particles in circulating fluidized beds. *Powder technology*, 78(2), 115-119.
- Li, H., Xia, Y., Tung, Y., & Kwauk, M. (1991). Micro-visualization of clusters in a fast fluidized bed. *Powder Technology*, 66(3), 231-235.
- Li, H., Zhu, Q., Liu, H., & Zhou, Y. (1995). The cluster size distribution and motion behavior in a fast fluidized bed. *Powder Technology*, 84(3), 241-246.
- Li, J., Zhang, X. P., Zhu, J., & Li, J. H. (1998). Effects of cluster behavior on gas-solid mass transfer in circulating fluidized beds. *9th Engineering Foundation Conference on Fluidization*, (pp. 17-22). DURANGO, CO.
- Lim, K. S., Zhu, J. X., & Grace, J. R. (1995). Hydrodynamics of gas-solid fluidization. *International Journal of Multiphase Flow*, 21, 141-193.
- Liu, J. (2016). Reactor Performances and Hydrodynamics of Various Gas-Solids Fluidized Beds, Ph.D. Diss. The University of Western Ontario
- Manyele, S. V., Pärssinen, J. H., & Zhu, J. X. (2002). Characterizing particle aggregates in a high-density and high-flux CFB riser. *Chemical Engineering Journal*, 88(1), 151-161.

Noymer, P. D., & Glicksman, L. R. (1998). Cluster motion and particle-convective heat transfer at the wall of a circulating fluidized bed. *International Journal of Heat and Mass Transfer*, 41(1), 147-158.

Shi, H., Wang, Q., Xu, L., Luo, Z., & Cen, K. (2008). Visualization of clusters in a circulating fluidized bed by means of particle-imaging velocimetry (PIV) technique. In *Proceedings of the 9th International Conference on Circulating Fluidized Beds*, Hamburg, Germany (pp. 1013-1019).

Soong, C. H., Tuzla, K., & Chen, J. C. (1994). Identification of particle clusters in circulating fluidized bed. *Circulating Fluidized Bed Technology*, 4, 615-620.

Wang, C. (2013). High density gas-solids circulating fluidized bed riser and downer reactors, Ph.D. Diss. The University of Western Ontario

Wang, C., Li, C., & Zhu, J. (2015). Axial solids flow structure in a high density gas-solids circulating fluidized bed downer. *Powder Technology*, 272, 153-164.

Wang, C., Zhu, J., Barghi, S., & Li, C. (2014). Axial and radial development of solids holdup in a high flux/density gas-solids circulating fluidized bed. *Chemical Engineering Science*, 108, 233-243.

Wu, R. L., Lim, C. J., Grace, J. R., & Brereton, C. M. H. (1991). Instantaneous local heat transfer and hydrodynamics in a circulating fluidized bed. *International journal of heat and mass transfer*, 34(8), 2019-2027.

Xu, J. (2010). Hydrodynamics studies on macro- and micro-flow structure with effects of particle properties in a circulating fluidized bed, Ph.D. Diss. The University of Western Ontario

Xu, J., & Zhu, J. (2011a). Effects of particle properties on flow structure in a 2-D circulating fluidized bed: Solids concentration distribution and flow development. *Chemical Engineering Science*, 66(21), 5064-5076.

- Xu, J., & Zhu, J. X. (2011b). Visualization of particle aggregation and effects of particle properties on cluster characteristics in a CFB riser. *Chemical Engineering Journal*, 168(1), 376-389.
- Yang, J. (2013). Studies on microscopic flow structure inside a rectangular circulating fluidized bed through image analysis, Ph.D. Diss. The University of Western Ontario
- Yang, N., Wang, W., Ge, W., & Li, J. (2003). CFD simulation of concurrent-up gas–solid flow in circulating fluidized beds with structure-dependent drag coefficient. *Chemical Engineering Journal*, 96(1), 71-80.
- Yang, Y. L., Jin, Y., Yu, Z. Q., & Wang, Z. W. (1992). Investigation on slip velocity distributions in the riser of dilute circulating fluidized bed. *Powder Technology*, 73(1), 67-73.
- Yerushalmi, J., Turner, D. H., & Squires, A. M. (1976). The fast fluidized bed. *Industrial & Engineering Chemistry Process Design and Development*, 15(1), 47-53.
- Yunhau, Z., Huilin, L., Yurong, H., Ding, J., & Lijie, Y. (2006). Numerical prediction of combustion of carbon particle clusters in a circulating fluidized bed riser. *Chemical Engineering Journal*, 118(1), 1-10.

CHAPTER 2

Literature Review

2.1 Introduction

Gas-solids circulating fluidized bed (GSCFB) was first developed in the early 1940s (Jahnig et al., 1980) and now it has a wide range of industrialized applications, including coal combustion and gasification, fluid catalytic cracking, biomass gasification and calcination, due to its advantages like good gas-solids contacting, reduced back-mixing, excellent heat transfer and high productivity (Lim et al., 1995; Zhu and Cheng, 2016; Wang et al., 2014).

CFB mainly consists of a riser, cyclones at riser top and a solids-returning system. Particles are transported upward by high-velocity gas in the riser and are recovered from gas in the cyclones. The collected particles are circulated to the riser bottom through the solids-returning system, which may be a standpipe or a regenerator. Normally, solids-returning system and cyclones are considered as auxiliary devices and reactions happen in the riser. Then, the performance of CFB highly relates to gas-solid contact in the riser.

In CFB risers, particles are fluidized both as dispersed particles and as aggregated clusters (Li et al., 1991; Cahyadi et al., 2017). Comparing with dispersed particles, cluster is much larger (Bi et al., 1993; Li et al., 1991), and much denser (Soong et al., 1994; Shi et al., 2008). As a result, gas has excellent contact with dispersed particles, but tends to bypass the clusters (Li et al., 1998; Yunhau et al., 2006;). Additionally, a vast volume of the riser is occupied by clusters and a large proportion of particles is transported in cluster form (Cocco et al., 2010; Chew et al., 2011; 2012a; 2012b;). Thus, key parameters, like slip velocity (Yang et al., 1992), drag force (Yang et al., 2003), back mixing (Noymer and Glicksman, 1998;), heat transfer (Wu et al., 1991; Noymer and Glicksman, 1998;), mass transfer (Li et al., 1998; Yunhau et al., 2006;) and reactor scale-up (Cocco et al., 2017;) are inevitably affected by the existence of clusters.

To summarize the studies on the instantaneous flow structure in the CFB, this literature review introduces measuring techniques, evolving understanding of clusters, cluster definitions, reported cluster properties and preliminary exploration.

2.2 Measurement techniques

In the literature, there are two types of instruments for cluster detection: high-speed camera and needle-type probe.

2.2.1 High-speed camera

Various types of illumination systems have been coupled with the high-speed camera. Takeuchi and Hirama (1991) coupled a camera with a borescope (10mm in diameter) and a light-guide probe. The borescope is connected with the camera and inserted into the riser. The light-guide probe, made of optical fibers, transmits the lights from a light source to the view field. It is installed facing the borescope and the distance is 0.01m. To have a wider view field, Takeuchi et al. (1996) attached the borescope with a prism and inserted a light guide parallelly with the borescope. To reduce the disturbance, a special probe has been designed to combine the borescope and light guide together. The special probe consists of a set of lenses and an optical fiber flashlight transmitter. The gas solid flow is illuminated by the flashlight through the transmitter and the view is recorded by the camera. (Li et al., 1991; Hatano et al., 1994; Zou et al., 1994;). For this technique, the maximum size of observable clusters is limited by the effective visual field (Li et al., 1991).

To visualize the flow in the particle scale, Particle Image Velocimetry (PIV) has been designed. It has a similar setup with the foresaid special probe but with a better resolution (Matsuda et al., 1996; Shi et al., 2008). As PIV has a scope smaller than a whole cluster, it cannot tell whether the particles recorded are inside or outside the cluster.

Horio and Kuroki (1994) coupled a video camera with the laser sheet techniques. The He-Ne laser light source passes through a glass rod to form the laser sheet, penetrate into the transparent riser and illuminate the particles. The flow can be visualized both vertically and horizontally depending on the direction of the laser sheet. However, once the solids circulating rate exceeds $0.6 \text{ kg/m}^2\text{s}$, this visualization fails due to the core annulus

structure. Van den Moortel and Tadrist (1996) and Van den Moortel et al. (1998) adopted this laser sheet technique and applied it in a square circulating fluidized bed. To visualize clusters at higher solids circulation rate, Kuroki and Horio (1994) employed three laser sheets, attached the light guide on the inside wall and placed a camera in the core region. Even though, the visualization still fails if the solids circulating rate is higher than $9 \text{ kg/m}^2\text{s}$. The main drawback of the laser sheet technique is that it is limited in the low solids circulation rate conditions.

The video camera has also been coupled with the transparent circulating fluidized bed column and the descending clusters along the wall were well visualized (Gidaspow et al., 1989; Rhodes and Hirama., 1992 and Lim et al., 1996). But the visualization is limited in the wall region due to the core-annulus structure. Bi and Zhu (1993) and Mondal et al., (2015) coupled a video camera with a transparent 2-D circulating fluidized bed. The annulus down flow only appears near the side walls and the visualization of the core region is achieved through the front and back walls. In order not to compress the clusters, Xu and Zhu (2010) constructed a transparent rectangular circulating fluidized bed (higher thickness/width ratio than 2-D riser) and found the solids holdup distribution is comparable in the rectangular bed and in the column bed. Then, Xu and Zhu (2011) and Yang and Zhu (2015a, 2015b, 2015c) conducted the visualization in the transparent rectangular circulating fluidized bed.

Wei et al. (1994) and Wei et al. (1995) detected the clusters in a CFB using a one-dimensional optical fiber image system which includes a 60-pixel optical fiber image sensor, 60 light emitting diodes, a photomultiplier tube and a computer interface. The sensor is fixed towards the flow direction and the cross section is $100 \times 2 \text{ mm}$. The particles are illuminated by the emitting diodes and the flow behavior is recorded with the image sensor.

2.2.2 Needle-type probe

Needle-type probes detect the capacitance or reflected-light intensity caused by local solids holdup and their measuring scopes are, from 1 mm to 1.5 mm, smaller than the cluster scale.

The acquired data reflects the instantaneous local average solids holdup. Based on the measurement principles (capacitance/light), we have needle capacitance probes and optical fiber probe.

Needle capacitance probe consists of an external sheath serving as the ground electrode, an extended-out central needle serving as the potential electrode and a concentric metal tube electrically insulating the outer sheath and the central needle. The effective sensing volume of this probe is a cone-shaped region around the exposed length of the central needle. The measurement volume is smaller than the typical cluster size, but orders of magnitude larger than the individual particle size. (Soong et al., 1994; Sharma et al., 2000;)

The optical fiber probe system differs in channel number (one, two and multiple) and fiber arrangement. However, the measuring principle is the same. Light from the source illuminates a measuring volume of particles through the light-emitting fibers. The light reflected by the particles is captured by the light receiving fibers and processed by a photo-multiplier. The light intensity is then converted into voltage signals and the voltage signals are further amplified and recorded with a computer. Two-channel probe is very popular, as (i) it can measure the solids holdup and velocity simultaneously and (ii) it has a small volume which reduces the disturbance. For the two-channel probe, each channel consists of many quartz fibers for light-emitting and receiving, arranged in alternating arrays. A glass cover is placed over the probe tip to eliminate the blind zone. Calibrate the effective distance between the two channels and calculate the time lag of the two signals using cross-correlation, the velocity is calculated by dividing the effective distance by the time lag. (Liu et al., 2003)

Calibrations

Yang and Zhu (2014a) correlated the grayscale with solids holdup using a liquid-solid fluidized bed. Yang and Zhu (2014b) further validated this correlation with optical fiber probe data. Besides, Casleton et al. (2010) estimated the voidage based on the particles on the focal plane, as particles are well visualized using PIV. For both the capacitance probe and optical fiber probe, the raw data obtained is a voltage signal which reflects the local capacitance or local light intensity reflected by particles. Zhang et al. (1998) created a

uniform suspension in a sim downer and calibrated the voltage with solids holdup (Wang, 2013; Manyele et al., 2002;).

2.3 The evolving understanding of clusters

Items like “swarms” (Rhodes and Hirama, 1992; Matsuda et al., 1996), “strands” (Rhodes and Hirama, 1992; Takeuchi et al., 1996), “packets” (Takeuchi and Hirama, 1991), and “clusters” have been used to describe the particle aggregations in fluidized bed. Later, “clusters” has been adopted as the general term to describe the particle aggregations. The study of clusters is a key to understand the fundamentals of CFB riser and has drawn more and more attention in recent 30 years (Cahyadi et al., 2017).

Wilhelm and Kwauk (1948) first observed “aggregative fluidization” where particles adhere in group and move together in conventional fluidized bed. Later, Yerushalmi et al. (1976) observed that particle aggregates in forms of strand and cluster within the fast-fluidization regime. Then, all particle aggregation was termed generically as clusters by Li and Kwauk (1980). Li et al. (1991) combined a high-speed camera with a special probe coupling borescope with a light source and, for the first time, systematically recorded clear pictures of clusters across the riser. Using this setup, Zou et al., (1994) found that a cluster further consists of sub-clusters and discrete particles. Afterward, Matsuda et al. (1996) employed a similar instrument with higher resolution and observed collisions of individual particles with the particle swarm: some particles bounced back while others join the swarm.

Takeuchi and Hirama (1991) combined a high-speed camera with a borescope as well as a separate light source and discovered the coexistence of relatively small and large dense packets. Based on this setup, Takeuchi et al. (1996) further analyzed the probability of cluster forms (parabolic, right increasing and left increasing).

Rhodes and Hirama (1992) coupled a high-speed camera with normal and magnifying lenses and identified three forms of particle motion at the wall of a transparent riser: dilute, swarm and dense flow. Bi et al. (1993) recorded clusters in a transparent two-dimensional riser using a high-speed camera and classified them into four forms, namely particle cluster, particle swarm, particle sheet and particle streamer. Shaffer et al. (2013) employed a high-

speed camera to record the flow at a transparent column wall and observed that voids formed after gas “jets” moves away is then filled with masses of particles in the form of large clusters. Yang and Zhu (2015a, 2015b) coupled a high-speed camera with a rectangular transparent riser and found that a cluster typically consists of a core region of the highest solids holdup and a surrounding region (cluster cloud) with intermediate solids holdup that is significantly higher than and distinctly different from that in the dilute phase.

Wei et al. (1994; 1995) arranged the mix of lighting fibers and receiving fibers linearly in an image sensor facing downward and found that cluster characteristics vary greatly at different conditions.

Horio and Kuroki (1994) developed an external picturing system using laser sheet as a lighting source and observed clusters three-dimensionally. Kuroki and Horio (1994) designed an internal picturing system with the camera inside the column and characterize cluster size. Using similar laser techniques, Van den Moortel and Tadriss (1996) discovered that the flow in a riser is characterized with particle aggregates and void regions and Van den Moortel et al. (1998) further studied the horizontal dimension of the gas pockets.

Besides high-speed camera, needle-type probes, including capacitance probe and optical fiber probe, have also been widely used to characterize clusters (Horio and Nishimuro, 1992; Soong et al., 1994; Sharma et al., 2000; Li et al., 1995; Rudnick and Werther 1998; Lu et al., 2005; Guenther and Breault, 2007; Yang and Leu, 2009; Chew et al. 2011, 2012a, 2012b;). The signal captures local capacitance or light intensity which reflects local solids holdup (Zhang et al., 1998; Wiesendorf and Werther, 2000). Several thresholds have been proposed to define clusters and details are summarized in the following section. Brereton and Grace (1993) assumed a cluster solids holdup of 0.6 and proposed an intermittency index, which would be zero for perfect core-annulus flow and one for perfect cluster flow, to characterize the flow in the CFB riser. Manyele et al. (2002) characterized clusters in a high-flux riser whose solids circulation rate is as high as $550 \text{ kg/m}^2 \text{ s}$ and found that cluster properties depend on local mean solids concentration. Xu and Zhu (2011a, 2011b) investigated the influence of particle properties on clusters and found that small and light particles have a higher potential to aggregate than large and heavy particles. Chew et al.

(2012a, 2012b) compared the clusters formed by monodisperse particles and polydisperse particles and found that they have similar trends of cluster characteristics.

2.4 Cluster definitions

A qualitative consensus has been reached on the cluster definition: the cluster has higher solids holdup than the individual particle region. But how to discriminate the clusters quantitatively is still not concluded yet. From 1993 to now, nine quantitative definitions have been proposed and applied to experimental data and simulated data.

“Rectangular threshold”

Horio and Nishimuro, (1992) detected clusters using an optical fiber probe and simplified the signal to rectangular signals. Cluster threshold, I_{th} , is 0.25 times light intensity for packed bed, I_0 . For each cluster, it has a maximum light intensity, I_{max} , and the cluster is defined to be where solids holdup is above $\frac{I_{max}+I_{th}}{2}$.

*“Mean +N*standard deviation”*

Soong et al. (1993) defined clusters using “Mean plus multiple(N=3) standard deviation(σ)” threshold, based on capacitance probe signals:

1. the solids fraction in a cluster must be significantly above the time-averaged solid fraction at the same operating condition at the local position;
2. the perturbation in solid fraction due to the occurrence of clusters must be greater than the random fluctuations in the background solid fraction;
3. the concentration increase must be sensed for a sampling volume with characteristic length scale greater than 100 particle diameters.

Sharma et al. (2000) also applied this definition to capacitance probe signals, but designated N with 0; Tuzlan et al. (1998), Xu and Zhu (2011) and Kiani et al. (2013) applied this definition to optical fiber probe signals and designated N with 2,2,1, respectively; Mondal et al. (2015) applied this definition to images acquired in a two-

dimensional riser and assigned $N=0.5$. Manyele et al. (2002) suggested that N shall change with the operating condition as well as positions and designated n from 1.0 to 1.4 according to sensitivity analysis of optical fiber probe signals. Besides experimental data, “Mean $+N$ *standard deviation” has also been widely used to extract cluster information from simulated data (Helland et al., 2002; Cabezas-Gomez et al., 2008; Wang et al., 2008; Shuyan et al., 2005; Liu and Lu, 2009;)

Visual detection

Li et al. (1995) visually sampled 848 clusters from the optical fiber probe signal based on visual observation of peaks and valleys.

“Gs-based threshold”

Rudnick and Werther (1998) suggested that the cluster detection shall only depend the local instantaneous solids holdup and proposed cluster definition based on solids circulation rate: (1) select a solids holdup threshold, (2) separate the signal into dense phase and lean phase based on the threshold, (3) calculate the dense phase velocity and lean phase velocity, (4) calculate and add up the solids circulation rate of dense phase and lean phase, (5) if the overall solids circulation rate is within $\pm 20\%$ of the external measured solids circulating rate, the threshold is considered to be sufficient; if not, adjust the solids holdup threshold and do this procedure again.

“Wavelet half peak”

Lu et al. (2005) detected clusters in a downer using optical fiber probe and defined the cluster boundary where the solid concentration is changed half from the concentration of the bed to that of the cluster center zone. To achieve that, the Mallat's pyramidal algorithm was employed for signal processing. Although this definition is proposed to analyze clusters in the downer, it is introduced here for a complete summary of cluster definitions.

“Median”

Johnsson et al. (1997) and Guenther and Breault (2007) pointed out the probability density distribution of solids holdup signals is not normally distributed and it makes the “Mean +N*standard deviation” physically meaningless. Then, Guenther and Breault (2007) defined clusters as where the transient solids holdup exceeded “fiftieth percentile (median)” with optical fiber probe signals. Afsahi et al. (2009) and Firuzian et L. (2014) adopted this definition and applied it to optical fiber probe signals.

“Wavelet cluster scale”

Ren et al. (2001) resolved optical fiber signals into three scales of components: micro-scale (particle size), meso-scale (cluster size) and macro-scale (unit size). Based on this understanding, Yang and Leu (2009) decomposed optical fiber probe signal using wavelet transform, analyzed the energy distribution for each wavelet scale, did a sensitivity test for different cluster discrimination scales and decided to chose A_{11} (approximate signal of scale 11) as the discrimination scale. Where the transient solids holdup exceeded the value of A_{11} was identified as clusters in the optical fiber probe signal by Yang and Leu (2009). Chew et al. (2011, 2012a, 2012b) adopted this cluster definition and applied it to optical fiber probe signals.

Wavelet transform can be viewed as a band filter applied at desired times to original solids holdup signal. For original signal, it contains information whose frequency spanning from 0 to sampling frequency. For scale 1, the original signal is decomposed to detail signal (d1) and approximate signal (a1). For scale 2, approximate signal (a1) is decomposed to detail signal (d2) and approximate signal (a2). For scale 3, approximate signal (a2) is decomposed to detail signal (d3) and approximate signal (a3). This process continues until the desired scale has been reached. For scale n, detail signal (dn) contains information whose frequency spanning from sampling frequency divided by 2^n to the requecy divided by 2^{n-1} ; approximate signal (an) contains information whose frequency spanning from 0 to sampling frequency divided by 2^n . The principle has already been elaborated in papers (Yang and Leu, 2009; Chew et al., 2011; 2012a; 2012b;). Based on this, cluster information was believed to be above 0.49 Hz or 0.39 Hz. The threshold frequency to demarcate cluster

information is referred as cluster bottom frequency. Cluster bottom frequencies for Yang and Leu (2009) and Chew et al. (2011, 2012a, 2012b) are listed in Table 2-1.

Table 2-1 Information of cluster bottom frequencies

Authors	Sampling frequency /Hz	Cluster scale	Cluster bottom frequency/Hz
Yang and Leu, 2009	1000	11	0.49
Chew et al., 2011 Chew et al., 2012a	1000	11	0.49
Chew et al., 2012a Chew et al., 2012b	100	8	0.39

In the following section, “wavelet cluster scale” was applied to sample data from optical fiber probe. Since sampling frequency is different from papers published by Yang and Leu (2009) and Chew et al. (2011, 2012a, 2012b), cluster bottom frequency was used as a reference.

“Threshold selection method”

Yang and Zhu (2014a, 2014b) recorded the gas-solids flow in a rectangular CFB riser using a high-speed camera and did a calibration between grayscale and solids holdup. Yang and Zhu (2015b) adopted a threshold section method (Otsu, 1975) which maximizes the inter-class variance between the background and foreground classes: apply it to discriminate dense and dilute phases and then apply it again in the dense phase to identify the clusters.

“Core wake method”

Varas et al. (2017) recorded the gas-solids flow in a transparent 2-D riser and proposed a cluster definition based on images: cluster exists if a dense particle core, whose solids holdup is above 0.4, appears and the cluster boundary around that core is defined as where solids holdup equals 0.2.

Remarks

The number of publications by the types of cluster definitions was plotted in Figure 2-1. “Rectangular threshold”, “Visual detection”, “Gs-based threshold”, “Wavelet half peak”, “Threshold selection method” and “Core wake method” only have one publication indicating that there is no adoption after their proposal. “Mean +N*standard deviation”, “Median” and “Wavelet cluster scale” have been widely adopted by several researchers and are all proposed based on the needle type probes. “Mean +N*standard deviation” have the highest publication, since it has a history of 25 years (Soong et al., 1993) and can be easily applied to experimental data. With the developing understanding of gas-solid interaction in the CFB riser, “Median” and “Wavelet cluster scale” have been proposed to deal with unnormal distribution of solids holdup probability and macro-scale fluctuation. In recent year, “Wavelet cluster scale” draws more and more attention. But, no consensus on cluster definition has been reached a yet.

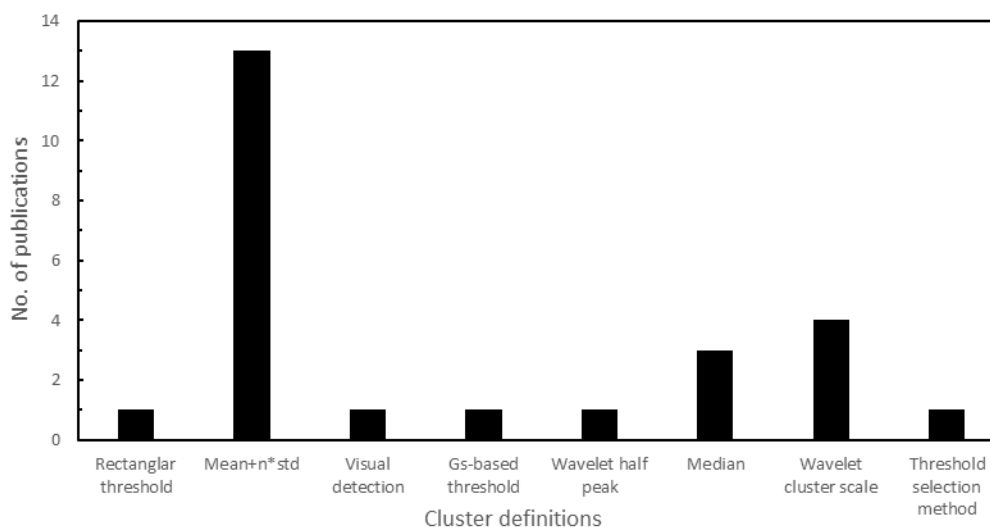


Figure 2-1 Number of publications for each cluster definition

2.5 Cluster properties in the literature

In the literature, the cluster has been characterized in terms of cluster solids holdup (or cluster voidage), cluster size, cluster frequency, cluster time fraction. Cahyadi et al. (2017)

have already well summarized reported cluster properties. Radial distribution of cluster voidage at the bottom, middle and top of the riser is shown in Figure 2-2. Cluster voidage is high in the riser center and reduces towards riser wall. Radial distribution of cluster size at the bottom, middle and top of a riser is shown in Figure 2-3. Cluster size has a discrepancy of one order of magnitude. Additionally, cluster size may (1) increases from riser center to riser wall, (2) first increases then decreases from riser center to riser wall, (3) first decreases then increases from riser center to riser wall. Radial distribution of cluster frequency at the bottom, middle and top of the riser is shown in Figure 2-4. Cluster frequency also has a discrepancy of one order of magnitude. Cluster frequency generally first increases then decreases from riser center to riser wall. Moreover, cluster time fraction is reported around 0.06 (Xu and Zhu, 2011a), around 0.10 (Manyele et al., 2002) or around 0.5 (Guenther and Breault, 2007; Afsahi et al., 2009; Firuzian et al., 2014; Chew et al., 2011; 2012a; 2012b;) and the difference is also almost one order of magnitude. Collectively, discrepancy on cluster properties still exists at similar operating conditions, which evidently hinders the understanding of flow structure in the riser and the development of numerical models. The particle type will influence the cluster property. But, if the measuring technique and definition are the same, the difference caused by particle type is much less than one order of magnitude (Xu and Zhu, 2011a; Xu and Zhu, 2011a; Chew et al., 2012a; Chew et al., 2012b;).

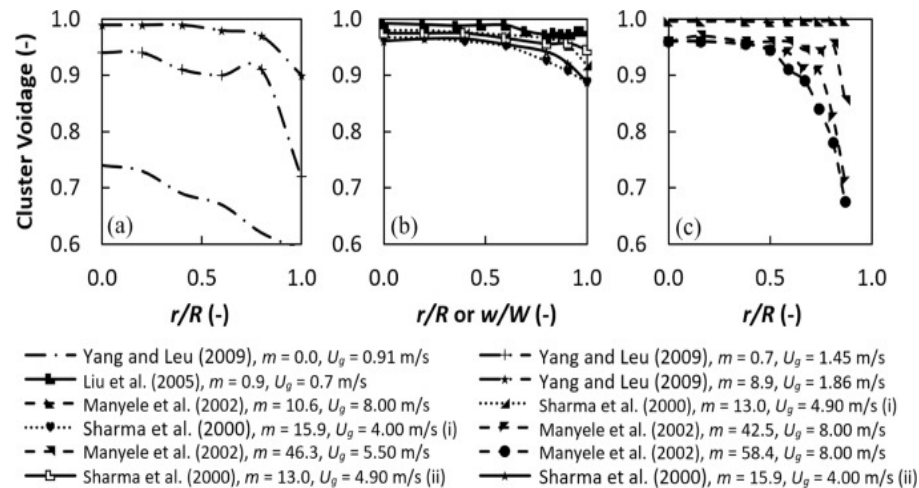


Figure 2-2 Summarization of cluster voidage in the literature (Cahyadi et al., 2017)

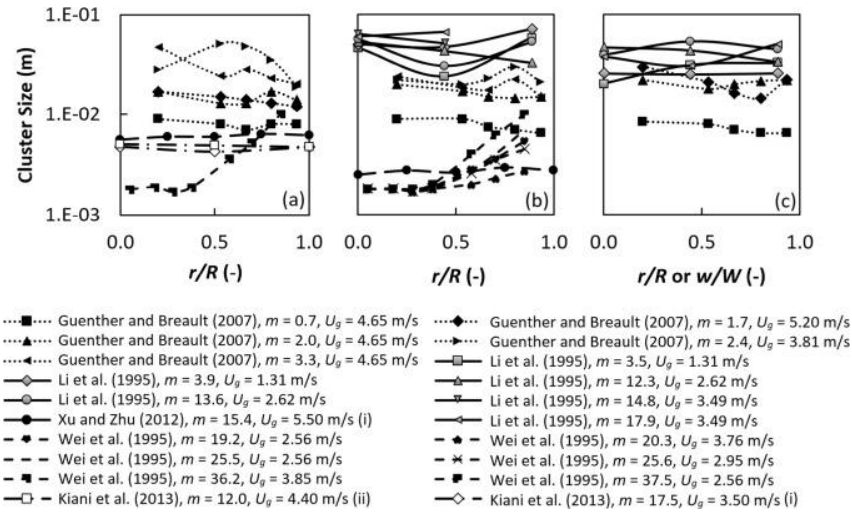


Figure 2-3 Summarization of cluster size in the literature (Cahyadi et al., 2017)

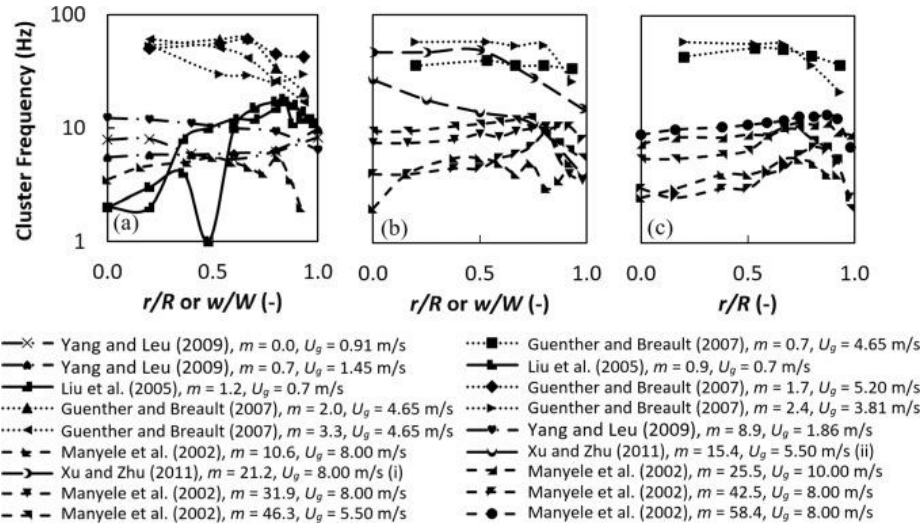


Figure 2-4 Summarization of cluster frequency in the literature (Cahyadi et al., 2017)

2.6 Preliminary exploration

Johnsson et al. (1997), Mondal et al (2015) and Varas et al. (2017) stated that cluster definitions may have evident influences on the magnitude of cluster properties (Johnsson et al., 1997; Mondal et al., 2015; Varas et al., 2017;). In-depth analysis of proposed cluster definitions is in urgent need, but still lacking. Preliminary analysis is conducted here by applying widely-adopted cluster definitions to the same experimental data, aiming to

explore the fundamentals of cluster defining and to investigate to what extent and how cluster definition influences the extracted cluster properties.

2.6.1 Analysis of example signal

In the literature, studies on clusters differ in particles, apparatuses, operating conditions, measurement devices, instrument resolution and measuring positions (Harris et al., 2002; Cahyadi et al., 2017;). To have a fair evaluation, the same series data should serve as the substrate for these cluster definitions, instead of data from the literature. After careful considerations, a signal captured using an optical fiber probe has been selected as the testing substrate. The reasons include: (1) optical fiber probe is a widely-used technique for cluster detection (Li et al., 1995; Rudnick and Werther, 1998; Manyele et al., 2002; Lu et al., 2005; Guenther and Breault, 2007; Yang and Leu, 2009; Afsahi et al., 2009; Xu and Zhu, 2011a; Xu and Zhu, 2011b; Chew et al., 2011; Chew et al., 2012a; Chew et al., 2012b; Kiani et al., 2013; Firuzian et al., 2014;); (2) out of nine cluster definitions, seven of them have been proposed based on optical fiber probe data; (3) popular cluster definitions, like “Mean+N*standard deviation”, “Median” and “Wavelet cluster scale”, are applicable to optical fiber probe data. The sampling position, operating condition, sampling frequency and sampling time for the testing substrate are $r/R=0$, $h/H=4.32\text{ m}/7.60\text{ m}$; $U_g=5\text{ m/s}$, $G_s=100\text{ kg/m}^2\text{ s}$; 100 kHz ; 13.1 s , respectively. The optical fiber probe used to acquire this signal is a dual-channel probe and its detailed dimensions can be found in previous papers (Xu and Zhu, 2011a; Xu and Zhu, 2011b;).

Cluster properties, including cluster solids holdup, cluster length, cluster frequency and cluster time fraction, were computed based on different cluster definitions (“Mean+3standard deviation”, “Mean+2standard deviation”, “Mean+standard deviation”, “Mean”, “Median” and “Wavelet cluster scale”) and the results are shown in Figure 2-5.

Cluster solids holdup, depending on cluster definition, ranges from 0.02 to 0.09 (4.5 times difference). “Mean+3standard deviation” corresponds to highest cluster solids holdup, followed by “Mean+2standard deviation”, “Mean+standard deviation”, “Mean”, “Wavelet cluster scale” and “Median”.

Cluster length, depending on cluster definition, spans from 0.002 m to 0.007 m (3.5 times difference). “Median” results in highest cluster length, followed by “Wavelet cluster scale”, “Mean”, “Mean+standard deviation”, “Mean+2standard deviation” and “Mean+3standard deviation”. Extracted cluster length is found to have a negative relationship with extracted cluster solids holdup.

Cluster time fraction reflects cluster volume fraction and it varies from 2% to 50% (25 times difference), depending on cluster definition. “Median” corresponds to highest cluster time fraction, followed by “Wavelet cluster scale”, “Mean”, “Mean+standard deviation”, “Mean+2standard deviation” and “Mean+3standard deviation”. Extracted cluster time fraction has a positive relation with extracted cluster length and a negative relation with extracted cluster solids holdup.

Cluster frequency, depending on cluster definition, varies from 75 to 680 (9 times difference). “Median” corresponds to highest cluster frequency, followed by “Wavelet cluster scale”, “Mean”, “Mean+standard deviation”, “Mean+2standard deviation” and “Mean+3standard deviation”. Extracted cluster frequency has a positive relation with extracted cluster length and cluster time fraction, but a negative relation with extracted cluster solids holdup.

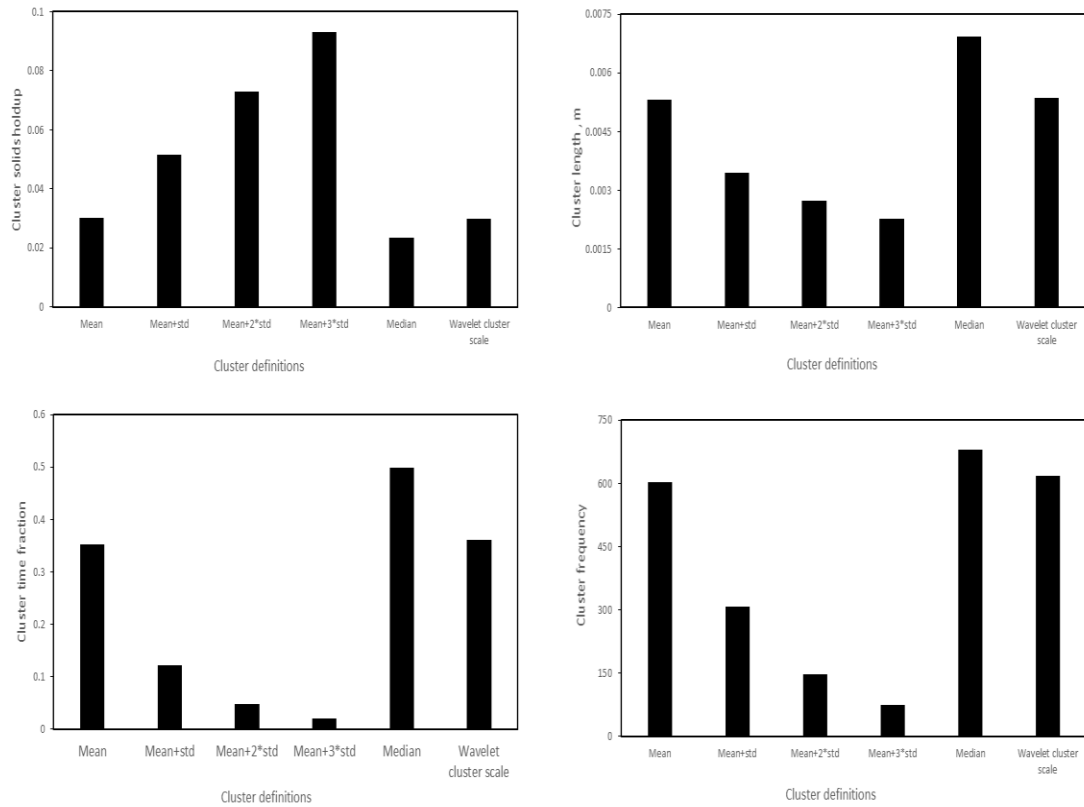


Figure 2-5 Clusters properties versus cluster definitions (100kHz)

In the literature, sampling frequency for optical fiber probe varies from 100Hz to 300kHz (Li et al., 1995; Rudnick and Werther, 1998; Manyele et al., 2002; Lu et al., 2005; Guenther and Breault, 2007; Yang and Leu, 2009; Afsahi et al., 2009; Xu and Zhu, 2011a; Xu and Zhu, 2011b; Chew et al., 2011; Chew et al., 2012a; Chew et al., 2012b; Kiani et al., 2013; Firuzian et al., 2014;). To guarantee the above understanding is generic, the sample signal was de-sampled from 100kHz to 98Hz using wavelet transform, then different cluster definitions were applied on the de-sampled signal. Extracted cluster properties were shown in Figure 2-6.

After de-sampling, the variations of cluster solids holdup, cluster length, cluster time fraction and cluster frequency are from 0.03 to 0.07 (lower difference), from 0.037 m to 0.145 m (higher difference), from 1% to 50% (higher difference), from 1.8 to 20.7 (higher difference), depending on the selection of cluster definitions. Before and after de-sampling,

cluster solids holdup and cluster time fraction have a similar magnitude, while cluster length and cluster frequency decrease more than an order of magnitude. However, the relative magnitude of cluster properties remains the same.

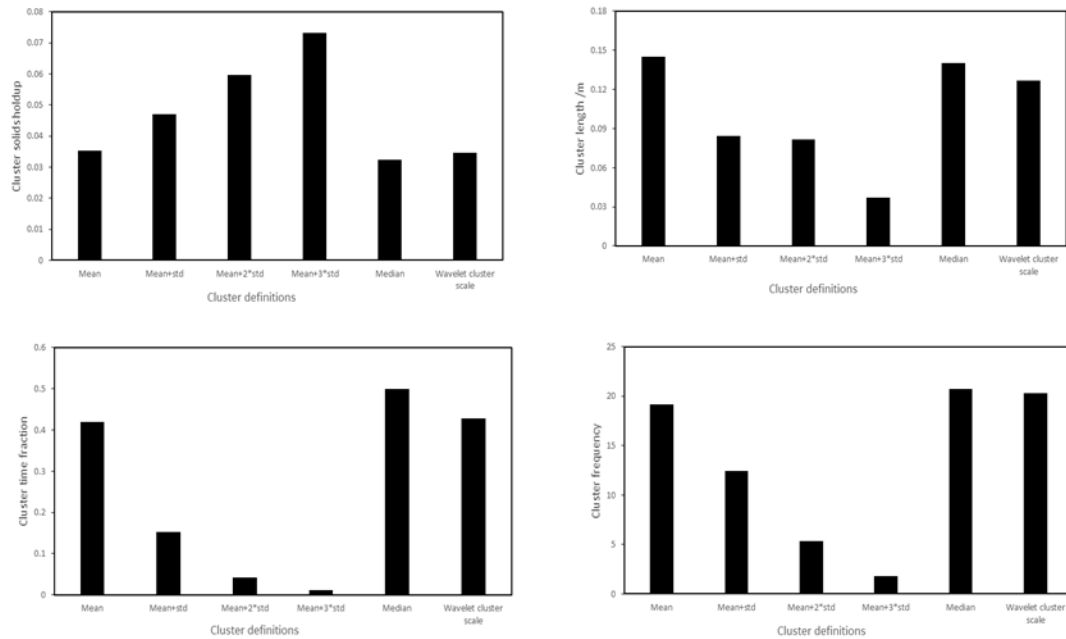


Figure 2-6 Clusters properties versus cluster definitions (100Hz)

Moreover, optical fiber signals at different positions, under different conditions, in different columns have been analyzed and the conclusions drawn are similar to this one. The cluster properties (cluster solids holdup, cluster size, cluster frequency and cluster time fraction) extracted are significantly dependent on the choice of the cluster definition and sampling frequency also has an evident influence on cluster length and cluster frequency.

2.6.2 Details of signal and thresholds

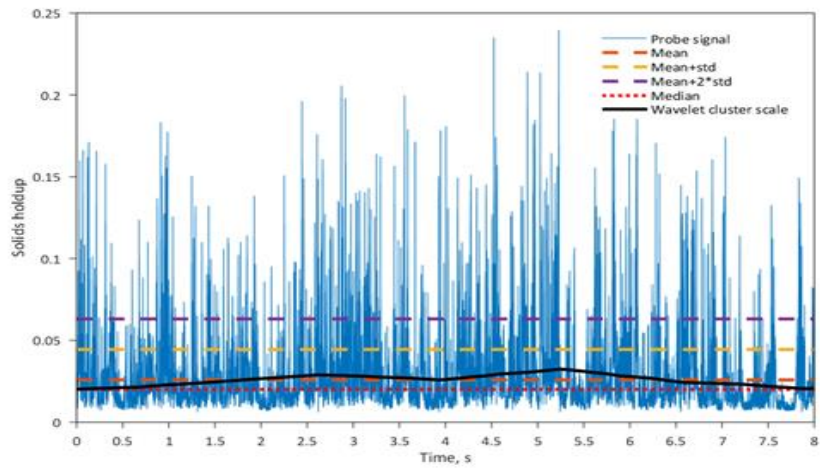
To analyze the rationality of these cluster definitions, the foresaid sample signal and various cluster thresholds corresponding to “Mean+3standard deviation”, “Mean+2standard deviation”, “Mean+standard deviation”, “Mean”, “Median” and “Wavelet cluster scale” are plotted in Figure 2-7. The sub-Figures have different time scales so that the whole-picture and the local details are both visualized.

“Mean+3*standard deviation” has the highest solids holdup threshold, followed by the “Mean+2*standard deviation”, “Mean+standard deviation”, “Mean” and “Median”. Referring to Figure 2-5 and Figure 2-6, higher threshold results in higher cluster solids holdup, lower cluster length, lower cluster time fraction and lower frequency. “Wavelet cluster scale” has a fluctuating threshold and its magnitude is close to “Median”, which is consistent with Yang and Leu, (2009).

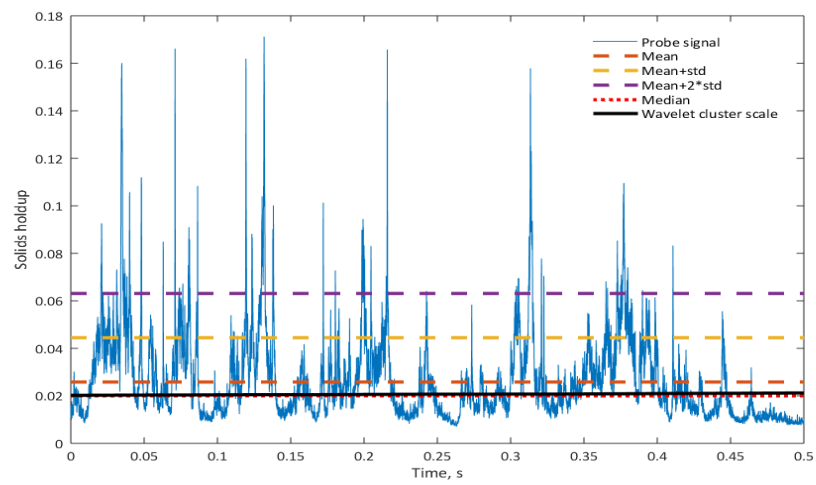
The foresaid sample signal is not a straight baseline with scattered peaks as commonly believed, but a hybrid of underneath crescents and troughs with narrow peaks (see Figure 2-7). The underneath crescents have a time scale around one order of magnitude larger than the narrow peaks. This pattern can also be found in signals presented by Yang and Leu (2009) and Guenther and Breault (2007). For this sample signal, “Mean+3*standard deviation”, “Mean+2*standard deviation” and “Mean+standard deviation” only characterize narrow peaks on the crescents. “Mean”, “Median” and “Wavelet cluster scale”, characterize both crescents and peaks in the troughs. In other words, “Mean+3*standard deviation”, “Mean+2*standard deviation” and “Mean+standard deviation” considers peaks on crescents as clusters, while “Mean”, “Median” and “Wavelet cluster scale” believes crescents and peaks in trough correspond to clusters.

As sampling frequency is also a key parameter for the cluster, signals before and after de-sampling signal are plotted in Figure 2-8. Low sampling frequency signal erases narrow peaks from the original signal and only captures underneath crescents. At low sampling frequency, clusters are considered to be only crescents.

Collectively, the coexistence of crescents and peaks explains the relative magnitude of cluster properties calculated using different definitions. But to know which cluster definition is more reasonable, peaks and crescents need to be interpreted physically.



(a)



(b)

Figure 2-7 Probe signal and thresholds originated from cluster definitions (a: whole picture, b: local details)

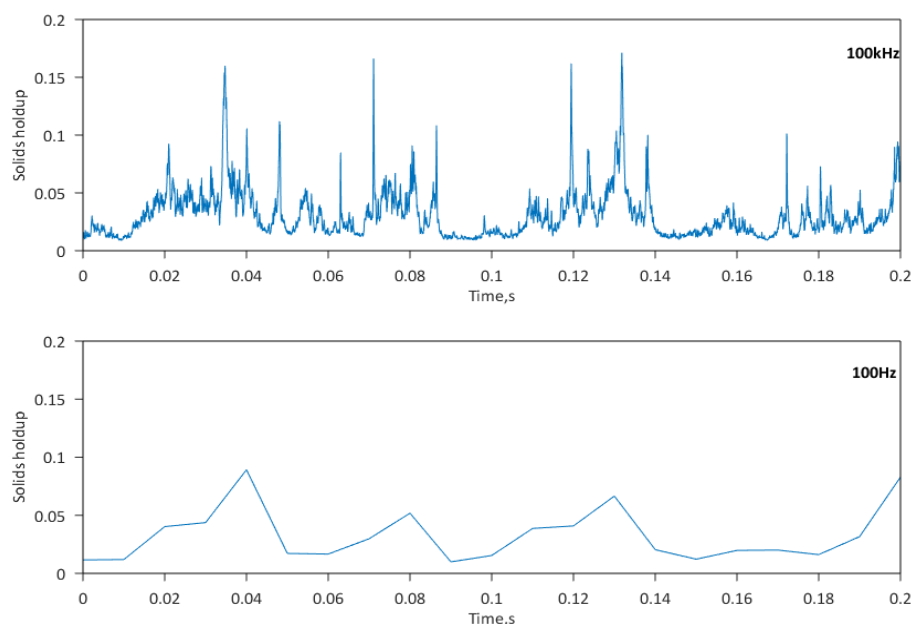


Figure 2-8 Probe signals acquired using different sampling frequencies

2.7 Conclusions

It has been almost 70 years after the first observation of particle aggregation (Wilhelm and Kwauk, 1948). Clusters have been visualized using the high-speed camera and detected using needle-type probes. Various cluster definitions have been proposed to extract cluster information from both experimental and modeling data. However, Cahyadi et al. (2017) well summarized reported cluster properties and found that cluster size and cluster frequency have a discrepancy in an order of magnitude. Moreover, cluster time fraction is reported around 0.06 (Xu and Zhu, 2011a), around 0.10 (Manyele et al., 2002) or around 0.5 (Guenther and Breault, 2007; Afsahi et al., 2009; Firuzian et al., 2014; Chew et al., 2011; 2012a; 2012b;) and the difference is also almost one order of magnitude. The discrepancy on cluster properties severely hinders the development of fluidization theory and numerical models.

To settle this dispute, preliminary analysis has been conducted by applying widely-adopted cluster definitions to the same experimental data. The selection of cluster definitions is found to cause cluster properties to vary significantly, as existing cluster definitions

characterize different characteristics in the CFB. Finally, it is imperative (1) to further investigate the instantaneous flow structure in the CFB, (2) to figure out the physical meanings of signal characteristics, (3) to propose more appropriate methods for phase discrimination.

References

- Afsahi, F. A., Sotudeh-Gharebagh, R., & Mostoufi, N. (2009). Clusters identification and characterization in a gas–solid fluidized bed by the wavelet analysis. *The Canadian Journal of Chemical Engineering*, 87(3), 375-385.
- Bi, H. T., Zhu, J. X., Jin, Y., & Yu, Z. Q. (1993, October). Forms of particle aggregations in CFB. In *Proceedings of the Sixth Chinese Conference on Fluidization, Wuhan, China* (pp. 162-167).
- Brereton, C. M. H., & Grace, J. R. (1993). Microstructural aspects of the behaviour of circulating fluidized beds. *Chemical Engineering Science*, 48(14), 2565-2572.
- Cahyadi, A., Anantharaman, A., Yang, S., Karri, S. R., Findlay, J. G., Cocco, R. A., & Chew, J. W. (2017). Review of cluster characteristics in circulating fluidized bed (CFB) risers. *Chemical Engineering Science*, 158, 70-95.
- Casleton, D. K., Shadle, L. J., & Ross, A. A. (2010). Measuring the voidage of a CFB through image analysis. *Powder Technology*, 203(1), 12-22.
- Chew, J. W., Hays, R., Findlay, J. G., Knowlton, T. M., Karri, S. R., Cocco, R. A., & Hrenya, C. M. (2012a). Cluster characteristics of Geldart Group B particles in a pilot-scale CFB riser. I. Monodisperse systems. *Chemical engineering science*, 68(1), 72-81.
- Chew, J. W., Hays, R., Findlay, J. G., Knowlton, T. M., Karri, S. R., Cocco, R. A., & Hrenya, C. M. (2012b). Cluster characteristics of Geldart group B particles in a pilot-scale CFB riser. II. Polydisperse systems. *Chemical engineering science*, 68(1), 82-93.
- Chew, J. W., Parker, D. M., Cocco, R. A., & Hrenya, C. M. (2011). Cluster characteristics of continuous size distributions and binary mixtures of Group B particles in dilute riser flow. *Chemical engineering journal*, 178, 348-358.
- Firuzian, N., Sotudeh-Gharebagh, R., & Mostoufi, N. (2014). Experimental investigation of cluster properties in dense gas–solid fluidized beds of different diameters. *Particuology*, 16, 69-74.

- Gidaspow, D., Tsuo, Y. P., & Luo, K. M. (1989). Computed and experimental cluster formation and velocity profiles in circulating fluidized beds. *Fluidization VI*, 81-88.
- Gopalan, B., & Shaffer, F. (2012). A new method for decomposition of high speed particle image velocimetry data. *Powder Technology*, 220, 164-171.
- Grace, J. R., & Tuot, J. (1979). A theory for cluster formation in vertically conveyed suspensions of intermediate density. *Trans. Inst. Chem. Eng*, 57(1), 49.
- Guenther, C., & Breault, R. (2007). Wavelet analysis to characterize cluster dynamics in a circulating fluidized bed. *Powder Technology*, 173(3), 163-173.
- Hatano, H., Kido, N., & Takeuchi, H. (1994). Microscope visualization of solid particles in circulating fluidized beds. *Powder Technology*, 78(2), 115-119.
- Horio, M., & Kuroki, H. (1994). Three-dimensional flow visualization of dilutely dispersed solids in bubbling and circulating fluidized beds. *Chemical Engineering Science*, 49(15), 2413-2421.
- Johnsson, F., Zhang, W., Johnsson, H., & Leckner, B. (1997). Optical and momentum probe measurements in a CFB furnace. *Circulating fluidized bed technology V*, 652.
- Kiani, A., Sotudeh-Gharebagh, R., & Mostoufi, N. (2013). Cluster size distribution in the freeboard of a gas–solid fluidized bed. *Powder technology*, 246, 1-6.
- Kuroki, H., & Horio, M. (1994). The flow structure of a three-dimensional circulating fluidized bed observed by the laser sheet technique. In *Proceedings of the 4th international Conference on Circulating Fluidized Beds (edited by Avidan AA), Hidden Valley, USA (Vol. 77)*.
- Lackermeier, U., Rudnick, C., Werther, J., Bredebusch, A., & Burkhardt, H. (2001). Visualization of flow structures inside a circulating fluidized bed by means of laser sheet and image processing. *Powder Technology*, 114(1), 71-83.

- Li, H., Xia, Y., Tung, Y., & Kwauk, M. (1991). Micro-visualization of clusters in a fast fluidized bed. *Powder Technology*, 66(3), 231-235.
- Li, H., Zhu, Q., Liu, H., & Zhou, Y. (1995). The cluster size distribution and motion behavior in a fast fluidized bed. *Powder Technology*, 84(3), 241-246.
- Li, J., Zhang, X. P., Zhu, J., & Li, J. H. (1998). Effects of cluster behavior on gas-solid mass transfer in circulating fluidized beds.
- Li, H. (2004). Multi-scale aggregation of particles in gas-solids fluidized beds. *China Particuology*, 2(3), 101-106.
- Lim, K. S., Zhou, J., Finley, C., Grace, J. R., Lim, C. J., & Brereton, C. M. H. (1996, May). Cluster descending velocity at the wall of circulating fluidized bed risers. In *5th International Conference on Circulating Fluidized Beds*, 218-223.
- Lu, X., Li, S., Du, L., Yao, J., Lin, W., & Li, H. (2005). Flow structures in the downer circulating fluidized bed. *Chemical Engineering Journal*, 112(1), 23-31.
- Manyele, S. V., Pärssinen, J. H., & Zhu, J. X. (2002). Characterizing particle aggregates in a high-density and high-flux CFB riser. *Chemical Engineering Journal*, 88(1), 151-161.
- Matsuda, S., Hatano, H., Takeuchi, H., Pyatenko, A. T., & Tsuchiya, K. (1996). Motion of individual solid particles in a circulating fluidized bed riser. In *Circulating Fluidized Bed Technology V* (pp. 176-181). Science Press Beijing.
- McMillan, J., Shaffer, F., Gopalan, B., Chew, J. W., Hrenya, C., Hays, R., ... & Cocco, R. (2013). Particle cluster dynamics during fluidization. *Chemical Engineering Science*, 100, 39-51.
- Mondal, D. N., Kallio, S., & Saxén, H. (2015). Length scales of solid clusters in a two-dimensional circulating fluidized bed of Geldart B particles. *Powder Technology*, 269, 207-218.

Noymer, P. D., & Glicksman, L. R. (1998). Cluster motion and particle-convective heat transfer at the wall of a circulating fluidized bed. *International Journal of Heat and Mass Transfer*, 41(1), 147-158.

Noymer, P. D., & Glicksman, L. R. (1998). Cluster motion and particle-convective heat transfer at the wall of a circulating fluidized bed. *International Journal of Heat and Mass Transfer*, 41(1), 147-158.

Otsu, N. (1975). A threshold selection method from gray-level histograms. *Automatica*, 11(285-296), 23-27.

Ren, J., Mao, Q., Li, J., & Lin, W. (2001). Wavelet analysis of dynamic behavior in fluidized beds. *Chemical Engineering Science*, 56(3), 981-988.

Rhodes, M., Mineo, H., & Hirama, T. (1992). Particle motion at the wall of a circulating fluidized bed. *Powder Technology*, 70(3), 207-214.

Rudnick, C., & Werther, J. (1998). The discrimination of cluster characteristics from fiberoptical probe signals in circulating fluidized beds. *Fluidization IX, Engineering Foundation*, 573-580.

Shaffer, F., Gopalan, B., Breault, R. W., Cocco, R., Karri, S. R., Hays, R., & Knowlton, T. (2013). High speed imaging of particle flow fields in CFB risers. *Powder technology*, 242, 86-99.

Sharma, A. K., Tuzla, K., Matsen, J., & Chen, J. C. (2000). Parametric effects of particle size and gas velocity on cluster characteristics in fast fluidized beds. *Powder Technology*, 111(1), 114-122.

Shi, H., Wang, Q., Xu, L., Luo, Z., & Cen, K. (2008). Visualization of clusters in a circulating fluidized bed by means of particle-imaging velocimetry (PIV) technique. In *Proceedings of the 9th International Conference on Circulating Fluidized Beds, Hamburg, Germany* (pp. 1013-1019).

Soong, C. H., Tuzla, K., & Chen, J. C. (1994). Identification of particle clusters in circulating fluidized bed. *Circulating fluidized bed technology*, 4, 615-620.

Takeuchi, H., & HIRAMA, T. (1991). Flow visualization in the riser of a circulating fluidized bed. *Circulating Fluidized Bed Technology III*, 177-182.

Takeuchi, H., Pyatenko, A. T., & Tatano, H. (1996). Flowing behavior of particles in the riser of a circulating fluidized bed. In *Circulating Fluidized Bed Technology V* (pp. 164-169). Science Press Beijing.

Tuzla, K., Sharma, A. K., Chen, J. C., Schiewe, T., Wirth, K. E., & Molerus, O. (1998). Transient dynamics of solid concentration in downer fluidized bed. *Powder Technology*, 100(2-3), 166-172.

Van den Moortel, T., & Tadriss, L. (1996). Experimental analysis of the two-phase flow structures in a circulating fluidized bed by image processing. In *Proceedings of the 5th International Conference on Circulating Fluidized Beds* (pp. 230-235). Science Press: Beijing, China.

Van den Moortel, T., Santini, R., Tadriss, L., & Pantaloni, J. (1998). Experimental analysis of the gas-particles flow structure in the dilute zone of a circulating fluidized bed by image processing. *Fluidisation IX*, 157-162.

Wang, C. (2013). *High density gas-solids circulating fluidized bed riser and downer reactors* (Doctoral dissertation, The University of Western Ontario).

Wei, F., Jin, Y., & Yu, Z. (1994). The visualization of macro structure of the gas-solids suspension in high density CFB. *Circulating Fluidized Bed Technology IV. AIChE, New York*, 588-593.

Wei, F., Yang, G. Q., Jin, Y., & Yu, Z. Q. (1995). The characteristics of cluster in a high density circulating fluidized bed. *The Canadian Journal of Chemical Engineering*, 73(5), 650-655.

Wu, R. L., Lim, C. J., Grace, J. R., & Brereton, C. M. H. (1991). Instantaneous local heat transfer and hydrodynamics in a circulating fluidized bed. *International journal of heat and mass transfer*, 34(8), 2019-2027.

Xu, J., & Zhu, J. (2011b). A new method for the determination of cluster velocity and size in a circulating fluidized bed. *Industrial & Engineering Chemistry Research*, 51(4), 2143-2151.

Xu, J., & Zhu, J. X. (2010). Experimental study on solids concentration distribution in a two-dimensional circulating fluidized bed. *Chemical Engineering Science*, 65(20), 5447-5454.

Xu, J., & Zhu, J. X. (2011a). Visualization of particle aggregation and effects of particle properties on cluster characteristics in a CFB riser. *Chemical engineering journal*, 168(1), 376-389.

Yang, J., & Zhu, J. (2014a). A novel method based on image processing to visualize clusters in a rectangular circulating fluidized bed riser. *Powder Technology*, 254, 407-415.

Yang, J., & Zhu, J. (2014b). An alternative method for mapping solids holdup in a narrow rectangular CFB riser through image calibration. *The Canadian Journal of Chemical Engineering*, 92(12), 2202-2210.

Yang, J., & Zhu, J. (2015a). Visualization of solids phase separation in a rectangular CFB riser using a novel image calibration method. *Powder Technology*, 273, 76-82.

Yang, J., & Zhu, J. (2015b). Cluster identification using image processing. *Particuology*, 23, 16-24.

Yang, J., & Zhu, J. (2015c). An Alternative Method to Quantify Solids Phase Separation in a Narrow Rectangular CFB Riser. *Procedia Engineering*, 102, 1064-1072.

Yang, T. Y., & Leu, L. P. (2009). Multiresolution analysis on identification and dynamics of clusters in a circulating fluidized bed. *AIChE journal*, 55(3), 612-629.

Yang, Y. L., Jin, Y., Yu, Z. Q., & Wang, Z. W. (1992). Investigation on slip velocity distributions in the riser of dilute circulating fluidized bed. *Powder technology*, 73(1), 67-73.

Zhang, H., Johnston, P. M., Zhu, J. X., De Lasa, H. I., & Bergougnou, M. A. (1998). A novel calibration procedure for a fiber optic solids concentration probe. *Powder Technology*, 100(2-3), 260-272.

Zou, B., Li, H., Xia, Y., & Ma, X. (1994). Cluster structure in a circulating fluidized bed. *Powder technology*, 78(2), 173-178.

Chapter 3

Experimental Apparatuses and Measurement Methods

3.1 Circulating fluidized beds

Two sets of circulating fluidized bed were used in the experiments. One set is a rectangular circulating fluidized bed made of transparent plexiglass. The other set is a cylindrical circulating fluidized bed mainly made of aluminum.

3.1.1 Rectangular circulating fluidized bed

Due to the existence of core-annulus structure in CFB, the solids holdup at column wall is much higher than that in riser center(Wang, 2013). In this work, a two-dimensional transparent circulating fluidized bed is used to visualize the flow structure across the column. It consists of a riser (7.6m in height, 19 mm in thickness, 114 mm in width), cyclones at riser top, a bag filter after cyclones, a downcomer and an inclined pipe conveying particles from downcomer to riser (see Figure 3-1). The downcomer has two sections: a cylindrical part (203 mm i.d.) to measure solids circulation rate and a rectangular part (203 mm in width and 38 mm in thickness) to store particles.

During operating, high-velocity gas is introduced from riser bottom through a distributor. In the riser, particles from the inclined pipe are transported upward by gas. At riser top, gas and solids mixture enter cyclones and bag filter with gas released to atmosphere and particles recovered to downcomer. In downcomer, particles flow downward to riser bottom through the inclined pipe. On the inclined pipe, a flip valve installed to control of solids circulation rate. Wider openness corresponds to lower resistance and results to higher solids circulation rate. To ensure the flowability of particles, aeration air is introduced to the inclined pipe. As the rectangular CFB riser is considered as a slice of cylindrical riser, radial positions and axial positions are employed to denote the lateral and vertical positions in the rectangular CFB.

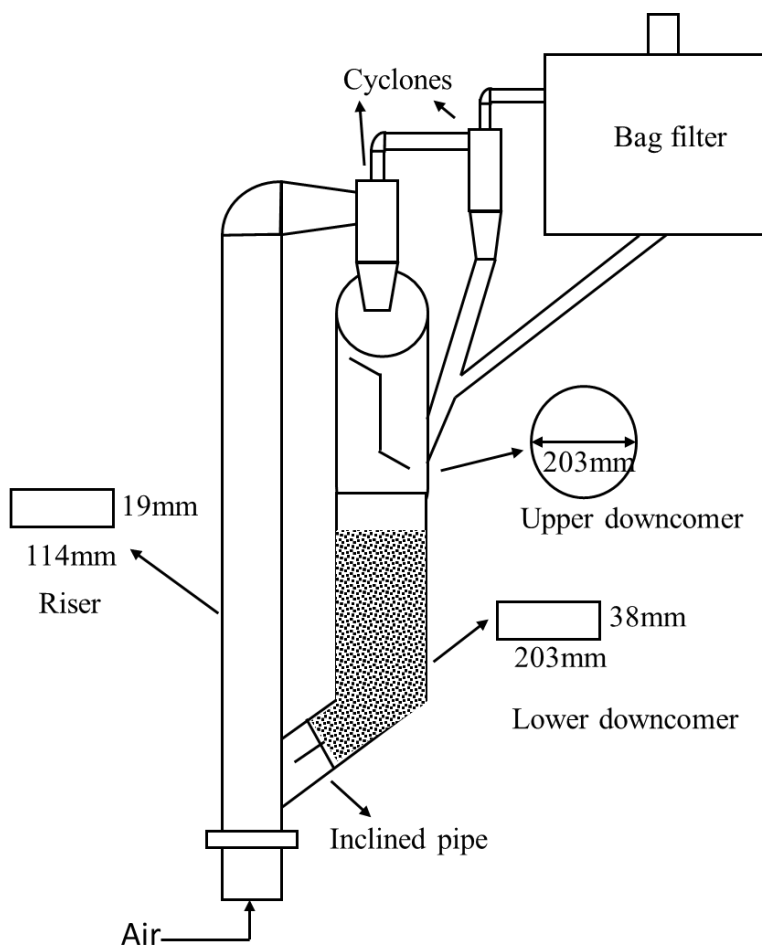


Figure 3-1 Schematic diagram of the rectangular circulating fluidized bed

3.1.2 Cylindrical circulating fluidized beds

The cylindrical circulating fluidized bed is a multifunctional system which can be operated in “Riser mode” and “Downer mode”. It consists of a riser (76 mm i.d. and 10 m in height), cyclones at riser top, a bag filter after cyclones, two downers (76 mm i.d. and 5.8 in height; 50 mm i.d. and 4.9 m in height), a downcomer (203 mm i.d.), a storage tank (457 mm i.d.) and an inclined pipe connecting the storage tank to the riser bottom (see Figure 3-2). The total solids inventory of FCC particles in the downcomer and storage tank could be up to 450 kg and approximately 6.0 m level of particles, providing enough back pressure to achieve high density operations. To ensure the flowability of particles during the solids circulation, fluidization in the inclined pipe and the storage tank is achieved by injecting aerate air during operation.

When operated in “Riser mode”, downers are sealed by adjusting the diverter valve below primary cyclone. High velocity gas is introduced from riser bottom through distributor. Solids are introduced to riser through an inclined pipe. In the riser, solids mix with gas thoroughly and are blown upward. Then, gas-solid mixture enters cyclones with gas released after bag filter and particles collected. The recovered particles enter storage tank via downcomer and go to riser for another cycle.

When operated in “Downer mode”, downcomer is sealed by adjusting the diverter valve below primary cyclone. The choice of downers is controlled by the diverter valve at the top of two downers. For each operation, one downer is sealed from top and the other one is open. Solids are lifted by high velocity gas in the riser and recovered by primary cyclone. Then the collected solids enter downer top where a distributor is installed (see Figure 3-3). This distributor consists of a chamber where particles are fluidized in minimum fluidization state, eight brass tubes (25mm i.d.) at the chamber bottom for solids feeding, a feeding funnel where particles get pre-accelerated by gravity and gas inlets which have 112 holes (6.3 mm diameter) evenly distributed around the circumference of the column. At the downer entrance, high velocity gas jets ensure a thorough mixing of gas and solids. In the downer, gas and particles flow concurrently downward. At the downer bottom, most particles are recovered to storage tank. Particles, transported to exhaust pipe by gas, are further separated by cyclones and bag filter and returned to downcomer.

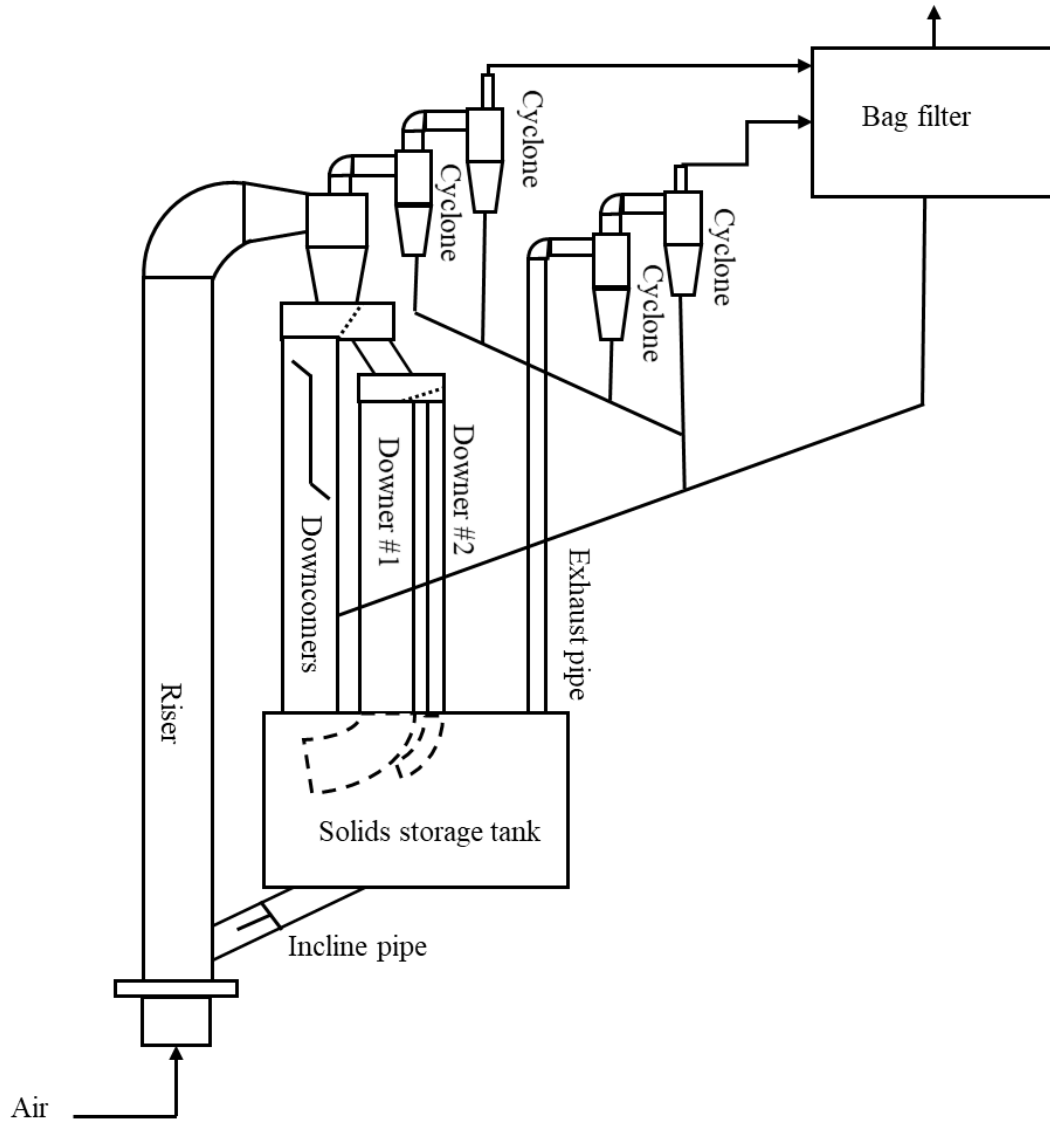


Figure 3-2 Schematic diagram of cylindrical circulating fluidized bed

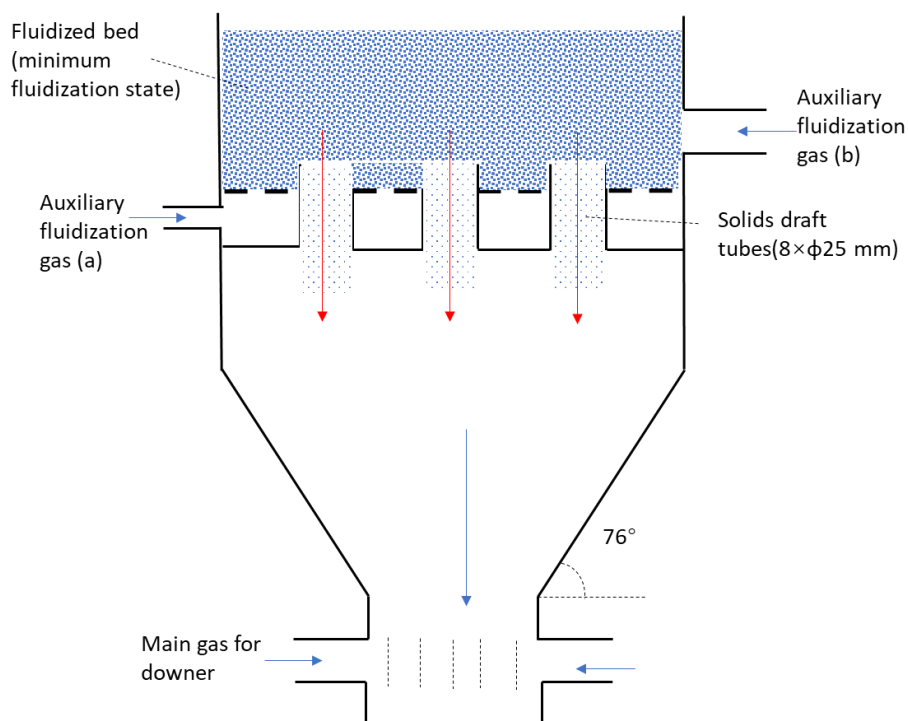


Figure 3-3 Schematic diagram of the distributor at downer top

3.2 Particle properties

Three types of particle were used in the experiments, namely FCC#1, FCC#2 and glass beads. Generally, FCC is group A powders while glass beads are group B powders.

Detailed particle properties, including particle diameter, particle density, sphericity and terminal velocity, are shown in table 3-1 (Xu and Zhu, 2011; Wang, 2013;). FCC#1 and glass beads served as fluidization medium in the “rectangular circulating fluidized bed”. FCC #2 was employed in the “cylindrical circulating fluidized bed”.

Table 3-1 Information of particle properties

Particles	FCC #1	FCC #2	Glass beads
Particle Sauter mean diameter (μm)	76	67	288
Particle density (kg/m^3)	1780	1877	2498
Bulk density (kg/m^3)	890	1125	1475
Sphericity (–)		0.95	~1
Particle terminal velocity (m/s)		0.26	3.73

3.3 Measurement of superficial gas velocity and solids circulation rate

Superficial gas velocity is controlled using a rotameter. Scales on the rotameter is gas flow rate in standard conditions ($P_c=101$ kPa, $T_c=293.15$ K). To measure gas flow rate in CFBs, a correction has been made with the pressure and temperature in columns (Equation 3-1).

$$Q_{\text{actual}} = Q_{\text{reading}} \sqrt{\frac{P_c T_a}{P_a T_c}} \quad \text{Equation 3-1}$$

Q_{actual} is actual gas flow rate, [m^3/s];

Q_{reading} is gas flow rate on rotameter, [m^3/s];

P_c actual pressure, [Pa];

T_a is actual temperature, [K];

The measurement of solids circulation rate is conducted in the upper part of the downcomer. A vertical plater is mounted in the column center, dividing it half and half. At the plate top and bottom installed the flapper valves. Closing the bottom valve to one side and open the top valve to the other side, the particles passing through this downcomer will accumulate on half column. With a scale attached along the column, the height of particles accumulated is measured in a certain time interval. Knowing particle density and column dimensions, solids circulation rate can be calculated using equation 3-2.

$$G_s = \frac{\Delta V \cdot \rho_p}{A \cdot \Delta t} \quad \text{Equation 3-2}$$

G_s is solids circulating rate, [$\text{kg}/\text{m}^2\text{s}$];

ΔV is the volume of particles accumulated during the measurement, [m^3];

A is the cross-section area of riser, [m^2];

ρ_p is particle bulk density, [kg/m³];

Δt is measurement time, [s];

3.4 Visualization system

A visualization system was established by coupling high-speed camera with rectangular transparent CFB riser (Yang and Zhu, 2014a; Yang and Zhu, 2014b;). A lamp is placed facing the riser and a high-speed camera is placed on the other side (see Figure 3-4). To eliminate the disturbance from other lightings, high-speed camera and the section of the videoed column were covered by a black box. The high-speed video camera employed is MotionScope M2 from Redlake. Its frame rate and resolution can be as high as 16,000 fps and 1280 × 1024 pixels, respectively. However, if the frame rate is higher than 500 fps, resolution reduces. The CMOS camera sensor contains self-calibrating circuitry and IR cut-off optical filter, which guarantees the image quality. The equipped lens is a Pentax C21228TH 12.5 mm F1.8 manual lens. Through a standard Firewire (IEEE-1394), the high-speed camera is connected to a computer. Software installed on a computer, Motionscope 2.0.3, allows the shooting video to be monitored and stored. The lamp employed has a 500 W quartz halogen bulb with irradiation of strong lights about 95,000 lx. A diffusion panel was placed between lamp and CFB riser to make the recorded area uniformly illuminated and to prevent overheating of the plexiglass of the CFB riser. This visualization system could capture the flow details two-dimensionally, but it is only applicable to low-density conditions in two-dimensional/rectangular CFB (Yang and Zhu, 2014a).

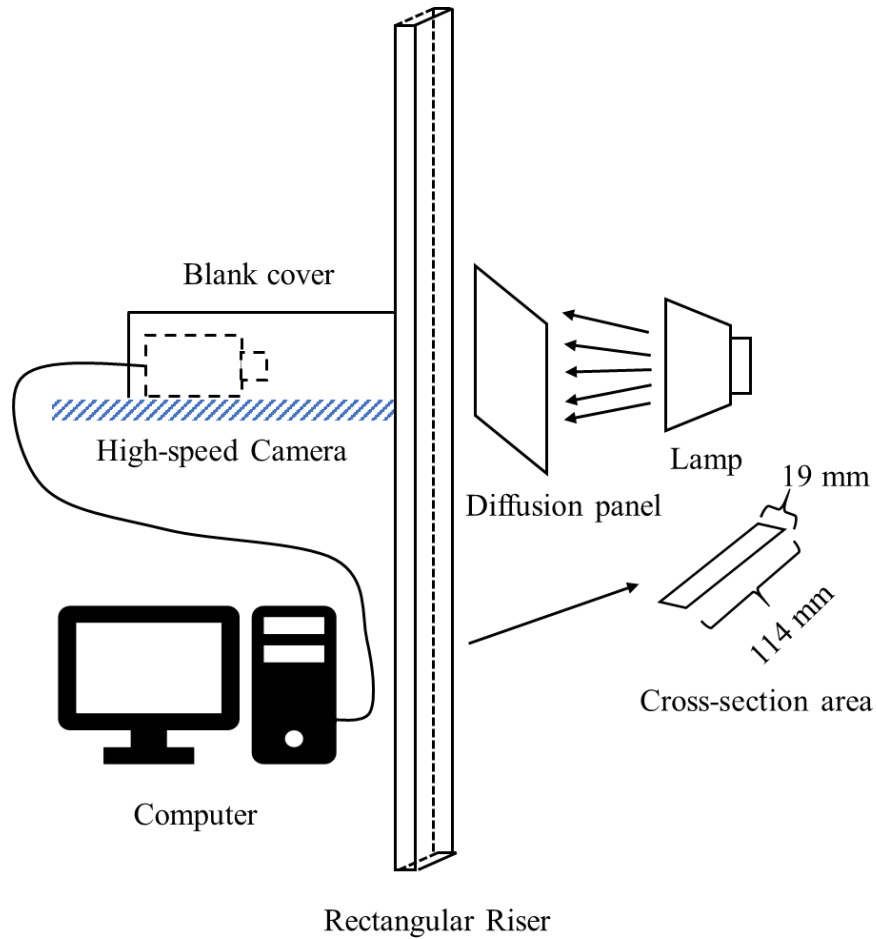


Figure 3-4 Schematic diagram of the visualization system

An image example recorded using this visualization system is shown in figure 3-5. The image recorded via the high-speed camera is a matrix of pixels consisting of 568 columns and 256 rows. Each pixel had a grayscale, ranging from 0 (darkest) to 255 (brightest). As the light penetrates the riser and finally receive by the camera sensor, a dense suspension results in low light intensity for pixels, while the dilute suspension results in high light intensity for pixels. Thus, white area and dark area in the images correspond to the dilute region and dense region, respectively.

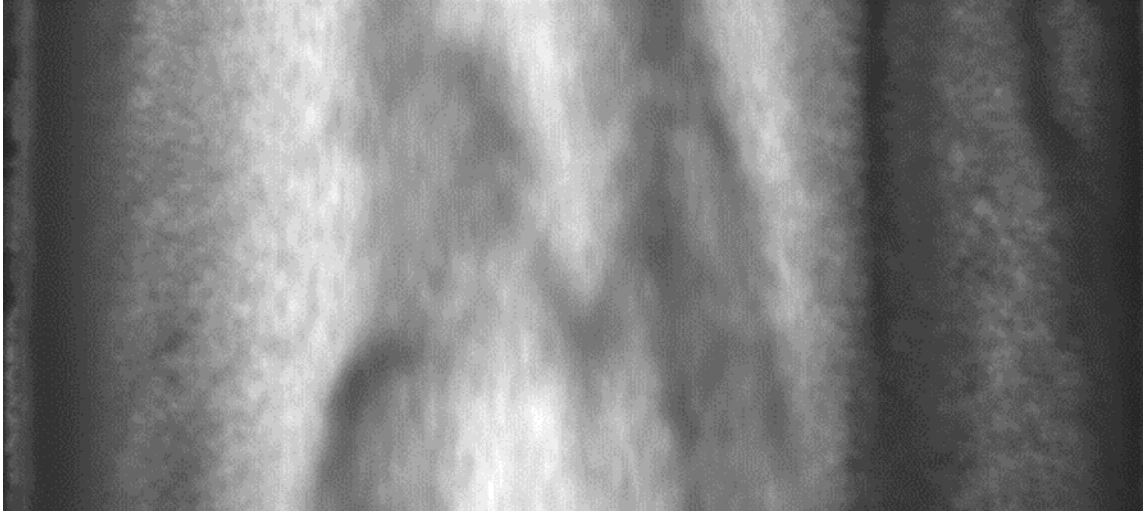


Figure 3-5 An image captured using the high-speed camera

3.4.1 Measurement of solids holdup

To quantitatively analyze local solids holdup, a calibration between grayscale and solids holdup had been developed (see Figure 3-6). Yang and Zhu (2014a) fluidized FCC using water and created a uniform distribution of solids. Mean solids holdup can be obtained according to pressure drop and mean grayscale is obtained from the images acquired using the high-speed camera. Then, grayscale has been correlated with solids holdup. As light transmittance of air and water is similar, this correlation was applied to gas-solid fluidization system. Moreover, Yang and Zhu (2014b) further validated this using an optical fiber probe.

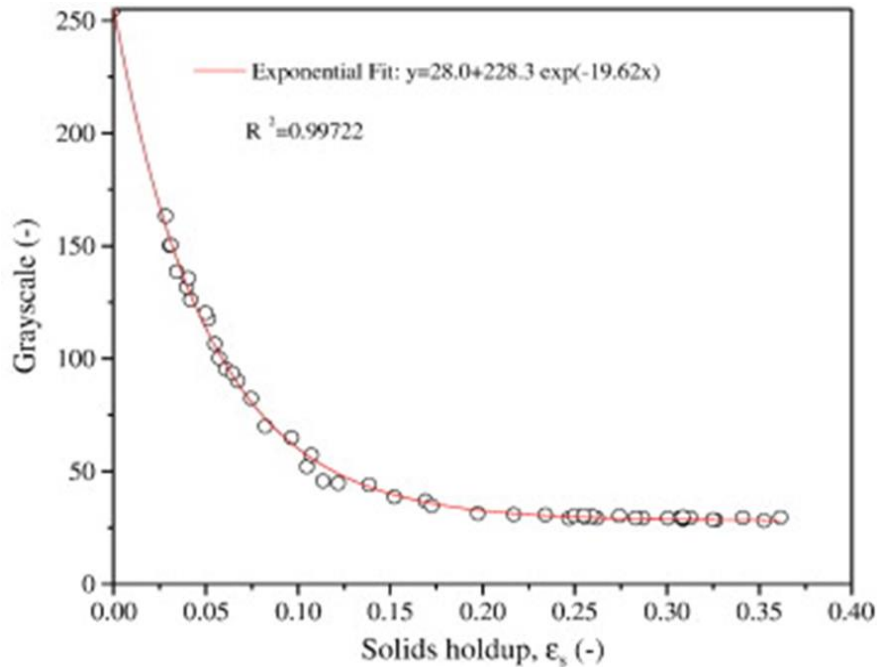


Figure 3-6 Correlation between solids holdup and grayscale

3.4.2 Measurement of particle velocity and solids flux

The image sequence was read into MATLAB and a 2-D average kernel (3 pixel \times 3 pixel) is first applied to remove noise. Then, an image block, 11.4mm in height and 5.7mm in width, is picked up from the image and its information, including pixel-wise grayscale and coordinate (x_1, y_1) , is stored. After that, the picked image block is used as a reference to search its location in the following images. The searching scope is around the coordinate (x_1, y_1) , but in a large region (25 pixels more to the left and right, 50 pixels more upward, 40 pixels more downward) (see Figure 3-7). The maximum velocity that can be determined with this searching scope is 4.75 m/s horizontally, 19 m/s upward and 3.8 m/s downward. The similarity of the image block and target-area is evaluated using two-dimensional cross-correlation (Lewis, 1995; Shapiro and Haralick, 1992;).

Correlation coefficient ranges from -1 to +1. The closer the correlation coefficient to +1, the more similarity the two signals share. Two signals are believed to have a good similarity if their correlation coefficient is above 0.6 (Wang, 2013). If only one most similar target-area is found in the searching scope and its correlation coefficient is higher than 0.6, the searching is effective and the coordinate (x_2, y_2) of target-area is stored.

Particle velocity can be calculated based on pixel shift using equation 3-3 and 3-4. Grayscale in that image block are converted to solids holdup based on a varied correlation between grayscale and solids holdup pixel-wisely (Yang and Zhu, 2014a). Then, the solids flux, is calculated by multiplying vertical velocity, with block-average solids holdup, and particle density, (see Equation 3-5). The minimum shift can be detected in the acquired image is $190 \mu\text{m}$ (one pixel) and the time interval is $1/2000 \text{ s}$. As a result, the velocity resolution is 0.38 m/s . To have a better velocity resolution, the target area is searched in the image after the adjacent image in this work. In this case, the minimum velocity resolution is 0.19 m/s . There are two direction components for both particle velocity and solids flux.

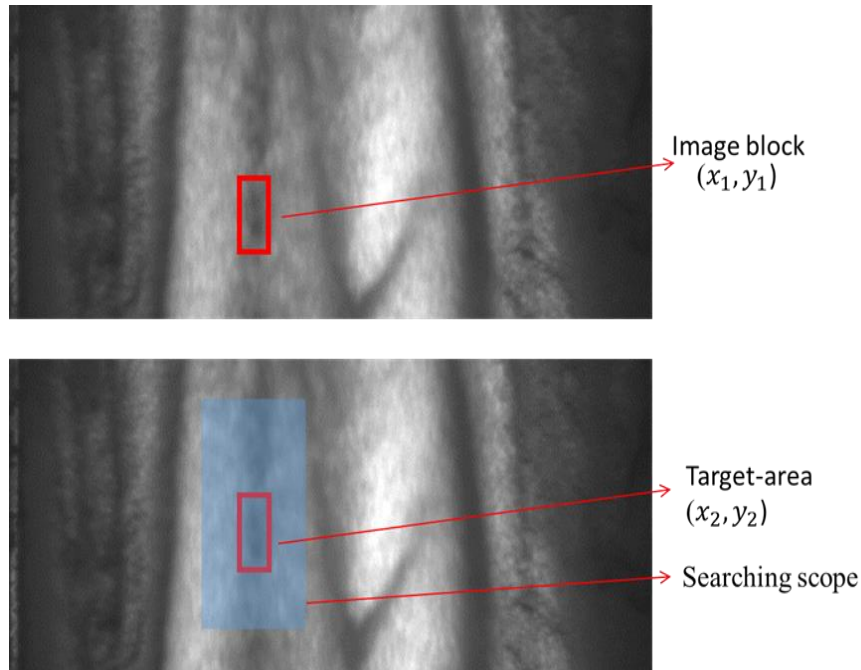


Figure 3-7 Demonstration of the image tracking

$$V_{pv} = \frac{y_1 - y_2}{\Delta t} d \quad \text{Equation 3-3}$$

$$V_{ph} = \frac{x_1 - x_2}{\Delta t} d \quad \text{Equation 3-4}$$

$$\mathbf{F}_s = \mathbf{V}_{pv} \times \epsilon_s \times \rho_p \quad \text{Equation 3-5}$$

(x_1, y_1) is the coordinate of the image block;

(x_2, y_2) is the coordinate of the target area;

d is the actual size of one pixel, [μm];

Δt is the time interval, [s];

V_{pv} is the particle velocity in vertical direction, [m/s];

V_{ph} is the particle velocity in horizontal direction, vertical velocity, [m/s];

F_s is the solids flux, [$\text{kg}/\text{m}^2 \text{ s}$];

ε_s is solids holdup of the image block;

ρ_p is particle density, [kg/m^3];

3.5 Optical fiber probe

In order to measure the flow information in high-density conditions, three optical fiber probes were employed in this thesis. Although the probes have the effective distance between two channels as 1.51 mm, 2.01mm and 2.02mm, respectively, the same measuring principle and setup are the same for all the three probes. Here we introduce one probe in details for concision.

The optical fiber probe is a multi-fiber probe, PV6, manufactured by the Institute of Processing Engineering, Chinese Academy of Sciences, Beijing, China (see Figure 3-8). This probe is 3.8 mm in diameter and has two measuring channels (1 mm \times 1 mm) aligned vertically. Each measuring channel consists of 8000 fibers (15 μm) either receiving or emitting light. Light from emitting fibers strikes particles appearing at the probe tip and reflected to receiving fibers. The intensity of reflected light is then translated to a voltage value. The sampling frequency is set to be 100kHz for all the experiments. Even though the optical fiber probe is applicable to high-density conditions,

it has a risk to influence the gas-solid flow and only captures one-dimensional information (Cocco et al., 2017).

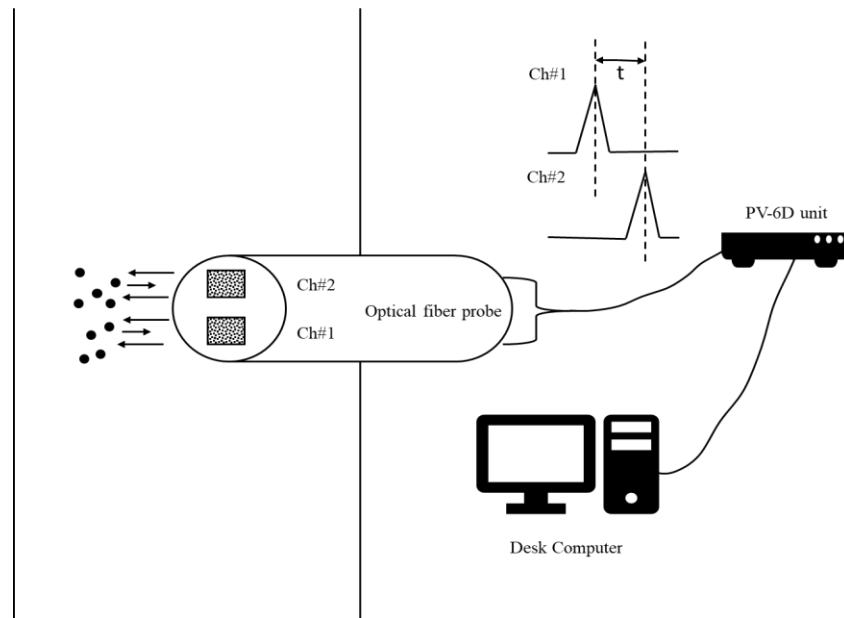


Figure 3-8 Measurement system of optical fiber probe

3.5.1 Measurement of solids holdup

To quantitatively analyze the gas-solid flow, the calibration of optical fiber probe signal with solids holdup was established using the method by Zhang et al. (1998). A calibration system is shown in Figure 3-9 and basically it has three parts: (1) the solids feed control system, (2) the solids concentration measurement system, and (3) the solids collection system. Solids is fluidized in a chamber and flow to a slim column through a vibrating solids feeder. After fully acceleration, solids in the lower part of the slim column is trapped by two sling valves. Trapped particles are collected and weighed by loose the sling of the lower valve. Knowing the particle density, particle volume in the trapped section is determined and solids holdup is calculated. On the other hand, the optical fiber probe is inserted into the trapped region and mean voltage is acquired. To achieve dense suspension, a back-pressure control system is used to slow down the particle velocity increase the solids concentration. The suspension density is adjusted via the valve installed in the vibrating solids feeder and the back-pressure control system. This process

is repeated from very dilute to extremely dense conditions. Based on that, the correlation between voltage and solids holdup is established for three types of particles (see the correlations below). Probe A, probe B and probe C refer to the probes whose effective distance between channels are 1.51 mm, 2.01 mm and 2.02 mm, respectively.

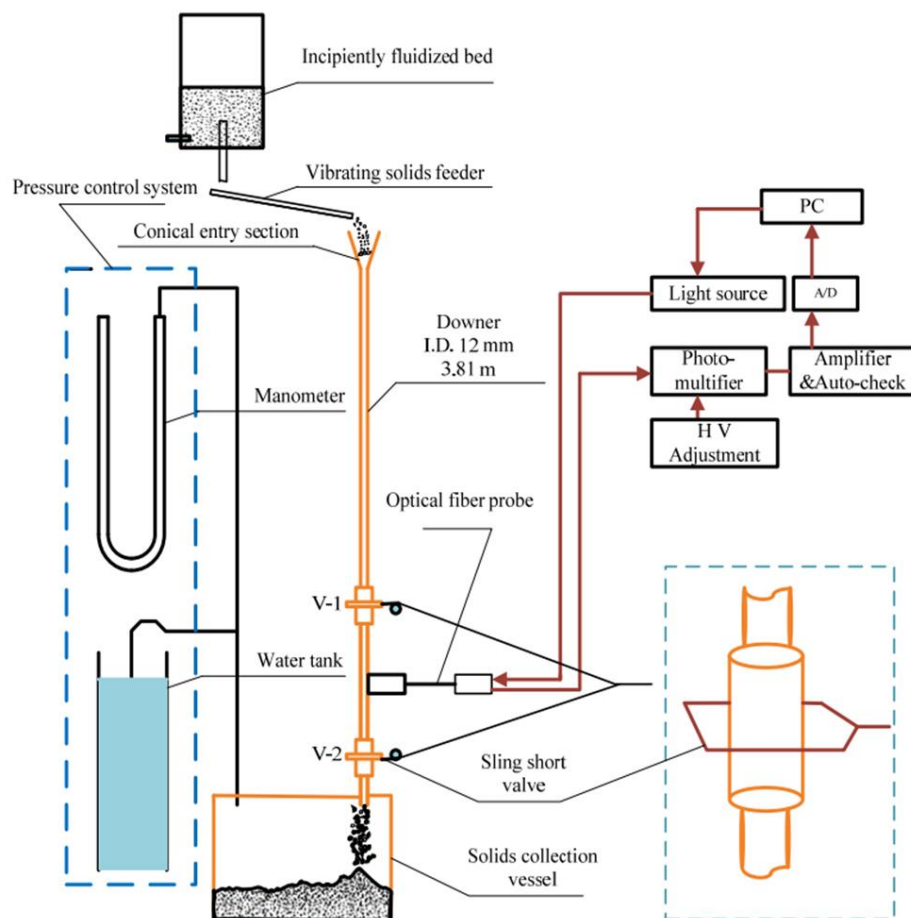


Figure 3-9 Calibration system of the optical fiber probe

For FCC #1:

$$\text{Probe A: } \varepsilon_s = 0.02227 \cdot V^2 - 0.0131 \cdot V + 0.00563 \quad (r/R \leq 0.75)$$

$$\text{Probe A: } \varepsilon_s = 0.02405 \cdot V^2 - 0.01767 \cdot V + 0.00734 \quad (r/R > 0.75)$$

For FCC #2:

$$\text{Probe B: } \varepsilon_s = 0.0297 \cdot V^2 - 0.00002 \cdot V + 0.0061$$

$$\text{Probe C: } \varepsilon_s = 0.0381 \cdot V^2 - 0.0409 \cdot V + 0.0113$$

For Glass Beads:

$$\text{Probe B: } \varepsilon_s = 0.0144 \cdot V^2 + 0.0716 \cdot V - 0.0107$$

$$\text{Probe C: } \varepsilon_s = 0.0140 \cdot V^2 + 0.0762 \cdot V - 0.0119$$

3.5.2 Measurement of particle velocity

As foresaid, there are two measuring channels aligned vertically for one optical fiber probe. Most particles pass channel one and then pass channel two. There is a time lag, between signal fragments on originated from two channels. Knowing the effective distance, between channels, instantaneous velocity is calculated with equation 3-6.

$$V_{pv} = \frac{L_e}{\tau} \quad \text{Equation 3-6}$$

V_{pv} is the particle velocity in the vertical direction;

τ is time lag;

L_e is the effective distance;

However, particle flow in fluidized bed is kind of arbitrary. In other words, some particles passing channel one may not appear on channel two. To deal with that, correlation coefficient is used to filter out those data. The instantaneous velocity is considered to be reliable only if their correlation coefficient is higher than 0.6 (Xu and Zhu, 2010; Wang, 2013).

3.6 Summary

The analysis in chapter 4, 5 and 6 is mainly based on the rectangular circulating fluidized bed and the visualization system. The analysis in chapter 7, 8 and 9 is mainly based on the cylindrical circulating fluidized bed and optical fiber probe.

References

- Lewis, J. P. (1995, May). Fast normalized cross-correlation. In *Vision interface* (Vol. 10, No. 1, pp. 120-123).
- Cocco, R. A., Karri, S. R., Knowlton, T. M., Findlay, J., Gauthier, T., Chew, J. W., & Hrenya, C. M. (2017). Intrusive probes in riser applications. *AIChE Journal*, 63(12), 5361-5374.
- Wang, C. (2013). High density gas-solids circulating fluidized bed riser and downer reactors, Ph.D. Diss. The University of Western Ontario.
- Xu, J., & Zhu, J. X. (2010). Experimental study on solids concentration distribution in a two-dimensional circulating fluidized bed. *Chemical Engineering Science*, 65(20), 5447-5454.
- Xu, J., & Zhu, J. X. (2011). Visualization of particle aggregation and effects of particle properties on cluster characteristics in a CFB riser. *Chemical Engineering Journal*, 168(1), 376-389.
- Yang, J., & Zhu, J. (2014a). A novel method based on image processing to visualize clusters in a rectangular circulating fluidized bed riser. *Powder Technology*, 254, 407-415.
- Yang, J., & Zhu, J. (2014b). An alternative method for mapping solids holdup in a narrow rectangular CFB riser through image calibration. *The Canadian Journal of Chemical Engineering*, 92(12), 2202-2210.
- Zhang, H., Johnston, P. M., Zhu, J. X., De Lasa, H. I., & Bergougnou, M. A. (1998). A novel calibration procedure for a fiber optic solids concentration probe. *Powder Technology*, 100(2-3), 260-272.

CHAPTER 4

Capturing the instantaneous flow structure in gas-solid circulating fluidized bed using high-speed imaging and fiber optic sensing

Abstract

Knowing the instantaneous flow structure in gas-solid circulating fluidized Bed (CFB) is crucial for the understanding of fast fluidization and the development of numerical models, but it is of great complexity due to the rapid movement of particle aggregations. Up to now, numerous studies have been reported on the instantaneous flow structure, but essential information, like phase classification, solids holdup mapping, macro-scale fluctuation and much more, still remains lacking. In this work, a high-speed camera is employed to capture the gas-particle flow behavior in a narrow transparent CFB riser, providing both large measuring window (11.4cm×5cm) and good resolution (190 μ m /pixel). Instantaneous solids holdup mapping across the riser is computed with a verified calibration between solids holdup and grayscale. Based on solids holdup characteristics, gas-solid flow in the CFB riser is classified into distinctive phases. Macroscopically, there are trough phase and crest phase. Within the trough phase, there are trough clusters and dispersed particles. Within the crest phase, there are crest clusters and coalesced particles. The alternating appearance of trough phase and crest phase could cause mean solids holdup across the riser to fluctuate significantly. To verify the above flow structure, instantaneous solids holdup was also measured in a large-scale cylindrical riser using an optical fiber probe. It has been found that solids holdup characteristics and phase scales detected using the optical fiber probe are consistent with those captured using highspeed camera. Collectively, this study deepens the understanding to fast fluidization, prepares for further phase characterization, contributes to the development of numerical modeling.

Keywords: aggregation; cluster, macro-fluctuation; instantaneous flow structure; high-speed camera; optical fiber probe; gas-solid circulating fluidized bed.

4.1 Introduction

Gas-solid circulating fluidized bed (CFB) riser has many industrial applications, including fluidized catalytic cracking (FCC), coal combustion, calcination, coal gasification and so forth (Lim et al., 1995; Wang et al., 2014; Zhu and Cheng, 2005;). Its performance, like mass and heat transfer, productivity, back mixing and so on, essentially relies on the fundamental interaction between gas and particles (Wu et al., 1991; Yang et al., 1992; Johnsson et al., 1997; Noymer and Glicksman, 1998; Shi et al., 2008). In the CFB riser, gas-particle interaction is determined by the instantaneous flow structure. Hence, many attempts have been made to understand the details of the instantaneous flow structure.

Particle clusters have been observed by many researchers, since the 1990s. Li et al. (1991) first recorded particle clusters systematically using a camera. Zou et al., (1994) proposed cluster roundness factor to characterize the cluster shape. Takeuchi et al. (1996) counted the number of clusters in different forms and analyzed the cluster flow directions. Li (2004) found that clusters consist of many sub-clusters inside. Takeuchi and Hirama (1991) found the coexistence of relatively small and large dense packets (clusters). Rhodes and Hirama (1992) identified three forms of particle motion at the wall: dilute, swarm and dense flow. Bi et al., (1993) grouped the clusters into four forms, namely particle cluster, particle swarm, particle sheet and particle streamer. Shi et al. (2008) classified the clusters into four categories: micro-clusters, core annulus clusters, compact clusters and sparse clusters. With a verified calibration between grayscale and solids holdup, Yang and Zhu (2014a; 2014b; 2015a; 2015b) studied solid phase separation in gas-solids CFB riser and identified clusters based on solids holdup histogram.

Moreover, macro-scale information has been revealed in the CFB riser. Ren et al., (2001) resolved the optical fiber probe signal into three scales: micro-scale (particle size), meso-scale (cluster size) and macro-scale (unit size). Yang and Leu (2009) and Chew et al. (2011, 2012a, 2012b) discriminated macro-scale information using wavelet analysis. Brown and Brue (2001) and Anantharaman et al. (2016) reported that pressure drops

along riser fluctuates significantly in low frequencies, indicating the existence of fluctuation in macroscope.

Despite these studies, Cahyadi et al. (2017) summarized cluster properties in the literature and found cluster information varies in an order of magnitude. Detailed information, like phase classification, solids holdup mapping, macro-scale fluctuation and much more, also remains lacking. This circumstance calls for a thorough and reliable analysis of the instantaneous flow structure in the CFB riser. In this work, flow behavior across riser was recorded in a “narrow rectangular” riser using a high-speed camera with a resolution of $190 \mu\text{m}/\text{pixel}$. Grayscale was converted to solids holdup based on a verified calibration between grayscale and solids holdup (Yang and Zhu, 2014a; 2014b). Based on solids holdup map, the instantaneous flow structure was analyzed in detail and essential phase information has been successfully revealed. Then, flow information was further verified in perspective of solids holdup characteristics and phase scales with signals detected in a “cylindrical riser (10m) using optical fiber probe.

4.2 Experimental

4.2.1 Circulating fluidized bed

Two sets of circulating fluidized beds were employed in this study. One has a “narrow transparent” riser (7.6m high, 19mm thick and 114mm wide) and the other has a “cylindrical” riser (10m high and 76mm in diameter). The gas-solids flow in two CFB systems share a similar operating principle (see Figure 4-1). Air is introduced through a distributor and entrains particles from riser bottom to rise top. At riser exit, this gas-solid mixture enters a series of cyclones and a bag filter where gas is released to atmosphere and particles are returned to downcomer. The collected particles fall downward to solids inventory and finally flow into riser again through an inclined pipe. In the upper section of the downcomer, there is a cylindrical section installed with two flapper valves and a vertical baffle. By adjusting the valves and record solids volume accumulates in unit time, solids circulation rate can be determined. To ensure particle flowability in solids inventory and incline pipe, aeration gas is introduced to maintain minimum fluidization during operating. The gas flow rate is controlled using a rotameter and solids circulation

rate is adjusted using a flip valve installed at the inclined pipe. Superficial gas velocity, U_g , ranged from 3.0 to 9.0 m/s and solids circulation rate, G_s , ranged from 50 to 200 kg/m²s. The particles were FCC catalysts, 67 μm (Sauter mean diameter) in size and 1877 kg/m³ in density. Further details of the CFB can be found in previous papers (Xu and Zhu, 2010; Xu and Zhu, 2011; Wang, 2013;).

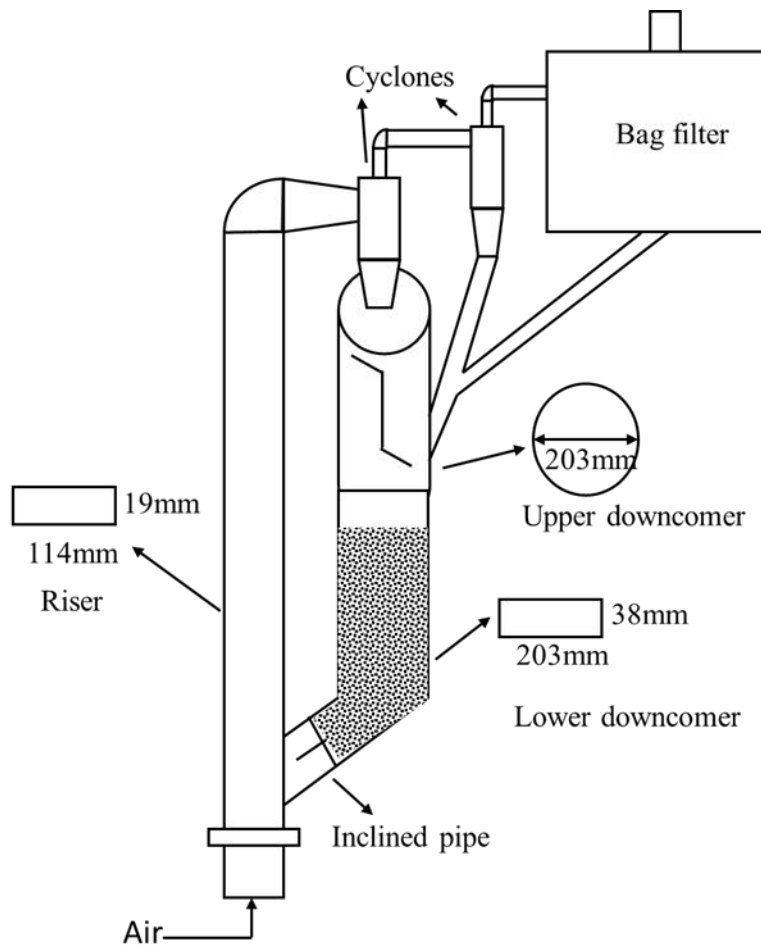


Figure 4-1 Schematic diagram of circulating fluidized bed

4.2.2 Visualization system

In the fully developed region of “narrow transparent” riser, instantaneous gas-solid flow structure has been recorded at $H=5.33\text{m}$ using a visualization system which consists of a high-speed camera coupled with a lens, a lamp, a diffusion panel, a blank box, a firewire and a computer (see Figure 4-2). The camera employed is MotionScope M2 from

Redlake. Its frame rate and resolution can be as high as 16,000 fps and 1280×1024 pixels, respectively. The CMOS camera sensor contains self-calibrating circuitry and IR cut-off optical filter, which guarantees the image quality. The equipped lens is a Pentax manual lens (C21228TH 12.5 mm F1.8). The lamp employs a 500 W quartz halogen bulb whose irradiation is consistent during the experiment. The camera and lamp were on different sides of this rectangular riser. In between the lamp and the riser is the diffusion panel which is for heat insulation and uniform light diffusion. The space from the riser to the camera is covered in a blank box for eliminating light from other sources. The high-speed camera is controlled via a computer through a standard Firewire (IEEE-1394) and a software (Motionscope 2.0.3). The detailed description of this visualization system can be found in previous papers (Yang and Zhu, 2014a; Yang and Zhu, 2014b;). If dense suspension appears in the recording section, the light would be blocked, and it results in low grayscale for the image. The following correlation between grayscale and solids holdup had been developed (Yang and Zhu, 2014a) and validated using an optical fiber probe (Yang and Zhu, 2014b).

$$G = 28.0 + 228.3e^{(-19.62\varepsilon_s)}$$

G is grayscale;

ε_s is solids holdup;

The images recorded via the high-speed camera is a matrix of pixels consisting of 568 columns and 256 rows and corresponds to an area of 114mm (width) \times 51mm (height). Each pixel denotes a $190 \mu\text{m} \times 190 \mu\text{m}$ area, is assigned a grayscale ranging from 0 to 255 based on light intensity and has a solids holdup value computed from grayscale. The coordinates in below figures are in terms of pixels and the factor to convert it to distance is 1.9×10^{-4} m/pixel. To ensure the analysis is statistical, 26887 images have been recorded and 978 clusters have been sampled from images.

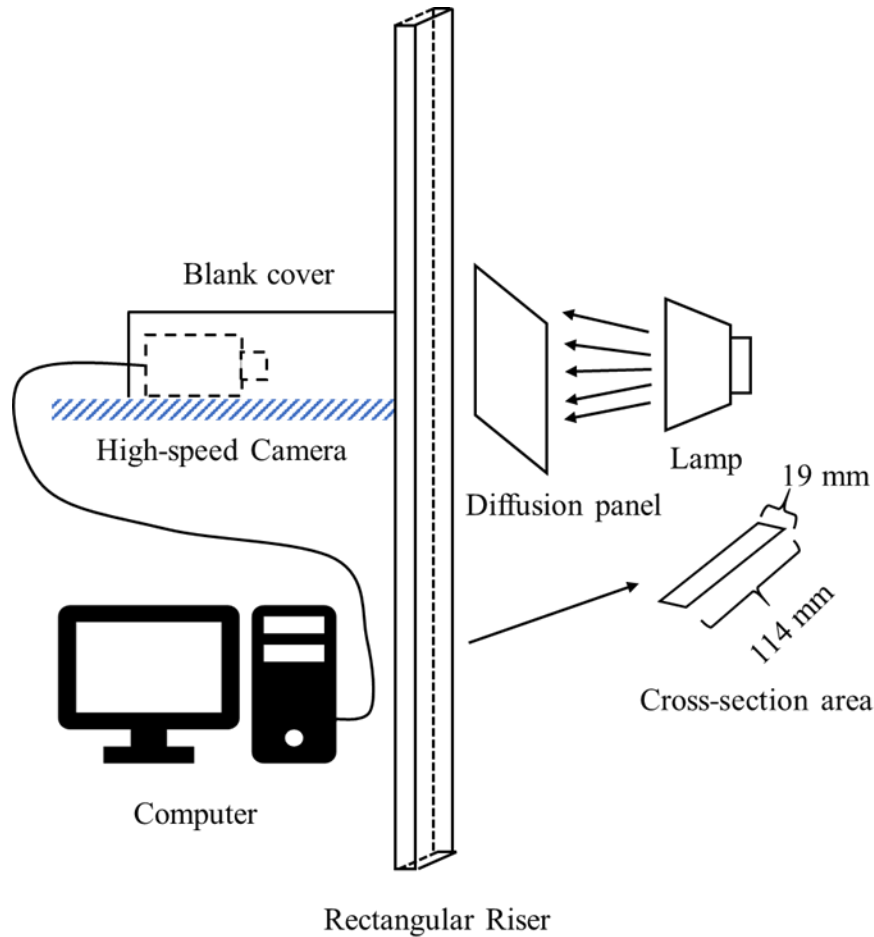


Figure 4-2 Schematic diagram of the visualization system

4.2.3 Optical fiber probe

Optical fiber probe is used to measure the local solids holdup in the “cylindrical riser”. The probe is model PV6D and it was manufactured by Institute of Process Engineering, Chinese Academy of Science, Beijing, China. This optical fiber probe has two sub probes aligned vertically. The overall outer diameter is 3.8 mm and the effective distance of sub-probes is 1.51mm. For each sub-probe, there are emitting fibers and receiving fibers. The light emitted from the emitting fibers hit the surface of particles, reflected to the probe and received by receiving fibers. Sampling frequency was set to be 100kHz, which ensures a good resolution. A calibration between voltage and solids holdup was established by creating a uniform suspension in a slim downer (Zhang et al., 1998). Particle velocity was calculated by cross-correlation the signals acquired by sub-probes.

Signals captured using the optical fiber probe signal is instantaneous solids holdup versus time. By multiplying time with particle velocity, instantaneous solids holdup can be plotted versus length. Details information of this probe and data processing was elaborated in previous papers (Wang, 2013).

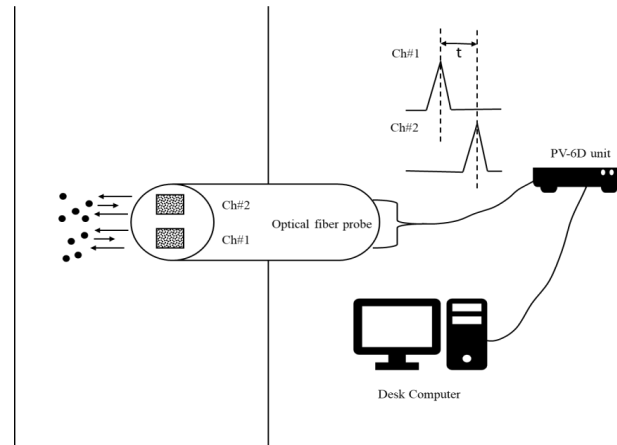
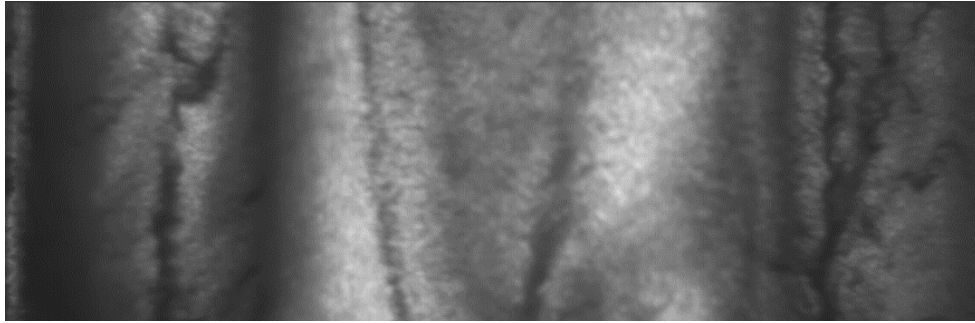


Figure 4-3 Schematic diagram of optical fiber probe

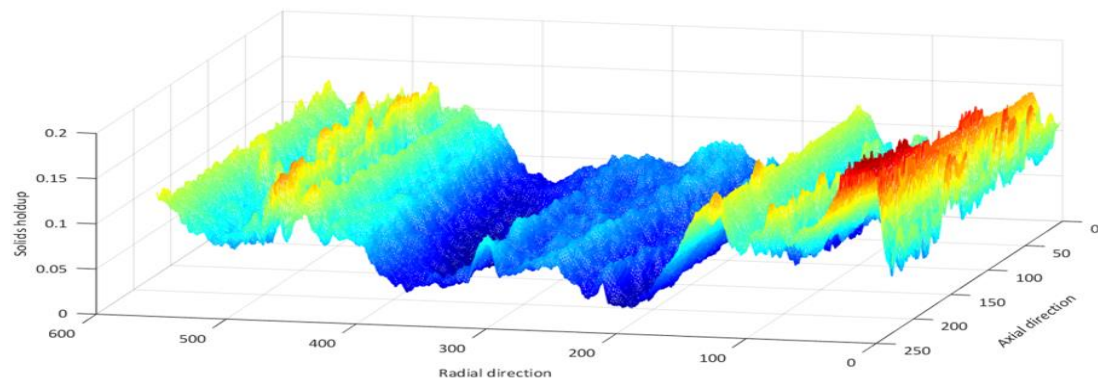
4.3 Results and discussion

4.3.1 Overall flow structure

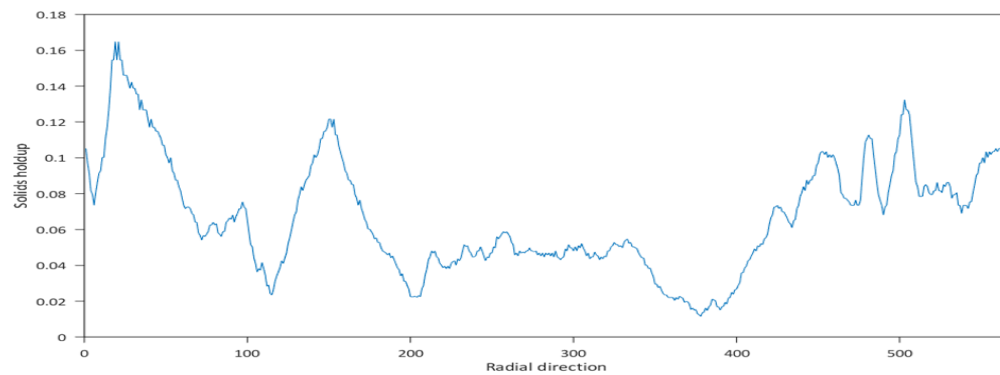
Flow structure across riser has been well visualized owing to the large measuring window of the high-speed camera. A typical mapping of instantaneous solids holdup across riser is shown in Figure 4-4 (a is the original image, captured at $H=5.33$ m, $U_g = 3$ m/s and $G_s=150$ kg/m²s; b is the corresponding solids holdup map; c is the instantaneous radial solids holdup distribution for one pixel-row). A smooth solids holdup slope exists between center region and wall region. Instantaneous solids holdup increases from riser center to wall, but not monotonically: solids holdup may have a significant drop, then increase again (see Figure 4-4b and 4-4c). There are dense regions ubiquitously existing in the CFB riser and their solids holdup is significantly higher than the surrounding (see Figure 4-4b). These dense regions are commonly believed to be clusters, according to the previous publications (Li et al., 1991; Bi et al., 1993; Soong et al., 1994; Shi et al., 2008;). Based on solids holdup mapping, clusters in the center region have lower solids holdup than those in wall region (see Figure 4-4b).



(a)



(b)



(c)

Figure 4-4 The instantaneous flow structure across riser ($H=5.33$ m, $U_g = 3$ m/s and $G_s=150$ kg/m²s, a: the original image, b: the solids holdup map across riser, c: instantaneous radial distribution of solids holdup)

4.3.2 Clusters

Many clusters have been well captured in a variety of operating conditions using the high-speed camera (see Figure 4-5). Contrast and brightness were adjusted for better visualization. The shape of clusters is irregular and has significant variations, which agrees with the previous observation (Takeuchi and Hirama, 1991; Zou et al., 1994;). Solids holdup map and contour of a typical cluster are also demonstrated in Figure 4-6: (a) is the original image, captured at $U_g = 5$ m/s and $G_s=50$ kg/m²s; (b) is the corresponding solids holdup map; (c) is the corresponding solids holdup contour. The solids holdup map shows that (1) the cluster is has its overall solids holdup far below packed solids holdup, (2) solids holdup increases monotonically and sharply from surrounding to cluster center, (3) difference in solids holdup between the cluster and its surrounding is evident (0.03 for this cluster). Further details are shown in solids holdup contour. Contour lines are concentrated at cluster surrounding, indicating that there is an abrupt increase of solids holdup around clusters.

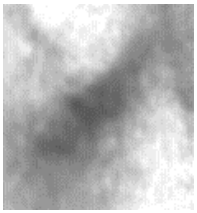
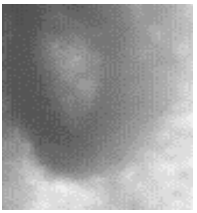






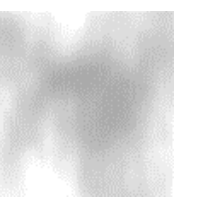
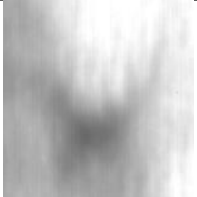


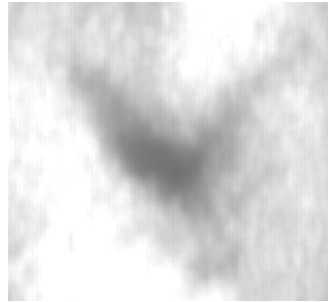
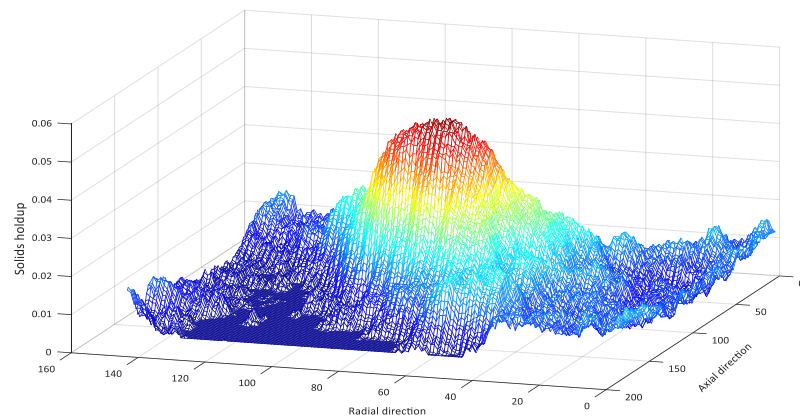
Operating conditions (Ug-Gs)	Cluster images		
3-50			
5-100			
5-150			
7-150			

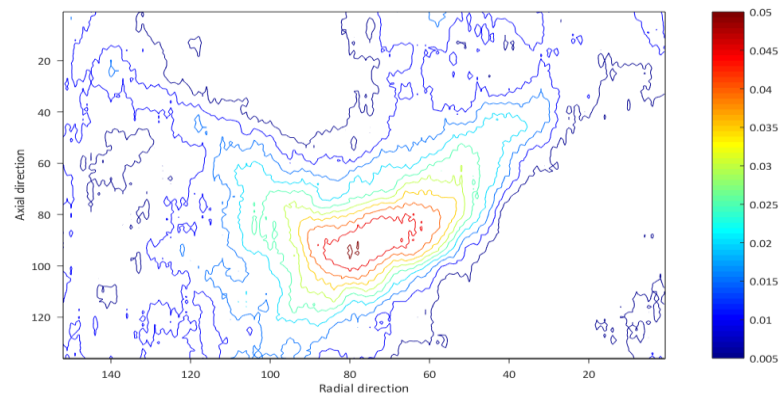
Figure 4-5 Clusters captured using the high-speed camera



(a)



(b)



(c)

Figure 4-6 Solids holdup details of a typical cluster ($H=5.33\text{m}$, $U_g = 5 \text{ m/s}$ and $G_s=50 \text{ kg/m}^2\text{s}$, a: the original image; b: the solids holdup map; c:the solids holdup contour)

Sample signals acquired in the “cylindrical riser” were plotted in Figure 4-7. These sample signals were characterized with sharp narrow peaks. As solids holdup for each peak is significantly higher than surrounding, these peaks are commonly considered to represent clusters (Soong et al., 1994; Manyele et al., 2002). For each cluster, solids holdup increases monotonically from surrounding and reaches a maximum in the center. Clusters also vary in both solids holdup and size. This information detected in “cylindrical riser” using an optical fiber probe agrees well with that derived from images. Although clusters have different shapes and sizes, they share the same solids holdup characteristics, well distinguishes from surrounding in solids holdup and is the basic unit of particle aggregations.

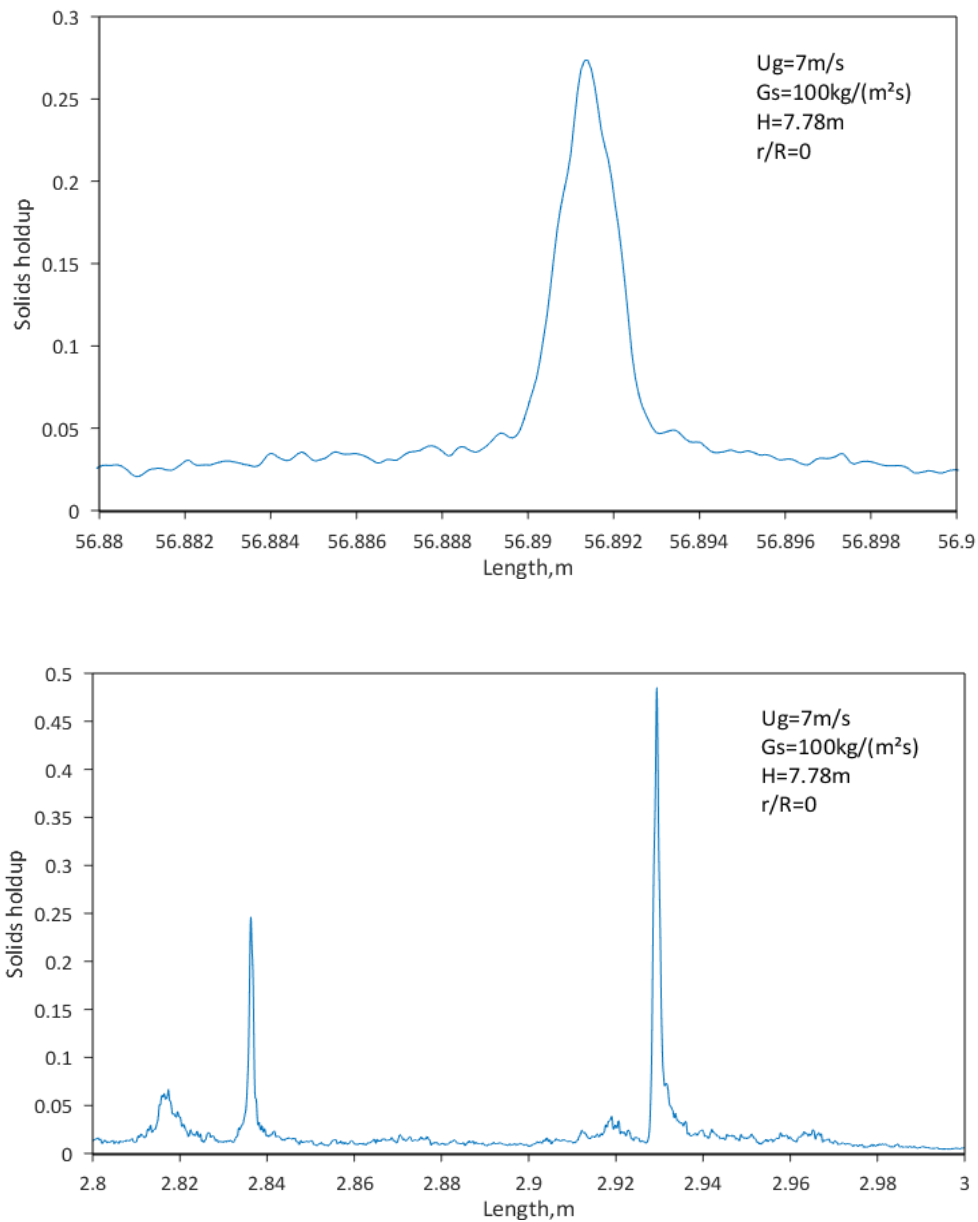


Figure 4-7 Cluster details captured using optical fiber probe

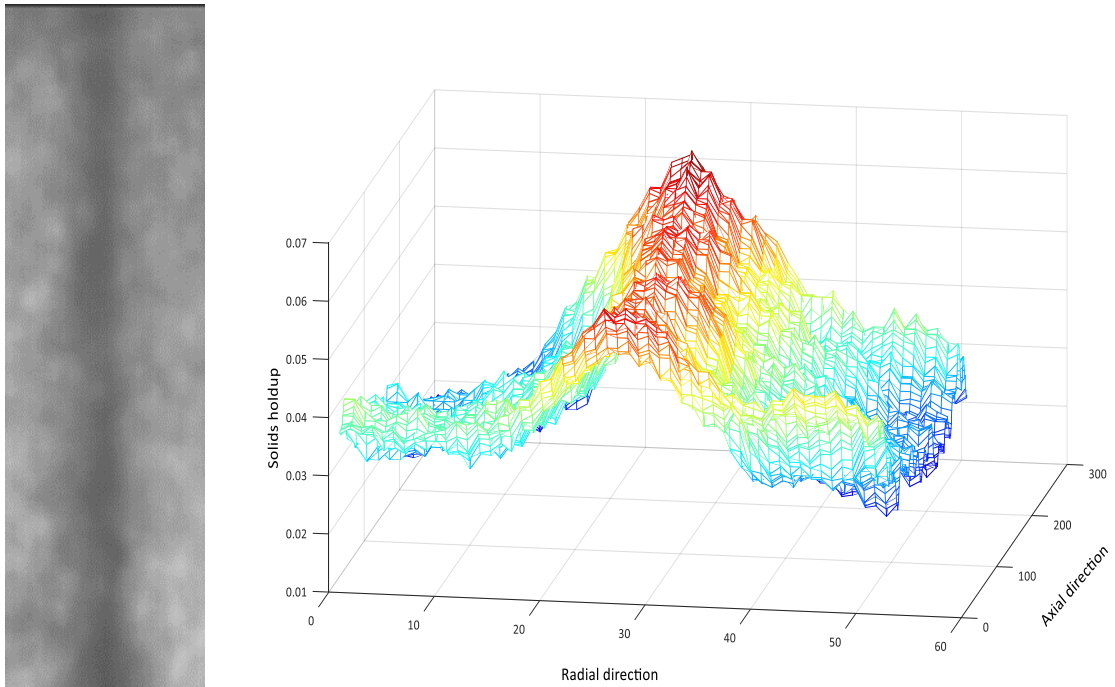
4.3.3 Crest phase

Many clusters are observed to exist within a cloud of coalesced particles whose solids holdup is lower than clusters but higher than surrounding regions, while other clusters exist in dispersed particles. In searching for the most approximate items, we suggest using crest clusters to name clusters surrounded by coalesced particles, and trough

clusters to name clusters surrounded by dispersed particles. Macroscopically, crest phase is suggested to denote crest clusters and coalesced particles, as they have continuous high solids holdup. Trough phase is suggested to denote trough clusters and dispersed particles, as they have continuous low solids holdup. According to the observation, crest phase is typically longer than 5 cm and there are two forms of crest phase: streamer (slim) and chunk (wide).

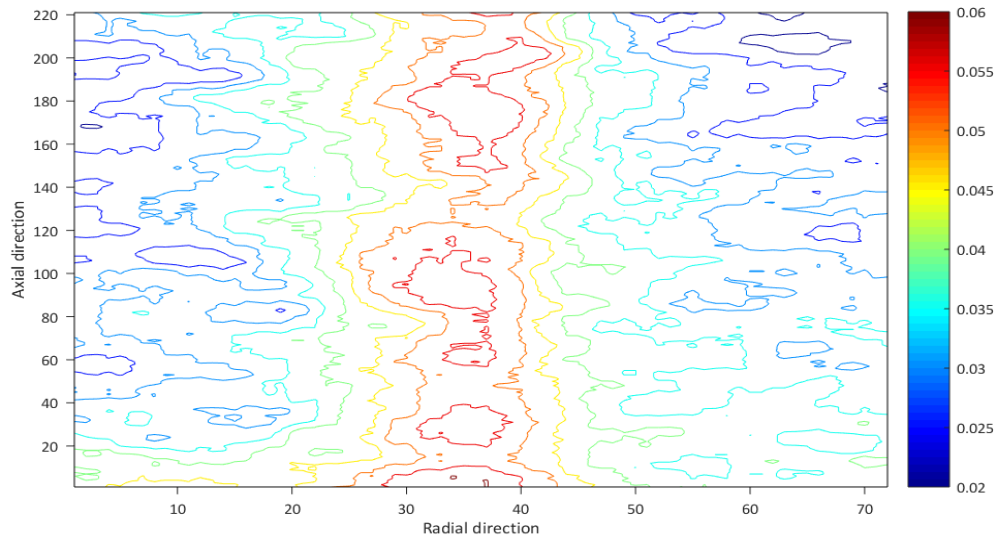
Streamers

Streamers have been reported by previous researchers (Yerushalmi et al., 1976; Bi et al., 1993; Shaffer et al., 2013), but its solids holdup structure has never been analyzed. Solids holdup map and contour of streamers are demonstrated based on a typical streamer acquired at $H=5.33$ m, $U_g=3$ m/s and $G_s=50$ kg/m²s (see Figure 4-8). As can be seen from solids holdup mapping, solids holdup increases symmetrically from left and right sides and reaches a maximum in the center. As can be seen from the solids holdup contour, streamer has several crest clusters aligned vertically inside. For these clusters, solids holdup increases monotonically from surrounding inward. Bi et al. (1993) observed that clusters further develop to resemble streamers in the CFB riser. In this work, clusters are observed to aligned perfect-vertically in the CFB riser (see Figure 4-9). As gas tends to go around clusters, a low-pressure wake is generated in the down-wind. Clusters in vicinity may be drawn to cluster wake and further develop to be streamer. However, this phenomenon is observed in a narrow rectangular CFB riser and this may owe to the restriction of front and back walls. Further observation in cylindrical column is needed to confirm this formation mechanism.



(a)

(b)



(c)

Figure 4-8 Solids holdup details of a typical streamer ($H=5.33$ m, $U_g = 3$ m/s and $G_s=50$ kg/m²s, a: the original image,; b: the solids holdup map; c:the solids holdup contour)

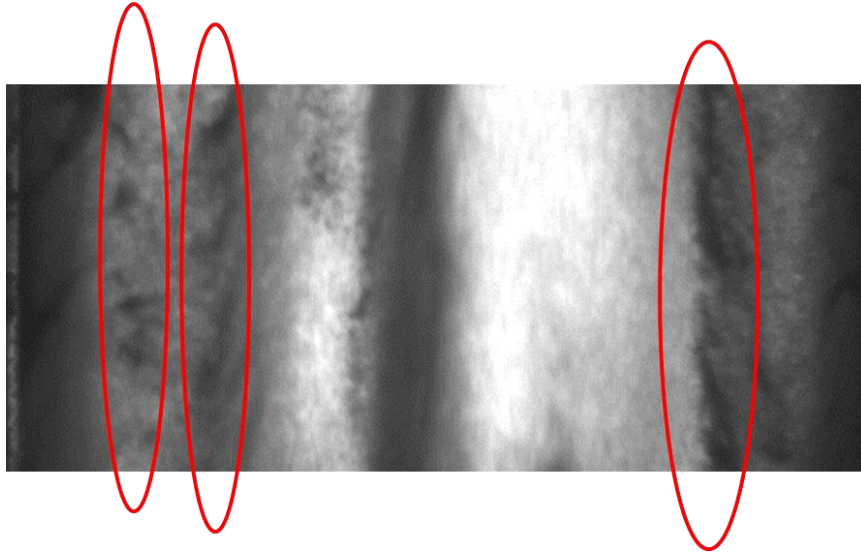


Figure 4-9 Formation of streamers

Chunk

Chunk is much wider comparing with streamer and usually occupies a good fraction of the cross-section area. A typical chunk acquired at $U_g = 5$ m/s and $G_s = 100$ kg/m²s is shown both in grayscale and solids holdup map (see Figure 4-10). As can be seen in Figure 4-10a, chunk in the riser center has higher solids holdup than its surrounding and the transition from trough phase is obvious. Even though this chunk occupies large cross-section area, the flow behavior at riser wall remains similar before and after the appearance of this chunk, indicating the hindering effect of coalesced particles is less evident than clusters. As can be seen in Figure 4-10b, several crest clusters are scattered in the chunk. Solids holdup of crest clusters is much higher than the rest of the chunk. Solids holdup increases monotonically for these crest clusters. The solids holdup increase around clusters is more abrupt than that around the chunk boundary. Formation of chunks may owe to the unsteady global flow structures, including: (1) the pulsed feed of particles from the inclined pipe; (2) distributor effect; (3) particle sheet scattered from the wall region to the center (Bi et al., 1993). Further investigation is required to draw a clear and solid conclusion on chunk formation.

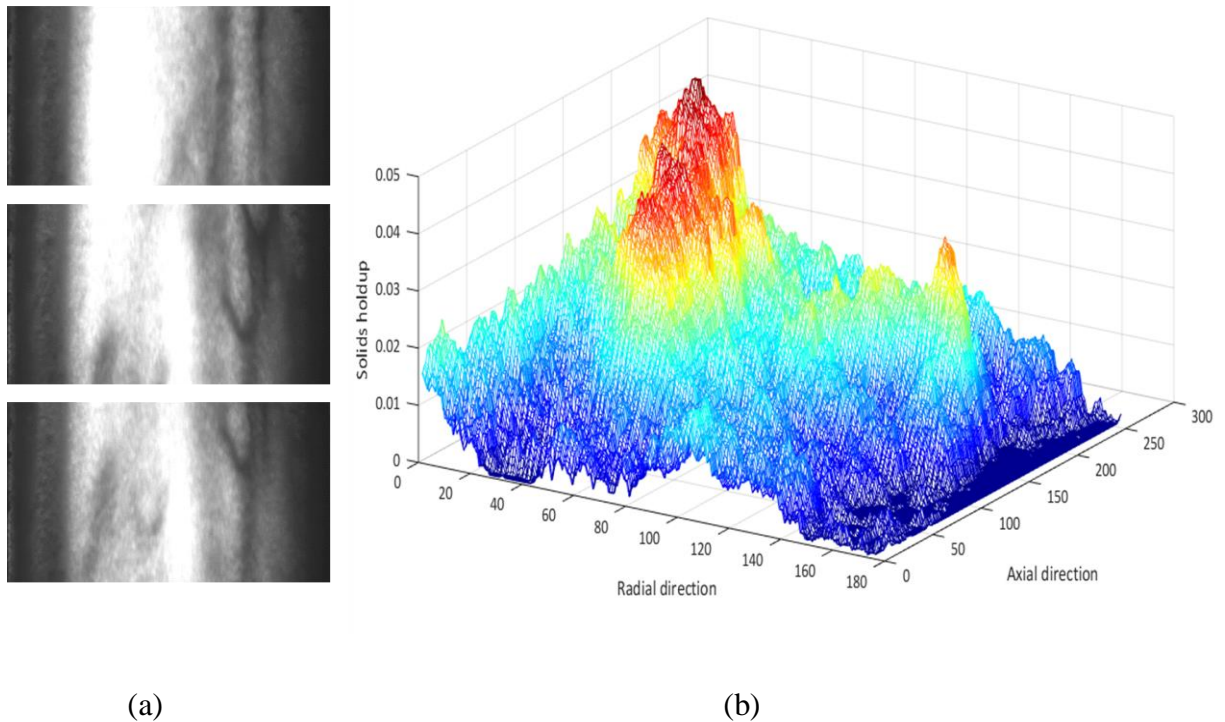


Figure 4-10 Solids holdup details of a typical chunk ($H=5.33$ m, $U_g = 5$ m/s and $G_s=100$ kg/m²s, a: the image sequence with a chunk in the riser center; b: the solids holdup map;)

Li (2004) and Zou et al. (2004) also mentioned the structure of “cluster of clusters” in the CFB riser, which is consistent with this work. Even though chunk contains more coalesced particles comparing with streamer, they share similar solids holdup structure. Counter to crest phase, there is continuous low solids holdup region, namely trough phase (see Figure 4-11). Trough phase has trough clusters immerse in dispersed particles. Collectively, the instantaneous flow structure in the CFB riser features in crest phase and trough phase in macroscope. In microscope, crest phase contains crest clusters and coalesced particles, while trough phase contains trough clusters and dispersed particles.

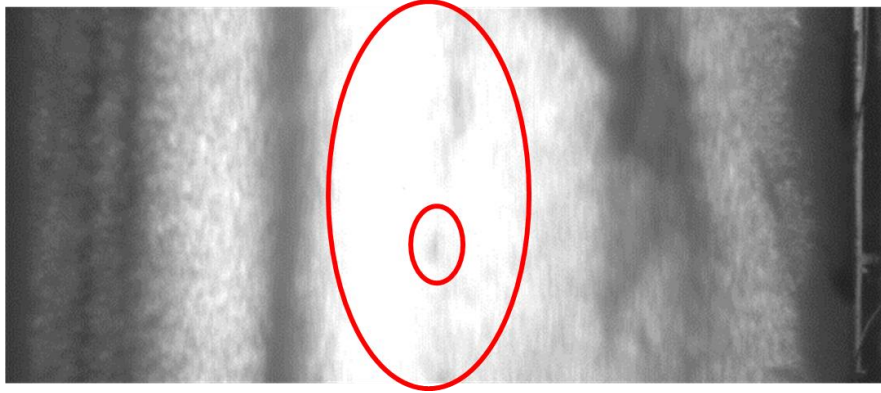


Figure 4-11 Trough phase and trough clusters

Sample signals acquired using an optical fiber probe were plotted to verify the phase classification (see Figure 4-12). The signals were featured with peaks and crescents. Some peaks exist in crescents. Solids holdup increase for crescent is flatter compared with that for peaks. The length of crescents is generally longer than 5cm. It can be concluded that crescent corresponds to crest phase and peaks within crescents represent crest clusters. Besides, there are peaks outside crescents, indicating the existence of clusters in trough phase, which is also consistent with images. According to the signals acquired in different radial positions, the phase classification has been verified across CFB riser.

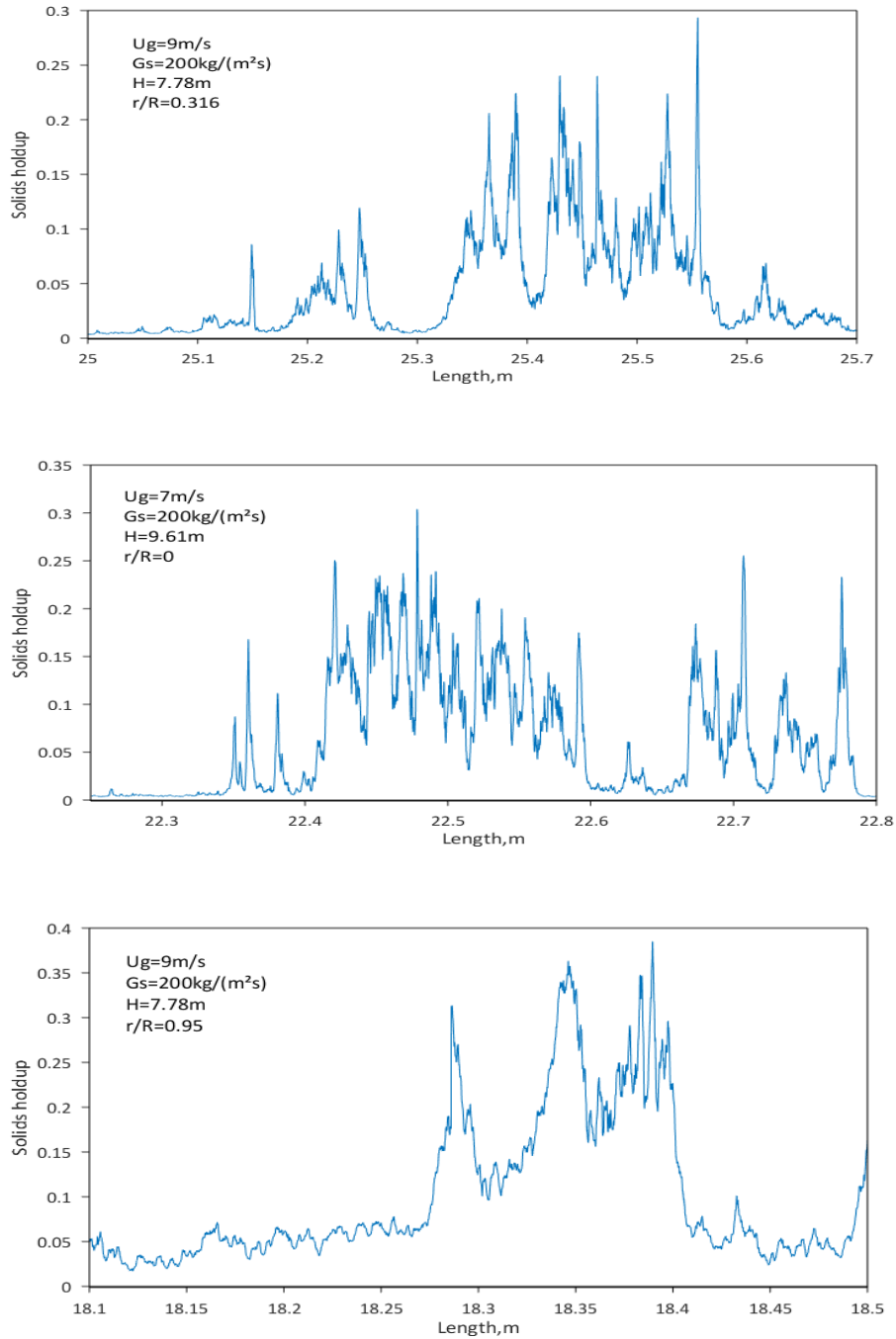


Figure 4-12 Phase details across riser captured using optical fiber probe

4.3.4 Macroscopic fluctuation

Fluctuations in macroscopic has been inferred to exist in the CFB riser based on the analysis of differential pressure along riser and optical fiber probe signals (Ren et al.,

2001; Yang and Leu, 2009; Chew et al., 2011, 2012a, 2012b; Brown and Brue, 200; Anantharaman et al. 2016;). To the best of our knowledge, the magnitude of this fluctuation has not been discussed in solids holdup and the corresponding flow structure remains unknown.

Mean solids holdup across riser was computed and plotted versus the image sequence in Figure 4-13. For each operating condition, many video clips are recorded and there is a time gap between video clips. Images from a consecutive video clip is represented using a consecutive fragment. Gaps in between consecutive fragments represent the time gap between clips. Mean solids holdup across riser fluctuates both frequently and significantly (as high as 0.05) in terms of solids holdup. The illumination intensity remains consistent for the whole lifetime of bulb (Yang and Zhu, 2014a), indicating this solids holdup fluctuation relates with flow structure inside CFB riser. The cause of solids holdup fluctuation was also explored by analyzing the solids holdup histogram of the top 10% dense images and top 10% dilute images (see Figure 4-14). For the top 10% dilute images, the probability decreases exponentially with increasing solids holdup. For the top 10% dense images, up to 60% of the area is occupied by high solids holdup suspension, indicating that the main cause of fluctuation is not certain extremely dense clusters, but large crest phase.

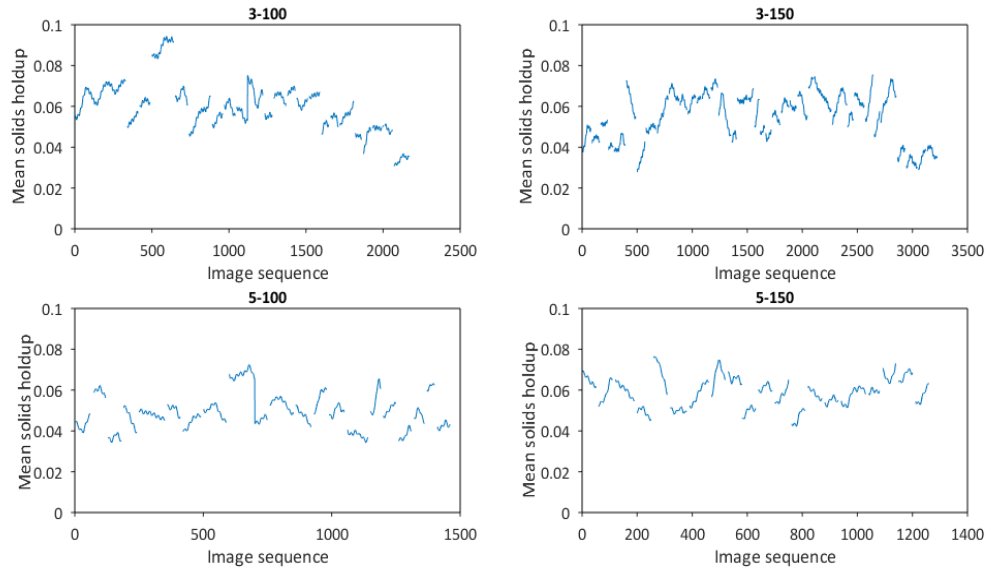


Figure 4-13 Macroscopic fluctuation of solids holdup

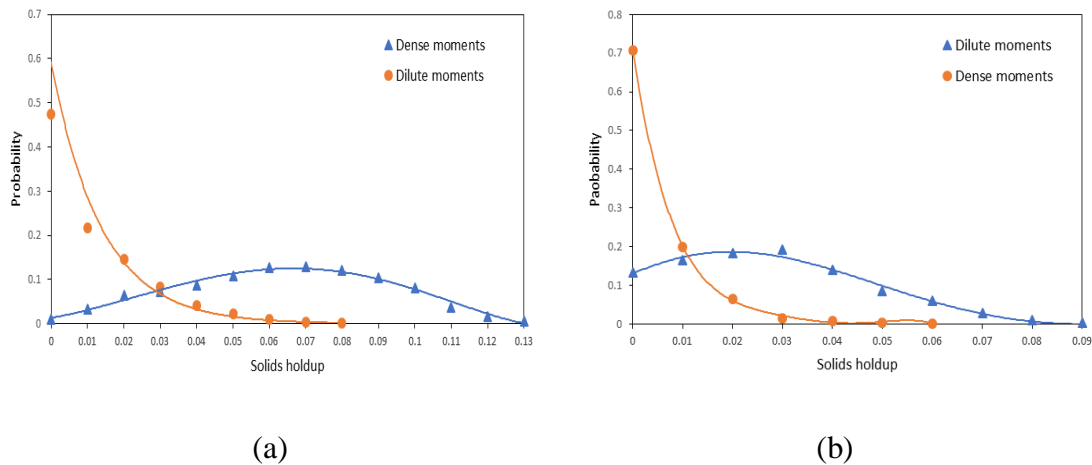


Figure 4-14 Histogram of solids holdup for dense moments and dilute moments
 (a: $U_g = 3 \text{ m/s}$ and $G_s = 100 \text{ kg/m}^2\text{s}$, b: $U_g = 5 \text{ m/s}$ and $G_s = 100 \text{ kg/m}^2\text{s}$)

4.4 Conclusions

Previously, it was believed that there are only two phases in a CFB riser: clusters and dispersed particles. Even though the characterization of clusters dates back to 1990s, the cluster properties in the literature still have a variation up to one order of magnitude. This circumstance hinders the development and validation of numerical models, so that a re-

visit of the instantaneous flow structure is in urgent need. In this work, gas-solid suspension in the CFB riser was both visualized in a narrow rectangular riser using a high-speed camera and measured in a cylindrical riser using optical fiber probe. Then, a thorough analysis of the instantaneous flow structure has been conducted both microscopically and macroscopically based on solids holdup characteristics.

Particle clusters, having their solids holdup increase monotonically and abruptly from the surrounding, are considered as the basic aggregation in the CFB riser. With the irregular shape and different size, particle clusters exist ubiquitously across CFB riser. Some clusters, named as crest clusters here, are surrounded by a cloud of coalesced particles, while other clusters, named as trough clusters here, are immersed in dispersed particles. In terms of solids holdup, (1) crest clusters and trough clusters are significantly denser than coalesced particles and dispersed particles, respectively, (2) coalesced particles are denser than dispersed particles, (3) solids holdup increase around coalesced particles is much less abrupt than those around crest clusters and trough clusters.

As coalesced particles and crest clusters exhibit continuous high solids holdup, they are named as crest phase in macroscope. Crest phase is usually longer than 5 cm and has two forms: slim streamer and wide chunk. Correspondingly, dispersed particles and trough clusters within are named as trough phase in macroscope, since exhibit continuous low solids holdup.

In macroscope, crest phase and trough phase appear alternatively, which could cause significant fluctuation of solids holdup in the CFB riser. In microscope, essential phases are identified as crest clusters, coalesced particles, trough clusters and dispersed particles. Collectively, this study deepens the understanding of fast fluidization, prepares for quantitative phase characterization and contributes to the development of numerical models.

References

- Anantharaman, A., Karri, S. R., Findlay, J. G., Hrenya, C. M., Cocco, R. A., & Chew, J. W. (2016). Interpreting Differential Pressure Signals for Particle Properties and Operating Conditions in a Pilot-Scale Circulating Fluidized Bed Riser. *Industrial & Engineering Chemistry Research*, 55(31), 8659-8670.
- Bi, H. T., Zhu, J. X., Jin, Y., & Yu, Z. Q. (1993). Forms of particle aggregations in CFB. In *Proceedings of the Sixth Chinese Conference on Fluidization*, Wuhan, China (pp. 162-167).
- Brown, R. C., & Brue, E. (2001). Resolving dynamical features of fluidized beds from pressure fluctuations. *Powder Technology*, 119(2-3), 68-80.
- Cahyadi, A., Anantharaman, A., Yang, S., Karri, S. R., Findlay, J. G., Cocco, R. A., & Chew, J. W. (2017). Review of cluster characteristics in circulating fluidized bed (CFB) risers. *Chemical Engineering Science*, 158, 70-95.
- Chew, J. W., Hays, R., Findlay, J. G., Knowlton, T. M., Karri, S. R., Cocco, R. A., & Hrenya, C. M. (2012a). Cluster characteristics of Geldart Group B particles in a pilot-scale CFB riser. I. Monodisperse systems. *Chemical engineering science*, 68(1), 72-81.
- Chew, J. W., Hays, R., Findlay, J. G., Knowlton, T. M., Karri, S. R., Cocco, R. A., & Hrenya, C. M. (2012b). Cluster characteristics of Geldart group B particles in a pilot-scale CFB riser. II. Polydisperse systems. *Chemical engineering science*, 68(1), 82-93.
- Chew, J. W., Parker, D. M., Cocco, R. A., & Hrenya, C. M. (2011). Cluster characteristics of continuous size distributions and binary mixtures of Group B particles in dilute riser flow. *Chemical engineering journal*, 178, 348-358.
- Johnsson, F., Zhang, W., Johnsson, H., & Leckner, B. (1997). Optical and momentum probe measurements in a CFB furnace. *Circulating fluidized bed technology V*, 652.
- Li, H. (2004). Multi-scale aggregation of particles in gas-solids fluidized beds. *China Particuology*, 2(3), 101-106.

- Li, H., Xia, Y., Tung, Y., & Kwauk, M. (1991). Micro-visualization of clusters in a fast fluidized bed. *Powder Technology*, 66(3), 231-235.
- Lim, K. S., Zhu, J. X., & Grace, J. R. (1995). Hydrodynamics of gas-solid fluidization. *International Journal of Multiphase Flow*, 21, 141-193.
- Manyele, S. V., Pärssinen, J. H., & Zhu, J. X. (2002). Characterizing particle aggregates in a high-density and high-flux CFB riser. *Chemical Engineering Journal*, 88(1), 151-161.
- Noymer, P. D., & Glicksman, L. R. (1998). Cluster motion and particle-convective heat transfer at the wall of a circulating fluidized bed. *International Journal of Heat and Mass Transfer*, 41(1), 147-158.
- Ren, J., Mao, Q., Li, J., & Lin, W. (2001). Wavelet analysis of dynamic behavior in fluidized beds. *Chemical Engineering Science*, 56(3), 981-988.
- Rhodes, M., Mineo, H., & Hirama, T. (1992). Particle motion at the wall of a circulating fluidized bed. *Powder Technology*, 70(3), 207-214.
- Shaffer, F., Gopalan, B., Breault, R. W., Cocco, R., Karri, S. R., Hays, R., & Knowlton, T. (2013). High speed imaging of particle flow fields in CFB risers. *Powder Technology*, 242, 86-99.
- Takeuchi, H., Pyatenko, A. T., & Tatano, H. (1996). Flowing behavior of particles in the riser of a circulating fluidized bed. In *Circulating Fluidized Bed Technology V* (pp. 164-169). Science Press Beijing.
- Shi, H., Wang, Q., Xu, L., Luo, Z., & Cen, K. (2008). Visualization of clusters in a circulating fluidized bed by means of particle-imaging velocimetry (PIV) technique. In *Proceedings of the 9th International Conference on Circulating Fluidized Beds, Hamburg, Germany* (pp. 1013-1019).
- Soong, C. H., Tuzla, K., & Chen, J. C. (1994). Identification of particle clusters in circulating fluidized bed. *Circulating fluidized bed technology*, 4, 615-620.

- Takeuchi, H., & Hiramata, T. (1991). Flow visualization in the riser of a circulating fluidized bed. *Circulating Fluidized Bed Technology III*, 177-182.
- Wang, C. (2013). High density gas-solids circulating fluidized bed riser and downer reactors (Doctoral dissertation, The University of Western Ontario).
- Wang, C., Zhu, J., Barghi, S., & Li, C. (2014). Axial and radial development of solids holdup in a high flux/density gas-solids circulating fluidized bed. *Chemical Engineering Science*, 108, 233-243.
- Wu, R. L., Lim, C. J., Grace, J. R., & Brereton, C. M. H. (1991). Instantaneous local heat transfer and hydrodynamics in a circulating fluidized bed. *International Journal of Heat and Mass Transfer*, 34(8), 2019-2027.
- Xu, J., & Zhu, J. (2011). Effects of particle properties on flow structure in a 2-D circulating fluidized bed: Solids concentration distribution and flow development. *Chemical Engineering Science*, 66(21), 5064-5076.
- Xu, J., & Zhu, J. X. (2010). Experimental study on solids concentration distribution in a two-dimensional circulating fluidized bed. *Chemical Engineering Science*, 65(20), 5447-5454.
- Yang, J., & Zhu, J. (2014a). A novel method based on image processing to visualize clusters in a rectangular circulating fluidized bed riser. *Powder Technology*, 254, 407-415.
- Yang, J., & Zhu, J. (2014b). An alternative method for mapping solids holdup in a narrow rectangular CFB riser through image calibration. *The Canadian Journal of Chemical Engineering*, 92(12), 2202-2210.
- Yang, J., & Zhu, J. (2015a). Visualization of solids phase separation in a rectangular CFB riser using a novel image calibration method. *Powder Technology*, 273, 76-82.
- Yang, J., & Zhu, J. (2015b). Cluster identification using image processing. *Particuology*, 23, 16-24.

- Yang, T. Y., & Leu, L. P. (2009). Multiresolution analysis on identification and dynamics of clusters in a circulating fluidized bed. *AIChE journal*, 55(3), 612-629.
- Yang, Y. L., Jin, Y., Yu, Z. Q., & Wang, Z. W. (1992). Investigation on slip velocity distributions in the riser of dilute circulating fluidized bed. *Powder Technology*, 73(1), 67-73.
- Yerushalmi, J., Turner, D. H., & Squires, A. M. (1976). The fast fluidized bed. *Industrial & Engineering Chemistry Process Design and Development*, 15(1), 47-53.
- Zhang, H., Johnston, P. M., Zhu, J. X., De Lasa, H. I., & Bergougnou, M. A. (1998). A novel calibration procedure for a fiber optic solids concentration probe. *Powder Technology*, 100(2-3), 260-272.
- Zhu, J., & Cheng, Y. (2005). Fluidized-Bed Reactors and Applications. In Crowe, C. T. *Multiphase Flow Handbook* (pp.55-93). CRC Press.
- Zou, B., Li, H., Xia, Y., & Ma, X. (1994). Cluster structure in a circulating fluidized bed. *Powder Technology*, 78(2), 173-178.

CHAPTER 5

Tracking the flow dynamics in gas-solid circulating fluidized bed through high-speed photographing

Abstract

In gas-solid circulating fluidized bed (CFB), particle velocity and solids flux are crucial parameters for hydrodynamics. In the literature, time-average information of particle velocity and solids flux has been intensively investigated and consensus has already been reached. However, instantaneous information of particle velocity and solids flux remains lacking, even though it relates directly with gas-solids interaction. In this work, flow behavior in a narrow rectangular circulating fluidized bed has been recorded using a high-speed camera. Then, grayscale is converted to solids holdup based on a verified correlation. Particle velocity is computed by tracking local solids holdup characteristics using two-dimensional cross-correlation. Solids flux is computed by multiplying particle velocity with particle density and local solids holdup. Time-average information of particle velocity and solids flux is found to have the same trend with previous publications. Instantaneous information of particle velocity and solids flux, including relations with local solids holdup, instantaneous radial distribution, instantaneous solids circulating rate and impacts of macro solids holdup fluctuation, is reported for the first time and discussed in detail.

Keywords: high-speed camera; circulating fluidized bed; cross-correlation; instantaneous solids flux; instantaneous particle velocity.

5.1 Introduction

Circulating fluidized bed (CFB) riser has been widely used in both chemical and energy industry, as it offers flexible control of gas/solids flow, high productivity, reduced back mixing, excellent gas-particle contact and so forth (Wang, 2013). In the CFB riser, particles are entrained upward using high-velocity gas and the flow field corresponds to overall reactor performance, including particle residence time, back mixing, solids flux, gas-solid contact and so forth. This study focuses on particle velocity and solids flux which are essential parameters for CFB hydrodynamics.

Up to now, enormous studies have already been conducted to measure the distribution of time-average particle velocity and time-average solids flux in the CFB riser. The devices employed includes laser Doppler velocimetry (Yang et al., 1992; Wei et al., 1998;), optical fiber probe (Pärssinen and Zhu, 2001; Wang et al., 2014;) and particle image velocimetry (Matsuda et al., 1996; Shi et al., 2008; Gopalan and Shaffer, 2012; Shaffer et al., 2013; McMillan et al., 2013;). Several consensuses have already been reached: (1) time-average particle velocity increases from riser wall to riser center, (2) time-average particle velocity may be negative in the riser wall, (3) time-average particle velocity increases with both superficial gas velocity and solids circulating rate, (4) time-average solids flux increases from riser wall toward riser center, (5) time-average solids flux may be negative in the riser wall.

Instantaneous particle velocity and solids flux relate directly with gas-particle interaction, but few studies has been reported. Van den Moortel et al. (1998) measured instantaneous particle velocity at a specific location in a dilute riser using laser Doppler velocimetry. Xu and Zhu (2011b) computed instantaneous cluster velocity based on cross-correlation of cluster signals acquired by optical fiber probe. Further studies are still needed, as the gas-solids suspension in the CFB riser is very complicated according to previous work (chapter 2; chapter 4). Microscopically, particles tend to form clusters due to hydrodynamics. Macroscopically, solids holdup across riser has significant fluctuations due to the appearance of crest phase. In this work, gas-solids suspension in a transparent rectangular riser was recorded at $H=5.33\text{m}$ (fully developed region) using a high-speed

camera. Particle velocity is computed based on two-dimensional cross-correlation of image blocks. With a verified correlation between grayscale and solids holdup (Yang and Zhu, 2014a; 2014b), solids flux is further calculated by multiplying block velocity with its average solids holdup. Then, time-average data was first computed and the trend, as well as magnitude, is consistent with the literature. After that, instantaneous flow characteristics, including relationships with local solids holdup, instantaneous radial distributions, microscopic and macroscopic fluctuations, are analyzed systematically and discussed in detail.

5.2 Experimental

5.2.1 Circulating fluidized bed (rectangular riser)

Circulating fluidized bed employed in this work has a rectangular riser (19 mm in thickness, 114 mm in width and 7.6m in height), two cyclones and a bag filter in series, a downcomer and an inclined pipe connecting riser and downcomer (see Figure 5-1). The downcomer has two sections: top section and bottom section. The top section is cylindrical and can be used to measure solids circulation rate by adjusting flapper valves. The bottom section is used to store particles. During operating, gas is introduced into riser through a distributor and particles enter riser through the inclined pipe. The gas-solid mixture flows concurrently upward in the CFB riser and gets separated in cyclones followed by a bag filter with gas released to atmosphere and particles eventually returned to bottom section of the downcomer. Then, particles will enter riser for a new cycle. Particles circulating in this CFB were FCC catalysts whose size and density are $67 \mu\text{m}$ (Sauter mean diameter) and of 1877 kg/m^3 respectively. Superficial gas velocity, ranging from 3.0 to 9.0 m/s, is controlled using a rotameter, while solids circulation rate, ranging from 50 to $150 \text{ kg/m}^2\text{s}$ is regulated using a valve installed in the middle of the inclined pipe. Details of this circulating fluidized bed is elaborated in previous papers (Yang and Zhu, 2014a; 2014b;).

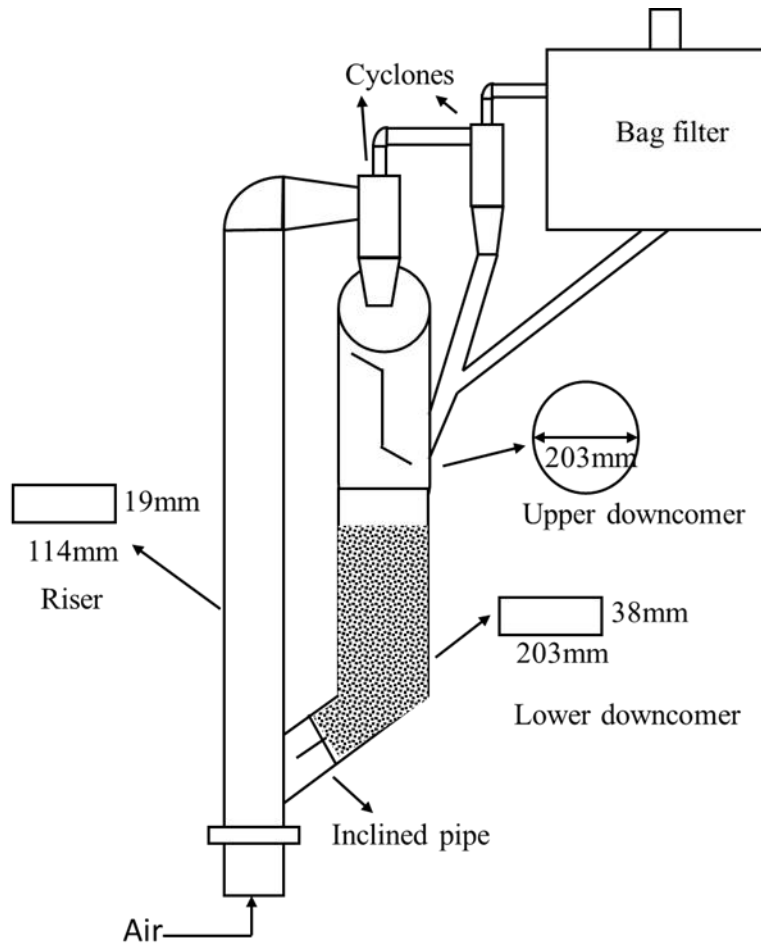


Figure 5-1 Schematic diagram of circulating fluidized bed

5.2.2 Visualization system

A lamp (500 W quartz halogen bulb) is placed facing the riser and provides uniform and consistent illumination with the help of a diffusion panel (see Figure 5-2). A high-speed camera (MotionScopeM2 from Redlake) is placed on the other side and covered in a blank box to avoid pollution of other light sources. If particles appear in the riser, the light would be blocked resulting in low grayscale. A correlation between grayscale and solids holdup (see Equation 5-1) had been developed and validated with optical fiber probe (Yang and Zhu, 2014a; 2014b;). Each pixel denotes a $190 \mu\text{m} \times 190 \mu\text{m}$ area physically and its solids holdup can be calculated based on the verified correlation. The camera was placed at 5.33m of CFB riser and retains stationary during recording. The frame rate is 2000 fps, indicating that time interval for adjacent images is $1/2000$ s. The

shift in the image sequence reflects the motion of particles in the CFB riser. In other words, particle velocity can be determined according to the pixel shift between images and solids flux can be computed by taking solids holdup into consideration. Details of this visualization system is elaborated in previous papers (Yang and Zhu, 2014a; 2014b;).

$$G = 28.0 + 228.3e^{(-19.62\varepsilon_s)} \quad \text{Equation 5-1}$$

G is grayscale;

ε_s is solids holdup;

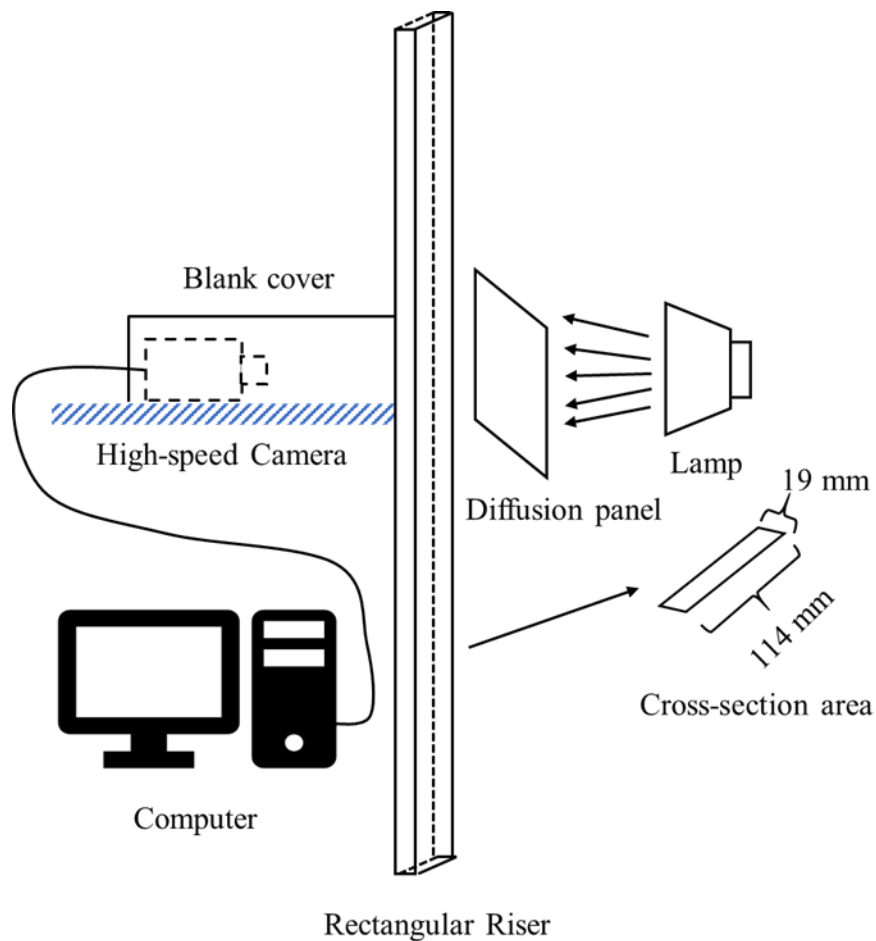


Figure 5-2 Schematic diagram of the visualization system

5.2.3 Data processing

The image sequence was read into MATLAB and a 2-D average kernel (3 pixel \times 3 pixel) is first applied to remove noise. Then, an image block, 11.4mm in height and 5.7mm in width, is picked up from the image and its information, including pixel-wise grayscale and coordinate (x_1, y_1) , is stored. After that, the picked image block is used as a reference to search its location in the following images. The searching scope is around coordinate (x_1, y_1) , but in a large region (25 pixels more to the left and right, 50 pixels more upward, 40 pixels more downward) (see Figure 5-3). The maximum velocity that can be determined with this searching scope is 4.75 m/s horizontally, 19 m/s upward and 3.8 m/s downward. The similarity of image block and target-area is evaluated using two-dimensional cross-correlation (Lewis, 1995; Shapiro and Haralick, 1992;). Correlation coefficient ranges from -1 to +1. The closer the correlation coefficient to +1, the more similarity the two signals share. Two signals are believed to have a good similarity if their correlation coefficient is above 0.6 (Wang, 2013). The probability distribution of correlation coefficients for sampled image blocks is shown in Figure 5-4. The distribution has an exponential shape and the majority is above 0.8, implying that the searching algorithm based on two-dimensional cross-correlation is reliable and accurate. Low correlation coefficients still occur in low probabilities. That may owe to that the grayscale change caused by cluster disintegration or collisions between two particle groups (chapter 4). If only one most similar target-area is found in the searching scope and its correlation coefficient is higher than 0.6, the searching is effective and the coordinate (x_2, y_2) of target-area is stored. Particle velocity can be calculated based on pixel shift using equation 5-2 and 5-3. Grayscales in that image block are converted to solids holdup based on a varied correlation between grayscale and solids holdup pixel-wisely (Yang and Zhu, 2014a). Then, the solids flux is calculated by multiplying vertical velocity with block-average solids holdup and particle density (see Equation 5-4). The minimum shift can be detected in the images is 190 μ m (one pixel) and the time interval is 1/2000 s. As a result, the velocity resolution is 0.38 m/s. To have a better velocity resolution, the target area is searched in the image after the adjacent image in this work. In this case, the minimum velocity resolution is 0.19 m/s. There are two direction components for both particle

velocity and solids flux. However, the horizontal motion of particles is neglectable and vertical motion is dominant (Van den Moortel et al., 1998). In the following discussion, velocity and flux refer to their components in the vertical direction. For each measurement location, numerous data has been collected and the median is taken for time-average information in order to filter out the influence of extreme value.

$$V_{pv} = \frac{y_1 - y_2}{\Delta t} d \quad \text{Equation 5-2}$$

$$V_{ph} = \frac{x_1 - x_2}{\Delta t} d \quad \text{Equation 5-3}$$

$$F_s = V_{pv} \times \varepsilon_s \times \rho_p \quad \text{Equation 5-4}$$

(x_1, y_1) is the coordinate of the image block;

(x_2, y_2) is the coordinate of the target area;

d is the actual size of one pixel, [μm];

Δt is the time interval, [s];

V_{pv} is the particle velocity in the vertical direction, [m/s];

V_{ph} is the particle velocity in the horizontal direction [m/s];

F_s is the solids flux, [$\text{kg}/\text{m}^2 \text{ s}$];

ε_s is solids holdup of the image block;

ρ_p is particle density, [kg/m^3];

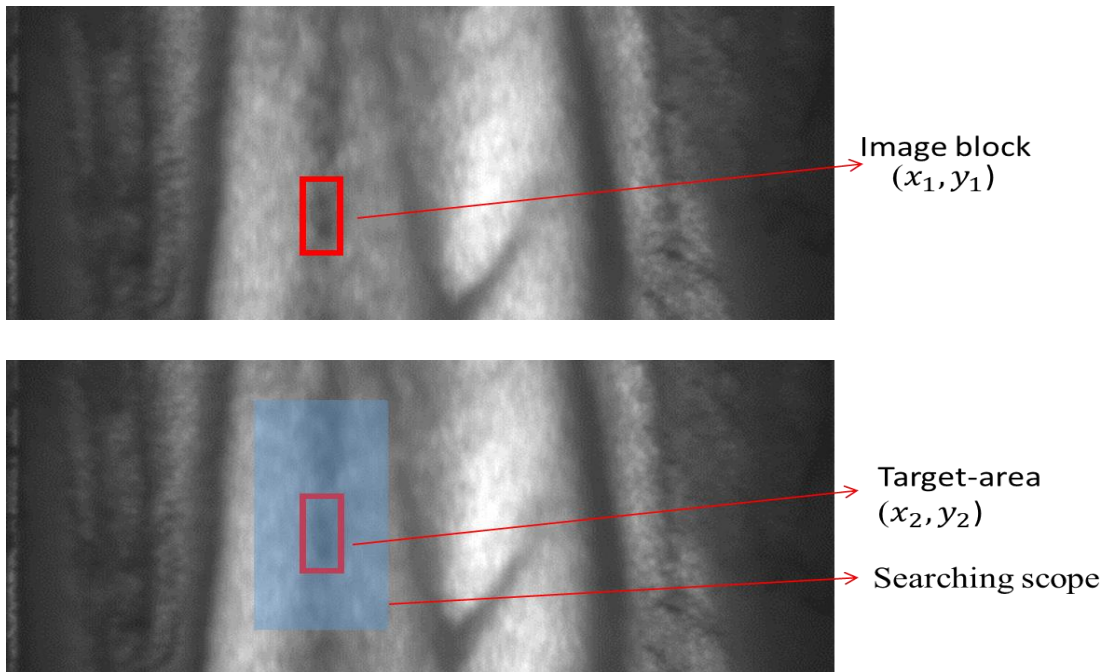


Figure 5-3 Demonstration of the image tracking

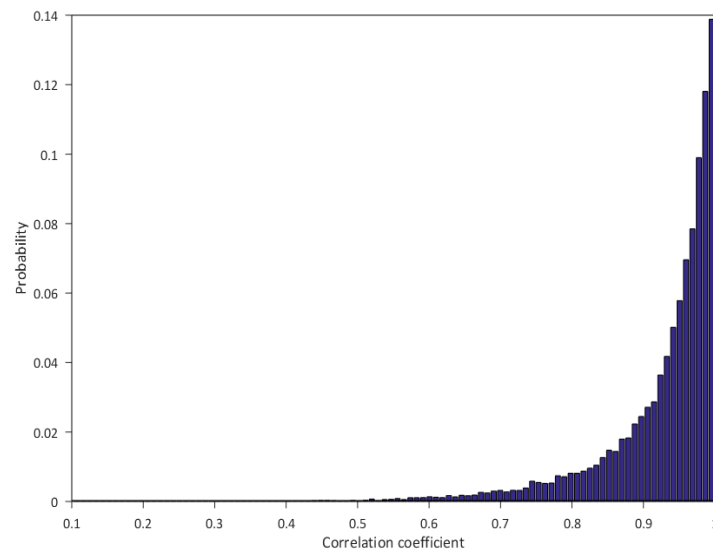


Figure 5-4 Probability density distribution of the cross-correlation coefficient

5.3 Results and discussion

5.3.1 Time-average particle velocity

Time-average particle velocity ($H=5.33\text{m}$) was plotted versus radial position (see Figure 5-5). Particle velocity increases monotonically from wall to center region. In the center region, particle velocity increases with superficial gas velocity and time-average particle velocity is higher than superficial gas velocity. In the wall region ($r/R=\pm 0.89$), particle flows downward at low gas velocity ($U_g = 3 \text{ m/s}$ and $U_g = 5 \text{ m/s}$), and upward at high gas velocities ($U_g = 9 \text{ m/s}$). Downflowing velocity is found to be less than 2 m/s in magnitude and thickness of down-flowing annulus shrinks with increasing gas velocity. The overall radial distribution is not symmetric, and this may owe to that particles enter riser from one side. These characteristics are all consistent with previous studies, indicating that the analysis of flow field is reliable in this work (Griffith and Louge, 1998; Noymer and Glicksman, 2000; Harris et al., 2002; Wang et al., 2014; Xu, 2010).

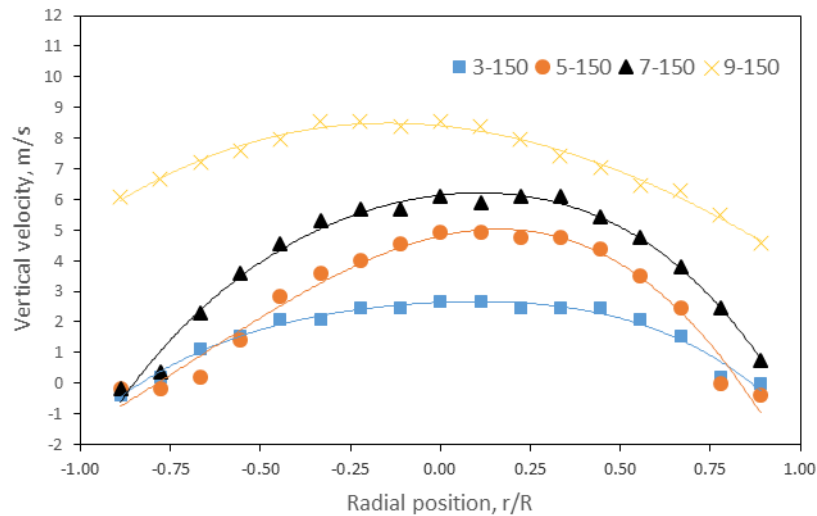


Figure 5-5 Radial distributions of the vertical velocity

Apparent slip velocity is the difference between gas velocity and average particle velocity (see Equation 5-5). Apparent slip velocity was plotted versus superficial gas velocity in figure 5-6. Apparent slip velocity increases with superficial gas velocity. This also agrees

well with previous papers (Islam et al.,2009; Wang et al., 2015;). Yunhau et al. (2006) found that the gas flow rate penetrating through cluster decreases with increasing superficial gas velocity and this explains why apparent slip velocity increases with superficial gas velocity. However, this trend may also relate with the radial distribution of solids holdup and further investigation is needed for a comprehensive understanding.

$$V_{slip} = \frac{U_g}{1 - \varepsilon_s} - \bar{V}_s \quad \text{Equation 5-5}$$

V_{slip} is apparent slip velocity, [m/s];

U_g is the superficial gas velocity, [m/s];

\bar{V}_s is the radial average velocity, [m/s];

ε_s is the spatial average solids holdup;

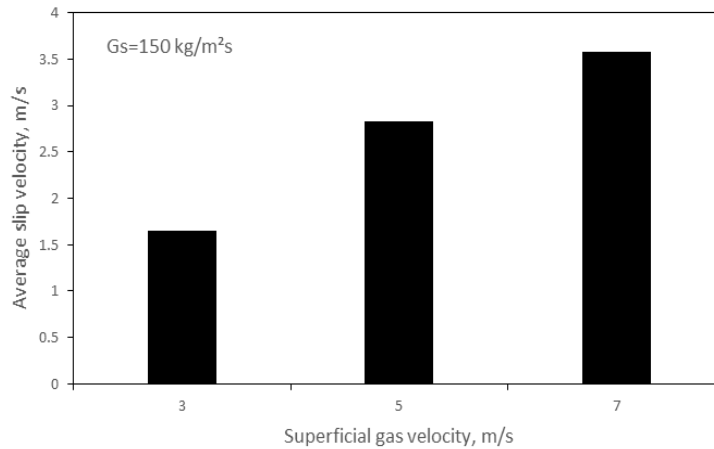


Figure 5-6 Slip velocity versus superficial gas velocity

5.3.2 Time-average solids flux

Time-average solids flux (H=5.33m) was plotted versus radial position (shown in figure 5-7). Time-average solids flux increases from riser wall to center monotonically. In the riser wall, solids flux is negative at low gas velocity and positive at high gas velocity.

These are consistent with previous research (Wang et al., 2014). At $U_g = 5$ m/s, solids flux in the center at $G_s = 100$ kg/m²s is lower than that at $G_s = 150$ kg/m²s. At $G_s = 150$ kg/m²s, solids flux at $U_g = 5$ m/s is higher in the center and lower in wall region comparing with that at $U_g = 3$ m/s.

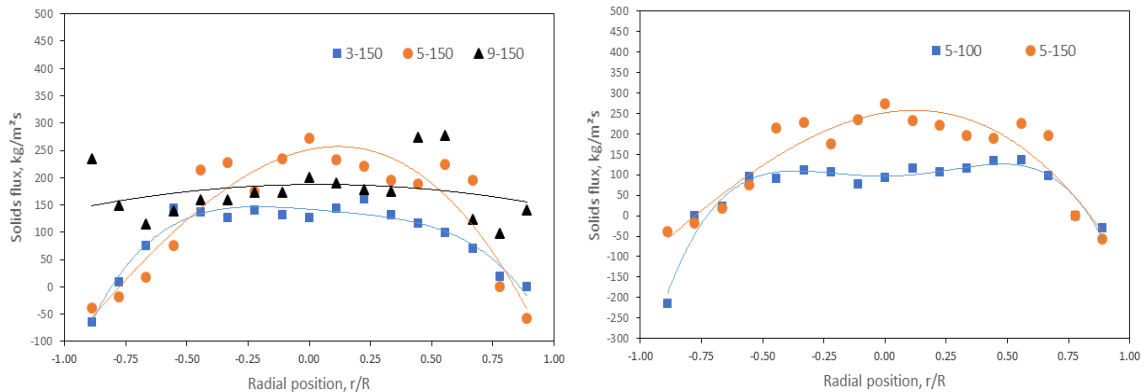


Figure 5-7 Radial distributions of the solids flux

5.3.3 Instantaneous information

Data in different operating conditions ($U_g = 3$ m/s, 5 m/s, 7 m/s, 9 m/s; $G_s = 50$ kg/m²s, 100 kg/m²s, 150 kg/m²s) has been analyzed to draw the conclusions in this section and the figures presented are examples for demonstration.

Relationship with local solids holdup

Instantaneous particle velocity at $r/R=0$ ($U_g = 5$ m/s, $G_s = 150$ kg/m²s) was plot versus its corresponding block-average solids holdup (see Figure 5-8). The particle velocity concentrates around 5 m/s and has a wide velocity distribution from 2 m/s to 6.5 m/s. However, particle velocity has a holistically decrease after 0.045 in solids holdup, indicating that the existence of slowing moving aggregations. But, particle aggregations differ not only in solids holdup, but also in size and shape, resulting in an ambiguous relationship between solids holdup and velocity. Xu and Zhu (2011b) analyzed the cluster velocity and cluster size using different particles and found no clear relation between them. To investigate the relationship between aggregation properties and velocity, it is

suggested to take the shape, size and solids holdup into consideration, other than only one factor among them for further studies.

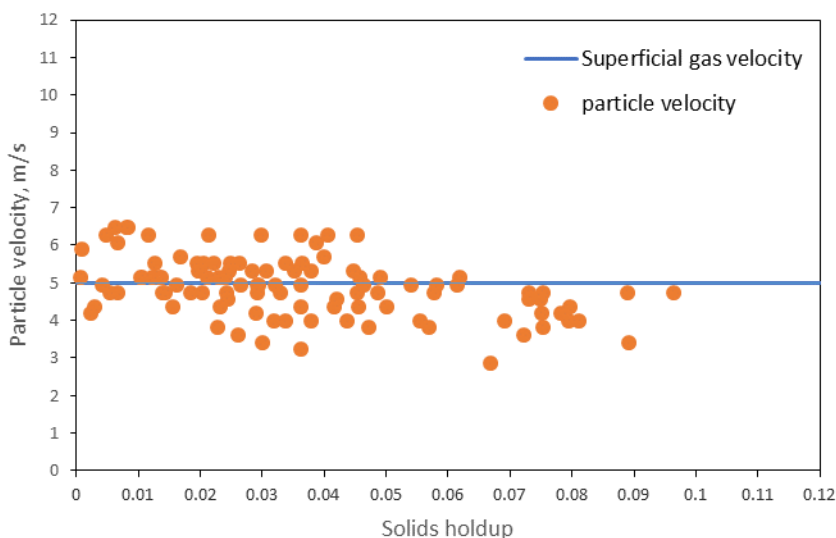


Figure 5-8 Instantaneous particle velocity versus solids holdup

Instantaneous solids flux at $r/R=0$ ($U_g = 5\text{ m/s}$, $G_s = 150\text{ kg/m}^2\text{s}$) was plotted versus its corresponding block-average solids holdup (see Figure 5-9). Solids flux is calculated by multiplying solids holdup with particle velocity and particle density. This explains why solids flux increases with solids holdup. Their relationship is close to linear for low solids holdup and tends to be chaotic for high solids holdup, indicating that gas-particle interaction has an abrupt change due to the increase of solids holdup. High solids holdup may correspond to aggregations and the velocity varies with their solids holdup, size and shape, resulting in the chaotic relationship for high solids holdup.

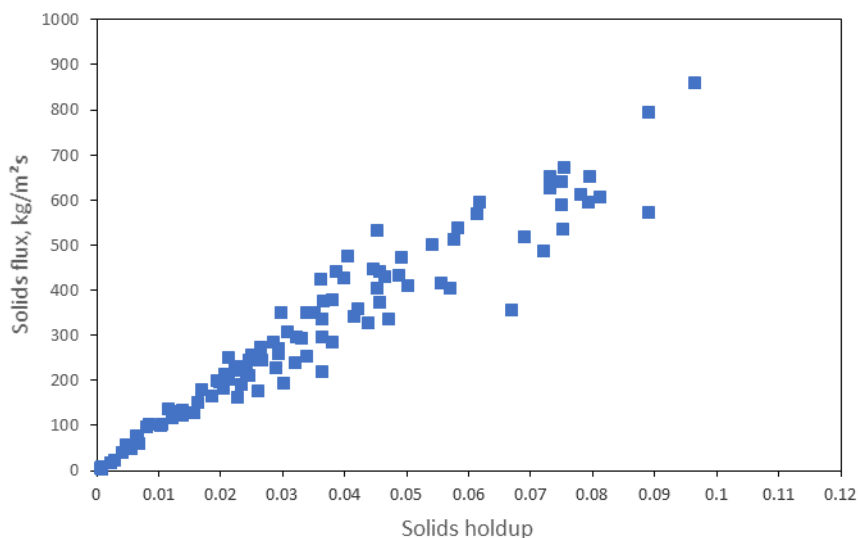
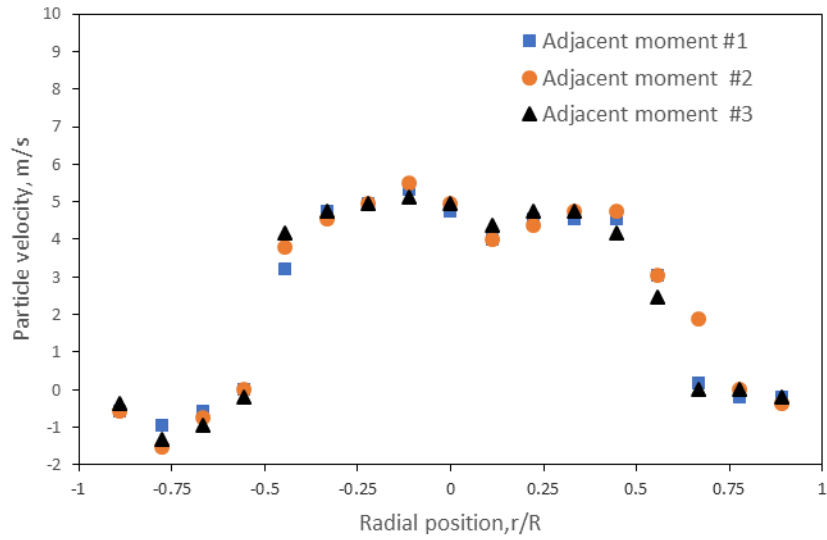


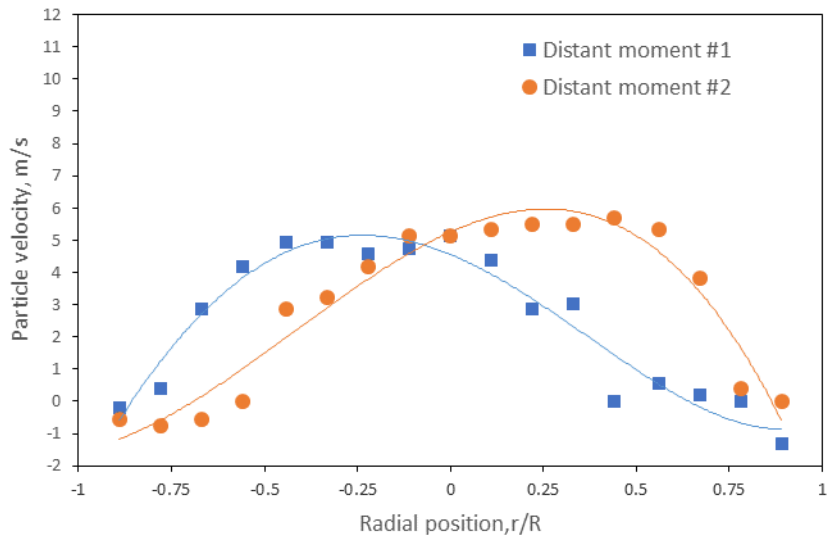
Figure 5-9 Instantaneous solids flux versus solids holdup

Instantaneous radial distribution

Instantaneous solids holdup distribution across riser has been discussed in detail (chapter 4). Here, Radial distribution of instantaneous flow dynamics are discussed both for adjacent moments and for distant moments. Instantaneous particle velocity was computed and plotted versus radial positions (see Figure 5-10). For 5-10a, image blocks were sampled radially at adjacent moments from example images ($H=5.33\text{m}$, $U_g = 5\text{m/s}$, $G_s = 150\text{ kg/m}^2\text{s}$). Their instantaneous particle velocity shares a similar pattern but differs slightly in magnitude. This indicates collision happens in the riser. Generally, instantaneous particle velocity increases from the wall region to the center region. This increase is not monotonical and drops may occur, which may owe to the existence of particle aggregations. For 5-10b, instantaneous particle velocity at distant moments was plotted versus radial positions ($U_g = 5\text{m/s}$, $G_s = 100\text{ kg/m}^2\text{s}$). The instantaneous distributions share similar characteristics with the distributions in 5-11a. At distant moments, instantaneous radial distributions of particle velocity change significantly in perspectives of both pattern and magnitude.



(a)



(b)

Figure 5-10 Radial distributions of instantaneous particle velocity (a: adjacent moments, b: distant moments)

Radial distributions of instantaneous solids flux were shown in figure 5-11. Solids flux increases from riser wall to riser center and this increase is not monotonical due to the

appearance of severe drops. The radial distributions of instantaneous solids flux are more chaotic than that of instantaneous particle velocity. Solids flux takes the fluctuations of both local solids holdup and particle velocity into consideration, which explains the significant chaos. At different moments, instantaneous radial distribution of solids flux also differs in both pattern and magnitude.

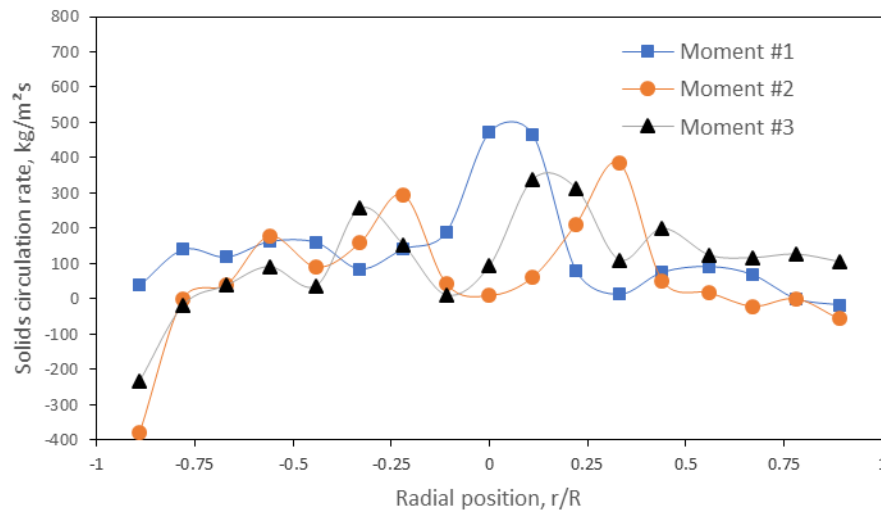


Figure 5-11 Radial distributions of instantaneous solids flux

Instantaneous solids circulating rate was further computed by taking the average of solids flux across riser. Many operating conditions have been analyzed and example data at $U_g = 5\text{m/s}$, $G_s = 100\text{ kg/m}^2\text{s}$ is shown in Figure 5-12. It has been found that instantaneous solids circulating rate keeps fluctuating significantly around experimental solids circulation rate and the fluctuation appears periodically. These may owe to (1) the pulsed particle feed from inclined solids return pipe, (2) the dense suspension scattered from the wall region to the center, (3) the appearance of crest phase in macroscope (chapter 4). Anantharaman et al., (2016) found that differential pressure along riser fluctuates in low frequency. The periodical fluctuation of instantaneous solids circulating rate may be a main cause of the pressure fluctuation. Even at adjacent moments, there are still variation of solids circulating rate, which may owe to the particle clusters.

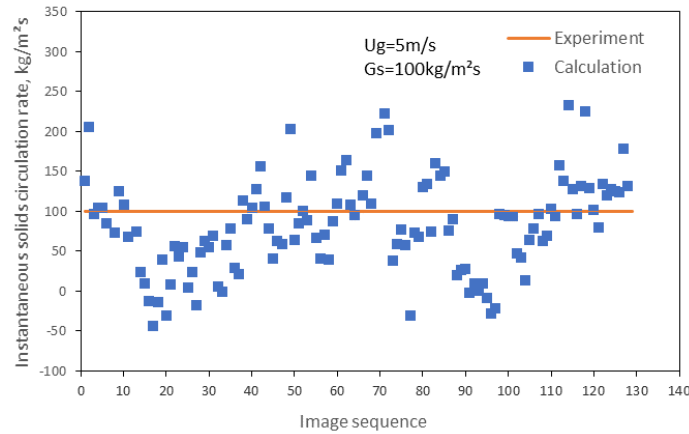


Figure 5-12 Periodical fluctuation of solids circulation rate

5.3.4 Impact of macro fluctuation

Based on the previous analysis, solids holdup across riser fluctuates significantly (chapter 4; Brown and Brue, 2001; Yang and Leu, 2009; Anantharaman et al., 2016; Chew et al., 2011, 2012a, 2012b;). To investigate the impacts of solids holdup fluctuation, top 20% dense images in the fully developed region ($H=5.33\text{m}$) are considered as dense moments and top 20% dilute images in the fully developed region ($H=5.33\text{m}$) are considered as dilute moments. The radial distribution of time-average solids holdup for dense moments and dilute moments are shown in figure 5-13. Solids holdup in dense moments is significantly higher than that in dilute moments across riser, indicating this classification is reasonable.

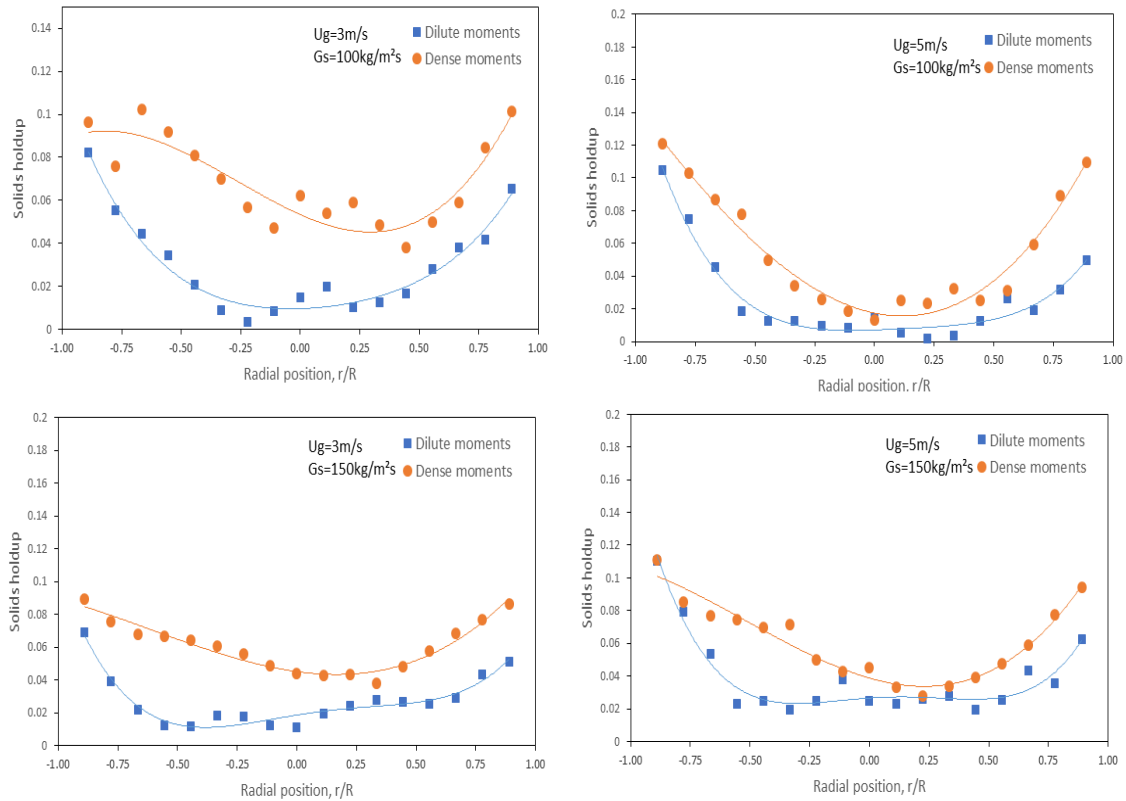


Figure 5-13 Radial distributions of the solids holdup for dense moments and dilute moments

Radial distributions of time-average particle velocity have been computed for dense moments and dilute moments, respectively (see Figure 5-14). At $G_s = 100\text{kg/m}^2\text{s}$, particle velocity in dense moments is lower in the center region and higher in wall region, compared with the that for dilute moments. At $G_s = 150\text{kg/m}^2\text{s}$, particle velocity in dilute and dense moments becomes similar. Radial distributions of time-average solids flux have also been computed in the fully developed region ($H=5.33\text{m}$) for dense moments and dilute moments, respectively (see Figure 5-15). In the center, the solids flux in dense moments is much higher than that in dilute moments. In the wall region, whether the solids flux in dense moments is higher or not is uncertain. The particle velocity in dense moments is either low or similar than that for dilute moments (see Figure 5-14), but dense moments have much higher solids holdup. Solids flux is the particle weight passed through unit cross-section area per second and is the product of solids holdup, particle

velocity and particle density. As a result, instantaneous solids flux in dense moments is significantly higher than that in dilute moments. In the previous study, it has been found dense moments and dilute moments appear alternatingly in the CFB riser (chapter 4), which explains why the instantaneous solids circulation rate keeps fluctuating periodically.

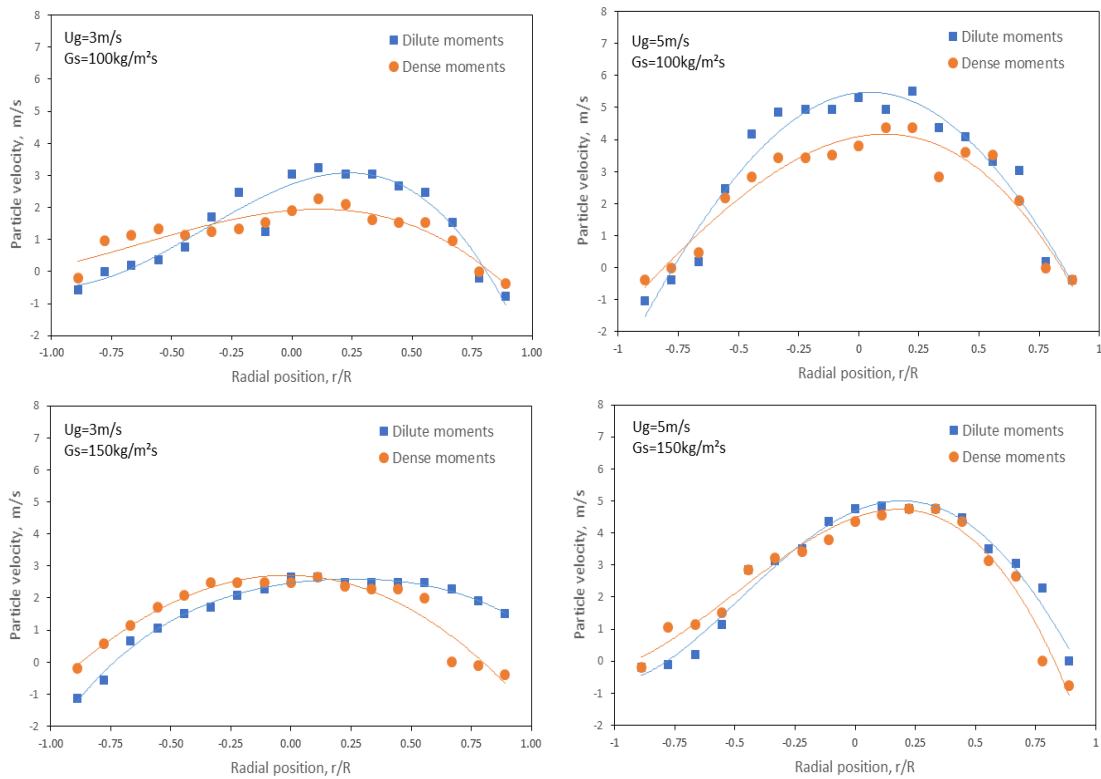


Figure 5-14 Radial distributions of particle velocity for dense moments and dilute moments

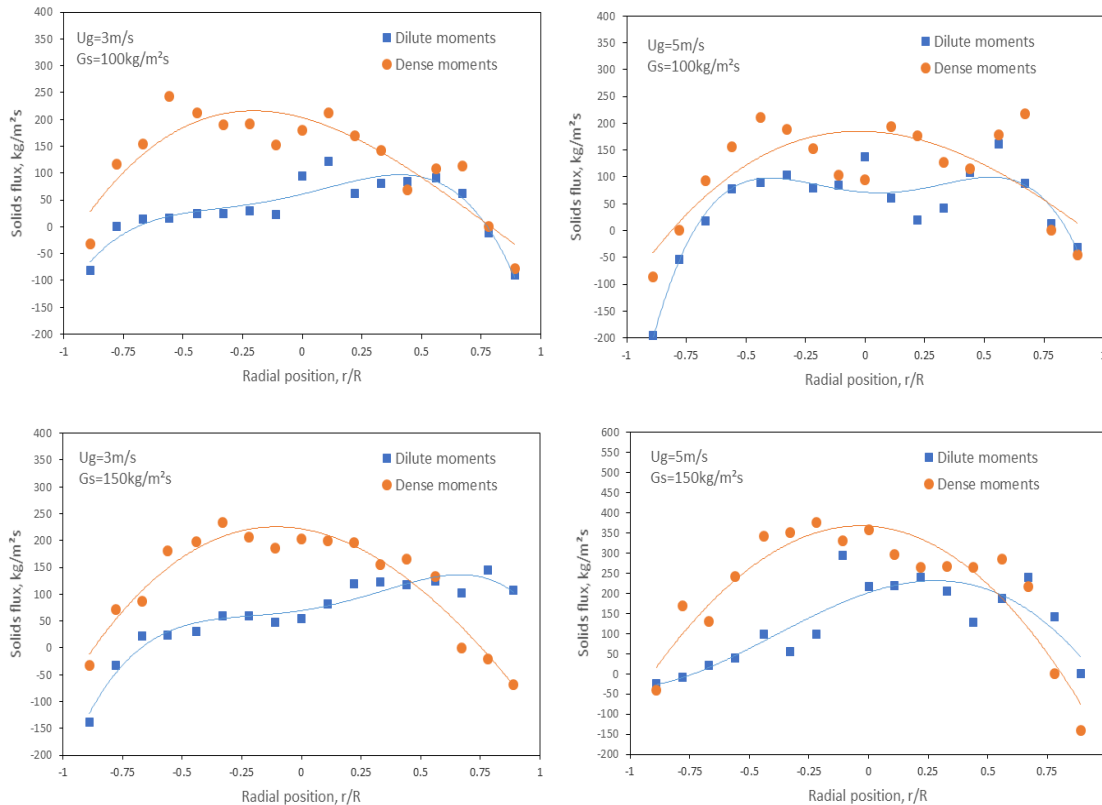


Figure 5-15 Radial distributions of solids flux for dense moments and dilute moments

5.4 Conclusions

Gas-solid flow in a CFB riser has been well recorded using a high-speed camera. This work provides a reliable way to detect flow dynamics using two-dimensional cross-correlation. Particle velocity was computed by tracking image blocks in the image sequences. With a verified correlation between solids holdup and grayscale, solids flux was calculated by multiplying particle velocity with solids holdup and particle density.

Time-average information is found to be consistent with literature:

1. Both time-average particle velocity and time-average solids flux increase monotonically from the riser wall towards the riser center.
2. Down flowing annulus disappears at high superficial gas velocity.

3. Apparent slip velocity increases with superficial gas velocity.

In addition, instantaneous flow information has been studied systematically. It has been found that:

1. Instantaneous particle velocity increases from riser wall to riser center, but not monotonically (drops may appear).
2. Instantaneous particle velocity decreases with local solids holdup holistically.
3. Instantaneous solids circulation rate fluctuates periodically and significantly.
4. At $G_s = 100 \text{ kg/m}^2\text{s}$, particle velocity in dense moments is lower in the center region and higher in wall region, compared with the that for dilute moments. At $G_s = 150 \text{ kg/m}^2\text{s}$, particle velocity in dilute and dense moments becomes similar.
5. Solids flux in dense moments is much higher than that in dilute moments in the center region. In wall region, whether the solids flux in dense moments is higher or not is uncertain.

References

- Anantharaman, A., Karri, S. R., Findlay, J. G., Hrenya, C. M., Cocco, R. A., & Chew, J. W. (2016). Interpreting Differential Pressure Signals for Particle Properties and Operating Conditions in a Pilot-Scale Circulating Fluidized Bed Riser. *Industrial & Engineering Chemistry Research*, 55(31), 8659-8670.
- Brown, R. C., & Brue, E. (2001). Resolving dynamical features of fluidized beds from pressure fluctuations. *Powder Technology*, 119(2-3), 68-80.
- Chew, J. W., Hays, R., Findlay, J. G., Knowlton, T. M., Karri, S. R., Cocco, R. A., & Hrenya, C. M. (2012a). Cluster characteristics of Geldart Group B particles in a pilot-scale CFB riser. I. Monodisperse systems. *Chemical engineering science*, 68(1), 72-81.
- Chew, J. W., Hays, R., Findlay, J. G., Knowlton, T. M., Karri, S. R., Cocco, R. A., & Hrenya, C. M. (2012b). Cluster characteristics of Geldart group B particles in a pilot-scale CFB riser. II. Polydisperse systems. *Chemical engineering science*, 68(1), 82-93.
- Chew, J. W., Parker, D. M., Cocco, R. A., & Hrenya, C. M. (2011). Cluster characteristics of continuous size distributions and binary mixtures of Group B particles in dilute riser flow. *Chemical Engineering Journal*, 178, 348-358.
- Gopalan, B., & Shaffer, F. (2012). A new method for decomposition of high speed particle image velocimetry data. *Powder Technology*, 220, 164-171.
- Griffith, A. E., & Louge, M. Y. (1998). The scaling of cluster velocity at the wall of circulating fluidized bed risers. *Chemical engineering science*, 53(13), 2475-2477.
- Harris, A. T., Davidson, J. F., & Thorpe, R. B. (2002). The prediction of particle cluster properties in the near wall region of a vertical riser (200157). *Powder Technology*, 127(2), 128-143.
- Islam, M. A., Krol, S., & de Lasa, H. I. (2009). Slip velocity in downer reactors: drag coefficient and the influence of operational variables. *Industrial & Engineering Chemistry Research*, 49(15), 6735-6744.

- Lewis, J. P. (1995, May). Fast normalized cross-correlation. In *Vision Interface* (Vol. 10, No. 1, pp. 120-123).
- Matsuda, S., Hatano, H., Takeuchi, H., Pyatenko, A. T., & Tsuchiya, K. (1996). Motion of individual solid particles in a circulating fluidized bed riser. In *Circulating Fluidized Bed Technology V* (pp. 176-181). Science Press Beijing.
- McMillan, J., Shaffer, F., Gopalan, B., Chew, J. W., Hrenya, C., Hays, R., ... & Cocco, R. (2013). Particle cluster dynamics during fluidization. *Chemical Engineering Science*, 100, 39-51.
- Noymer, P. D., & Glicksman, L. R. (2000). Descent velocities of particle clusters at the wall of a circulating fluidized bed. *Chemical Engineering Science*, 55(22), 5283-5289.
- Pärssinen, J. H., & Zhu, J. X. (2001). Particle velocity and flow development in a long and high-flux circulating fluidized bed riser. *Chemical Engineering Science*, 56(18), 5295-5303.
- Shaffer, F., Gopalan, B., Breault, R. W., Cocco, R., Karri, S. R., Hays, R., & Knowlton, T. (2013). High speed imaging of particle flow fields in CFB risers. *Powder Technology*, 242, 86-99.
- Shapiro, L., & Haralick, R. (1992). Computer and robot vision. *Reading: Addison-Wesley*, 8.
- Shi, H. X. (2007). Experimental research of flow structure in a gas-solid circulating fluidized bed riser by PIV. *Journal of Hydrodynamics*, Ser. B, 19(6), 712-719.
- Shi, H., Wang, Q., Xu, L., Luo, Z., & Cen, K. (2008). Visualization of clusters in a circulating fluidized bed by means of particle-imaging velocimetry (PIV) technique. In *Proceedings of the 9th International Conference on Circulating Fluidized Beds*, Hamburg, Germany (pp. 1013-1019).

Van den Moortel, T., Azario, E., Santini, R., & Tadrif, L. (1998). Experimental analysis of the gas-particle flow in a circulating fluidized bed using a phase Doppler particle analyzer. *Chemical Engineering Science*, 53(10), 1883-1899.

Wang, C., Li, C., Zhu, J., & Barghi, S. (2015). A comparison of flow development in high density gas - solids circulating fluidized bed downer and riser reactors. *AIChE Journal*, 61(4), 1172-1183.

Wang, C., Zhu, J., Li, C., & Barghi, S. (2014). Detailed measurements of particle velocity and solids flux in a high density circulating fluidized bed riser. *Chemical Engineering Science*, 114, 9-20.

Wei, F., Lin, H., Cheng, Y., Wang, Z., & Jin, Y. (1998). Profiles of particle velocity and solids fraction in a high-density riser. *Powder Technology*, 100(2-3), 183-189.

Xu, J., & Zhu, J. (2011). A new method for the determination of cluster velocity and size in a circulating fluidized bed. *Industrial & Engineering Chemistry Research*, 51(4), 2143-2151.

Yang, J., & Zhu, J. (2014a). A novel method based on image processing to visualize clusters in a rectangular circulating fluidized bed riser. *Powder Technology*, 254, 407-415.

Yang, J., & Zhu, J. (2014b). An alternative method for mapping solids holdup in a narrow rectangular CFB riser through image calibration. *The Canadian Journal of Chemical Engineering*, 92(12), 2202-2210.

Yang, T. Y., & Leu, L. P. (2009). Multiresolution analysis on identification and dynamics of clusters in a circulating fluidized bed. *AIChE journal*, 55(3), 612-629.

Yang, Y. L., Jin, Y., Yu, Z. Q., & Wang, Z. W. (1992). Investigation on slip velocity distributions in the riser of dilute circulating fluidized bed. *Powder Technology*, 73(1), 67-73.

Yunhau, Z., Huilin, L., Yurong, H., Ding, J., & Lijie, Y. (2006). Numerical prediction of combustion of carbon particle clusters in a circulating fluidized bed riser. *Chemical Engineering Journal*, 118(1), 1-10.

Zhu, J., & Cheng, Y. (2016). Applications of Fluidized Bed Reactors. In Michaelides, E., Crowe, C. T., & Schwarzkopf, J. D. (Eds.). *Multiphase Flow Handbook* (pp.1029-1058). CRC Press.

CHAPTER 6

Analysis of phase segregation in gas-solid circulating fluidized bed with direct image calibration

Abstract

As a widely-used reactor, circulating fluidized bed (CFB) riser aims to offer an efficient space for gas-particle contact. However, particles in the CFB riser aggregate to form clusters which are denser than surrounding and much larger than individual particles. As a result, particles inside clusters are “sheltered” from main gas stream, resulting in the reduction of contact efficiency. To predict the performance of CFB riser and to build numerical models, many previous attempts have been made to characterize the clusters. However, cluster properties in the literature deviate significantly, up to one order of magnitude, even at similar operating conditions. This, to a large extent, attributes to subjective methods to identify cluster boundary. In this study, flow behavior in the CFB riser was recorded using a high-speed camera and solids holdup gradient was used to analyze cluster boundary. With validation using an optical fiber probe, an abrupt increase of solids holdup is found to exist around clusters, evidencing the phase segregation. Then, cluster boundary is determined to be where solids holdup increases most abruptly, and clusters are characterized systematically across riser in terms of solids holdup, projected width, projected length, equivalent diameter and circularity. Collectively, this study provides an objective and effective method to qualify clusters based on solids holdup distribution, so as to achieve a reliable characterization of clusters.

Keywords: image processing; cluster boundary; cluster characterization; high-speed camera; circulating fluidized bed.

6.1 Introduction

Gas-solid circulating fluidized bed (CFB) riser is widely used in oil refining, electricity generation, gasification, metallurgy and calcination, as it provides excellent heat and mass transfer, reduced back mixing, high productivity and independent control of gas and solids (Zhu and Cheng, 2016). Inside CFB riser, particles are fluidized by up-flowing gas and particle cluster is formed due to hydrodynamic force (Cahyadi et al., 2017). As clusters have high solids holdup and large size, particles inside the cluster are sheltered from gas, resulting in the reduction of gas-particle contact (Li et al., 1998; Shi et al., 2008). Thus, understanding and characterization of particle cluster are crucial for the prediction of reactor performance and the development of numerical models.

Since the 1990s, cluster has been quantitatively characterized by many researchers (Harris et al., 2002; Cahyadi et al., 2017;). Cahyadi et al. (2017) well summarized reported cluster properties and found they have a severe discrepancy in magnitude. Johnsson et al. (1997), Mondal et al. (2015) and Varas et al. (2017) found that cluster properties extracted from experimental data are sensitive to cluster definitions. By applying the widely-used cluster definitions to the same experimental substrate, it has been found that the choose of cluster definitions can cause cluster time fraction and cluster size vary even in an order of magnitude (review). Thus, further exploration of cluster definition is imperative for cluster characterization.

In the literature, “Mean+N*std”, “Median” and “Wavelet cluster scale” are the most popular definitions to discriminate clusters (review). Soong et al. (1993) identified clusters using “Mean solids holdup plus N times standard deviation(σ)” as threshold : (1) the solid fraction in a cluster must be significantly above the time-averaged solid fraction at the same operating condition at the local position; (2) the perturbation in solid fraction due to the occurrence of clusters must be greater than the random fluctuations in the back ground solid fraction; (3) the concentration increase must be sensed for a sampling volume with characteristic length scale greater than 100 particle diameters. However, the choice of N is subjective to researchers. N has been assigned as 0 (Sharma et al., 2000), 2 (Tuzlan et al., 1998; Xu and Zhu, 2011), 1(Kiani et al., 2013) and 0.5 (Mondal et al., 2015). Manyele et

al. (2002) designated N with a value ranging from 1.0 to 1.4 based on sensitivity analysis. Later, Guenther and Breault (2007), Afsahi et al. (2009) and Firuzian et al. (2014) identified regions whose solids holdup is above “Median” solids holdup as clusters. But, this threshold results in that cluster time fraction remains 0.5 for all cases. Then, Yang and Leu (2009), as well as Chew et al. (2011, 2012a, 2012b), decomposed optical fiber probe signal using wavelet transform and discriminated clusters as regions where transient solids holdup exceeded the approximate signal of certain scale. Collectively, these cluster definitions determined cluster boundary using subjective thresholds. To settle this dispute on cluster characterization, a physically-meaningful method is in urgent need to determine cluster boundary.

In this work, flow details in a narrow rectangular riser have been well captured using a high-speed camera. With a verified correlation between grayscale and solids holdup (Yang and Zhu, 2014a; 2014b;), grayscale in images is converted to solids holdup pixel by pixel. Then, the solids holdup gradient is proposed to characterize the abrupt change of solids holdup in images. A sharp increase of solids holdup is found to exist around clusters and this is further confirmed using optical fiber probe. As the sharp increase of solids holdup is a physically-meaningful sign of phase segregation, clusters are defined as dense regions which are surrounded by abrupt solids holdup increase and cluster boundary is defined where solids holdup increases most abruptly. Finally, 978 clusters have been separated from their surrounding and characterized systematically in perspective of cluster threshold, cluster solids holdup, cluster length, cluster width, cluster equivalent diameter and cluster shape.

6.2 Experimental

6.2.1 Circulating fluidized bed (rectangular riser)

Circulating fluidized bed employed in this work consists of a riser, two cyclones at riser top, a bag filter, a downcomer and an inclined pipe connecting downcomer and riser bottom (see Figure 6-1). The riser is 7.6m high and has a rectangular cross-section which is 19 mm in thickness and 114 mm in width. Air is introduced from riser bottom and entrains particles from the inclined pipe to riser top. After that, gas-solid mixture enters

two cyclones in series and a bag filter where particles are collected to downcomer and air is released to the atmosphere. The upper part of downcomer is a cylindrical column (1.85m high and 203mm in diameter) and the lower part of downcomer is a rectangular column (203mm in width and 38 mm in thickness). In downcomer, solids fall to the particle storage tank and flow into riser again for another cycle through the inclined pipe at the bottom. Solids circulation rate is controlled using a flip valve installed at the inclined pipe and measured in the cylindrical column in the downcomer top. The air flow rate is controlled using a rotameter and its reading is further calibrated based on pressure at riser bottom. Particles circulating in this CFB were FCC (67 μm in Sauter mean diameter, 1877 kg/m^3 in density). Solids circulation rate, G_s , ranged from 50 to 150 $\text{kg}/(\text{m}^2 \text{ s})$, while the superficial gas velocity, U_g , ranged from 3.0 to 9.0 m/s .

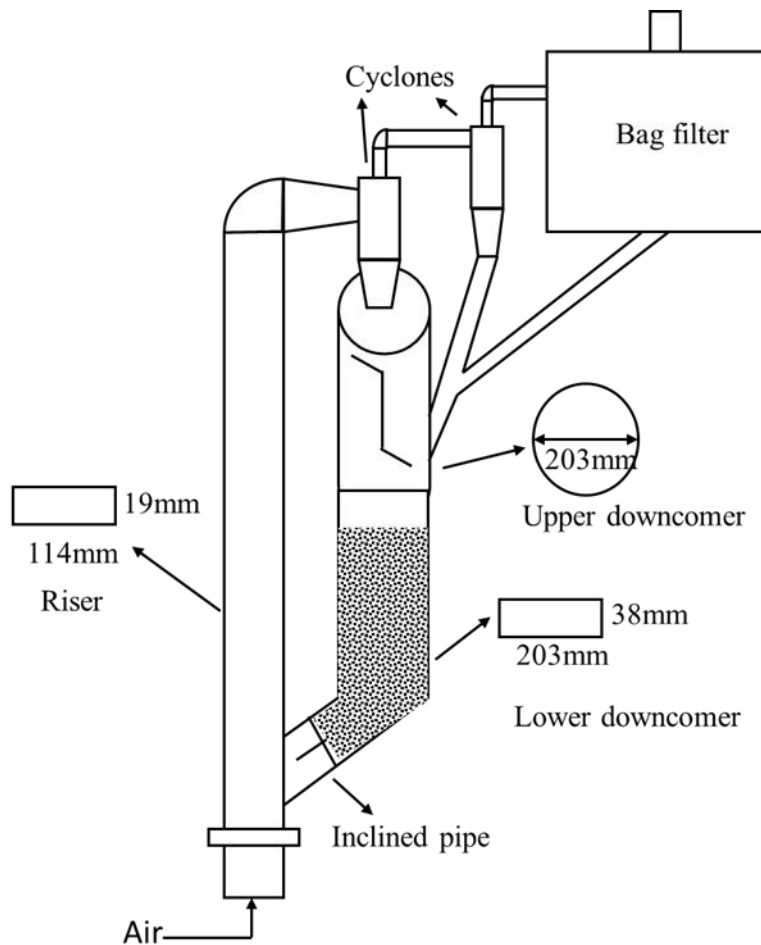


Figure 6-1 Schematic diagram of the circulating fluidized bed

6.2.2 Visualization system

A visualization system, consisting of a lamp, a diffusion panel, a high-speed camera, a blank box and a computer, was set up in the fully developed region ($H=5.33\text{m}$) of CFB riser (see Figure 6-2). The lamp is placed facing the riser and, through the diffusion panel, the visualization section is uniformly illuminated. Installed in the lamp is a 500 W quartz halogen bulb (4 - 5/8", T-3 lamp, L-16, The Designers Edge, USA), which can provide consistent lighting for 1500 h. The high-speed camera, Motion ScopeM2 from Redlake, is placed on the other side of the riser and covered in a blank box to eliminate lights from other sources. This high-speed video camera was equipped with a Pentax C21228TH 12.5 mm F1.8 manual lens. Frame rate has been set as 2000fps (frame per second) in order to capture the rapid flow behavior in the CFB riser. The recorded image covers this CFB riser from the left wall to the right wall. Each image is a matrix of pixels consisting of 568 columns and 256 rows. Every pixel denotes a $190\mu\text{m}$ square and is assigned a grayscale, ranging from 0 (darkest) to 255 (brightest). A correlation (Equation 6-1) between grayscale and solids holdup has been established and validated using optical fiber probe data (Yang and Zhu, 2014a; 2014b). A detailed description of this system has been elaborated in previous papers (Yang and Zhu, 2014a; 2014b;).

$$G = 28.0 + 228.3e^{(-19.62\varepsilon_s)} \quad \text{Equation 6-1}$$

G is grayscale;

ε_s is solids holdup;

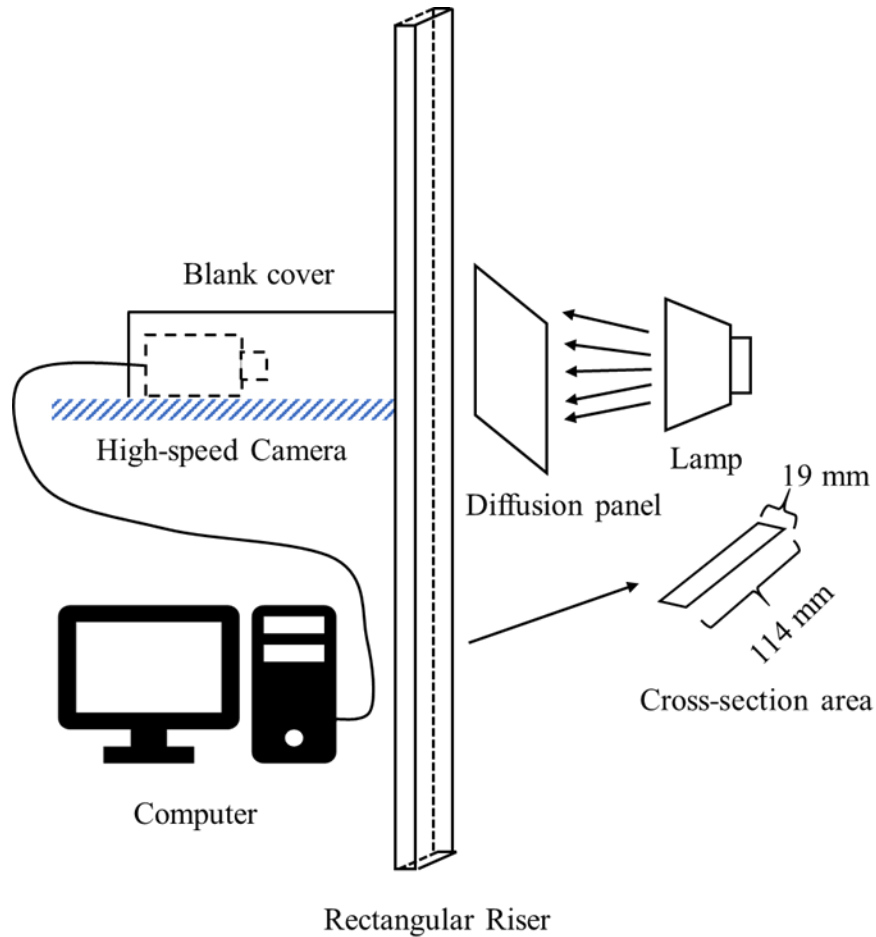


Figure 6-2 Schematic diagram of the visualization system

6.3 Results and discussion

6.3.1 Solids holdup gradient

In the CFB, grayscale does not directly correlate with the flow information and the analysis is suggested to be conducted in solids holdup domain (Liu et al., 2016). Images recorded using high-speed camera were read into MATLAB and the grayscale was converted to solids holdup through a verified correlation (Yang and Zhu, 2014a; 2014b). In image processing, the grayscale gradient is a commonly used parameter for boundary detection. Here, solids holdup gradient is proposed to analyze phase information in the CFB (see Equation 6-2, 6-3 and 6-4). For each pixel, there is a horizontal slope of solids

holdup and vertical slope of solids holdup. The magnitude of solids holdup gradient is computed based on solids holdup slopes.

$$S_h(i, j) = 0.5 \frac{\varepsilon_s(i, j-1) - \varepsilon_s(i, j+1)}{L} \quad \text{Equation 6-2}$$

$$S_v(i, j) = 0.5 \frac{\varepsilon_s(i-1, j) - \varepsilon_s(i+1, j)}{L} \quad \text{Equation 6-3}$$

$$Gr(i, j) = \sqrt{S_h(i, j)^2 + S_v(i, j)^2} \quad \text{Equation 6-4}$$

$\varepsilon_s(i-1, j)$ is the solids holdup at (i-1, j);

$\varepsilon_s(i+1, j)$ is the solids holdup at (i+1, j);

$\varepsilon_s(i, j-1)$ is the solids holdup at (i, j-1);

$\varepsilon_s(i, j+1)$ is the solids holdup at (i, j+1);

L is the distance between pixels, $190\mu m$;

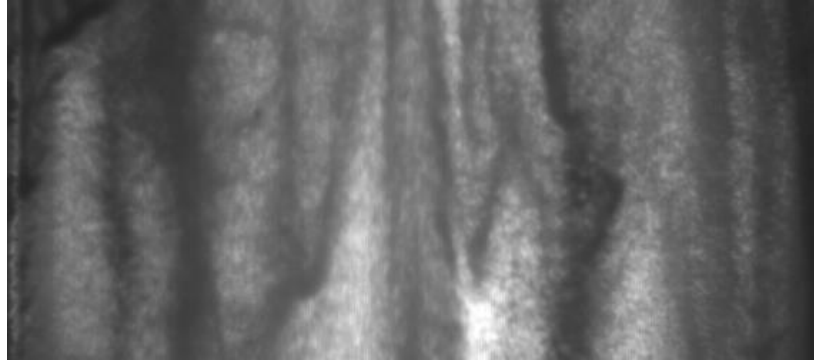
$S_h(i, j)$ is the solids holdup slope at (i, j) in horizontal direction;

$S_v(i, j)$ is the solids holdup slope at (i, j) in vertical direction;

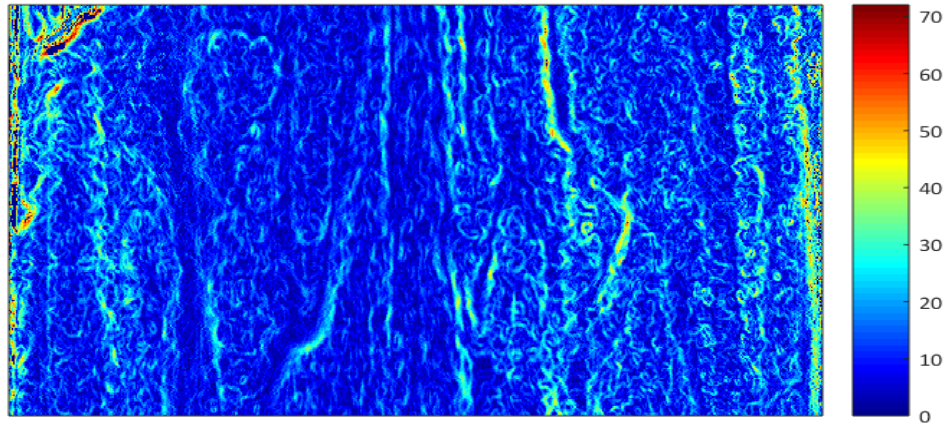
$Gr(i, j)$ is the solids holdup gradient at (i, j);

Map of solids holdup gradient was plotted for an example image (see Figure 6-3). The scope of images covers the CFB riser from left to right. High solids holdup gradient is ubiquitous across riser. Referring to the original image, high solids holdup gradient usually exists around dense regions. Moreover, there is more high solids holdup gradients in the wall region than that in the center region, indicating that gas-particle interaction is different in the riser center and riser wall. It has reached a quantitative consensus that clusters have much higher solids holdup than surrounding (review). To analyze the cluster boundary, clusters (dense regions) have been cropped from original images and their mapping of solids holdup gradient are shown in figure 6-4 where 1a-3a denotes the images for large clusters, 4a denotes the image for small clusters and 1b-4b are the

corresponding solids holdup gradient distribution. Regions in the cluster center and cluster surrounding have low solids holdup gradient. High solids holdup gradient is found to exist around clusters, but its magnitude varies from cluster to cluster. Solids holdup gradient around small clusters is less distinct than that for large clusters. Outlines of solids holdup gradient are not completely consecutive. Upwind regions tend to have high solids holdup gradient. For some clusters, cluster top may also have high solids holdup gradient, and this may relate to low-pressure zones behind clusters formed by gas flowing-around. An abrupt increase of solids holdup around cluster may correspond to high gas resistance and be responsible for sheltering particles from gas. Even though further study is needed to address how solids holdup gradient influences gas-particle interaction, it is reasonable to consider the abrupt increase of solids holdup as a sign of phase segregation.



(a)



(b)

Figure 6-3 Distribution of solids holdup gradient across riser (a: the original image, b: the map of solids holdup gradient)

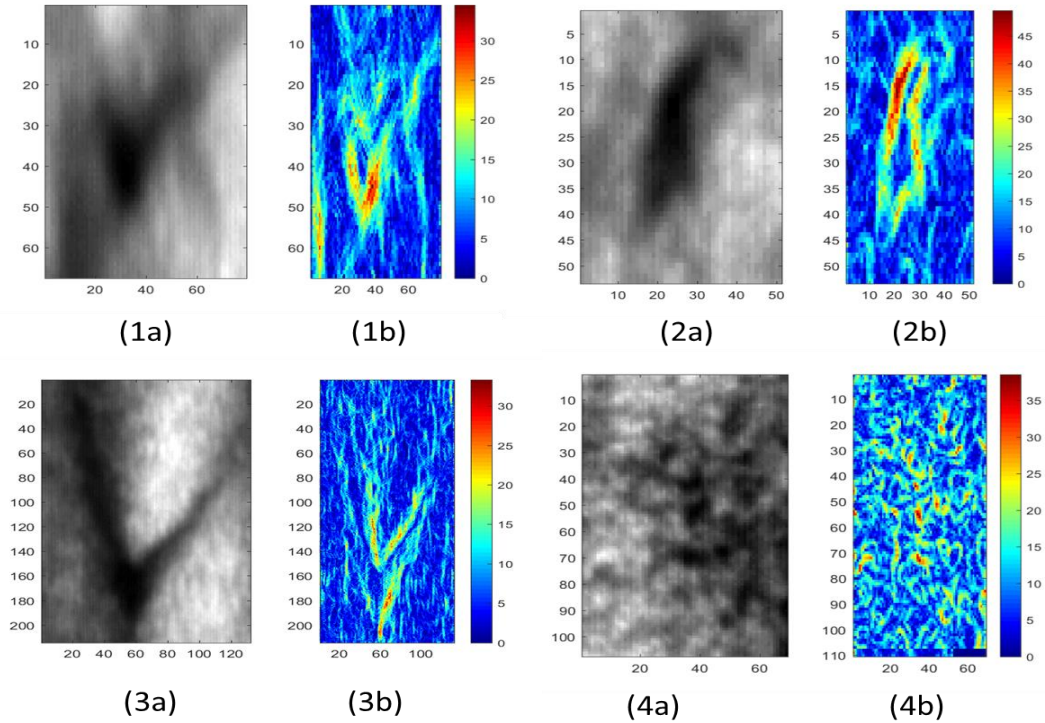


Figure 6-4 Distribution of solids holdup gradient around clusters

To verify the existence of abrupt increase of solids holdup around clusters, instantaneous solids holdup has been detected using an optical fiber probe. Optical fiber probe was inserted into CFB riser. At probe tip, there is measuring windows consisting of thousands of fibers (emitting fibers and receiving fibers). Light emitted from emitting fibers hits particles and reflected to receiving fibers. More particles appear, higher light intensity reflected. Based on that, light intensity was calibrated with solids holdup (Zhang et al., 1998). As optical fiber probe only captures one-dimensional solids holdup information, solids holdup slope, the absolute difference between adjacent points, has been used to characterize the abrupt solids holdup change. After denoise using wavelet transform, solids holdup signal and its slope information were plotted versus time in figure 6-5. Peaks in signal represent particle clusters according to the previous study (chapter 4; Soong et al., 1994). Higher solids holdup slope is found to exist around clusters (inside dash rectangular), which agrees well with the information obtained from images. However, this characteristic is missing for some clusters (inside solid-line rectangular),

which may owe that (1) abrupt solids holdup increase is not consecutive around clusters (2) one-dimensional signal may miss high solids holdup increase region around some clusters.

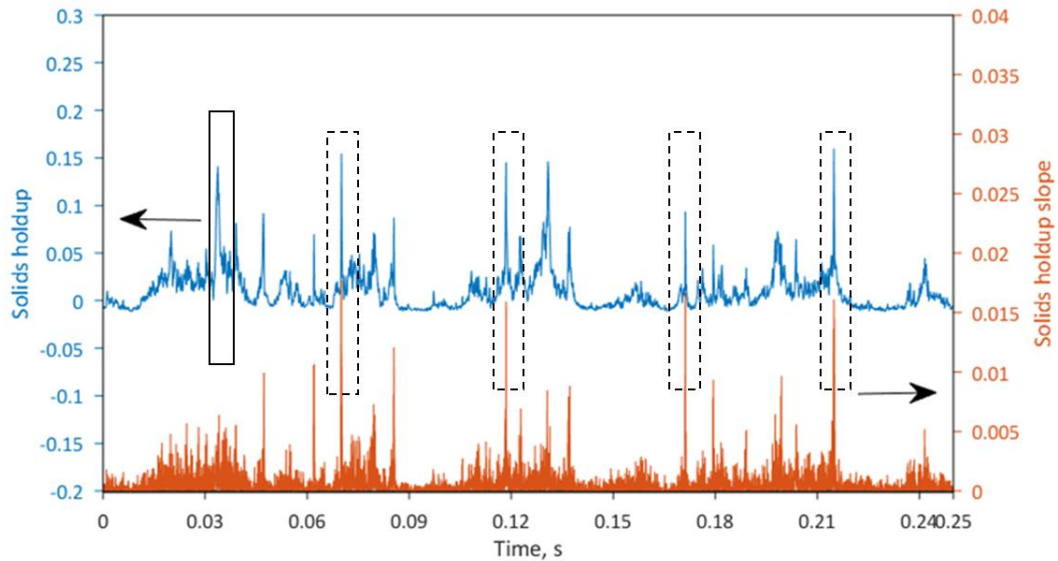


Figure 6-5 Solids holdup slopes captured using optical fiber probe

6.3.2 Determination of cluster boundary

Based on previous observation, the cluster is defined as dense regions whose solids holdup increases monotonically and sharply from surrounding (chapter 2; chapter 4). Solids holdup gradient, as an evident sign for phase segregation, provides a clue for the physically meaningful determination of cluster boundary. Here, cluster boundary is defined where solids holdup increases most abruptly. Then, a MATLAB procedure has been proposed to locate cluster boundary, to isolate clusters from surrounding and to analyze cluster information, including solids holdup, radial position (centroid), project width, projected length and equivariant diameter (demonstrated in Figure 6-6):

1. Read the acquired images to MATLAB, convert the grayscale to solids holdup pixel-wisely and draw the solids holdup map.
2. Interact with the solids holdup map and crop a rectangular region, which contains one major cluster (see 6-6b).

3. Calculate the map of solids holdup gradient for the selected region using the equation 6-2, 6-3, 6-4, pixel-wisely. “Salt-and-pepper” noise presents itself as sparsely occurring white and black pixels and may generate extremely high solids holdup gradient. According to statistical analysis, pixels whose solids holdup gradient is higher than 53 m^{-1} are considered to be noise pixels and discarded in the following analysis.
4. Binarize cropped the image using thresholds varying from 0 to 0.15 with a step as low as 0.0015, record the coordinates of cluster outline for each threshold, then take the average of solids holdup gradient (referring to solids holdup gradient map in step 3) on outline coordinates (see 6-6c).
5. Consider solids holdup which corresponds to the highest solids holdup gradient as the physically meaningful threshold.
6. Discriminate the major cluster using the physically meaningful threshold (see 6-6d), consider the largest consecutive area as major cluster, then compute cluster properties, including solids holdup threshold, cluster solids holdup, cluster area, cluster size (equivalent diameter), radial position (centroid), cluster perimeter, cluster projection length and cluster projection width.

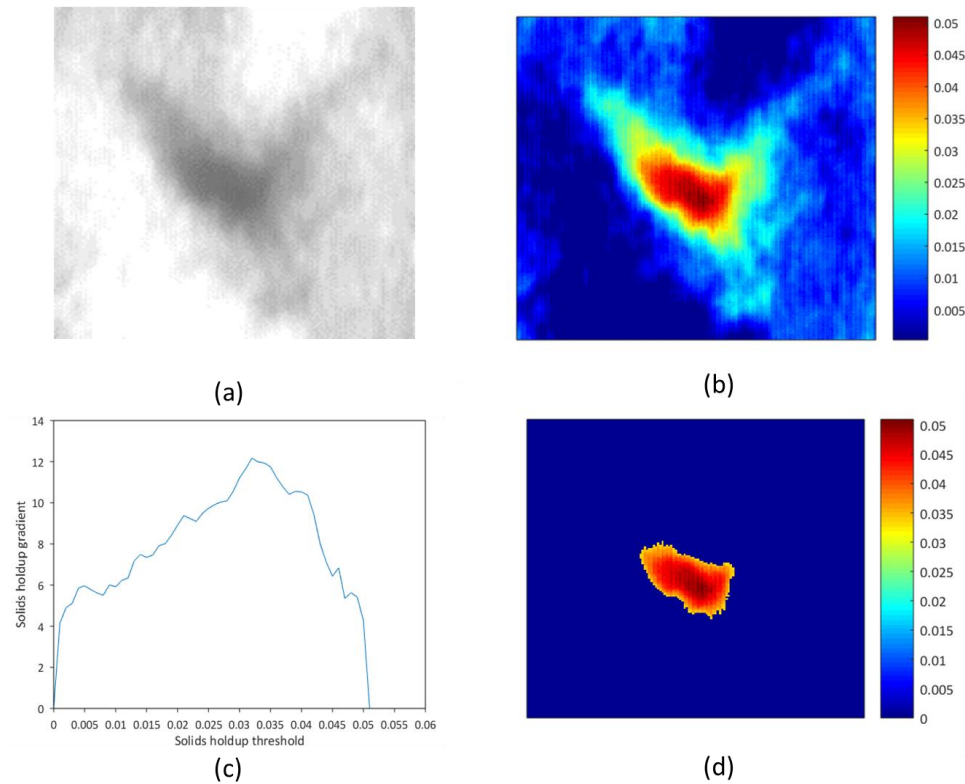


Figure 6-6 Determination of cluster boundary

6.3.3 Cluster dimensions and shape

As clusters have irregular and different shapes (Bi et al., 1993; Zou et al., 1994; chapter 4), projected length, projected width and equivalent diameter are employed to characterize cluster dimensions and shape in this work. The projected length and Projected width are the lengths of projections in vertical and horizontal directions. Equivalent diameter is the diameter of a circle whose area is the same with the acquired cluster. Cluster dimensions were first plotted versus the corresponding radial positions (see Figure 6-7). Clusters near the riser wall have lower projected length, lower projected width and lower equivalent diameter than clusters in the riser center. Moreover, the variation of these parameters is also lower in the wall region than that in the riser center. This may attribute to the vigorous collision between particle-cluster and cluster-cluster in the riser wall, as solids holdup in the riser wall is much higher than that in the riser center (Wang et al. 2014).

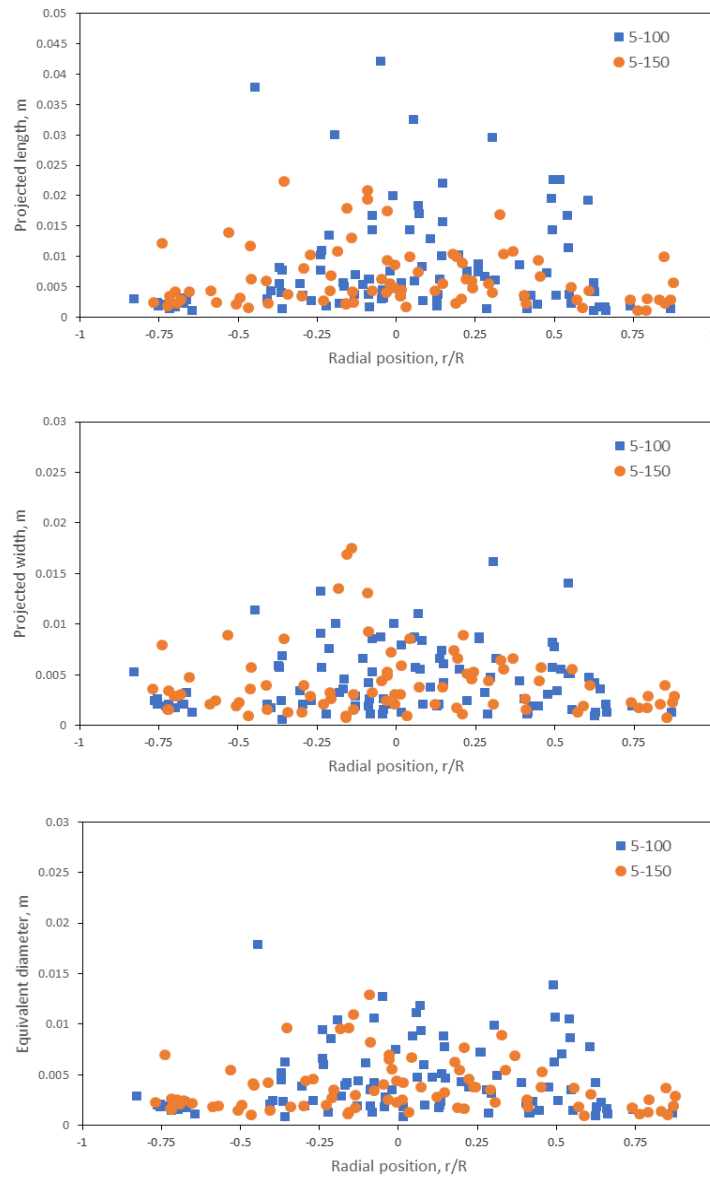


Figure 6-7 Radial distributions of cluster dimensions

To analyze cluster shape, projected length and projected width were further plotted versus equivalent diameter (see Figure 6-8). Both projected length and projected width increase with equivalent diameter. However, the increase of projected length is more significant than that of projected width, indicating that large clusters tend to have a higher ratio between projected length and projected width. Additionally, projected length is

higher than the projected width for most clusters. In the CFB riser, gas entrains particle upward and projected width directly relates with upwind area. Shear force would increase dramatically with projected width and clusters are elongated vertically.

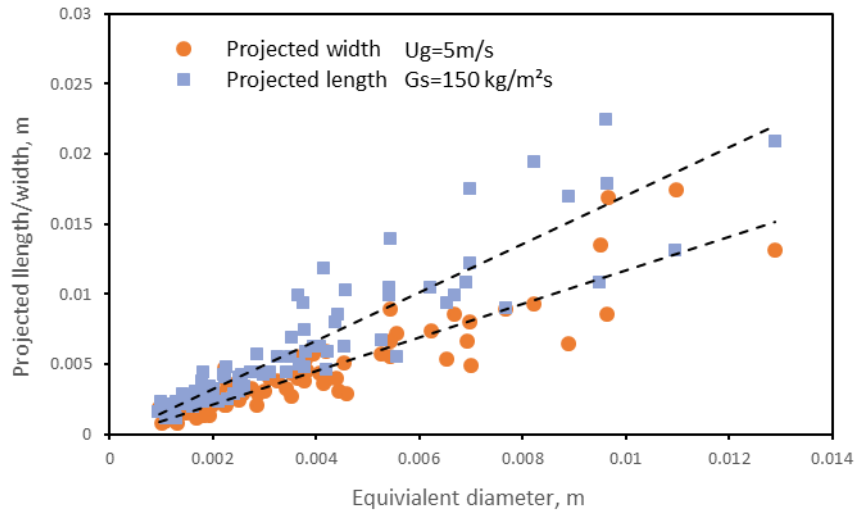


Figure 6-8 Relationship between projected length/ width and equivalent diameter

In addition, circularity, a ratio between area and square of the perimeter (see Equation 6-5), is also employed to qualitatively analyze cluster shape. Circularity is one for a perfect circle. The closer circularity is to one, the more similar the shape is to circle. Cluster circularity was plotted versus equivalent diameter (see Figure 6-9). Generally, circularity decreases with equivalent diameter, indicating small clusters tend to be more similar to a sphere than large clusters.

$$e = \frac{4\pi S}{P^2} \quad \text{Equation 6-5}$$

e is circularity;

S is cluster area, [m^2];

P is cluster perimeter, [m];

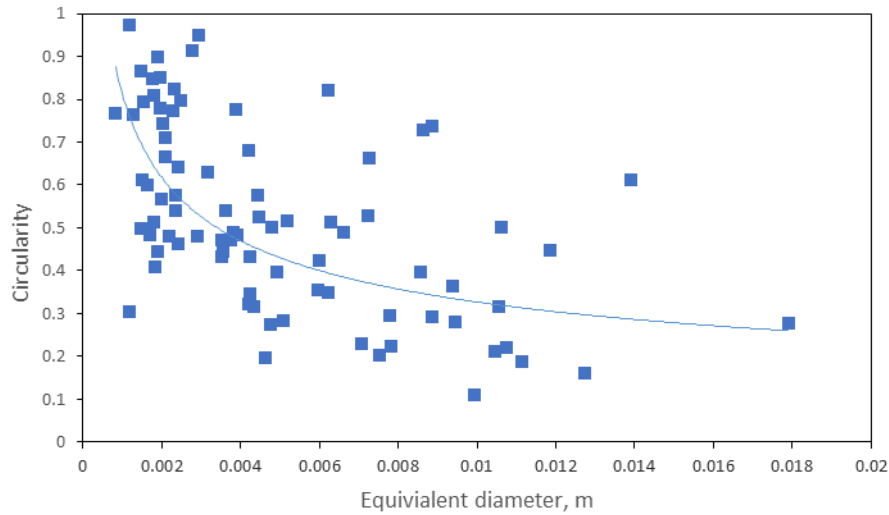


Figure 6-9 Circularity versus equivalent diameter

Here, average projected length, average projected width and average equivalent diameter at different operating conditions were computed and plotted versus operating conditions in figure 6-10. Generally, average projected length, average projected width and average equivalent diameter are in the same order of magnitude and change in the same tendency with operating conditions. As for the relative magnitude, the average projected length is the largest, the average projected width is medium and the average equivalent diameter is smallest. The average projected width and average equivalent diameter are close at all operating conditions, while the average projected length is much larger than them, especially at high superficial gas velocity. This may owe to that higher superficial gas velocity elongates the clusters. Collectively, the equivalent diameter is recommended to represent cluster size, as it both reflects cluster dimension two-dimensionally and is close to projected width which is a crucial parameter for gas drag. Hereafter, the equivalent diameter is referred as cluster size. At $U_g = 3$ m/s, average cluster size remains stable with solids circulation rate. At $U_g = 5$ m/s, average cluster size first increases, then decreases with solids circulation rate. At $U_g = 7$ m/s and $U_g = 9$ m/s, average cluster size first increases with solids circulation rate. The average cluster size has a complicated relationship with operating conditions. Further investigation at a wider range is suggested for a comprehensive understanding.

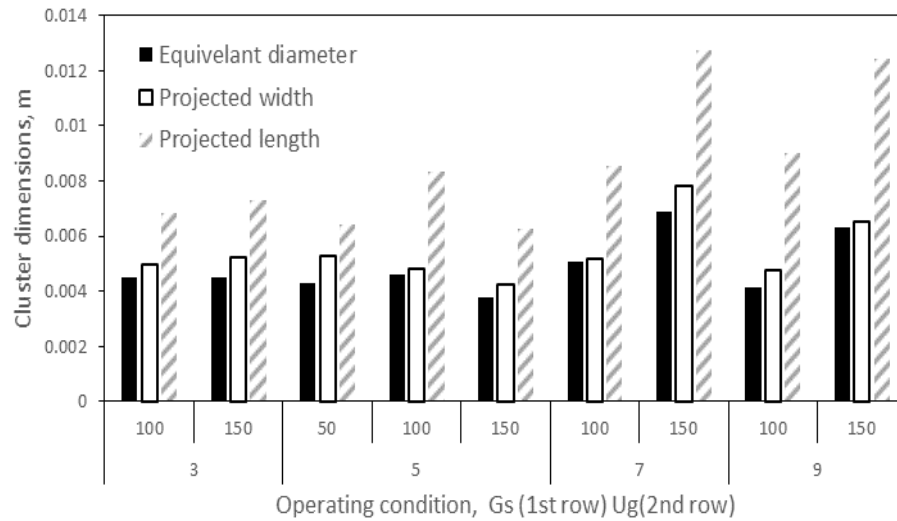


Figure 6-10 cluster dimensions versus operating conditions

Probability density distribution of cluster size was plotted in Figure 6-11. The probability decreases significantly with the increasing cluster size, which agrees well with previous studies (Li et al., 1995). Large clusters may easily get disintegrated, as their large size may induce a high probability of collision.

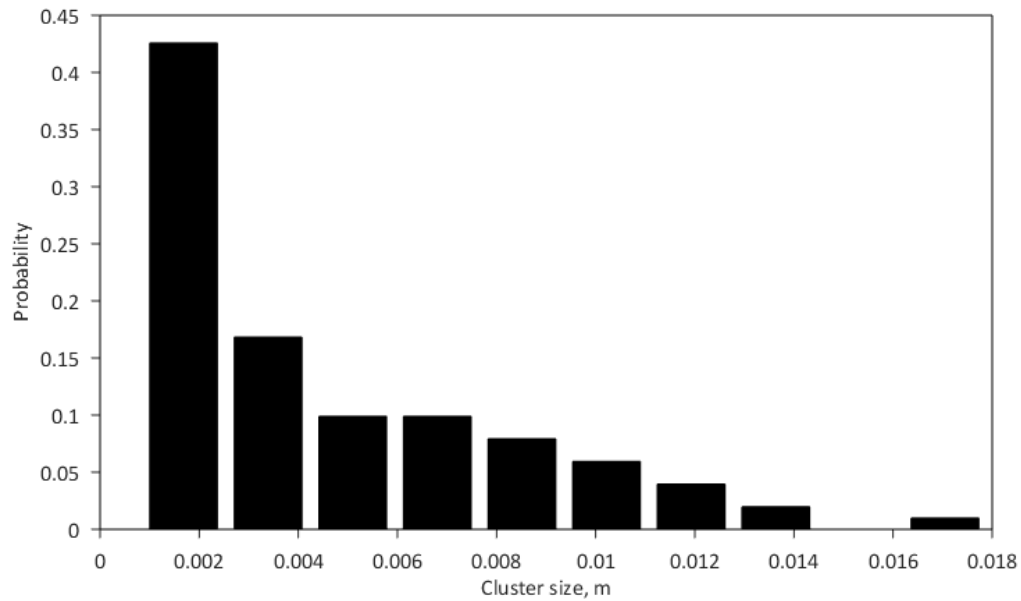


Figure 6-11 Probability density distribution of cluster size

6.3.4 Cluster solids holdup

Cluster solids holdup is a key parameter to indicate the degree of aggregation. Cluster solids holdup was plotted versus the corresponding radial positions in Figure 6-12. In general, cluster solids holdup increases from riser center to riser wall and clusters tend to have high solids holdup at high solids circulation rate. Cluster solids holdup has a high variation, even at similar radial positions, implying cluster solids holdup may relate directly with the instantaneous local conditions. According to previous observation, the alternative appearance of the crest phase and trough phase in the CFB causes evident solids holdup fluctuation in macroscope, which may result in the variation of cluster solids holdup (chapter 4). Cluster solids holdup was also plotted versus cluster size (see Figure 6-13). Small clusters have a wider cluster solids holdup span, compared with large clusters. This trend may be attributed to the facts that (1) clusters in the riser wall have higher solids holdup than that in the riser center, (2) small clusters appear across riser, (3) large clusters mainly exist in the riser center. Statistic cluster solids holdup was plotted versus operating conditions in Figure 6-14. Generally, the statistic cluster solids holdup decreases with superficial gas velocity. Statistic cluster solids holdup at $G_s=100 \text{ kg/m}^2\text{s}$ decreases more significantly with superficial gas velocity than that at $G_s=150 \text{ kg/m}^2\text{s}$.

This trend of cluster solid holdup is consistent with mean solids holdup (Xu and Zhu, 2010).

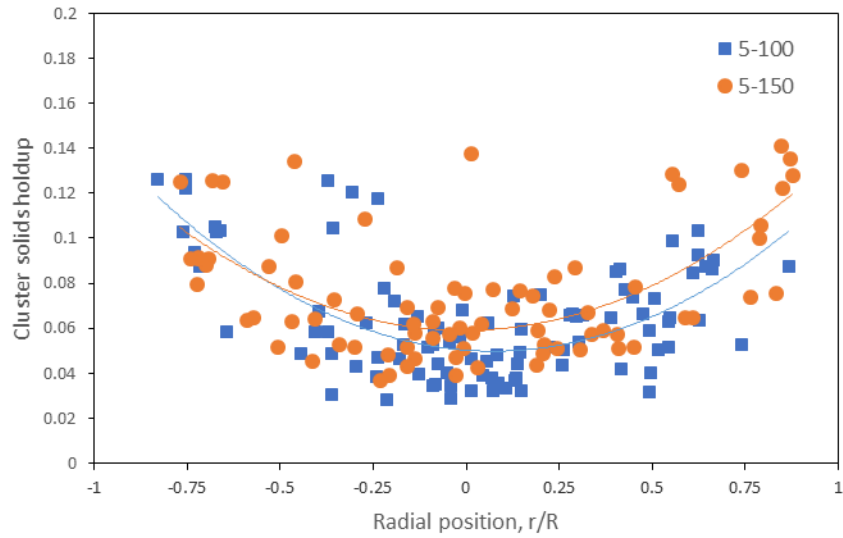


Figure 6-12 Radial distributions of cluster solids holdup

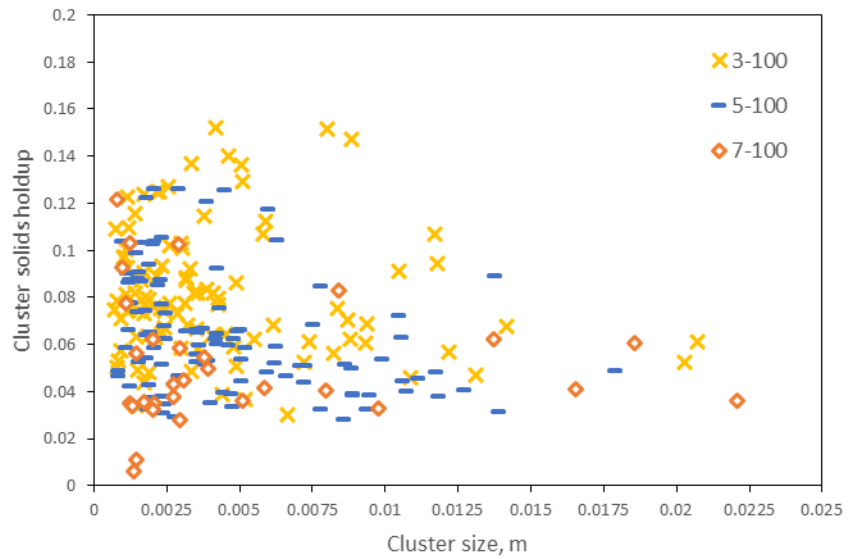


Figure 6-13 Relationship between cluster solids holdup and cluster size

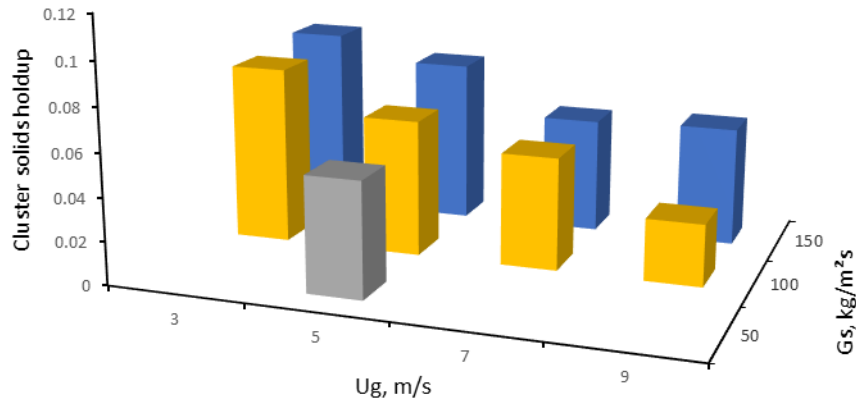


Figure 6-14 Cluster solids holdup versus operating conditions

6.4 Conclusions

Aiming to settle the severe discrepancy of cluster properties in the literature, this work seeks a physically-meaningful method to determine of cluster boundary. First, gas-solid suspension in the CFB riser has been well recorded using a high-speed camera. With the help of a verified correlation, grayscales were converted to solids holdup. Then, the solids holdup gradient is proposed to analyze the phase boundary in the CFB. With the verification using an optical fiber probe, the abrupt increase of solids holdup has been identified around the cluster, indicating the existence of objective boundary around clusters. Based on the previous study, the cluster has been defined as dense regions whose solids holdup increases monotonically and sharply from the surrounding. In this work, the cluster boundary is defined where solids holdup increase is sharpest. Using MATLAB, clusters are characterized in terms of cluster solids holdup, projected length, projected width, equivalent diameter and radial position. It has been found that:

1. Generally, cluster dimensions reduce from riser center to riser wall and cluster dimensions in the riser center vary much more significantly than that in the riser wall.

2. Circularity decreases with increasing cluster size. Large clusters tend to have higher ratio between projected length and projected width.
3. Appearance probability decreases with increasing cluster size.
4. Projected length, projected width and cluster size (equivalent diameter) change with operating conditions in the same tendency, but projected length becomes much larger at high superficial gas velocity due to the elongation effect.
5. Cluster solids holdup is generally higher in the riser wall and lower in the riser center. Variation of cluster solids holdup still exists even at the same radial positions and it may owe to the fluctuation of solids holdup in macroscope.
6. Small clusters tend to have a higher span of solids holdup than large clusters.
7. Cluster solids holdup decreases with superficial gas velocity.

References

- Afsahi, F. A., Sotudeh - Gharebagh, R., & Mostoufi, N. (2009). Clusters identification and characterization in a gas - solid fluidized bed by the wavelet analysis. *The Canadian Journal of Chemical Engineering*, 87(3), 375-385.
- Bi, H. T., Zhu, J. X., Jin, Y., & Yu, Z. Q. (1993, October). Forms of particle aggregations in the CFB. In *Proceedings of the Sixth Chinese Conference on Fluidization*, Wuhan, China (pp. 162-167).
- Cahyadi, A., Anantharaman, A., Yang, S., Karri, S. R., Findlay, J. G., Cocco, R. A., & Chew, J. W. (2017). Review of cluster characteristics in circulating fluidized bed (CFB) risers. *Chemical Engineering Science*, 158, 70-95.
- Firuzian, N., Sotudeh-Gharebagh, R., & Mostoufi, N. (2014). Experimental investigation of cluster properties in dense gas-solid fluidized beds of different diameters. *Particuology*, 16, 69-74.
- Guenther, C., & Breault, R. (2007). Wavelet analysis to characterize cluster dynamics in a circulating fluidized bed. *Powder Technology*, 173(3), 163-173.
- Harris, A. T., Davidson, J. F., & Thorpe, R. B. (2002). The prediction of particle cluster properties in the near wall region of a vertical riser (200157). *Powder Technology*, 127(2), 128-143.
- Johnsson, F., Zhang, W., Johnsson, H., & Leckner, B. (1997). Optical and momentum probe measurements in a CFB furnace. *Circulating fluidized bed technology V* (pp. 652-657). Science Press Beijing.
- Kiani, A., Sotudeh-Gharebagh, R., & Mostoufi, N. (2013). Cluster size distribution in the freeboard of a gas-solid fluidized bed. *Powder technology*, 246, 1-6.
- Li, H., Zhu, Q., Liu, H., & Zhou, Y. (1995). The cluster size distribution and motion behavior in a fast fluidized bed. *Powder Technology*, 84(3), 241-246.

Li, J., Zhang, X. P., Zhu, J., & Li, J. H. (1998). Effects of cluster behavior on gas-solid mass transfer in circulating fluidized beds. 9th Engineering Foundation Conference on Fluidization, (pp. 17-22). DURANGO, CO.

Liu, X., Jiang, Y., Zhang, N., & Li, J. (2016). Gas penetrating flow through dynamic particle clusters. *Powder Technology*, 297, 409-414.

Manyele, S. V., Pärssinen, J. H., & Zhu, J. X. (2002). Characterizing particle aggregates in a high-density and high-flux CFB riser. *Chemical Engineering Journal*, 88(1), 151-161.

Mondal, D. N., Kallio, S., & Saxén, H. (2015). Length scales of solid clusters in a two-dimensional circulating fluidized bed of Geldart B particles. *Powder Technology*, 269, 207-218.

Sharma, A. K., Tuzla, K., Matsen, J., & Chen, J. C. (2000). Parametric effects of particle size and gas velocity on cluster characteristics in fast fluidized beds. *Powder Technology*, 111(1), 114-122.

Shi, H., Wang, Q., Xu, L., Luo, Z., & Cen, K. (2008). Visualization of clusters in a circulating fluidized bed by means of particle-imaging velocimetry (PIV) technique. In *Proceedings of the 9th International Conference on Circulating Fluidized Beds*, Hamburg, Germany (pp. 1013-1019).

Soong, C. H., Tuzla, K., & Chen, J. C. (1994). Identification of particle clusters in circulating fluidized bed. *Circulating fluidized bed technology*, 4, 615-620.

Tuzla, K., Sharma, A. K., Chen, J. C., Schiewe, T., Wirth, K. E., & Molerus, O. (1998). Transient dynamics of solid concentration in downer fluidized bed. *Powder Technology*, 100(2-3), 166-172.

Varas, A. C., Peters, E. A. J. F., & Kuipers, J. A. M. (2017). Experimental study of full field riser hydrodynamics by PIV/DIA coupling. *Powder Technology*, 313, 402-416.

Wang, C., Zhu, J., Barghi, S., & Li, C. (2014). Axial and radial development of solids holdup in a high flux/density gas–solids circulating fluidized bed. *Chemical Engineering Science*, 108, 233-243.

Xu, J., & Zhu, J. (2011). A new method for the determination of cluster velocity and size in a circulating fluidized bed. *Industrial & Engineering Chemistry Research*, 51(4), 2143-2151.

Xu, J., & Zhu, J. X. (2010). Experimental study on solids concentration distribution in a two-dimensional circulating fluidized bed. *Chemical Engineering Science*, 65(20), 5447-5454.

Yang, J., & Zhu, J. (2014a). A novel method based on image processing to visualize clusters in a rectangular circulating fluidized bed riser. *Powder Technology*, 254, 407-415.

Yang, J., & Zhu, J. (2014b). An alternative method for mapping solids holdup in a narrow rectangular CFB riser through image calibration. *The Canadian Journal of Chemical Engineering*, 92(12), 2202-2210.

Yang, T. Y., & Leu, L. P. (2009). Multiresolution analysis on identification and dynamics of clusters in a circulating fluidized bed. *AIChE journal*, 55(3), 612-629.

Zhang, H., Johnston, P. M., Zhu, J. X., De Lasa, H. I., & Bergougnou, M. A. (1998). A novel calibration procedure for a fiber optic solids concentration probe. *Powder Technology*, 100(2-3), 260-272.

Zhu, J., & Cheng, Y. (2016). Applications of Fluidized Bed Reactors. In Michaelides, E., Crowe, C. T., & Schwarzkopf, J. D. (Eds.). *Multiphase Flow Handbook* (pp.1029-1058). CRC Press.

Zou, B., Li, H., Xia, Y., & Ma, X. (1994). Cluster structure in a circulating fluidized bed. *Powder Technology*, 78(2), 173-178.

CHAPTER 7

A comprehensive characterization of aggregative flow in gas- solid circulating fluidized bed using wavelet analysis

Abstract

The gas-solid circulating fluidized bed (CFB) riser has many applications in chemical industry and its performance essentially relies on the thorough contact between gas and particles. However, particles tend to form dense aggregations in the CFB riser, resulting in the reduction of the contact efficiency. Thus, analysis of particle aggregations is imperative for a thorough understanding of CFB. With the help of a high-speed camera and optical fiber probe, the instantaneous flow structure in the CFB riser has already been analyzed in our early studies. In macroscope, trough phase and crest phase are identified as continuous dilute and continuous dense regions. Within the trough phase, there are trough clusters and dispersed particles. Within the crest phase, there are crest clusters and coalesced particles. Aiming to quantitatively characterize these phases across riser, optical fiber probe was employed in this work to detect local instantaneous solids holdup. Wavelet analysis, which can analyze signal characteristics accurately both in temporal and frequency domain, was used to extract phase information from time-series signals. With verification using a high-speed camera, phase information was discussed in perspectives of solids holdup, length, frequency and time fraction. In order to explore the flow mechanism, phases in the CFB are also compared between FCC system and glass beads system. Collectively, this study deepens the understanding of flow behavior in the CFB and is owed to contribute to the development of numerical models.

Keywords: crest clusters; trough clusters; crest phase; aggregation; optical fiber probe; circulating fluidized bed; wavelet analysis;

7.1 Introduction

The gas-solid circulating fluidized bed (CFB) riser has been applied to catalytic reactions where particles serve as catalyst (fluid catalytic cracking, Fischer–Tropsch synthesis) and non-catalytic reactions where particles are reactant (calcination, gasification and combustion) in industry. In either case, it is desired to have a through contact between gas and particles. However, some particles form dense aggregations which shelter internal particles away from the main gas stream (chapter 4; Yunhau et al., 2006). Thus, many researchers have been working on the observation, identification and characterization of particle aggregations.

Wilhelm and Kwauk (1948) first observed “aggregative fluidization” in the fluidized bed. Then, particle aggregations were recorded with the help of a high-speed camera (Li et al., 1991; Takeuchi and Hirama, 1991; Rhodes et al., 1992; Bi et al., 1993; Zou et al., 1994; Matsuda et al., 1996; Takeuchi et al., 1996; Horio and Kuroki, 1994; Shaffer et al., 2013;). Bi et al. (1993) and Shi et al. (2008) preliminarily classified particle aggregations based on qualitative observation. However, solids holdup analysis of images was not achieved until Yang and Zhu (2015a, 2015b) calibrated grayscale with solids holdup. Based on the flow behaviors captured using a high-speed camera, multiscale structure co-exists in the CFB riser (chapter 4). Macroscopically, there is trough phase and crest phase. Within the trough phase, there are dispersed particles and trough clusters in microscope. Within the crest phase, there is coalesced particles and crest clusters in microscope. Then, this understanding has been verified using optical fiber probe (review). Solids holdup signals acquired with an optical fiber probe is a hybrid of narrow peaks and crescents which correspond to clusters and crest phase respectively.

Besides qualitative observation, particle aggregations have also been quantitatively characterized in the literature. Brereton and Grace (1993) proposed an intermittency index to characterize gas-particle segregation in the CFB riser. Manyele et al. (2002) analyzed particle aggregations in a high-flux riser (up to $550 \text{ kg/m}^2 \text{ s}$) using an optical fiber probe. Xu and Zhu (2011a, 2011b) compared particle aggregations formed by various particles using both the high-speed camera and optical fiber probe. Chew et al.

(2012a, 2012b) investigated how particle size distribution influence cluster properties using optical fiber probe. However, there are several types of particle aggregation and detailed analysis of each aggregation phase remains lacking (review).

In this work, instantaneous solids holdup has been measured using a dual-channel optical fiber probe. Acquired solids holdup signals were decomposed to narrow peaks (corresponding to clusters) and macro waves (corresponding to crest phase) using wavelet transform. Cluster information in this work is found to agree well with that originated from images. Then, clusters are further classified into trough clusters and crest clusters based on whether they are surrounded by dispersed particles or coalesced particles. Finally, phase information has been quantitatively characterized in terms of solids holdup, length, frequency and time fraction. In addition, phases formed by FCC (group A) and glass beads (group B) are also compared systematically in order to explore the flow mechanism,

7.2 Experimental

7.2.1 Circulating fluidized bed (rectangular riser)

The circulating fluidized bed we used consists of a rectangular riser (19 mm in thickness, 114 mm in width, 7.6m in height), two cyclones in series, a bag filter, a downcomer and an inclined pipe connecting riser bottom and downcomer bottom (see Figure 7-1). At riser bottom, gas is introduced through a distributor and particles flow into riser through the inclined pipe with the help of aeration gas. Then, this gas-solid mixture flow to riser top and enters cyclones and the bag filter for separation. After that, gas is released to atmosphere and particles are recovered to downcomer. Finally, particles flow to the downcomer bottom, then to the riser for another circulation. The air flow rate is regulated using a rotameter and solids circulation rate is controlled using a valve installed on the inclined pipe connecting riser bottom and downcomer bottom. A detailed description of this CFB apparatus can be found in previous papers (Yang and Zhu, 2014a; Yang and Zhu, 2014b;). The particles circulating in this CFB were FCC (group A powder, 67 μm , 1877 kg/m^3) and glass beads (group B powder, 288 μm , 2498 kg/m^3). Detailed particle properties are shown in Table 7-1 (Xu and Zhu,2010). Solids circulation rate, G_s , ranged

from 50 to 200 kg/m² s, while the superficial gas velocity, U_g , ranged from 3.5 to 6.5 m/s.

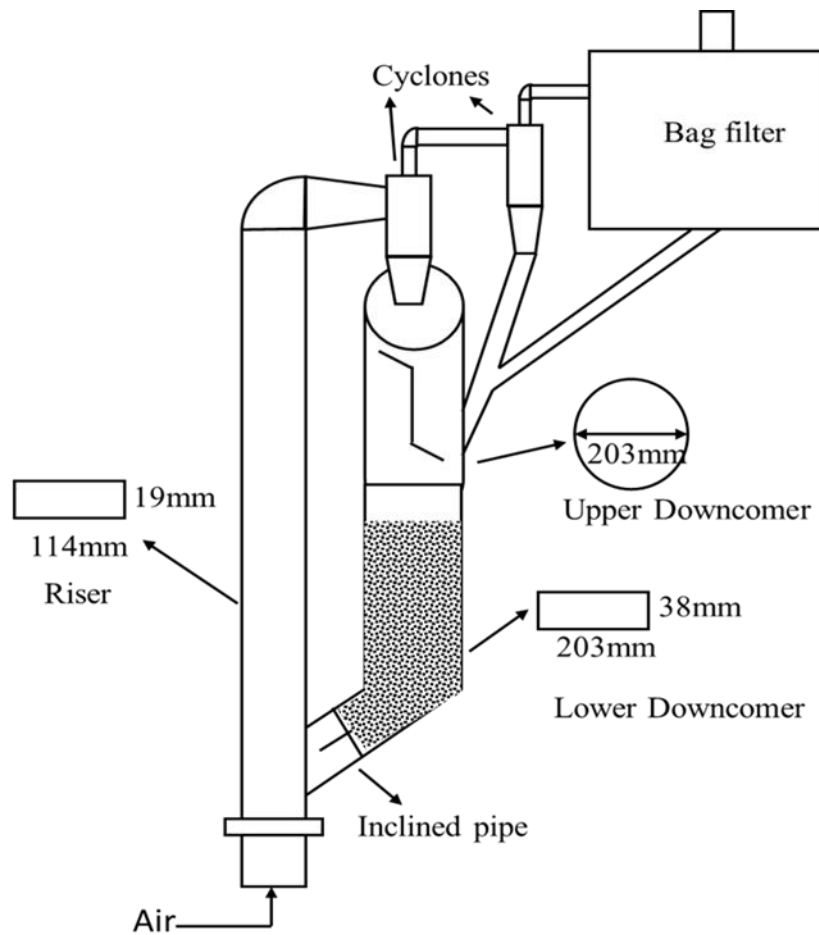


Figure 7-1 Schematic diagram of the circulating fluidized bed

Table 7-1 Information of particle properties

Particles	FCC Glass beads	
Particle Sauter mean diameter (μm)	67	288
Particle density (kg/m^3)	1877	2498
Bulk density (kg/m^3)	1125	1475
Sphericity (-)	0.95	~ 1
Particle terminal velocity (m/s)	0.26	3.73
Particle Group	A	B

7.2.2 Optical fiber probe

Optical fiber probe has been positioned in the CFB riser to detect local solids holdup. The optical fiber probe in this work is a multi-fiber probe, PV6, with a diameter of 3.8 mm. It has two measuring windows (1mm ×1mm) aligned vertically. Each measuring window consists of 8000 fibers (15 μ m) either receiving or emitting light. Light from emitting fibers strikes particles appearing at the probe tip and reflected to receiving fibers. The sampling frequency is set to be 100kHz for a good resolution. The intensity of reflected light is then translated to a voltage value. The calibration between solids holdup and signal voltage has been established using a slim downer. Particle velocity is calculated based on the cross-correlation of the signals obtained from two measuring windows. Details of the measuring principle and calibration were elaborated in previous papers (Xu and Zhu, 2010; Wang, 2013). Along CFB riser, there is acceleration region where particles are accelerating and fully developed region where solids have already been fully accelerated. The measuring locations include 6 heights (H=1.27m, 2.29m, 3.30m, 4.32m, 5.33m, 6.35m) and each height contains 9 lateral positions ($r/R=-0.98, -0.75, -0.5, -0.25, 0, 0.25, 0.5, 0.75, 0.98$). According to the previous study on the hydrodynamics, 1.27m, 2.29m and 3.30m located in acceleration region and 4.32m, 5.33m and 6.35m belong to the fully developed region (Xu and Zhu, 2010).

7.2.3 Signal details

With the help of a high-speed camera, solids holdup signals acquired using optical fiber probe have already been interpreted physically: peaks inside crescents, remaining regions in crescents, peaks outside crescents, remaining regions outside crescents correspond to crest clusters, coalesced particles, trough clusters and dispersed particles, respectively (see Figure 7-2). Here, the wavelet transform was employed to analyze signal details and to extract phase inform from probe signals. Essentially, wavelet transform views signal as a summation of various wavelets and the wavelets, according to its characteristics, are classified into a series of scales (frequency bands). The original signal is first decomposed to detail signal (d1) and approximate signal (a1) in scale 1. d1 contains information spanning from 0.5^* sampling frequency to sampling frequency, while a1 contains information spanning from 0 to 0.5^* sampling frequency. Then, approximate

signal (a1) is decomposed to detail signal (d2) and approximate signal (a2) in scale 2. d2 contains information spanning from $0.25 \times$ sampling frequency to $0.5 \times$ sampling frequency, while a2 contains information spanning from 0 to $0.25 \times$ sampling frequency. This process is continued until the desired scale has been reached (see Figure 7-3). Worth noted is that, original solids holdup signal can be well reconstructed by adding up $d1, d2, d3 \dots dn$ and a_n . Collectively, the waveforms in the signal are localized in both time and scale. Details of the principle have been elaborated in previous papers (Chew et al., 2011; 2012a; 2012b;). In this work, DB3 (Daubechies Wavelet of order three) is used, since it is symmetrical and results in low residues (Chew et al., 2011).

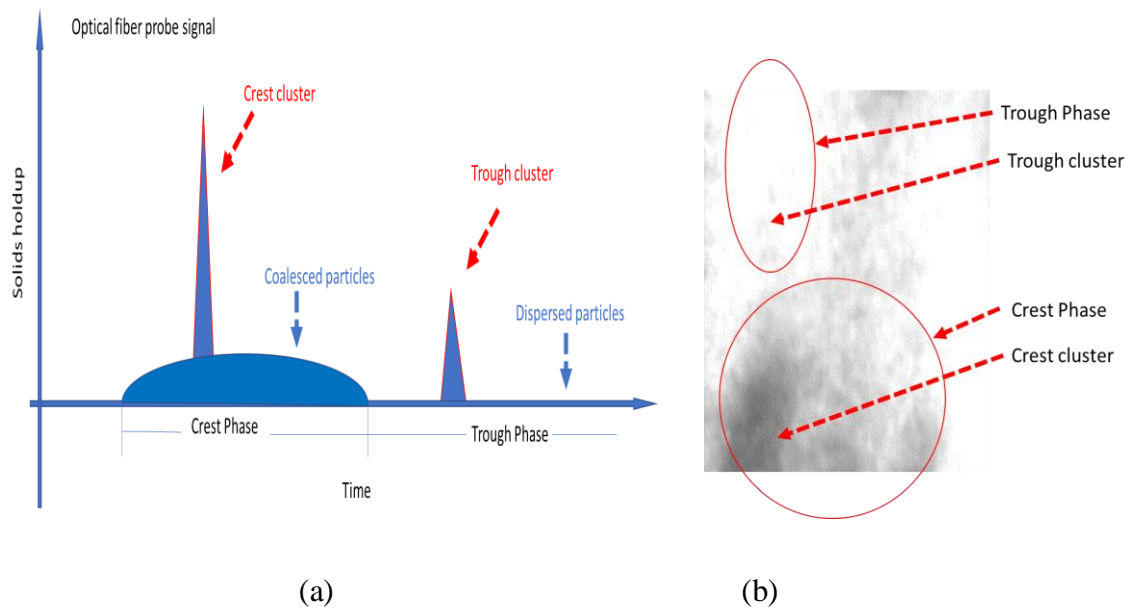


Figure 7-2 The instantaneous flow structure in the CFB (a: phase interpretation from signal captured by optical fiber probe, b: phase interpretation from the image captured by the high-speed camera)

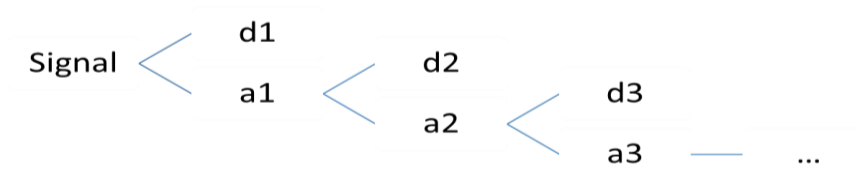


Figure 7-3 Demonstration of wavelet transform

The optical fiber probe employed has two channels and both of them record instantaneous solids holdup signals. Solids holdup signals were first decomposed using wavelet transform. Then, the time lags of detail scales between two channels were calculated based on cross-correlations and the result was shown in Figure 7-4. The time lag for d1 and d2 is zero, indicating the waves of d1 and d2 appear at the two channels simultaneously. Starting from d3, time lag increases with wavelet scale. Based on this, d1 and d2 are considered as noises imposed by the electronics on signals. For further analysis, a2 is considered as the denoised signal.

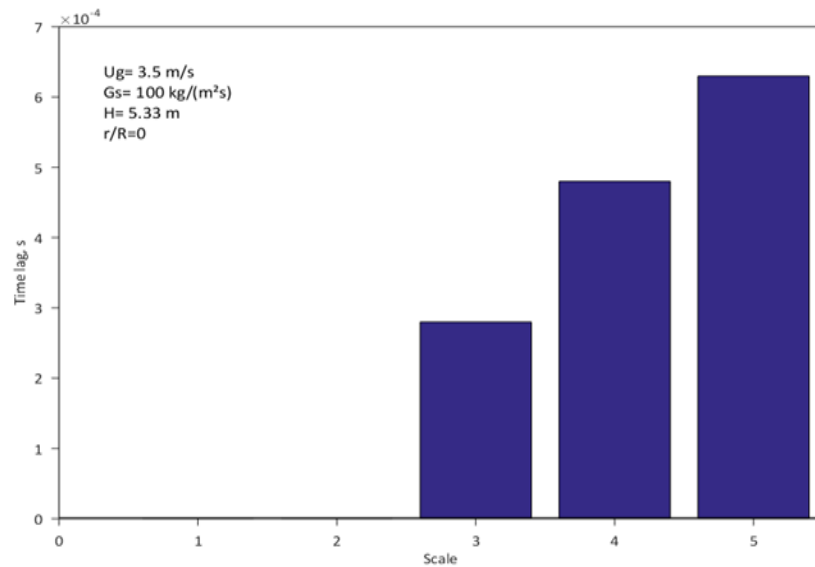


Figure 7-4 Time lag versus wavelet scale

Approximate signals from a3 to a17 were plotted versus the original solids holdup signal (see Figure 7-5). For lower scales (<5), approximate signal coincides with the original

signal. Increasing scale, approximate signal loses the peaks, but still maintains good coincidence with crescents in the signal. After scales 11, approximate signal gradually loses crescents. For scale 17, the approximate signal is basically a straight line. The correlation coefficient between approximate signals and original solids holdup signal were calculated and shown in figure 7-6. Before scale 5, the correlation coefficient is close to 1, indicating well coincidence. From scale 5 to 10, the correlation coefficient begins to drop slowly and still above 0.6, due to the loss of peak (cluster) information. After scale 10, the correlation coefficient drops rapidly and approach 0 due to the loss of crescent (crest phase) information. Approximate signals (a10 and a17) were plotted versus the original solids holdup signal in Figure 7-7. Peaks in optical fiber probe signals are well discriminated as fragments in the original signal whose solids holdup is above a10. Crescents can be identified as fragments in a10 whose solids holdup are above a17.

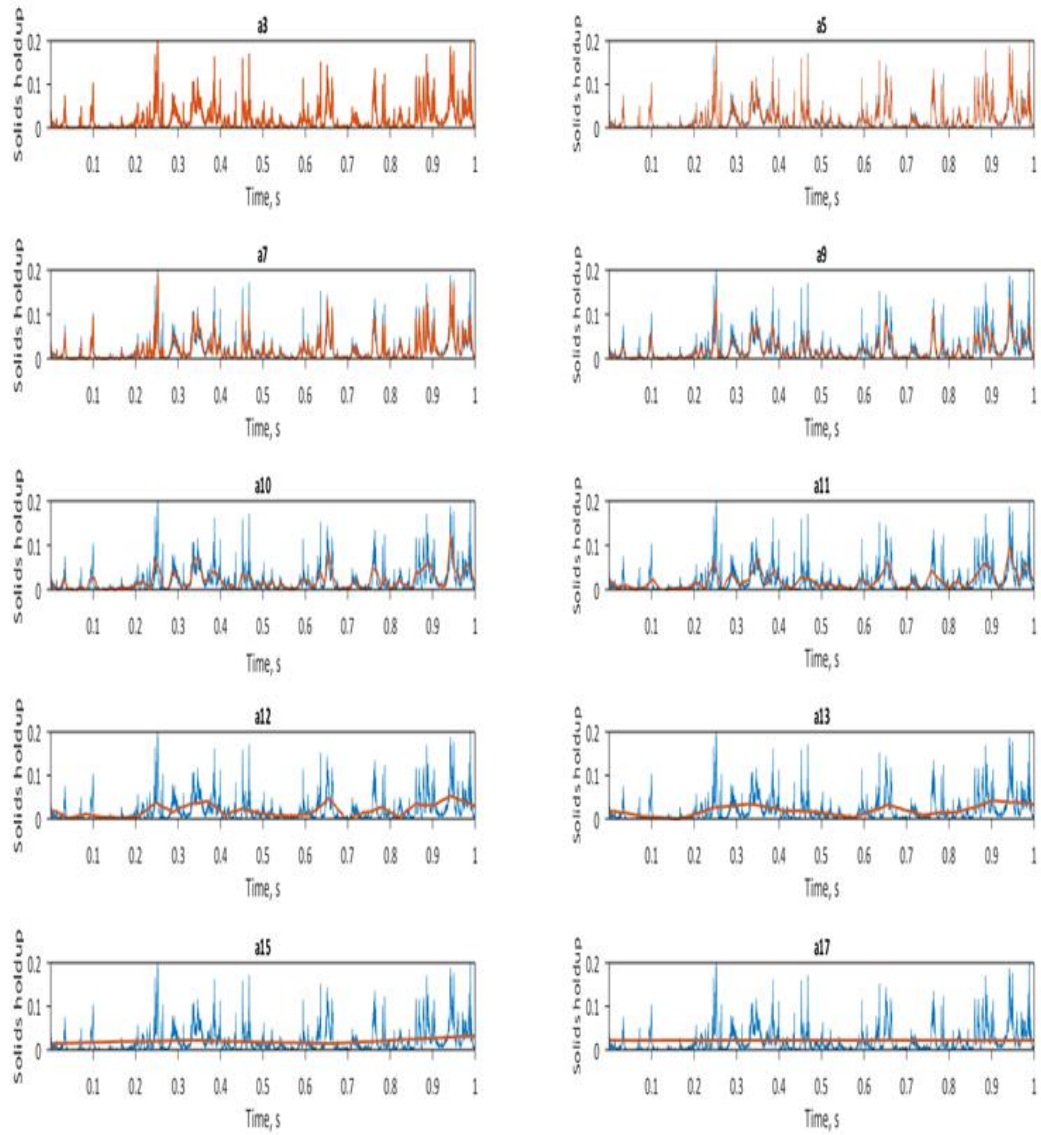


Figure 7-5 Probe signal and approximate signals

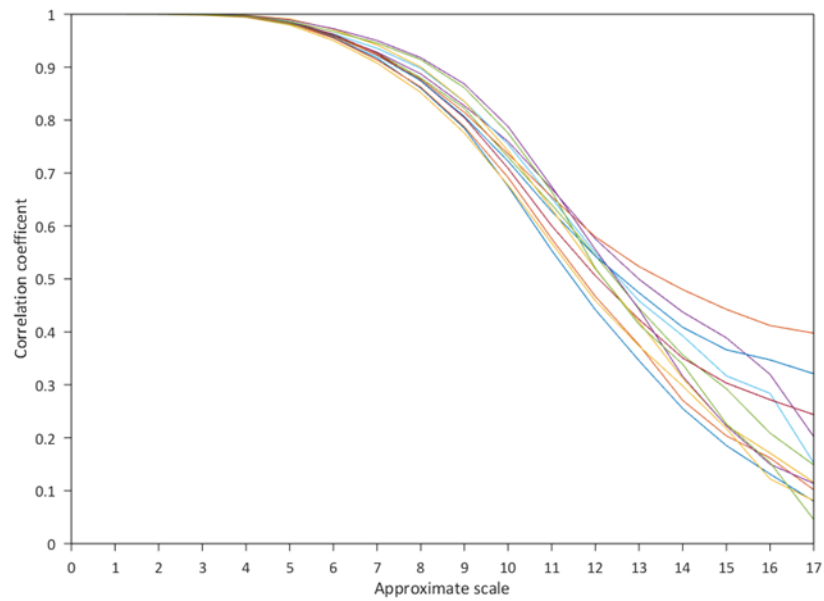


Figure 7-6 Correlation coefficient versus the wavelet scale

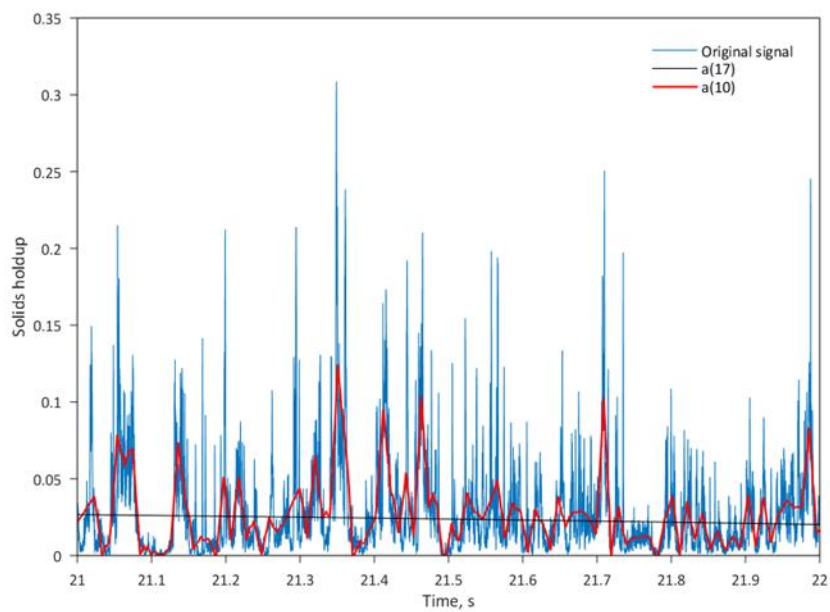


Figure 7-7 Probe signal and approximate signals (a10, a17)

Based on the above analysis, scale 10 can be used to discriminate the frequency band of clusters and crest phase in the CFB riser:

1. d1 and d2 correspond to the signal noise and a2, instead of the original signal, is used for further analysis.
2. Fragments in a2, whose solids holdup is higher than a10, correspond to crest clusters and trough clusters.
3. Fragments in a2, where solids holdup in a10 is above a17, correspond to crest phase.

In addition, cluster and crest phase shall have their maximum solids holdup at least 0.01 higher than their threshold and their sizes are at least 5 times of particle diameter (380 μ m) and 2 cm, respectively (Table 7-2). Otherwise, they are considered to be aggregations passing probe tip in a distance or fluctuations caused by lateral movement. The cluster is the basic aggregation unit with solids holdup increasing monotonically and sharply from the surrounding. Then, clusters are further classified into trough clusters and crest clusters based on whether they are surrounded by dispersed particles or coalesced particles. Then, trough clusters, crest clusters and crest phase are characterized in terms of solids holdup, duration time, time fraction and frequency. Their length is computed by multiplying duration time with the corresponding instantaneous velocity which is calculated by cross-correlating intervals(0.01s). Finally, information of coalesced particles and dispersed particles are also calculated using equation 7-1, 7-2, 7-3 and 7-4 where T_{pc} is time fraction of coalesced particles, T_{cp} is time fraction of crest phase, T_{cc} is time fraction of crest clusters, T_{tc} is time fraction of trough clusters, ε_{pc} is solids holdup of coalesced particles, ε_{ip} is solids holdup of dispersed particles, ε_{cp} is solids holdup of crest phase, ε_{cc} is solids holdup of crest clusters, ε_{tc} is solids holdup of trough clusters, ε_{ip} is solids holdup of dispersed particles, ε_m is mean solids holdup. For glass beads, the corresponding solids holdup signals share the same characteristics with signals originated from FCC. Based on sensitivity analysis, scale 10 is also selected to discriminate clusters and crest phase for glass beads.

$$T_{pc} = T_{cp} - T_{cc} \quad \text{Equation 7-1}$$

$$T_{ip} = 1 - T_{cp} - T_{tc} \quad \text{Equation 7-2}$$

$$\varepsilon_{pc} = \frac{\varepsilon_{cp}*(T_{cc}+T_{pc})-\varepsilon_{cc}*T_{cc}}{T_{pc}} \quad \text{Equation 7-3}$$

$$\varepsilon_{ip} = \frac{\varepsilon_m - T_{cp}*\varepsilon_{cp} - T_{tc}*\varepsilon_{tc}}{1 - T_{cp} - T_{tc}} \quad \text{Equation 7-4}$$

Table 7-2 Phase classification using wavelet transform

Signal scales	Physical meaning	Minimum size	Significance
d1, d2	Noise		
From d3 to d10	Trough clusters Crest clusters	>5*d _p	>0.01
From d11 to d17	Crest phase	>2cm	>0.01

7.3 Results and discussion

7.3.1 Phase components

To have an overview of the phase components, phase information was plotted versus local-mean solids holdup (see Figure 7-4). Crest clusters have highest solids holdup, followed by trough clusters, coalesced particles and dispersed particles. This is consistent with the solids holdup mapping using the high-speed camera and the characteristics of probe signals (chapter 4). Solids holdup of crest clusters, trough clusters, coalesced particles and dispersed particles increases with local solids holdup. The solids holdup difference between the dispersed particles and other phases increases with local solids holdup, indicating the aggregation is severe in high-solids holdup atmosphere. Dispersed particles have highest time fraction, followed by coalesced particles, crest clusters and trough clusters. Time fraction of dispersed particles decreases with local solids holdup, while time fraction of coalesced particles, trough clusters and crest clusters increases with local solids holdup. This is intuitively reasonable, as high solids holdup leads to more aggregations. Length of both trough clusters and crest clusters decreases with local solids holdup. The decrease is abrupt at low solids holdup and smooth at high solids holdup. This trend may relate to the facts that collision intensity increases with local solids holdup. Comparing with crest clusters, trough clusters have lower solids holdup, higher length and lower time fraction. However, the data for solids holdup, length and time

fraction has an evident variation among the overall trend, suggesting that other factors may also play an important role to particle aggregation. Further study on the aggregation mechanism is required to fully understand the phase characteristics.

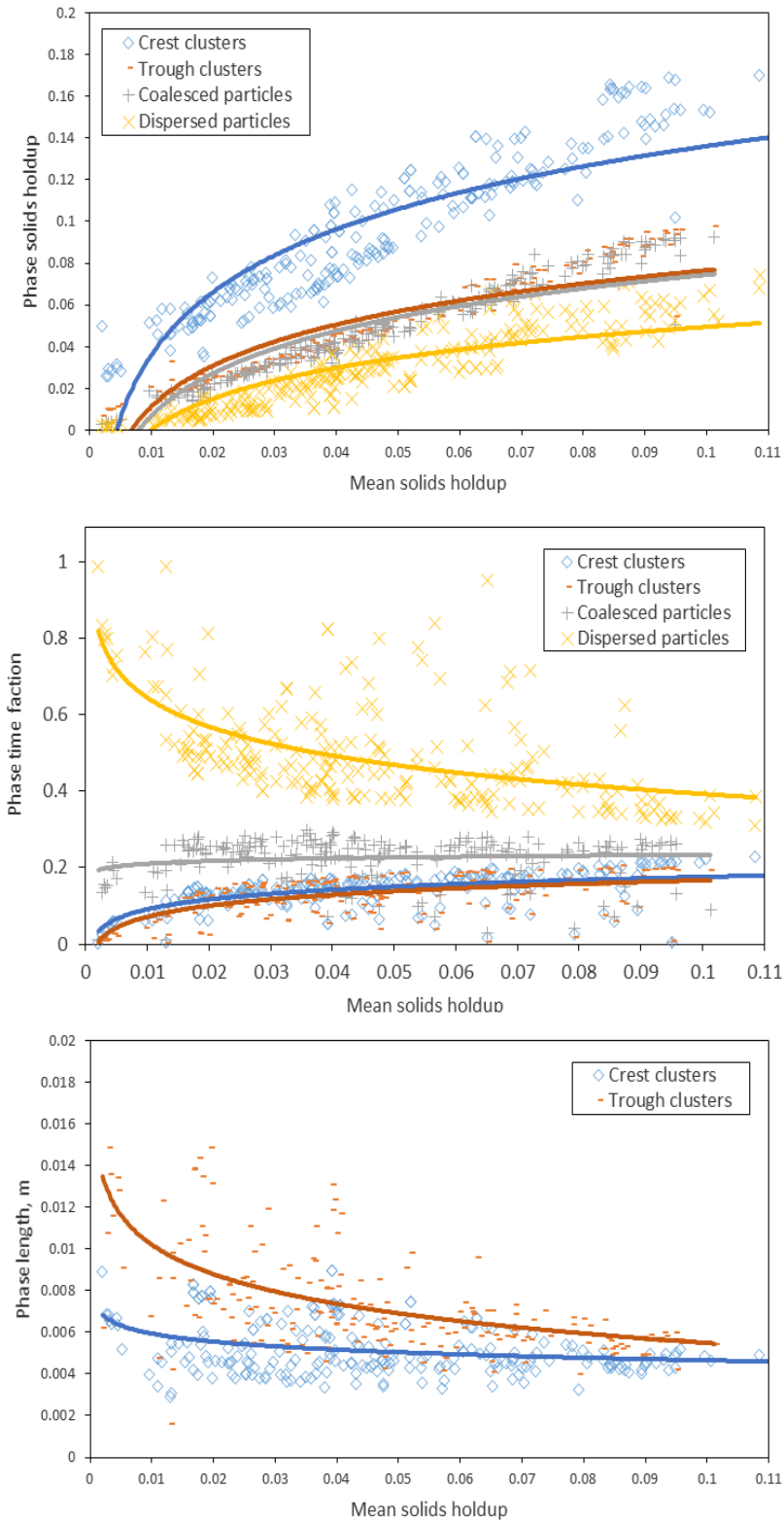


Figure 7-8 Phase properties versus local-mean solids holdup

To deepen the understanding of fast-fluidized, to develop and validate numerical model of CFB riser, statistic phase information in the fully developed region, including solids holdup, length and time fraction, was also computed and plotted versus operating conditions (see Figure 7-5). Solids holdup for trough clusters and crest clusters both increases with solids circulation rate and decreases with superficial gas velocity. Comparatively, trough cluster has lower solids holdup than crest cluster, which is consistent with a previous paper (chapter 4). Solids holdup difference between them increases with solids circulation rate and decreases with superficial gas velocity. Time fraction, to some extent, represents the volume fraction of reactor occupied by a specific phase. Time fraction of dispersed particles decreases with solids circulation rate and increases with superficial gas velocity. Time fraction of trough clusters and crest clusters increases with solids circulation rate and decreases with superficial gas velocity. Comparatively, the time fraction of trough clusters is slightly higher than that of crest clusters. As for phase dimension, trough cluster is longer than crest cluster and the length difference is more significant at high superficial gas velocity. At $U_g=3.5$ m/s, length of trough clusters decreases with solids circulation rate and length of crest clusters remains constant. At $U_g=5.5$ m/s, length of trough clusters and crest clusters first increases then decreases with solids circulation rate. Investigation in a wider range of operating conditions is suggested to analyze the overall trend.

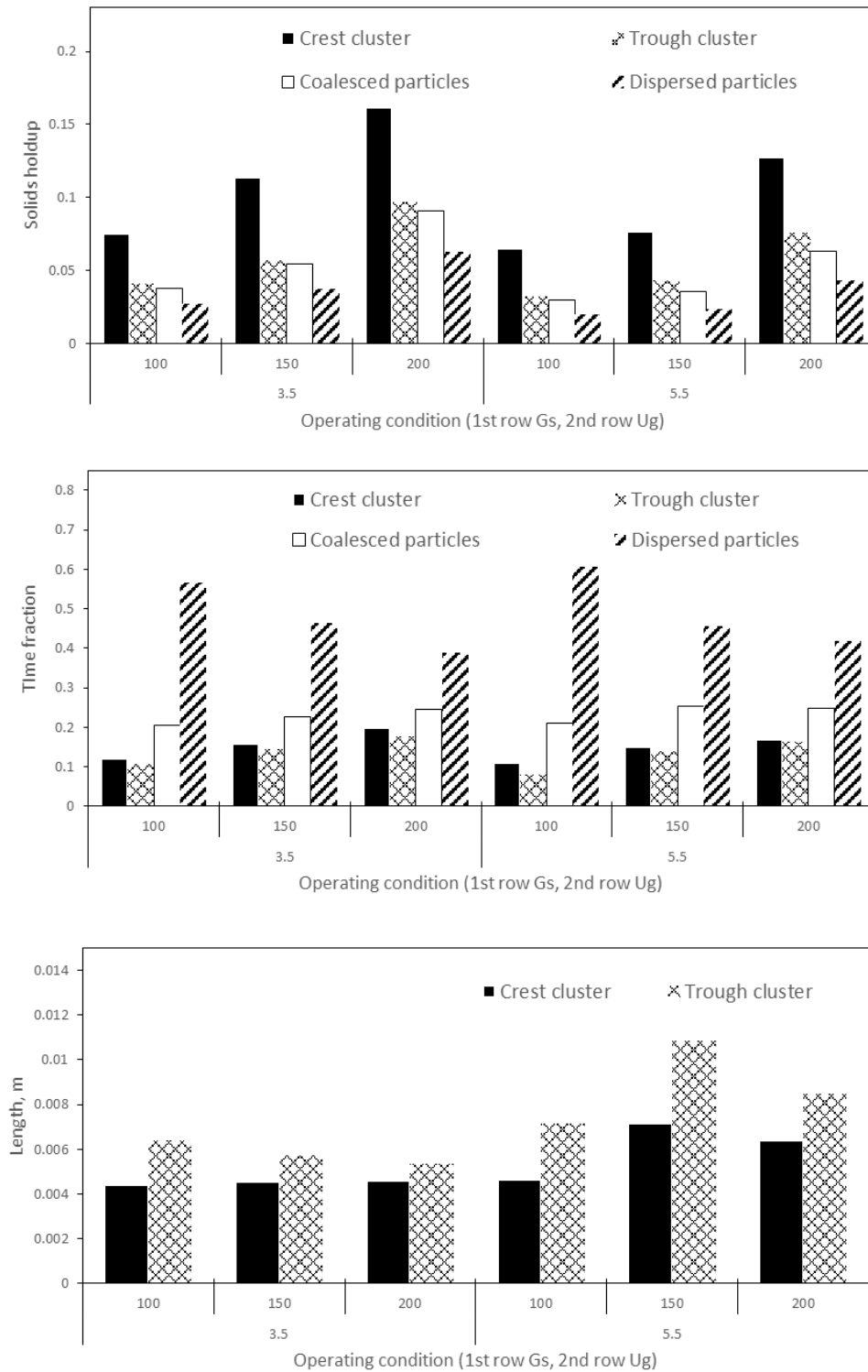


Figure 7-9 Statistic properties of crest clusters and trough clusters versus operating conditions

7.3.2 Crest phase

As crest clusters and coalesced particles possess continuous high solids holdup, they are referred to crest phase in macroscope. As crest phase is usually large than 5 cm, may occupy up to 60% of CFB riser and causes macro solids holdup fluctuation, it is characterized thoroughly in terms of solids holdup, length, frequency and cluster number per crest phase (see Figure 7-6). Solids holdup of crest phase is the average solids holdup of crest clusters and coalesced particles. According to the images and signals acquired using an optical fiber probe, the crest cluster is the dominant component of crest phase in solids holdup (chapter 4). Solids holdup of crest phase decreases with superficial velocity and increases with solids circulation rate, which is consistent with solids holdup of crest clusters. Length of crest phase, spanning from 0.07m to 0.23m, increases with both superficial gas velocity and solids circulation rate. The scale of crest phase is one order of magnitude larger than clusters, which is consistent with quantitative observation based on the high-speed camera (chapter 4). Time fraction of crest phase decreases with superficial velocity and increases with solids circulation rate. Frequency of crest phase increases with solids circulation rate and decreases with superficial gas velocity. Crest phase frequency has a magnitude less than 1 and this may owe to its large scale. Crest phase is a complex where clusters scattered in coalesced particles. Number of clusters in crest phase is average number of clusters within crest phase. Number of clusters in crest phase, spanning from 6 to 14.5, increases with both superficial gas velocity and solids circulation rate. Large crest phase tends to have more clusters than small crest phase, which explains why the number of clusters in the crest phase has the same trend with the length of crest phase.

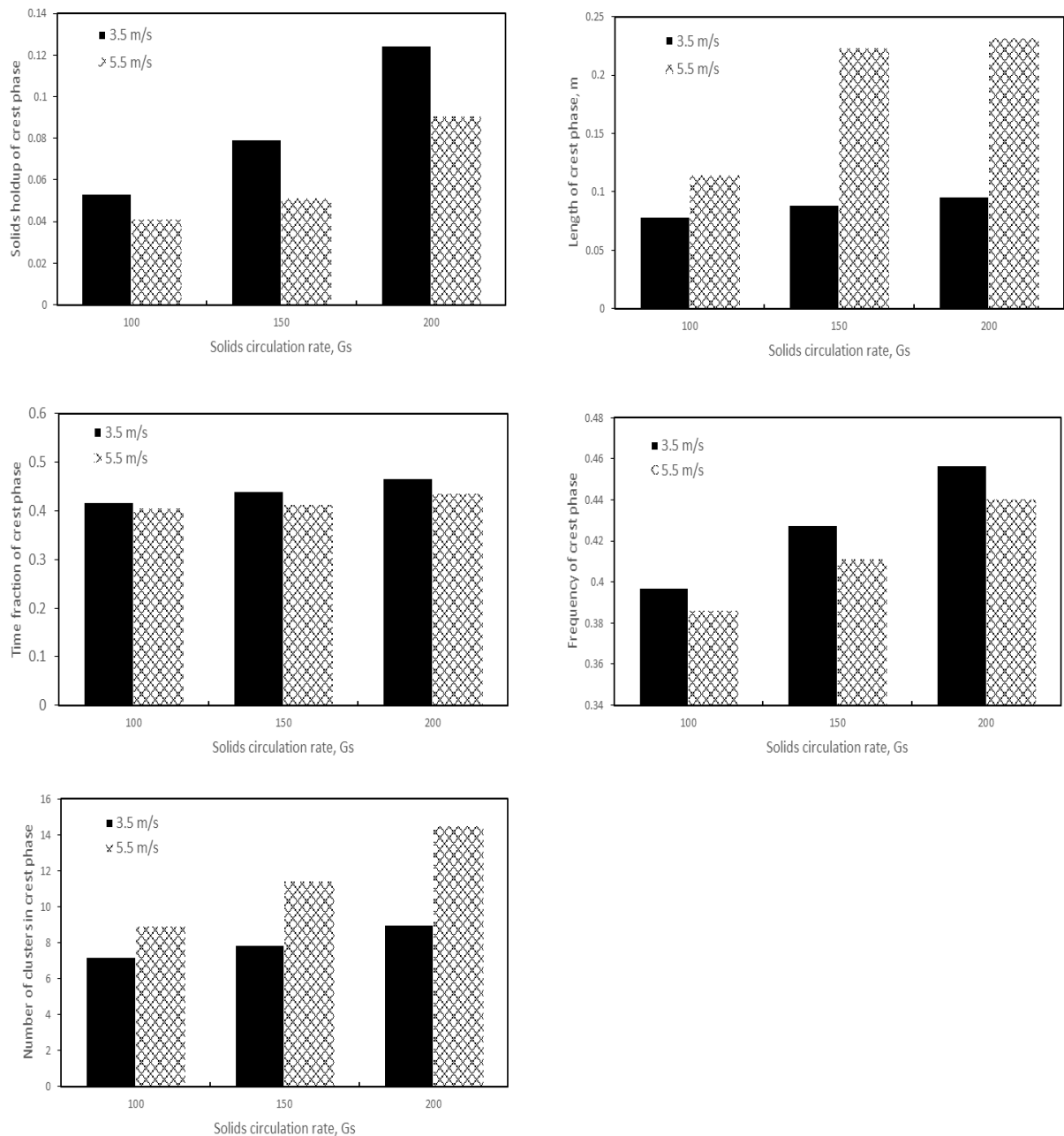


Figure 7-10 Properties of crest phase versus operating conditions

7.3.3 Validation using high-speed camera

Cahyadi et al., (2017) well summarized the cluster properties in the literature and found that some properties have a discrepancy in an order of magnitude. In the previous study,

gas-solid flow has been well recorded using a high-speed camera in the same CFB riser using the same FCC particles (chapter 6). With the help of a verified correlation between solids holdup and grayscale, cluster boundary is, for the first time, determined physically meaningfully based on the sharp increase of solids holdup around clusters. To verify the phase characterization in this work, cluster information, combining trough cluster and crest cluster, was compared with the information originated from the high-speed camera. Probability density distribution of cluster length was analyzed plotted in Figure 7-7. Cluster length ranges from millimeters to centimeters. Probability decreases exponentially with cluster length, indicating small clusters are dominant in numbers. This agrees well with previous studies (chapter 4; chapter 6; Zou et al.,1994; Li et al.,1995;) and may attribute to large clusters are more easily to break due to the collision. Then, cluster solids holdup was also plotted with the corresponding cluster length in Figure 7-8. There is no clear relationship between cluster solids holdup and cluster length, indicating the chaos of flow behavior in the CFB. Small clusters have wider solids holdup span. This is also consistent with results originated from images (chapter 6).

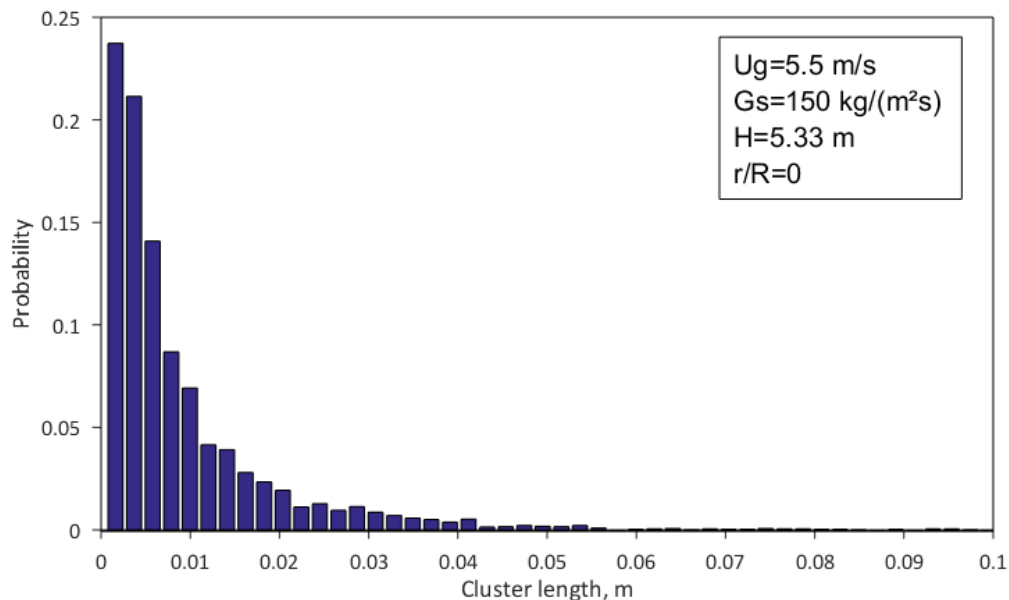


Figure 7-11 Histogram of cluster length

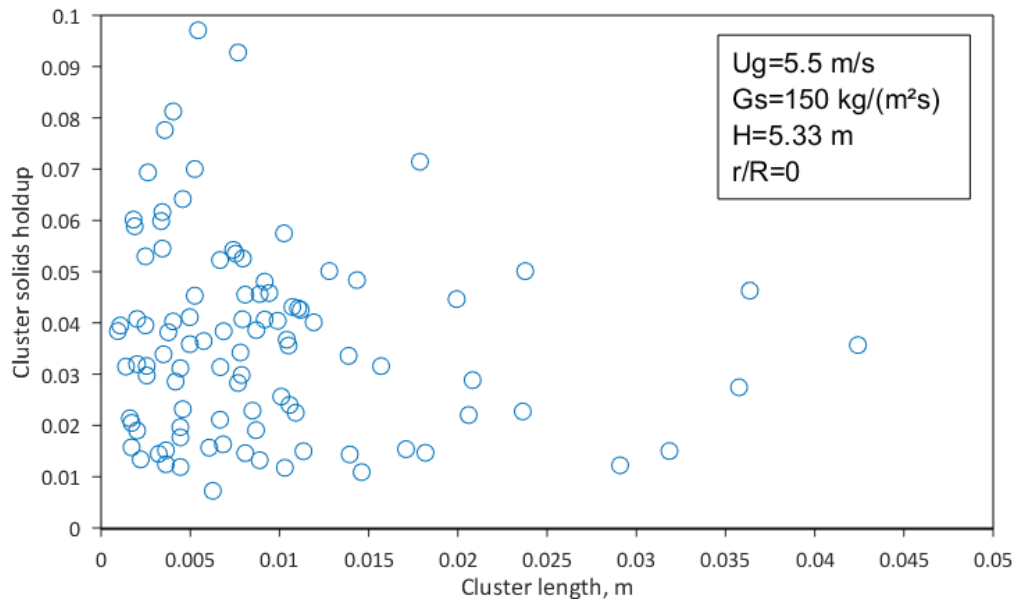


Figure 7-12 Relationship between cluster solids holdup and cluster length

Due to the difference in resolution and measuring window between optical fiber probe and the high-speed camera, clusters whose length ranges from 0.0015m and 0.01m were sampled to compare the cluster length captured using optical fiber probe and cluster equivalent diameter acquired using the high-speed camera (see Figure 7-9). In the literature, cluster dimensions have a discrepancy in an order of magnitude (Cahyadi et al., 2017; review). In this work, cluster length originated from an optical fiber probe is found to be close with cluster area-equivalent diameter originated from a high-speed camera.

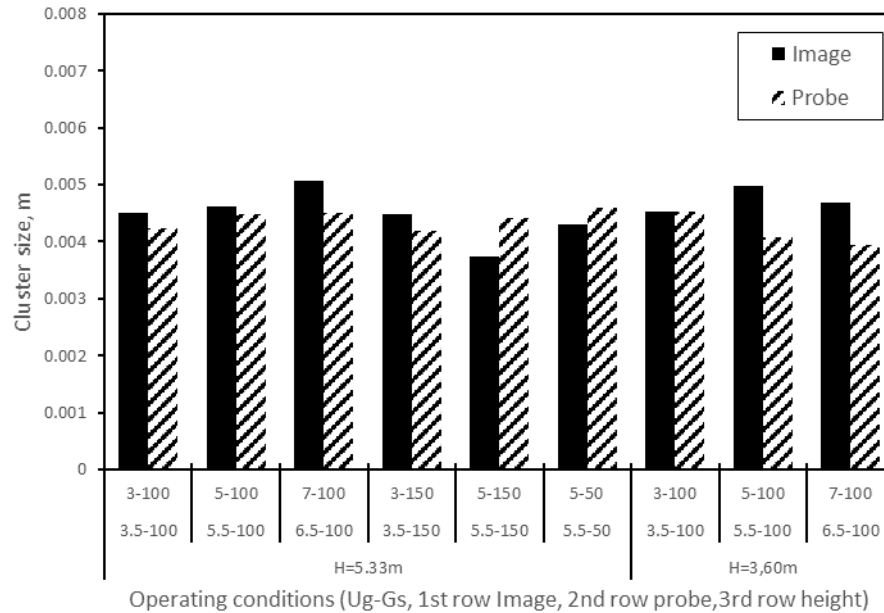


Figure 7-13 Comparison of cluster size between the optical fiber probe and high-speed camera

7.3.4 Impact of the particle group

To explore the flow mechanism, phases formed by FCC (group A) and glass beads (group B) are compared systematically. At the same solids circulation rate, solids holdup in the CFB differs significantly due to the difference in particle density (Xu and Zhu, 2010). To have a fair comparison, the comparison of crest clusters and trough clusters was conducted on the basis of local-mean solids holdup (see Figure 7-10 and 7-11).

For both glass beads and FCC, solids holdup of crest clusters increases with mean solids holdup. At similar mean solids holdup, crest clusters formed by glass beads have higher solids holdup than that formed by FCC. Length of crest clusters formed by FCC is generally higher than that of glass beads, indicating crest clusters formed by glass beads may be subject to severe collision due to high inertia. Length of crest clusters decreases exponentially for FCC and increases for glass beads with local solids holdup.

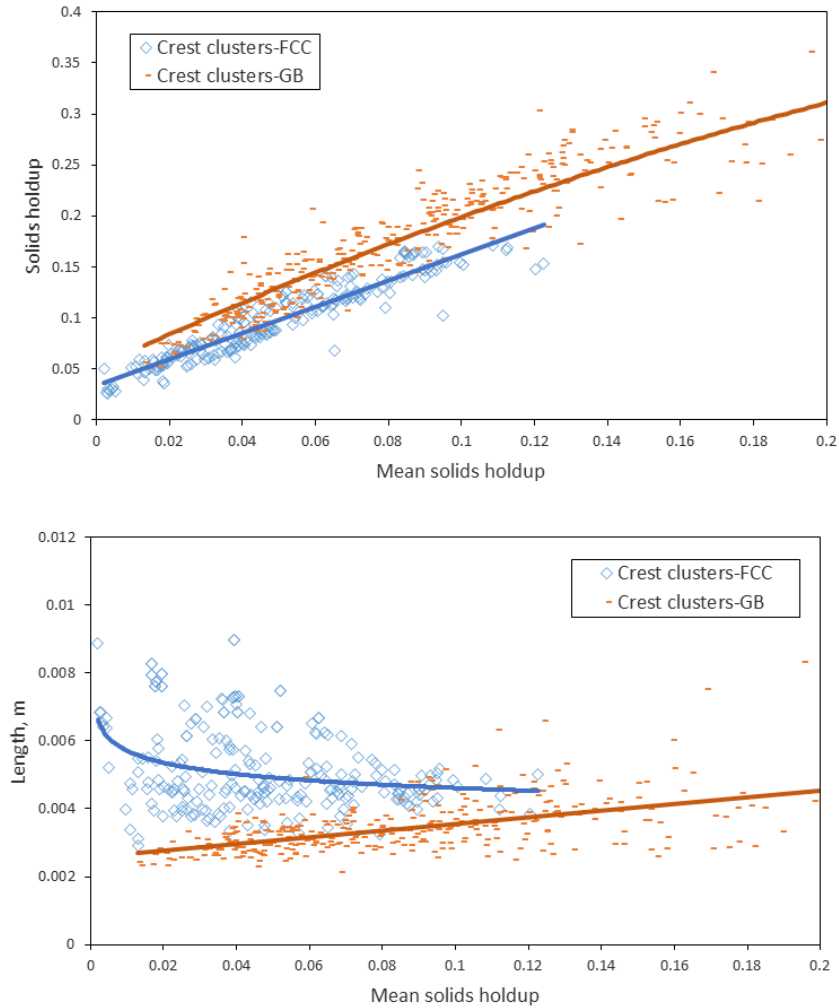


Figure 7-14 Comparison of crest clusters formed by FCC and glass beads

Solids holdup of trough clusters also increases with mean solids holdup for both FCC and glass beads. Trough clusters formed by FCC and glass beads have similar solids holdup, when local solids holdup is similar. Length of trough clusters formed by FCC is generally higher than that of glass beads. Length of trough clusters also decreases exponentially for FCC and increases for glass beads with local solids holdup.

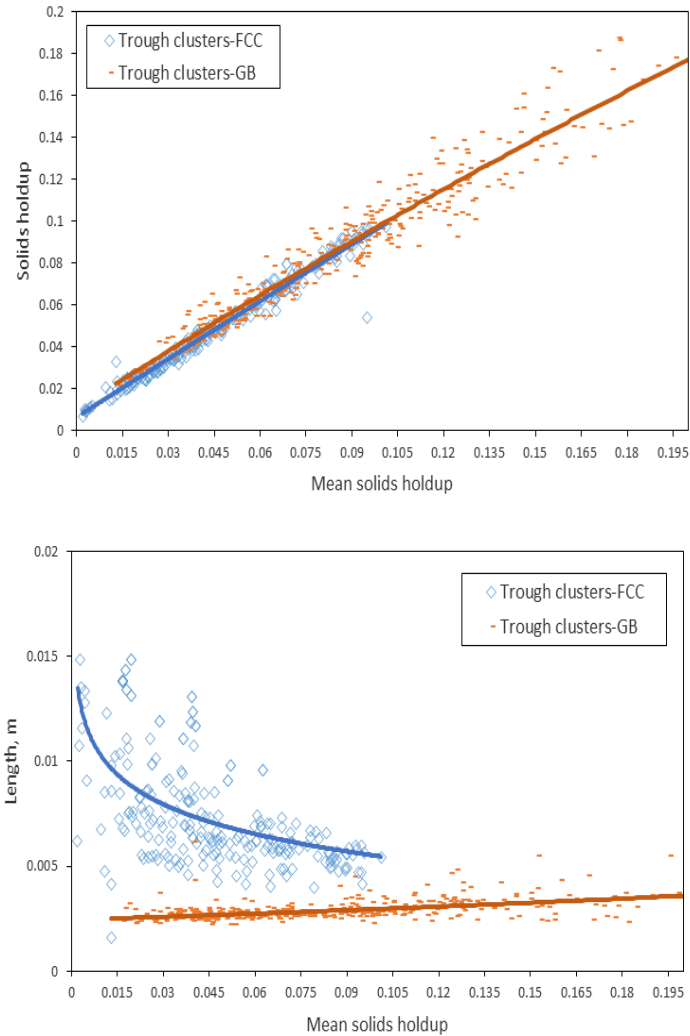


Figure 7-15 Comparison of trough clusters formed by FCC and glass beads

As the crest phase is in macroscopic phenomenon, the comparison of crest phase was conducted based on similar volumetric solids circulation rate instead of local solids holdup (see Figure 7-12). The crest phase formed by FCC and glass beads has the same trend with operating conditions. Comparatively, crest phase formed by FCC has lower solids holdup and lower length than that formed by glass beads. The difference in solids holdup is more significant than the length. Further analysis of the mechanism is needed to further explain the difference.

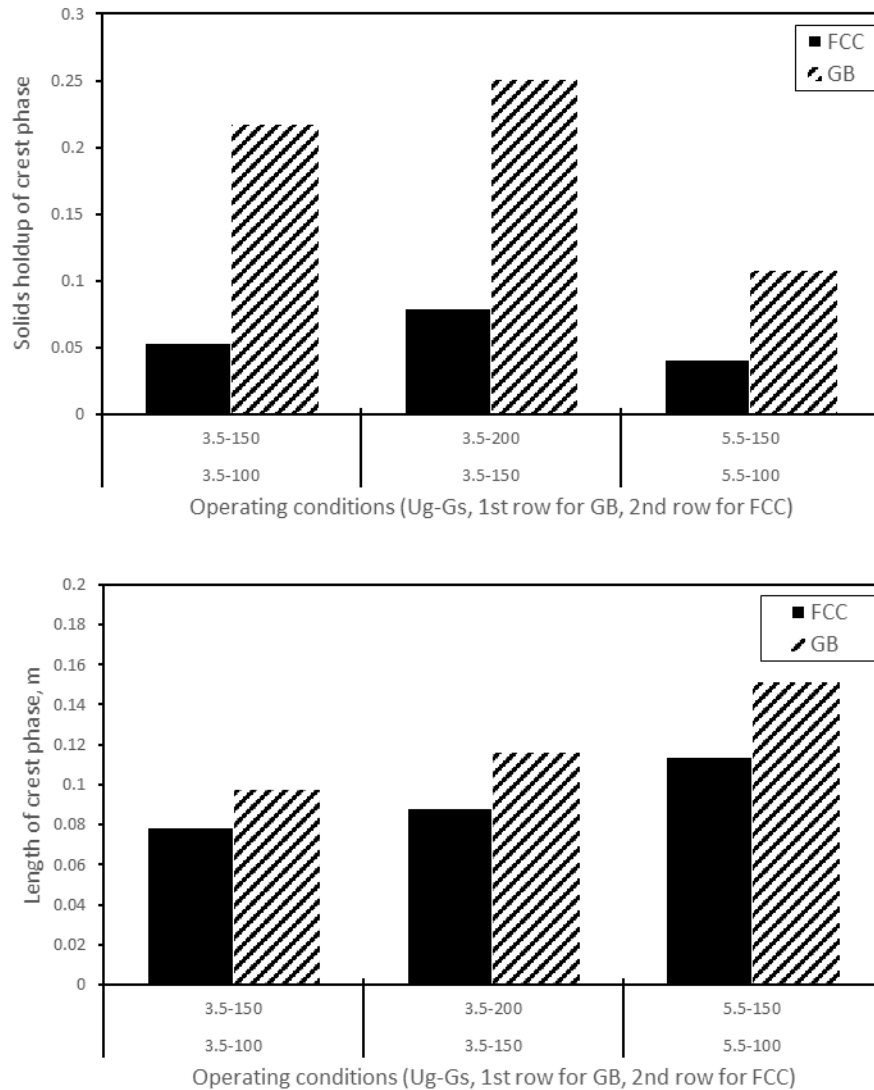


Figure 7-16 Comparison of crest phase formed by FCC and glass beads

7.4 Conclusions

Based on the observation and solids holdup map in the CFB riser, it has already found that there are trough clusters, dispersed particles, crest clusters and coalesced particles in the CFB riser. In this work, local solids holdup in the CFB riser has been measured using an optical fiber probe. Using wavelet transform, phase information, including solids holdup, length, time fraction and frequency, has been successfully extracted from solids holdup signals. Phase properties have been plotted versus both local-mean solids holdup

and operating conditions. Moreover, cluster characteristics extracted in this work were found to be consistent with that acquired from images. Finally, phase information formed by FCC were compared with that formed by glass beads in perspectives of solids holdup and length.

Collectively, phase in the CFB have been quantitatively characterized systematically and how particle type influences the phase information was also investigated experimentally. These phase properties may help to understand gas-particle interaction, to predict heat and mass transfer, and to develop or validate numerical models. However, further study is still needed to further characterize phase information in high-density conditions and to further explore the aggregation mechanism both experimentally and numerically.

Nomenclature

U_g is superficial gas velocity, [m/s];

G_s is solids circulation rate, [kg/m²s];

T_{pc} is time fraction of coalesced particles;

T_{cp} is time fraction of crest phase;

T_{cc} is time fraction of crest clusters;

T_{tc} is time fraction of trough clusters;

ϵ_{pc} is solids holdup of coalesced particles;

ϵ_{ip} is solids holdup of dispersed particles;

ϵ_{cp} is solids holdup of crest phase;

ϵ_{cc} is solids holdup of crest clusters;

ϵ_{tc} is solids holdup of trough clusters;

ϵ_{ip} is solids holdup of dispersed particles;

ϵ_m is mean solids holdup;

References

- Anantharaman, A., Karri, S. R., Findlay, J. G., Hrenya, C. M., Cocco, R. A., & Chew, J. W. (2016). Interpreting differential pressure signals for particle properties and operating conditions in a pilot-scale circulating fluidized bed riser. *Industrial & Engineering Chemistry Research*, 55(31), 8659-8670.
- Brereton, C. M. H., & Grace, J. R. (1993). Microstructural aspects of the behaviour of circulating fluidized beds. *Chemical Engineering Science*, 48(14), 2565-2572.
- Bi, H. T., Zhu, J. X., Jin, Y., & Yu, Z. Q. (1993, October). Forms of particle aggregations in CFB. In *Proceedings of the Sixth Chinese Conference on Fluidization*, Wuhan, China (pp. 162-167).
- Cahyadi, A., Anantharaman, A., Yang, S., Karri, S. R., Findlay, J. G., Cocco, R. A., & Chew, J. W. (2017). Review of cluster characteristics in circulating fluidized bed (CFB) risers. *Chemical Engineering Science*, 158, 70-95.
- Chew, J. W., Hays, R., Findlay, J. G., Knowlton, T. M., Karri, S. R., Cocco, R. A., & Hrenya, C. M. (2012a). Cluster characteristics of Geldart Group B particles in a pilot-scale CFB riser. I. Monodisperse systems. *Chemical Engineering Science*, 68(1), 72-81.
- Chew, J. W., Hays, R., Findlay, J. G., Knowlton, T. M., Karri, S. R., Cocco, R. A., & Hrenya, C. M. (2012b). Cluster characteristics of Geldart group B particles in a pilot-scale CFB riser. II. Polydisperse systems. *Chemical engineering science*, 68(1), 82-93.
- Chew, J. W., Parker, D. M., Cocco, R. A., & Hrenya, C. M. (2011). Cluster characteristics of continuous size distributions and binary mixtures of Group B particles in dilute riser flow. *Chemical engineering journal*, 178, 348-358.
- Horio, M., & Kuroki, H. (1994). Three-dimensional flow visualization of dilutely dispersed solids in bubbling and circulating fluidized beds. *Chemical Engineering Science*, 49(15), 2413-2421.

- Li, H., Xia, Y., Tung, Y., & Kwauk, M. (1991). Micro-visualization of clusters in a fast fluidized bed. *Powder Technology*, 66(3), 231-235.
- Li, H., Zhu, Q., Liu, H., & Zhou, Y. (1995). The cluster size distribution and motion behavior in a fast fluidized bed. *Powder Technology*, 84(3), 241-246.
- Manyele, S. V., Pärssinen, J. H., & Zhu, J. X. (2002). Characterizing particle aggregates in a high-density and high-flux CFB riser. *Chemical Engineering Journal*, 88(1), 151-161.
- Matsuda, S., Hatano, H., Takeuchi, H., Pyatenko, A. T., & Tsuchiya, K. (1996). Motion of individual solid particles in a circulating fluidized bed riser. In *Circulating Fluidized Bed Technology V* (pp. 176-181). Science Press Beijing.
- Rhodes, M., Mineo, H., & Hirama, T. (1992). Particle motion at the wall of a circulating fluidized bed. *Powder Technology*, 70(3), 207-214.
- Shaffer, F., Gopalan, B., Breault, R. W., Cocco, R., Karri, S. R., Hays, R., & Knowlton, T. (2013). High speed imaging of particle flow fields in CFB risers. *Powder Technology*, 242, 86-99.
- Shi, H., Wang, Q., Xu, L., Luo, Z., & Cen, K. (2008). Visualization of clusters in a circulating fluidized bed by means of particle-imaging velocimetry (PIV) technique. In *Proceedings of the 9th International Conference on Circulating Fluidized Beds*, Hamburg, Germany (pp. 1013-1019).
- Takeuchi, H., & Hirama, T. (1991). Flow visualization in the riser of a circulating fluidized bed. *Circulating Fluidized Bed Technology III*, 177-182.
- Takeuchi, H., Pyatenko, A. T., & Tatano, H. (1996). Flowing behavior of particles in the riser of a circulating fluidized bed. In *Circulating Fluidized Bed Technology V* (pp. 164-169). Science Press Beijing.
- Wang, C. (2013). High density gas-solids circulating fluidized bed riser and downer reactors. Ph.D. Diss. The University of Western Ontario.

- Wilhelm, R. H., & Kwauk, M. (1948). Fluidization of solid particles. *Chemical Engineering Progress*, 44(3), 201-218.
- Xu, J., & Zhu, J. (2011a). A new method for the determination of cluster velocity and size in a circulating fluidized bed. *Industrial & Engineering Chemistry Research*, 51(4), 2143-2151.
- Xu, J., & Zhu, J. X. (2011b). Visualization of particle aggregation and effects of particle properties on cluster characteristics in a CFB riser. *Chemical Engineering Journal*, 168(1), 376-389.
- Xu, J., & Zhu, J. X. (2010). Experimental study on solids concentration distribution in a two-dimensional circulating fluidized bed. *Chemical Engineering Science*, 65(20), 5447-5454.
- Yang, J., & Zhu, J. (2015a). Visualization of solids phase separation in a rectangular CFB riser using a novel image calibration method. *Powder Technology*, 273, 76-82.
- Yang, J., & Zhu, J. (2015b). Cluster identification using image processing. *Particuology*, 23, 16-24.
- Yunhau, Z., Huilin, L., Yurong, H., Ding, J., & Lijie, Y. (2006). Numerical prediction of combustion of carbon particle clusters in a circulating fluidized bed riser. *Chemical Engineering Journal*, 118(1), 1-10.
- Zhang, H., Johnston, P. M., Zhu, J. X., De Lasa, H. I., & Bergougnou, M. A. (1998). A novel calibration procedure for a fiber optic solids concentration probe. *Powder Technology*, 100(2-3), 260-272.
- Zou, B., Li, H., Xia, Y., & Ma, X. (1994). Cluster structure in a circulating fluidized bed. *Powder Technology*, 78(2), 173-178.

CHAPTER 8

A comprehensive characterization of aggregative flow in gas- solid circulating fluidized bed using wavelet analysis: high-density riser

Abstract

The circulating fluidized bed (CFB) has a variety of industrial applications and the solids circulation rate, typically, ranges from 5 to 1400 kg/ m² s. Due to the difficulties to achieve high solids circulation rate in pilot CFB, studies, in the literature, concentrated on solids circulation rate below 300 kg/ m² s. Only in our group, high solids circulation rate, up to 700 kg/ m² s, has been achieved with an optimization of the CFB system. Optical fiber probe has been employed in the CFB riser to measure the instantaneous local solids holdup. Utilizing the previous experimental data, instantaneous flow behavior has been analyzed with phase identification and characterization. In the riser wall, a “dense structure”, featured with particulate phase whose solids holdup above 0.45, has been identified in the wall region of CFB riser at high solids circulation rate. The transition to “dense structure” has also been explored with time fraction of the particulate phase. In the riser center, solids holdup characteristics remain similar in both low and high solids circulation rate. With a verified discrimination method, phases in the riser center, namely crest clusters, coalesced particles, trough clusters and dispersed particles, are discriminated and characterized in terms of solids holdup, length, frequency and time fraction. Collectively, this is the first time that the instantaneous flow structure in the CFB has been thoroughly analyzed at such a high solids circulation rate (700 kg/ m² s), which shall contribute to the understanding of industrial CFB, the development and validation of numerical models in high-density conditions.

Keywords: high-density; circulating fluidized bed; optical fiber probe; clusters; aggregations; flow structure.

8.1 Introduction

The circulating fluidized bed is the major reactor type for combustion, gasification and FCC (fluid catalytic cracking) in energy and chemical industries. In CEB riser, solids are transported upward using high-velocity gas and the concurrent up-flow offers advantages like reduced back mixing, high gas output, excellent heat and mass transfer, independent control of gas and solids (Lim et al., 1995).

Main parameters for CFB operation are superficial gas velocity and solids circulation rate and they typically range from 2 to 12 m/s and 5 to 1400 kg/m²s, respectively. The laboratory studies on CFB riser concentrate on solids circulation rate below 300 kg/m²s (Wang, 2014a; 2014b;). Aiming to bridge the gap between academia and industry, high solids circulation rate, 550 kg/m²s and 1000 kg/m²s was achieved by Manyele et al., (2002) and Wang (2013), respectively. Detailed hydrodynamics, including distribution of solids holdup, particle velocity and solids flux, have been reported in detail (Wang, 2014a; 2014b). Additionally, Ozone decomposition was employed as a sample reaction to evaluate riser performance (Wang, 2014c).

However, the study on instantaneous flow behavior remains scarce in high-density conditions, although it is the link between hydrodynamics and reactor performance. Manyele et al., (2002) analyzed particle clusters with the solids circulation rate as high as 550 kg/m²s. All other studies on clusters have their solids circulation rate below 300 kg/m²s (Harris et al.,2002; Cahyadi et al., 2017).

Recently, phase information in the CFB riser has been thoroughly analyzed in the CFB riser using a high-speed camera and optical fiber probe (chapter 2; chapter 4; chapter 6). Particle clusters, having their solids holdup increase monotonically and sharply from the surrounding, are considered as basic aggregations. Some clusters, namely crest cluster, immersed in a cloud of coalesced particles, while other clusters, namely trough clusters, are surrounded by dispersed particles. In other words, there are four distinctive phases in the CFB riser, namely crest clusters, coalesced particles, trough clusters and dispersed particles. Then, a phase discrimination method has been proposed to extract phase information from optical fiber probe signals (chapter 2; chapter 7). Phase information

originated from this phase discrimination method was verified in terms of phase characteristics using a high-speed camera (chapter 7:).

As optical fiber probe is feasible in high-density conditions and probe signals have been well interpreted with the help of the high-speed camera, this work employed optical fiber probe to measure the instantaneous solids holdup in a large scale CFB riser (10m high). Superficial gas velocity spans from 5 to 9 m/s and solids circulation rate ranges from 200 kg/m²s to 700 kg/m²s. Then, “dilute structure” and “dense structure” are identified in the CFB based on signal characteristics. A transition from “dilute structure” to “dense structure” has been identified in the wall region at high-density conditions. With a verified discrimination method, phases, namely crest clusters, coalesced particles, trough clusters and dispersed particles, are discriminated and characterized in terms of solids holdup, length, frequency and time fraction. After that, phase properties were further analyzed in both radial and axial directions. Moreover, statistic phase properties in the fully developed region were plotted versus operating conditions.

8.2 Experimental

8.2.1 Circulating fluidized bed (cylindrical riser)

The experiments were conducted in a multifunctional circulating fluidized bed (MCFB) system (see Figure 8-1). This system contains one riser (76 mm i.d. and 10 m high) and two downers (76 mm i.d. and 5.8 m high; 50 mm i.d. and 4.9 m high;). For the operating of CFB riser, superficial gas velocity ranges from 3 to 9 m/s and solids circulation rate spans from 200 kg/m²s to 700 kg/m²s. Air is introduced from riser bottom through a distributor. Particles (FCC, 67 μm, 1780 kg/m³) in solids storage tank enter riser through an inclined pipe. After a though mixing, gas entrains particles upward. Once the air-solids mixture is out of riser, it goes to cyclones and a bag filter in series with gas released and particles recovered. Then, the recovered particles go to the storage tank through a downcomer. To increase the flowability of particles, aerated gas is also introduced into solids storage tank to maintain minimum fluidization. Superficial gas velocity is regulated using a rotameter and solids circulation rate is controlled using a valve installed in the inclined pipe between the storage tank and riser bottom. By adjusting the valves

installed in the upper downcomer, how much particles accumulated in unit time is obtained to monitor the solids circulation rate. Details of this CFB was elaborated in previous papers (Wang, 2013).

8.2.2 Optical fiber probe

Optical fiber probe was used to measure local solids holdup in the CFB riser. The probe, model PV6D, was manufactured in Institute of Process Engineering, Chinese Academy of Science, Beijing, China. This optical fiber probe is 3.8 mm in diameter and has two sub-probes aligned vertically. For each sub-probe, there are emitting fibers and receiving fibers. Light emitted from fibers hit the surface of particles, reflected to probe and receiver by receiving fibers. Light intensity is then converted to voltages. Sampling frequency was set to be 100kHz for a good resolution. A calibration between voltage and solids holdup was established by creating a uniform suspension in a slim downer (Zhang et al., 1998). As the effective distance of sub-probes is 1.51mm, particle velocity can be computed with the time lag between sub-probes. To map the entire riser, optical fiber probe was inserted into 10 heights ($z=0.59$ m, 1.02 m, 1.94, 2.85 m, 3.77 m, 4.78 m, 5.84 m, 7.78 m, 9.61 m and 10.09 m) and 6 radial positions ($r/R=0, 0.316, 0.548, 0.707, 0.837$ and 0.950), where r is the distance from riser center and R is riser radius. Details information of this probe and data processing was elaborated in previous papers (Wang, 2013; chapter 2; chapter 7;).

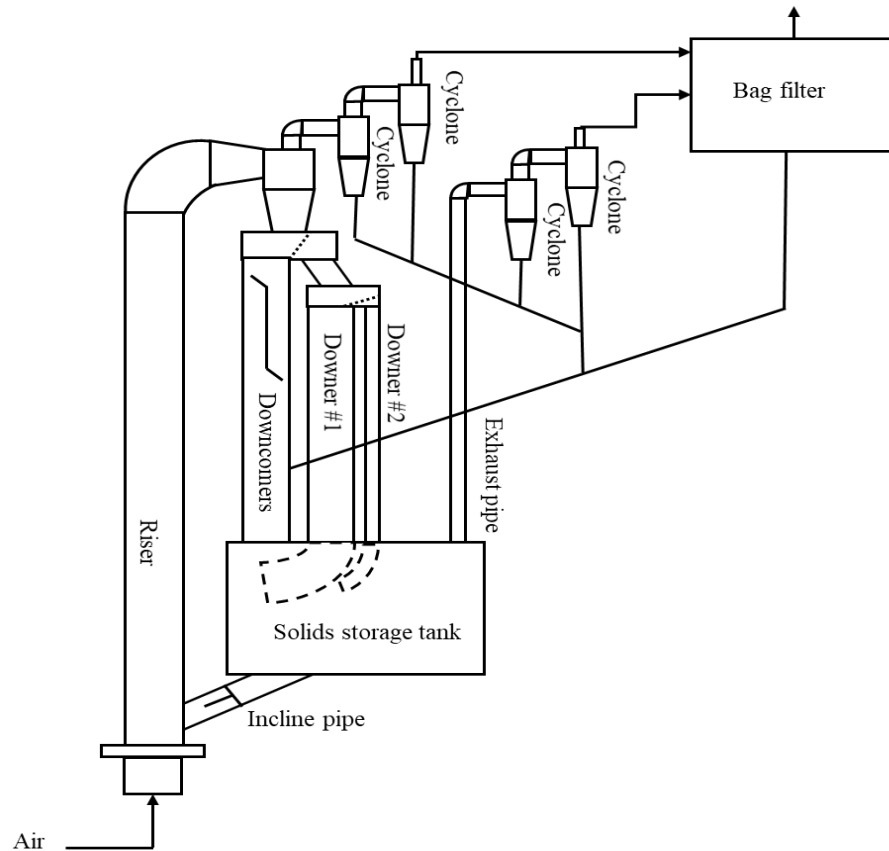


Figure 8-1 Schematic diagram of the circulating fluidized bed

8.2.3 Signal details

With the help of the high-speed camera and optical fiber probe, it has been confirmed that there are four distinctive phases, namely crest clusters, coalesced particles, trough clusters and dispersed particles, coexisting in the CFB riser (chapter 4). With the solids holdup characteristics, solids holdup signals are well interpreted: peaks inside crescents, remaining regions in crescents, peaks outside crescents, remaining regions outside crescents correspond to crest clusters, coalesced particles, trough clusters and dispersed particles, respectively (see Figure 8-2). Crest clusters and their surrounding coalesced particles are considered as crest phase, as they have continuous high solids holdup. Correspondingly, trough clusters and their surrounding dispersed particles are considered as trough phase, as they have continuous low solids holdup. In the previous study, a phase discrimination method, applicable to optical fiber probe signals, has been proposed and

verified quantitatively using a high-speed camera (chapter 7). Details information has been elaborated in previous papers (chapter 2, chapter 4, chapter 6, chapter 7).

Essentially, this phase discrimination decomposes solids holdup signal into a series of scales using wavelet transform. With the analysis and sensitivity test, information in different scales are interpreted physically:

1. $d1$ and $d2$ correspond to the signal noise and $a2$, instead of the original signal, is used for further analysis.
2. Fragments in $a2$, whose solids holdup is higher than $a10$, correspond to crest clusters and trough clusters.
3. Fragments in $a2$, where solids holdup in $a10$ is above $a17$, correspond to crest phase.

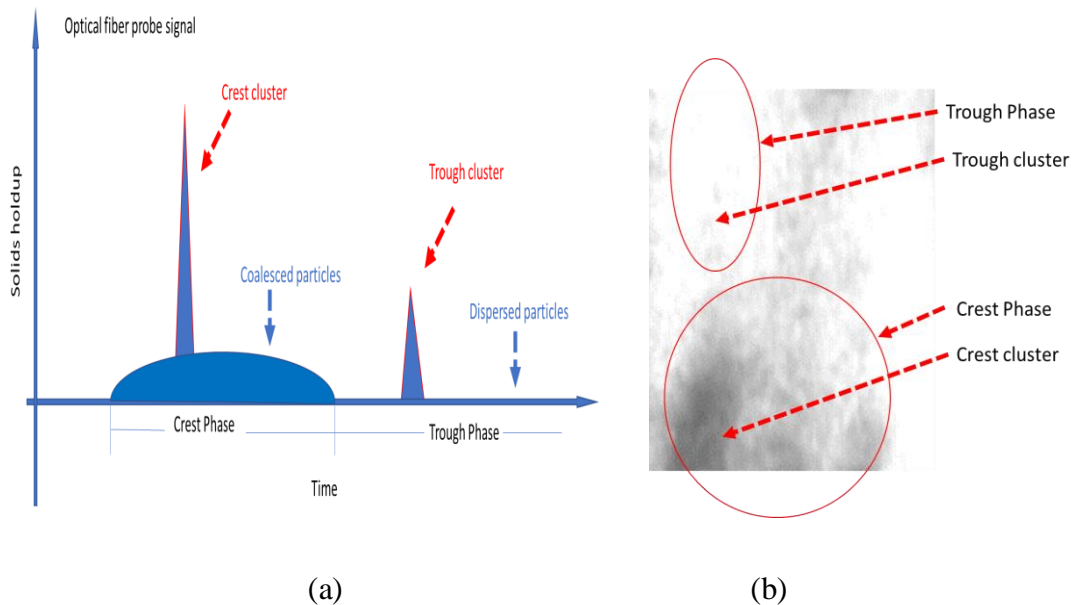


Figure 8-2 The instantaneous flow structure in the CFB (a: phase interpretation for signals captured by optical fiber probe, b: phase interpretation for images captured by the high-speed camera)

To remove natural oscillation of solids holdup, clusters shall have their size at least 5 times particle diameter (d_p), crest phase shall be larger than 2 cm, maximum cluster solids holdup shall be at least 0.01 higher than a10, and maximum solids holdup of crest phase shall be at least 0.01 higher than a17. Then, clusters are further classified into crest clusters and trough clusters, according to whether clusters are in crest phase or not. After that, crest clusters, trough clusters and crest phase were characterized in terms of solids holdup, duration time, frequency and time fraction. Their length was further computed by multiplying duration time with particle velocity. Finally, coalesced particles and dispersed particles are also characterized in solids holdup and time fraction using equations 8-1, 8-2, 8-3 and 8-4 where T_{pc} is time fraction of coalesced particles, T_{cp} is time fraction of crest phase, T_{cc} is time fraction of crest clusters, T_{tc} is time fraction of trough clusters, ε_{pc} is solids holdup of coalesced particles, ε_{ip} is solids holdup of dispersed particles, ε_{cp} is solids holdup of crest phase, ε_{cc} is solids holdup of crest clusters, ε_{tc} is solids holdup of trough clusters, ε_{ip} is solids holdup of dispersed particles, ε_m is mean solids holdup.

$$T_{pc} = T_{cp} - T_{cc} \quad \text{Equation 8-1}$$

$$T_{ip} = 1 - T_{cp} - T_{tc} \quad \text{Equation 8-2}$$

$$\varepsilon_{pc} = \frac{\varepsilon_{cp}*(T_{cc}+T_{pc})-\varepsilon_{cc}*T_{cc}}{T_{pc}} \quad \text{Equation 8-3}$$

$$\varepsilon_{ip} = \frac{\varepsilon_m - T_{cp}*\varepsilon_{cp} - T_{tc}*\varepsilon_{tc}}{1 - T_{cp} - T_{tc}} \quad \text{Equation 8-4}$$

8.3 Results and discussion

8.3.1 Overall flow structure

Solids holdup signals in the riser center and riser wall were plotted in both low and high solids circulation rate (see Figure 8-3). At low solids circulation rate, solids holdup signals are characterized by sharp peaks and beneath crescents across riser, which is consistent with previous studies (review; chapter 1). At high solids circulation rate, solids

holdup signals in the riser center are also featured with narrow sharp peaks and beneath crescents. However, these sharp peaks (crest clusters and trough clusters) possess higher solids holdup (even above 0.3) than those at low solids circulation rate. At high solids circulation rate, a new flow pattern has been identified in the riser wall: a straight line scattered with dilute gorges. Characteristics of this pattern is similar to flow structure of bubbling or turbulent fluidized bed where straight line represents continuous particulate phase and dilute gorge represents dispersed bubbles (Zhu et al., 2013). Thus, we suggest naming this signal pattern as “dense structure”, as it is featured with the particulate phase whose solids holdup is above 0.45. Correspondingly, the instantaneous flow structure in the riser center is suggested naming as “dilute structure”, as its solids holdup is significantly lower than that of “dense structure”. Moreover, the transition between “dilute structure” and “dense structure” was also recorded using the optical fiber probe (see Figure 8-4). This probe signal combines those two patterns where sharp peaks still exist and the particulate phase begins to appear.

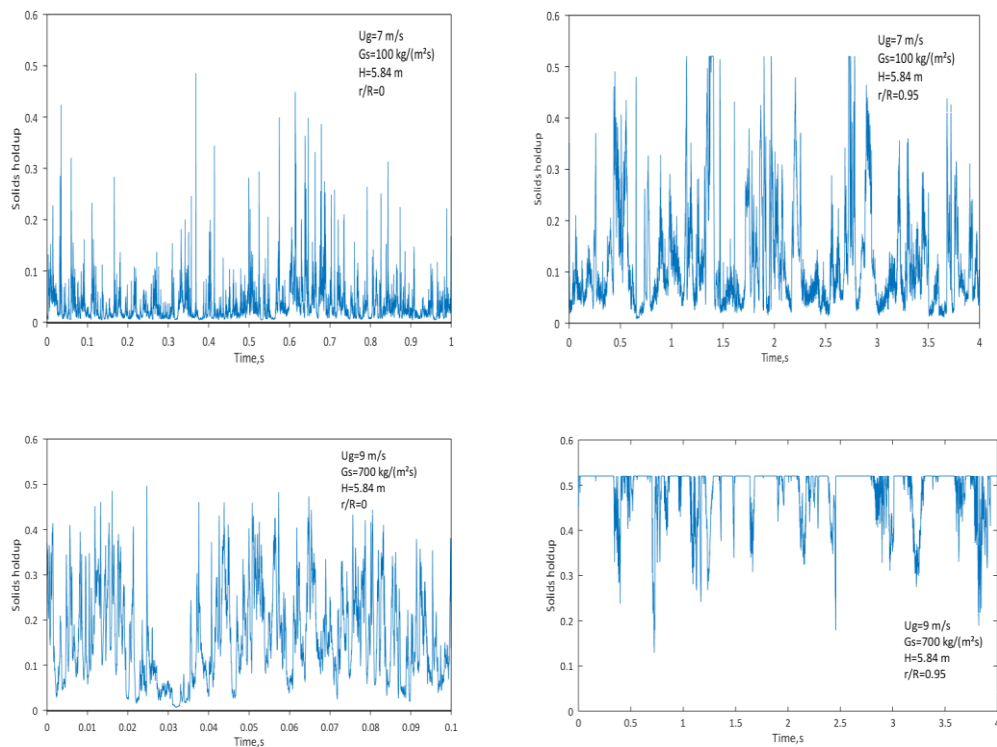


Figure 8-3 Solids holdup signals captured in low density and high density conditions

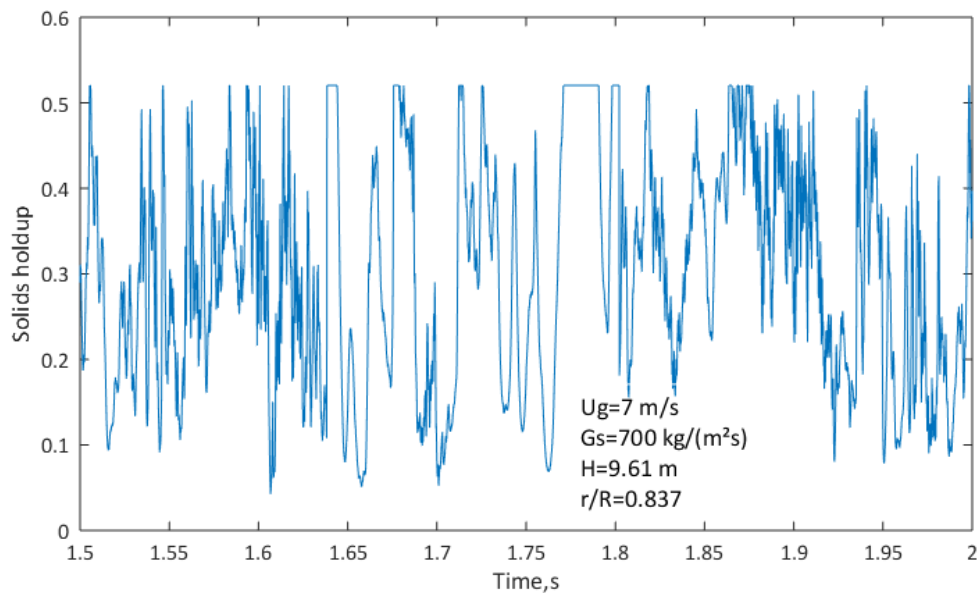


Figure 8-4 A transition signal from “dilute structure” and to “dense structure”

These two structures provide different ways for gas-particle contact, which could result in different mechanism for heat and mass transfer. As the major difference between two structures is the appearance of particulate phase, time fraction of particulate phase (solids holdup is higher than 0.45) was calculated to estimate the portion of the dense structure (see Figure 8-5). At high solids circulation rate, time fraction of the particulate phase is low in the riser center, but close to 1 in the riser wall. Along riser, the radial portion where particulate phase appears first increases then decreases. This distribution of dense structure is consistent with the thickness of the annulus region (Kim et al., 2004). This is the first time that dense structure has been reported in the annulus region of high solids circulation rate condition. Data from other instruments is needed for further verification.

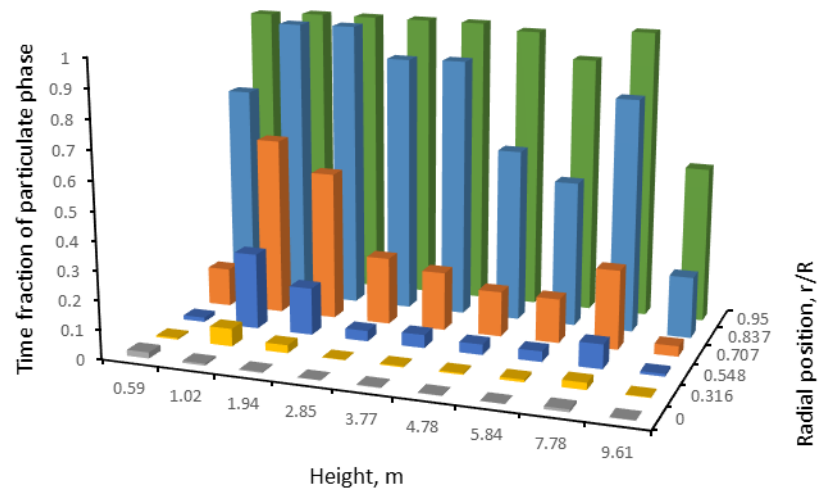


Figure 8-5 Distribution of particulate phase ($U_g = 7$ m/s and $G_s = 700$ kg/m²s)

As foresaid, there are four basic phases in the riser center: crest clusters, coalesced particles, trough clusters and dispersed particles. According to the previous study on hydrodynamics, most of gas and solids are entrained through core region, owing to the high gas velocity and high solids flux in the riser center (Wang et al., 2014b). Thus, the phase characterization in the riser core is crucial for the overall performance of CFB riser. With the discrimination method elaborated in “data processing”, phase solids holdup in fully developed region ($H=7.78$) was plotted versus radial positions ($r/R=0, 0.316, 0.548, 0.707$) in Figure 8-6. Phase solids holdup increases from $r/R=0$ to $r/R=0.707$. Comparatively, crest clusters have the highest solids holdup, followed by trough clusters, coalesced particles and dispersed particles, which agrees well with previous studies (chapter 2; chapter 4; chapter 7;).

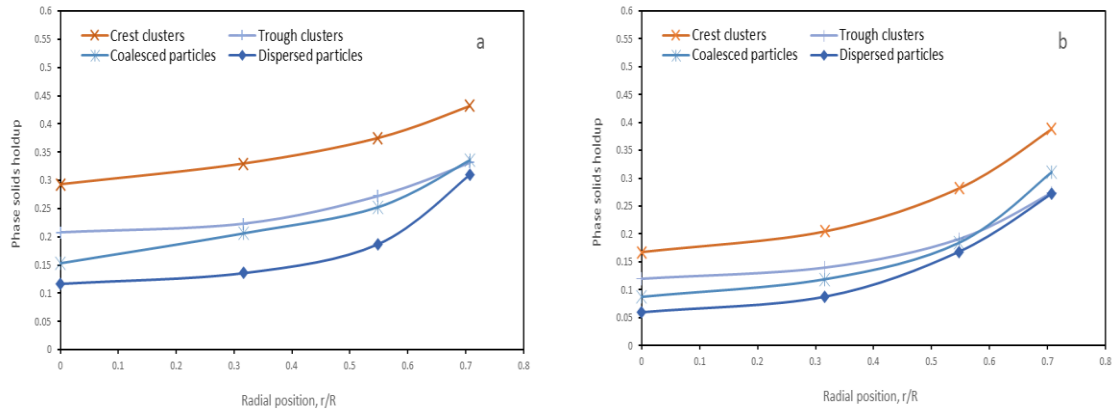


Figure 8-6 Radial distributions of phase solids holdup (a: 7 m/s-700 kg/m²s, b:5 m/s-400 kg/m²s)

8.3.2 Trough clusters and crest clusters

As trough clusters and crest clusters are dominant in terms of solids holdup, their solids holdup, length, frequency and time fraction were discussed in perspectives of radial distributions (at 7.78 m), axial distributions and statistic properties in the fully developed region. Axial distributions were calculated based on the spatial-average phase properties in the riser core ($r/R=0, 0.316, 0.548, 0.707$). Statistics properties in the fully developed region were calculated based on data acquired at heights (4.78 m, 5.84 m, 7.78 m, 9.61 m and 10.09m).

Radial distributions were plotted in Figure 8-7. Solids holdup of crest clusters and trough clusters increases from $r/R=0$ to $r/R=0.707$, which agrees well with Figure 8-6. This increase is more profound in high solids circulation rate conditions. Length of crest clusters decreases from $r/R=0$ to $r/R=0.707$ at $G_s = 100 \text{ kg/m}^2\text{s}$, but increases from $r/R=0$ to $r/R=0.707$ at $G_s = 300, 400, 700 \text{ kg/m}^2\text{s}$. Length of trough clusters first increases then decreases from $r/R=0$ to $r/R=0.707$ at $G_s = 100, 300 \text{ kg/m}^2\text{s}$. Length of trough clusters increases from $r/R=0$ to $r/R=0.707$ at $G_s = 400, 700 \text{ kg/m}^2\text{s}$.

Collectively, the length of crest clusters and trough clusters have their radial distribution dependent on operating conditions. The frequency of crest clusters and trough clusters is first constant, then decreases at low solids circulation rate ($G_s = 100, 300 \text{ kg/m}^2\text{s}$). The

frequency of crest clusters and trough clusters decreases from $r/R=0$ to $r/R=0.707$ at high solids circulation rate ($G_s = 400, 700 \text{ kg/m}^2\text{s}$). The frequency of certain phase denotes to how many times a specific phase appears in unit time, indicating that frequency is a function of cluster probability and velocity. The previous study has reported that (1) particle velocity is flat then decreases toward riser wall, when solids circulation rate is low, (2) particle velocity decreases toward riser wall, when solids circulation rate is high (Wang et al., 2014b). This may explain why the frequency of crest clusters and trough clusters is dependent on solids circulation rate. Time fraction of certain phase, to some extent, reflects volumetric fraction occupied by certain phase. Time fraction of crest clusters remains constant across riser center at $G_s = 100, 300 \text{ kg/m}^2\text{s}$. Time fraction of crest clusters decreases after $r/R=0.5$ at $G_s = 400, 700 \text{ kg/m}^2\text{s}$. Time fraction of trough clusters is constant and starts to decrease after $r/R=0.5$. The decrease of time fraction may relate with (1) the transition of flow structure at high solids circulation rate, (2) shear force generated due to the velocity difference between riser center and riser wall. In the radial direction, crest clusters and trough clusters have their properties in the same magnitude and share similar distributions in terms of solids holdup, length, frequency and time fraction.

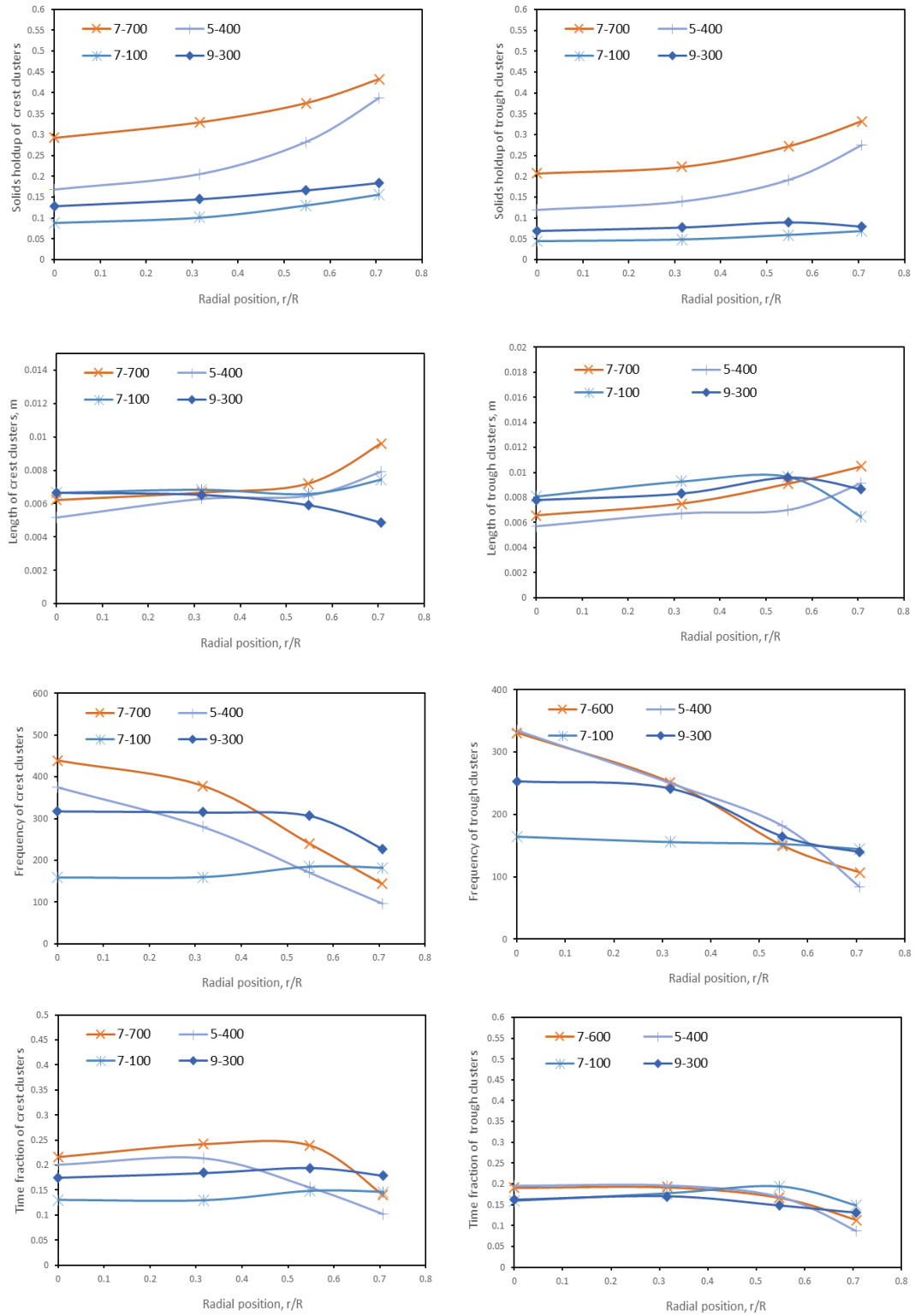


Figure 8-7 Properties of crest clusters and trough clusters versus radial positions

Axial distributions were plotted to explore the evolution of crest clusters and trough cluster along riser (see Figure 8-8). Axially, there are two regions along riser, namely acceleration region and fully developed region (Wang et al., 2014a; Wang et al., 2014b; Li et al., 2013). Particles are accelerated by high-velocity gas in acceleration region, and get fully accelerated in fully developed region.

Solids holdup of crest clusters and trough clusters decrease with height in acceleration region and becomes stable in the fully developed region. This indicates crest clusters and trough clusters are dense at solids entrance and becomes dilute due to the gas-particle interaction. Length of crest clusters first decreases then becomes constant at low solids circulation rate. At high solids circulation rate, length of crest clusters remains stable along CFB riser. Length of trough clusters is constant along CFB riser, when solids circulation rate is low. Length of trough clusters first increases then becomes constant, when solids circulation rate is high. The frequency of crest clusters and trough clusters increases with height in acceleration region and becomes constant in the fully developed region. As foresaid, the frequency of certain phase is positively related to velocity. The axial trends can be explained by the acceleration of particles. Collectively, these axial distributions are consistent with the existence of acceleration region and fully developed region along CFB riser. However, the crest cluster and trough cluster have different trends in axial directions in terms of length. Crest clusters are surrounded by coalesced particles, while trough clusters are immersed in dispersed particles. Coalesced particles have higher solids holdup than dispersed particles, which may result in a different mechanism of particle collision. This study only reports the trend of axial distributions. Further study on the aggregation mechanism is still needed to explain these trends.

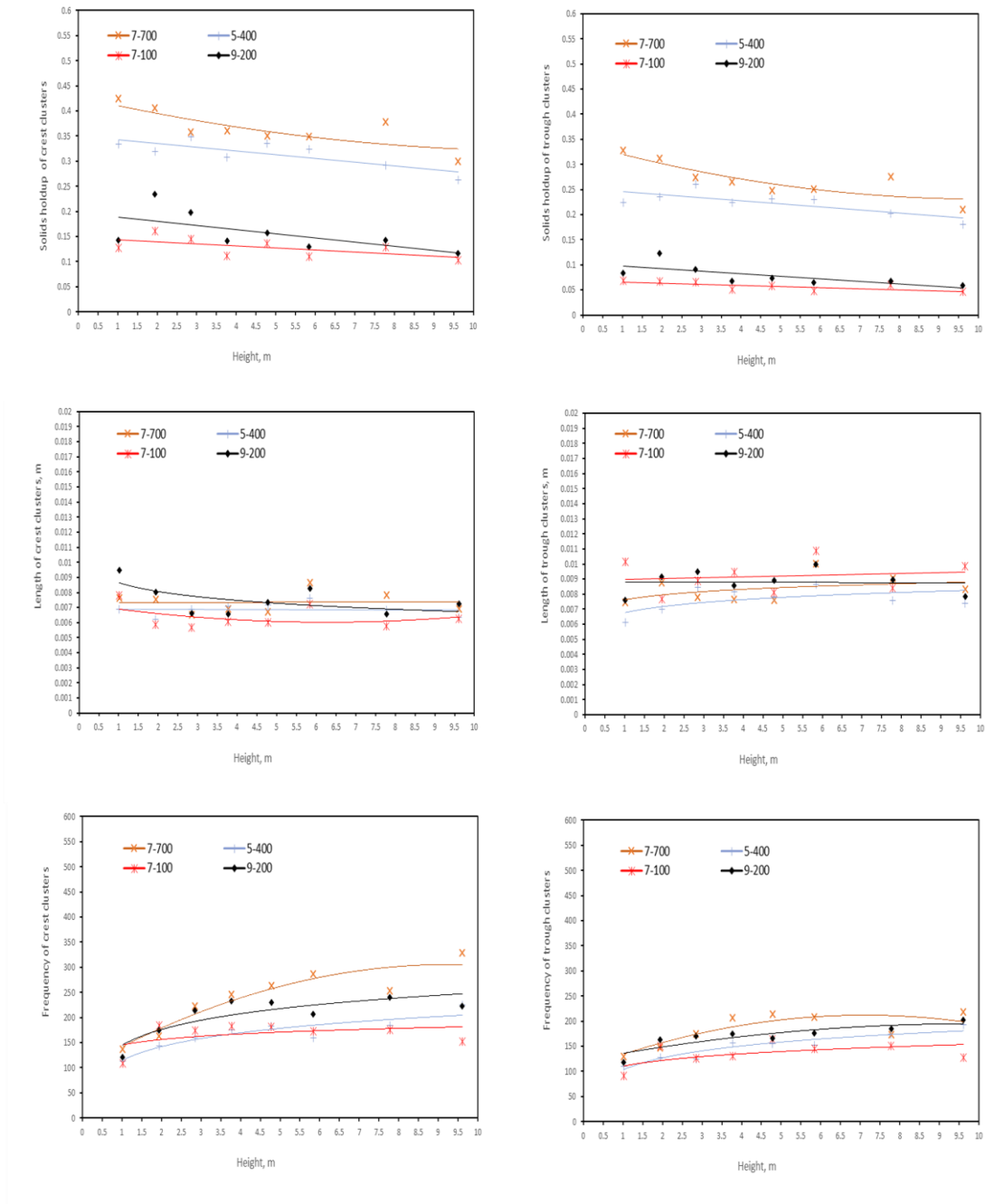


Figure 8-8 Properties of crest clusters and trough clusters versus axial positions

In order (1) to investigate how phase properties change with operating conditions, (2) to facilitate the development and validation of numerical modeling, statistic properties of crest clusters and trough clusters in the fully developed region were plotted versus operating conditions (see Figure 8-9). Solids holdup of crest clusters and trough clusters

increases with solids circulation rate and decreases with superficial gas velocity, which is consistent with how mean solids holdup change with operating conditions (Wang et al., 2015). In addition, solids holdup of crest clusters and trough clusters are more sensitive to solids circulation rate at $U_g = 5$ m/s comparing with that at $U_g = 7, 9$ m/s. Length of crest clusters first increases, then decreases with solids circulation rate. Length of trough clusters decreases monotonically with solids circulation rate. For both crest clusters and trough clusters, the length difference between $U_g = 7$ m/s and $U_g = 9$ m/s reduces with solids circulation rate. The frequency of crest and trough clusters increases with both superficial gas velocity and solids circulation rate. Frequency denotes to the number of a specific phase detected in unit time. High solids circulation rate may increase the number of aggregations due to the enrichment of particles, while high superficial gas velocity results in the fast motion of aggregations. Time fraction of crest clusters is not sensitive to superficial gas velocity, but increases with solids circulation rate. Time fraction of trough clusters is not sensitive to solids circulation rate, but increases with superficial gas velocity. This figure reports the trend on how phase properties change with operating conditions. Further analysis is needed to address the causes of the differences between crest clusters and trough clusters.

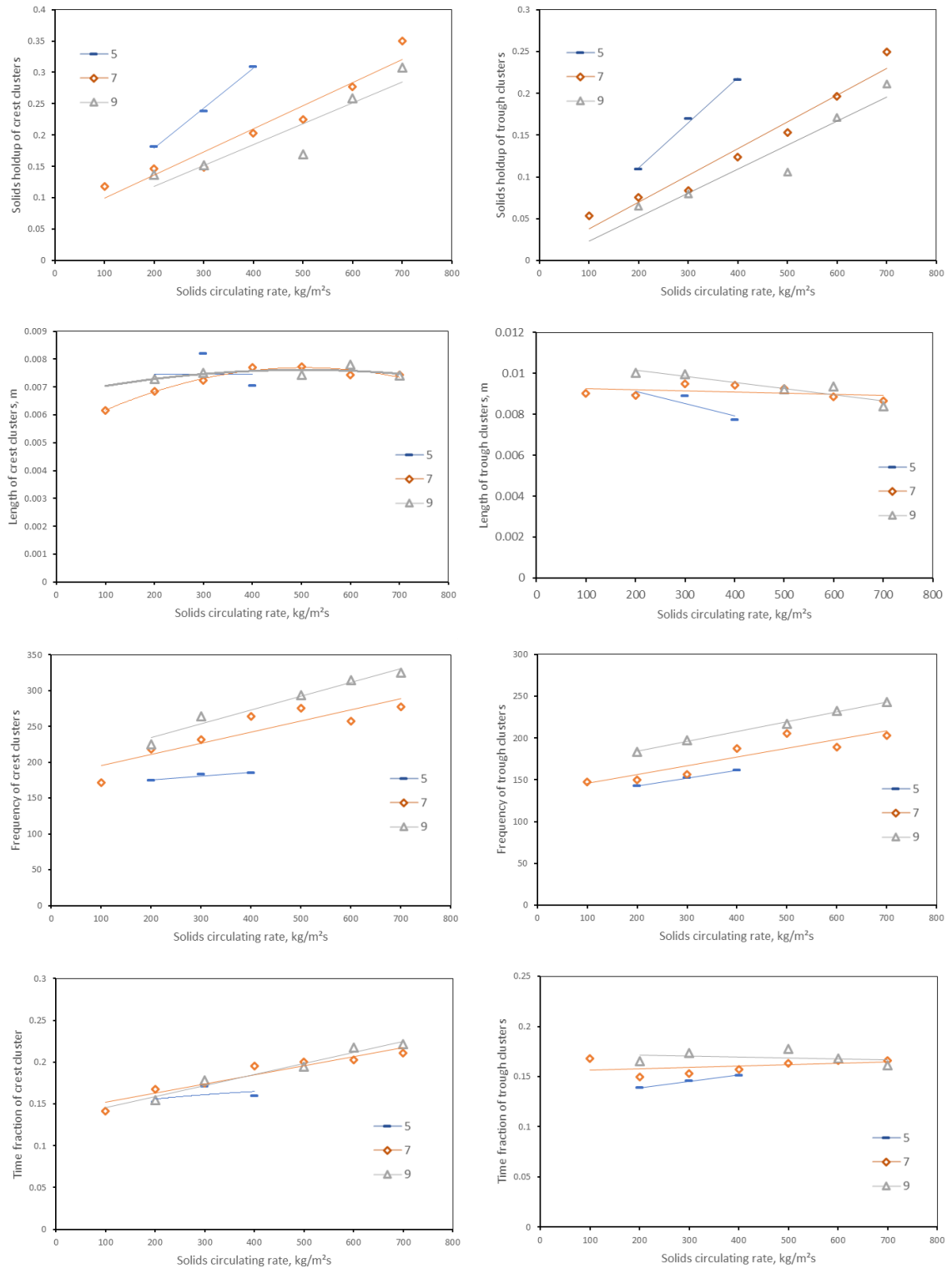
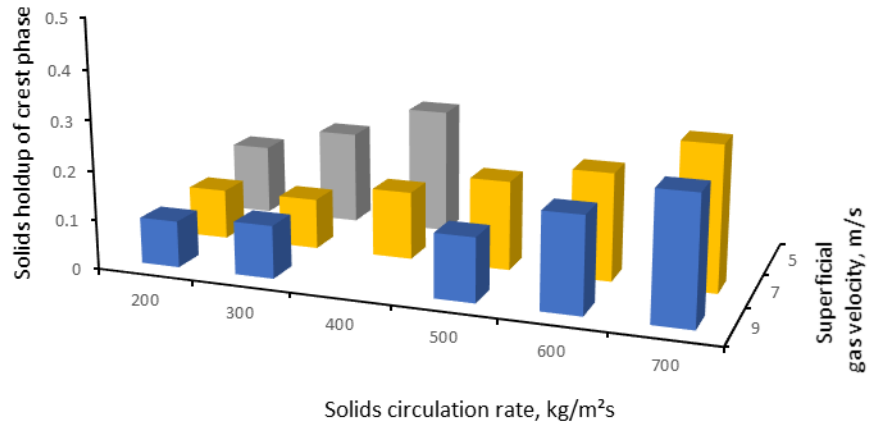


Figure 8-9 Statistic phase information versus operating conditions

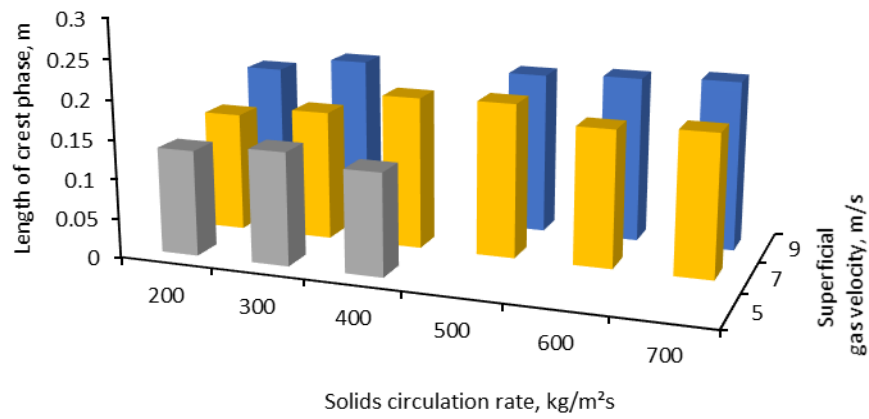
8.3.3 Crest phase

Given that crest clusters and their surrounding coalesced particles have continuous high solids holdup, they are named as crest phase in macroscope (chapter 2; chapter 4).

Additionally, crest phase has been characterized in solids holdup and length (see Figure 8-10). Solids holdup of crest phase increases with solids circulation rate and decreases with superficial gas velocity. Solids holdup of crest phase at $U_g = 5$ m/s is more sensitive to solids circulation rate than that at $U_g = 7$ m/s and $U_g = 9$ m/s. Statistically, crest phase has its length around 20cm in this work. Length of crest phase is not sensitive to solids circulation rate, but increases with superficial gas velocity.



(a)



(b)

Figure 8-10 Information of crest phase versus operating conditions (a: solids holdup, b: length)

8.4 Conclusions

In this work, instantaneous flow behavior has been explored using an optical fiber probe in a wide range of operating conditions. “Dilute structure” and “dense structure” have been identified based on solids holdup characteristics. A transition from Dilute structure” to “dense structure” has been identified in the riser wall at high solids circulation rate. Then, the radial fraction occupied by “dense structure” first increases then decreases along riser height. With a verified discrimination method, essential phases, including crest clusters, coalesced particles, trough clusters and dispersed particles, are characterized in solids holdup, length, frequency and time fraction. It has been found that crest clusters and trough clusters are found to be dominant in terms of solids holdup. Then, crest clusters and trough clusters are further discussed in radial distributions, axial distributions and statistical data in the fully developed region. To the best of our knowledge, this is the first time that the instantaneous flow structure in the CFB has been thoroughly analyzed at such a high solids circulation rate ($700 \text{ kg/ m}^2 \text{ s}$), which well prepares for the development and validation of numerical models in high-density conditions.

Nomenclature

U_g is superficial gas velocity, [m/s];

G_s is solids circulation rate, [kg/m²s];

T_{pc} is time fraction of coalesced particles;

T_{cp} is time fraction of crest phase;

T_{cc} is time fraction of crest clusters;

T_{tc} is time fraction of trough clusters;

ϵ_{pc} is solids holdup of coalesced particles;

ϵ_{ip} is solids holdup of dispersed particles;

ϵ_{cp} is solids holdup of crest phase;

ϵ_{cc} is solids holdup of crest clusters;

ϵ_{tc} is solids holdup of trough clusters;

ϵ_{ip} is solids holdup of dispersed particles;

ϵ_m is mean solids holdup;

References

- Bi, H. T., Zhu, J. X., Jin, Y., & Yu, Z. Q. (1994). Forms of particle aggregations in CFB. In *Proceedings of the Sixth Chinese Conference on Fluidization*, Wuhan, China (pp. 162-167).
- Cahyadi, A., Anantharaman, A., Yang, S., Karri, S. R., Findlay, J. G., Cocco, R. A., & Chew, J. W. (2017). Review of cluster characteristics in circulating fluidized bed (CFB) risers. *Chemical Engineering Science*, 158, 70-95.
- Harris, A. T., Davidson, J. F., & Thorpe, R. B. (2002). The prediction of particle cluster properties in the near wall region of a vertical riser (200157). *Powder Technology*, 127(2), 128-143.
- Hatano, H., Kido, N., & Takeuchi, H. (1994). Microscope visualization of solid particles in circulating fluidized beds. *Powder Technology*, 78(2), 115-119.
- Horio, M., & Kuroki, H. (1994). Three-dimensional flow visualization of dilutely dispersed solids in bubbling and circulating fluidized beds. *Chemical Engineering Science*, 49(15), 2413-2421.
- Kim, S. W., Kirbas, G., Bi, H., Lim, C. J., & Grace, J. R. (2004). Flow behavior and regime transition in a high-density circulating fluidized bed riser. *Chemical Engineering Science*, 59(18), 3955-3963.
- Li, H., Xia, Y., Tung, Y., & Kwauk, M. (1991). Micro-visualization of clusters in a fast fluidized bed. *Powder Technology*, 66(3), 231-235.
- Lim, K. S., Zhu, J. X., & Grace, J. R. (1995). Hydrodynamics of gas-solid fluidization. *International journal of multiphase flow*, 21, 141-193.
- Li, D., Ray, M. B., Ray, A. K., & Zhu, J. (2013). A comparative study on hydrodynamics of circulating fluidized bed riser and downer. *Powder technology*, 247, 235-259.

- Li, X. T., Grace, J. R., Lim, C. J., Watkinson, A. P., Chen, H. P., & Kim, J. R. (2004). Biomass gasification in a circulating fluidized bed. *Biomass and bioenergy*, 26(2), 171-193.
- Manyele, S. V., Pärssinen, J. H., & Zhu, J. X. (2002). Characterizing particle aggregates in a high-density and high-flux CFB riser. *Chemical Engineering Journal*, 88(1), 151-161.
- Shaffer, F., Gopalan, B., Breault, R. W., Cocco, R., Karri, S. R., Hays, R., & Knowlton, T. (2013). High speed imaging of particle flow fields in CFB risers. *Powder Technology*, 242, 86-99.
- Wang, C., Wang, G., Li, C., Barghi, S., & Zhu, J. (2014c). Catalytic ozone decomposition in a high density circulating fluidized bed riser. *Industrial & Engineering Chemistry Research*, 53(16), 6613-6623.
- Wang, C., Zhu, J., Barghi, S., & Li, C. (2014a). Axial and radial development of solids holdup in a high flux/density gas–solids circulating fluidized bed. *Chemical Engineering Science*, 108, 233-243.
- Wang, C., Zhu, J., Li, C., & Barghi, S. (2014b). Detailed measurements of particle velocity and solids flux in a high density circulating fluidized bed riser. *Chemical Engineering Science*, 114, 9-20.
- Wang, C., Li, C., Zhu, J., Wang, C., Barghi, S., & Zhu, J. (2015). A comparison of flow development in high density gas - solids circulating fluidized bed downer and riser reactors. *AIChE Journal*, 61(4), 1172-1183.
- Wilhelm, R. H., & Kwauk, M. (1948). Fluidization of solid particles. *Chemical Engineering Progress*, 44(3), 201-218.
- Xu, J., & Zhu, J. X. (2011). Visualization of particle aggregation and effects of particle properties on cluster characteristics in a CFB riser. *Chemical Engineering Journal*, 168(1), 376-389.

Yang, J., & Zhu, J. (2014a). A novel method based on image processing to visualize clusters in a rectangular circulating fluidized bed riser. *Powder Technology*, 254, 407-415.

Yang, J., & Zhu, J. (2014b). An alternative method for mapping solids holdup in a narrow rectangular CFB riser through image calibration. *The Canadian Journal of Chemical Engineering*, 92(12), 2202-2210.

Zhang, H., Johnston, P. M., Zhu, J. X., De Lasa, H. I., & Bergougnou, M. A. (1998). A novel calibration procedure for a fiber optic solids concentration probe. *Powder Technology*, 100(2-3), 260-272.

Zhu, J. X., & Bi, H. T. (1995). Distinctions between low density and high density circulating fluidized beds. *The Canadian Journal of Chemical Engineering*, 73(5), 644-649.

Zhu, J., & Cheng, Y. (2016). Applications of Fluidized Bed Reactors. In Michaelides, E., Crowe, C. T., & Schwarzkopf, J. D. (Eds.). *Multiphase Flow Handbook* (pp.1029-1058). CRC Press.

Zhu, J., Qi, M., & Barghi, S. (2013). Identification of the flow structures and regime transition in gas–solid fluidized beds through moment analysis. *AIChE Journal*, 59(5), 1479-1490.

CHAPTER 9

A comprehensive characterization of aggregative flow in gas- solid circulating fluidized bed using wavelet analysis: high-density downer

Abstract

To overcome the drawbacks of circulating fluidized bed (CFB) riser, CFB downer has been proposed to provide narrow residence time distribution, reduced back mixing, reduced radial nonuniformity and short contact time. However, almost all studies on CFB downer has their solids circulation rate below $200 \text{ kg/m}^2 \text{ s}$. Low solids circulation rate limits the reaction intensity in the CFB downer, which further reduces reactor efficiency. Our group achieved a wide range of solids circulation rate (ranging from $100 \text{ kg/m}^2 \text{ s}$ to $700 \text{ kg/m}^2 \text{ s}$) in a large-scale downer. In our early study, instantaneous solids holdup has been measured over the whole downer using an optical fiber probe. Utilizing previously acquired data, essential phases, namely crest clusters, trough clusters, coalesced particles and dispersed particles, have been discriminated and characterized in perspectives of solids holdup, length, time fraction and frequency. Then, statistic phase properties in the fully developed region, radial and axial distributions of phase properties are plotted and discussed in detail. Finally, phase information in the CFB downer has been compared between riser and downer. It has been found that aggregation in the downer is less severe than that in the riser. Collectively, this work provides insights on the instantaneous flow behavior of CFB downer in a wide range of operating conditions, which is owed to serve for the understanding of flow mechanism, the development and validation of numerical models.

Keywords: circulating fluidized bed downer; instantaneous flow structure; wavelet analysis, optical fiber probe; high density.

9.1 Introduction

The gas-solid circulating fluidized bed (CFB) riser has wide-spread industrial applications, including combustion and gasification of coal and biomass, FCC (fluid catalytic cracking), calcination, since it provides low pressure drop, solids circulation, high gas and solids output and good contact between gas and solids. However, CFB riser suffers from asymmetry flow, solids back mixing and radial segregation. Then, CFB downer, where gas and solids flow concurrently downward, was proposed to overcome these drawbacks.

Several comparative studies between riser and downer have been done in terms of time-average information, including axial development, radial uniformity and Ozone decomposition. It has been found that (1) solids holdup in the downer is more uniform than that in the riser both axially and radially (Zhang et al., 2001; Zhang et al., 2003; Zhu et al., 1995; Wang et al., 2015a; Wang et al., 2015b); (2) radial distribution of particle velocity in the downer is more uniform than that in the riser (Zhang et al., 2001; Zhang et al., 2003); (3) residence time distribution of solids in the downer is much narrower than that in the riser (Zhu et al., 1995; Wei and Zhu, 1996); (5) gas flow in the downer is closer to plug flow than that in the riser (Wang et al., 2015b).

Similar to CFB riser, CFB downer is essentially a heterogeneous reactor. The overall reactor performances are basically determined by the instantaneous flow information in the CFB downer. Lu et al. (2005) found that particle aggregates to form clusters in the CFB downer using a micro-camera. As cluster has higher solids holdup than surrounding (Soong et al., 1994; Shi et al., 2008) and is much larger compared with particles (Bi et al., 1993; Li et al., 1991), it shelters internal particles away from flowing gas (Yunhau et al., 2006). Tuzla et al. (1998) characterized clusters in terms of solids holdup and duration time using a capacitance probe and the solids circulation rate is below $100 \text{ kg/m}^2\text{s}$. Manyele et al., (2003) analyzed the instantaneous solids holdup using an optical fiber probe and the solids circulation rate is below $200 \text{ kg/m}^2\text{s}$. Collectively, a systematic investigation on the instantaneous flow behavior in the CFB downer remains lacking in the following perspectives: (1) phase classification based on solids holdup characteristics,

(2) phase information in high-density conditions, (3) axial distributions of phase properties, (4) statistics phase properties in the fully developed region.

In this work, optical fiber probe was positioned in the CFB downer to detect the instantaneous solids holdup. Superficial gas velocity in this downer ranges from 3 to 9 m/s. High-density conditions have been achieved with solids circulation rate spanning from 100 kg/m²s to 700 kg/m²s. Then, signals of instantaneous solids holdup were analyzed in solids holdup characteristics and phase classification was conducted using wavelet transform. Phases were characterized in solids holdup, length, frequency and time fraction. Finally, phase properties were plotted versus radial positions, axial positions and operating conditions. Collectively, this systematic investigation on the instantaneous flow information deepens the understanding of the flow behavior in the CFB downer, prepares for further study of heat and mass transfer, and contributes to the development and validation of numerical models.

9.2 Experimental

9.2.1 Circulating fluidized bed (cylindrical downer)

The experiments were conducted in a multifunctional circulating fluidized bed (MCFB) system (see Figure 9-1). This system contains one riser (76 mm i.d. and 10 m high) and two downers (76 mm i.d. and 5.8 m high; 50 mm i.d. and 4.9 m high;). For this work, the experiments were conducted in the downer which is 50 mm i.d. and 4.9 m high. Sketch of downer distributor is shown in figure 2. Solids from riser are recovered using cyclones and enter a chamber where they are fluidized in a minimum fluidization state (see Figure 9-2). Eight brass tubes (25mm i.d.) was installed at chamber bottom. Particles fall from the brass tubes and enter a feeding funnel where they get pre-accelerated by gravity. Below the feeding funnel is the main gas inlet. Downer main gas is introduced through 112 holes of 6.3 mm diameter evenly distributed around the circumference of the column. High-velocity gas jets ensure a thorough mixing of gas and solids at downer entrance. Then, the gas-solid mixture flows concurrently downward in the downer. At downer exit, gas and solids are separated preliminarily with centrifugal force. Gas is released through the exhaust pipe. The remaining solids in gas were further recovered using cyclones and

the bag filter. The recovered particles are returned to the solids storage tank and ready for another cycle through the riser. Axial height in this work refers to the distance from downer entrance. For the operating of CFB downer, superficial gas velocity ranges from 3 m/s to 9 m/s and solids circulation rate can be as high as 700 kg/m²s. Details of this CFB was elaborated in the previous paper (Wang et al., 2015a). The particles we used are FCC of 67 μm (Sauter mean diameter) with a particle density of 1780 kg/m³.

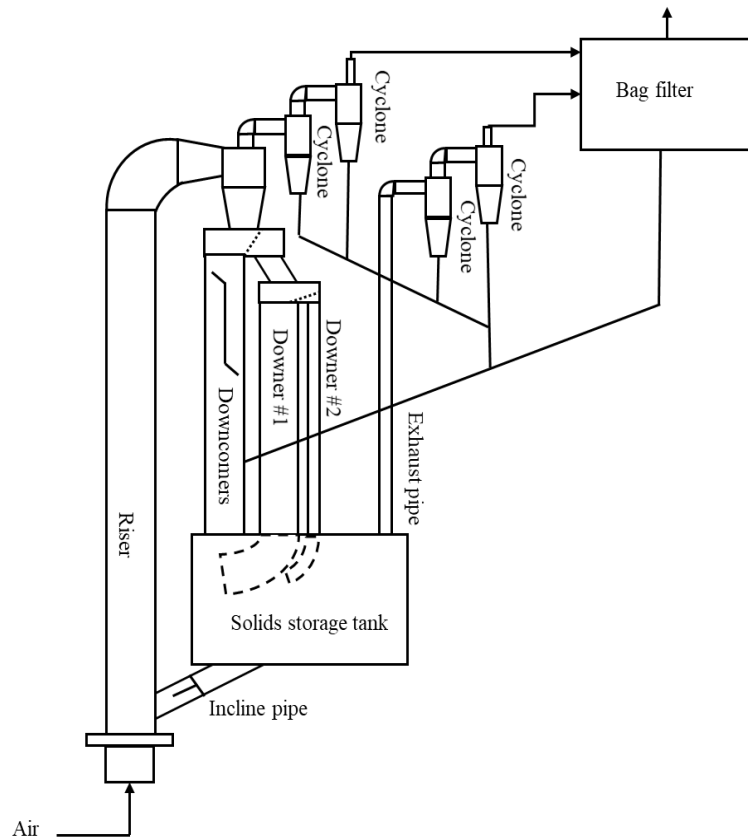


Figure 9-1 Schematic diagram of the multifunctional circulating fluidized bed

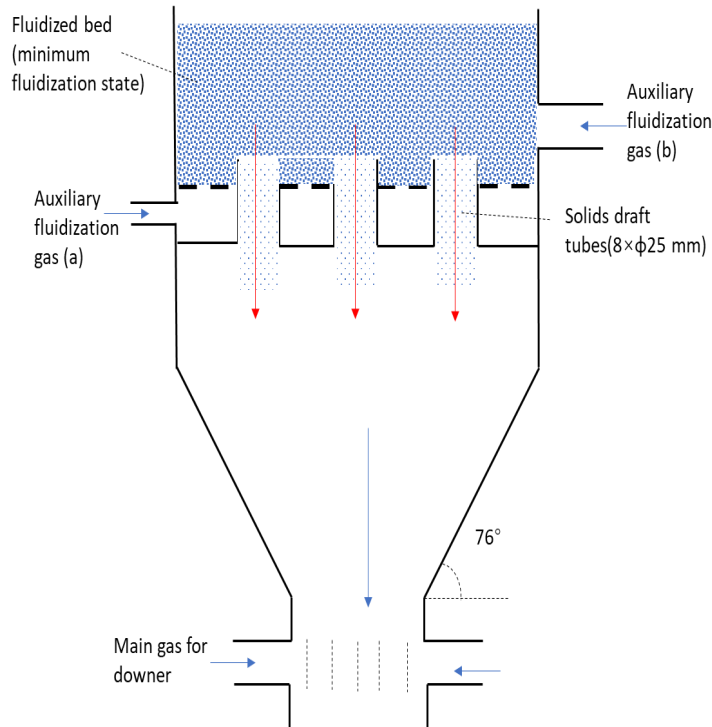


Figure 9-2 Schematic diagram of downer inlet

9.2.2 Optical fiber probe

Optical fiber probe, model PV6D, was employed to detect local solids holdup with a frequency of 100kHz. The probe was manufactured in Institute of Process Engineering, Chinese Academy of Science, Beijing, China. This probe is 3.8 mm in diameter and contains two subprobe. For each subprobe, 8000 optical fibers are arranged arbitrarily. Some fibers emit light and other fibers receive light reflected by particles. Then, the light intensity relates to local solids holdup and it was recorded in voltage. A calibration between voltage and solids holdup was established by creating a uniform suspension in a slim downer (Zhang et al., 1998). The subprobes are arranged vertically and the effective distance between them is 1.51mm. Knowing the distance, particle velocity can be computed with the time lag of the signals. Details information of this probe was elaborated in previous papers (Wang et al., 2015a; 2015b;). To map the entire downer, optical fiber probe was inserted into 10 heights ($z = 0.76, 1.27, 1.78, 2.35, 3.26$ and 4.18 m) and 6 radial positions ($r/R = 0, 0.316, 0.548, 0.707, 0.837$ and 0.950), where r is the distance from downer center and R is downer radius.

9.2.3 Signal details

Example signals acquired Optical fiber probe at $U_g = 7 \text{ m/s}$; $G_s = 300 \text{ kg/m}^2\text{s}$ was shown in figure 9-3. Across riser, signals are a hybrid of peaks and crescents. Comparing with crescents, peaks have higher solids holdup, steeper solids holdup slope. This pattern agrees well with signals in the CFB riser. In the CFB riser, four basic phases have been identified in probe signals with the help of the high-speed camera (see Figure 9-4): crest clusters (peaks within crescents), coalesced particles (regions in crescents excluding peaks), trough clusters (peaks outside crescents) and dispersed particles (region excluding peaks and crescents). As the probe signals in this work have the same solids holdup characteristics with that in the CFB riser, this understanding was adopted to analyze phase information in the CFB downer. Then, a phase discrimination method has been proposed using wavelet analysis.

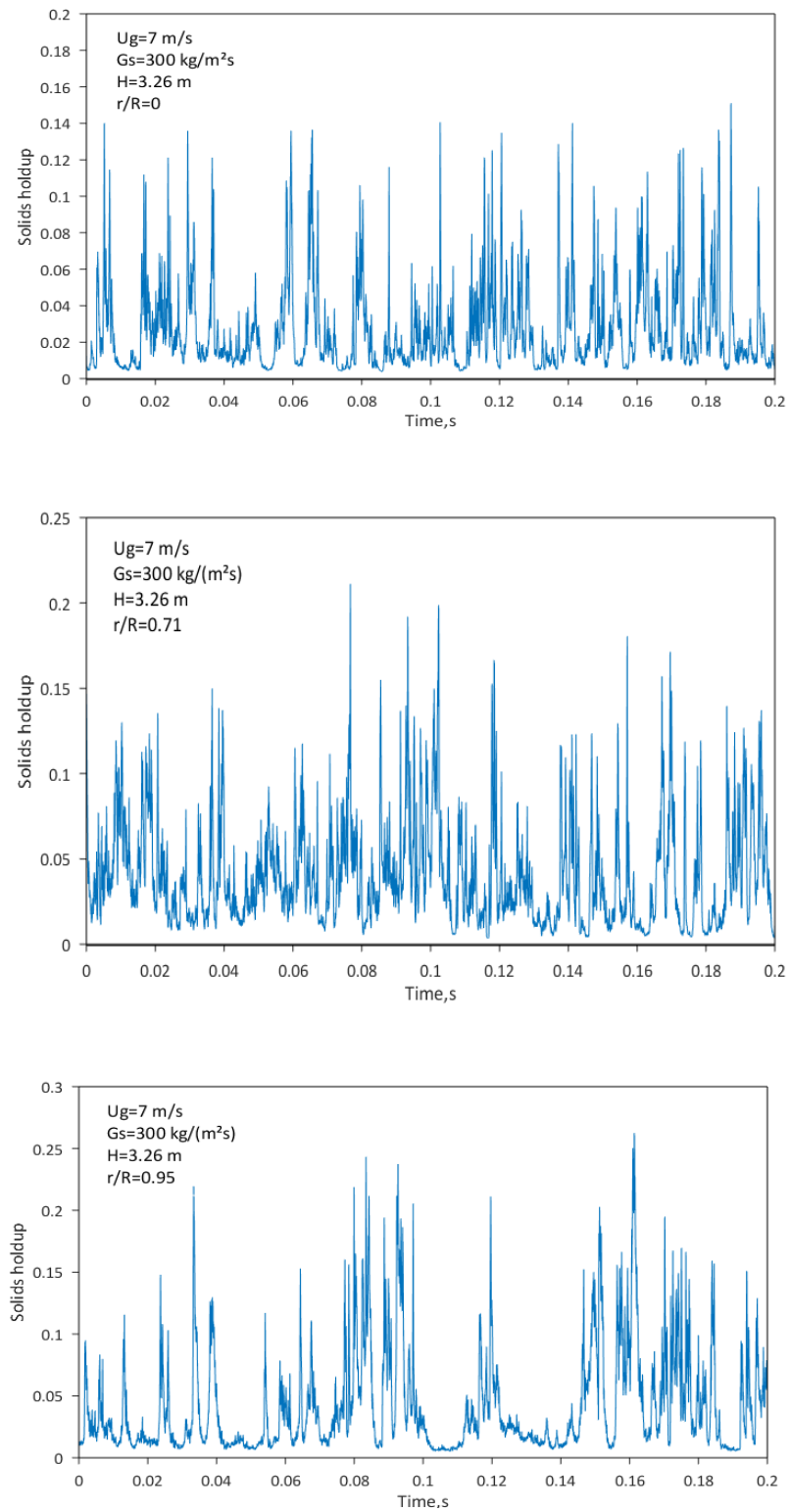


Figure 9-3 Example signals across CFB downer

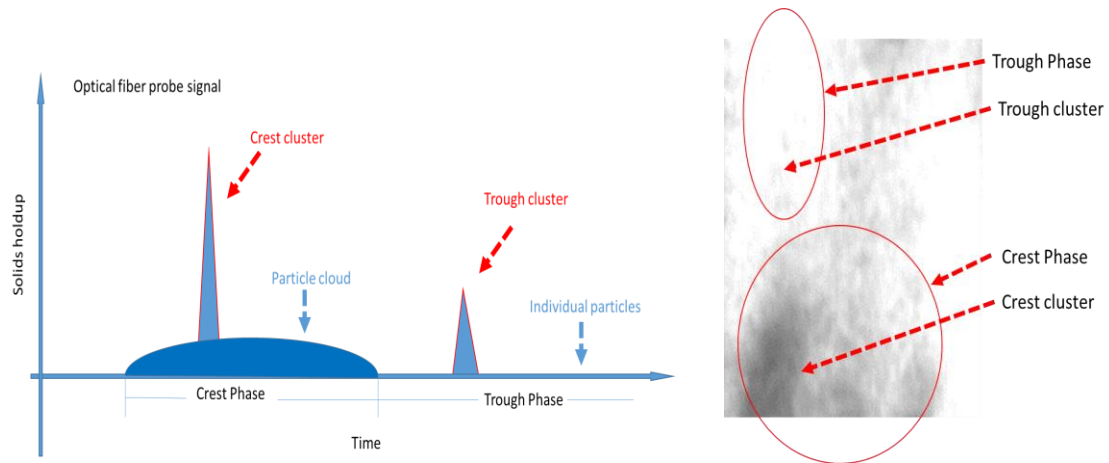


Figure 9-4 The instantaneous flow structure in the CFB (a: phase interpretation for signals captured by optical fiber probe, b: phase interpretation for images captured by the high-speed camera)

The basic principle of wavelet analysis is to decompose signals into different scales. The original signal is first decomposed to d_1 (detail signal) and a_1 (approximate signal). Then, a_1 is further decomposed to d_2 (detail signal) and a_2 (approximate signal). This process continues until the desired scale has been reached. For each scale, the detail signal contains the extracted information and the approximate signal contains the remaining after information extraction. The sharpest and narrowest peaks are first extracted into detail signals, followed by the wide and flat crescents. Then, the fluctuation in the signal is divided into wavelets in different scales. The original signal can be well constructed by adding up the detail signals and the last approximate signal. Details of wavelet analysis have been elaborated in previous papers (Chew et al., 2011; 2012a; 2012b;). The following analysis is based on DB3 (Daubechies Wavelet of order three), as it is symmetrical and results in low residues.

As foresaid, optical fiber probe has two channels and the signals originated from channel 1 and channel 2 were decomposed to 17 scales using wavelet analysis. Cross-correlation of each scale was conducted between two channels and the time lag was plotted versus scale in figure 9-5. d_1 and d_2 have no time lag indicating that they appear in two channels simultaneously, indicating that information in d_1 and d_2 may correspond to noises imposed by electronic components.

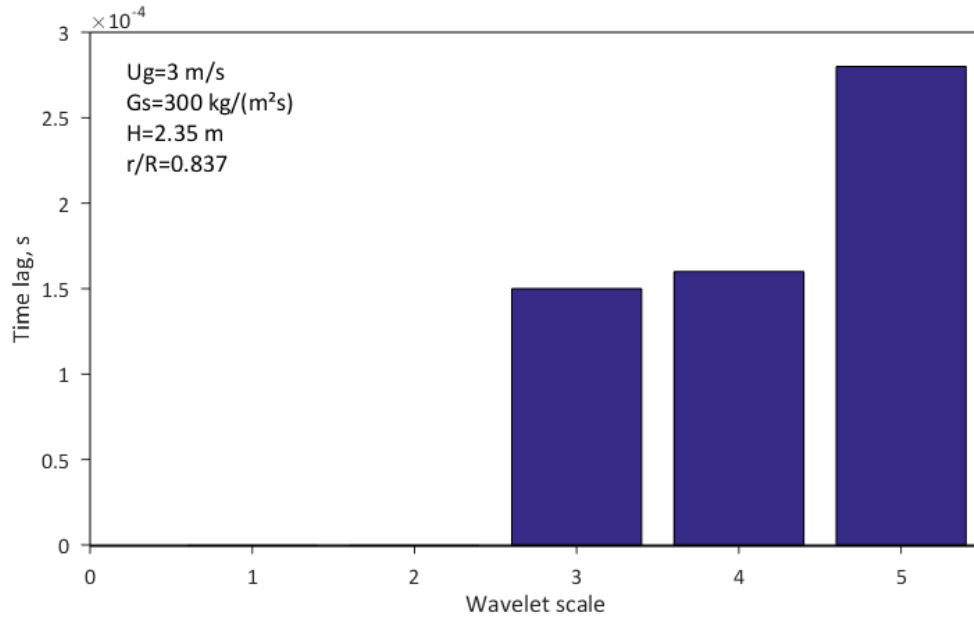


Figure 9-5 Time lag versus wavelet scale

As foresaid, optical fiber probe signals in the CFB downer were also found to be a hybrid of peaks and crescents. Original probe signal was decomposed to 17 scales and each detailed signal was correlated with the original signal. The correlation coefficient was plotted versus its scale in figure 9-6. For d1 and d2, their correlation coefficients are close to 1, indicating the signal to noise ratio is very high. From d3 to d9, the correlation coefficient decreases slowly. After d9, the correlation coefficient has a steep drop. Original solids holdup signal was plotted versus a9 and a17 in figure 9-7. Peaks in solids holdup signal can be well separated from surroundings using a9 as the instantaneous threshold. Crescents can be well identified as regions where a9 is higher than a17. This explains the trend in Figure 9-6. Before d9, the correlation coefficient decreases slowly and this attribute to the removal of peaks. After d9, the correlation coefficient decreases steeply and this attribute to the removal of crescents.

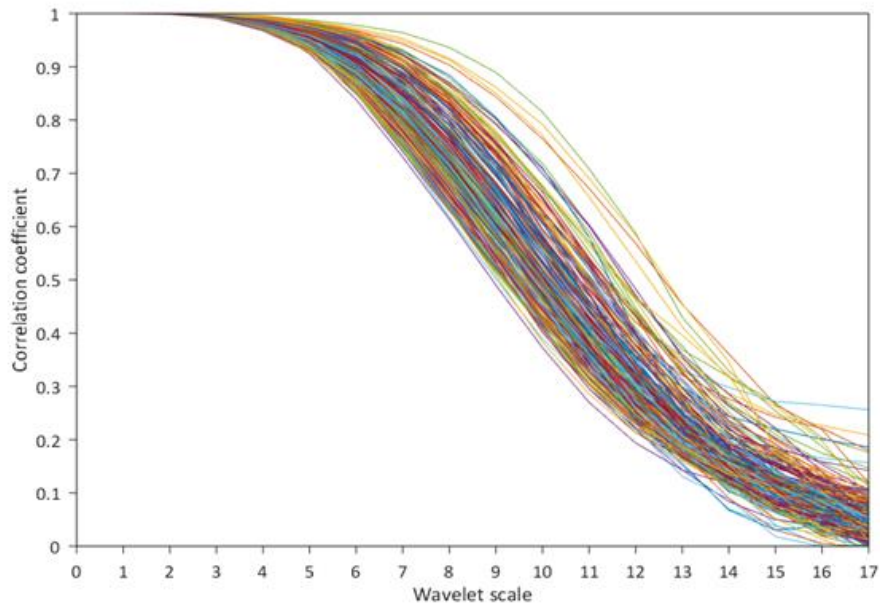


Figure 9-6 Correlation coefficient versus wavelet scale

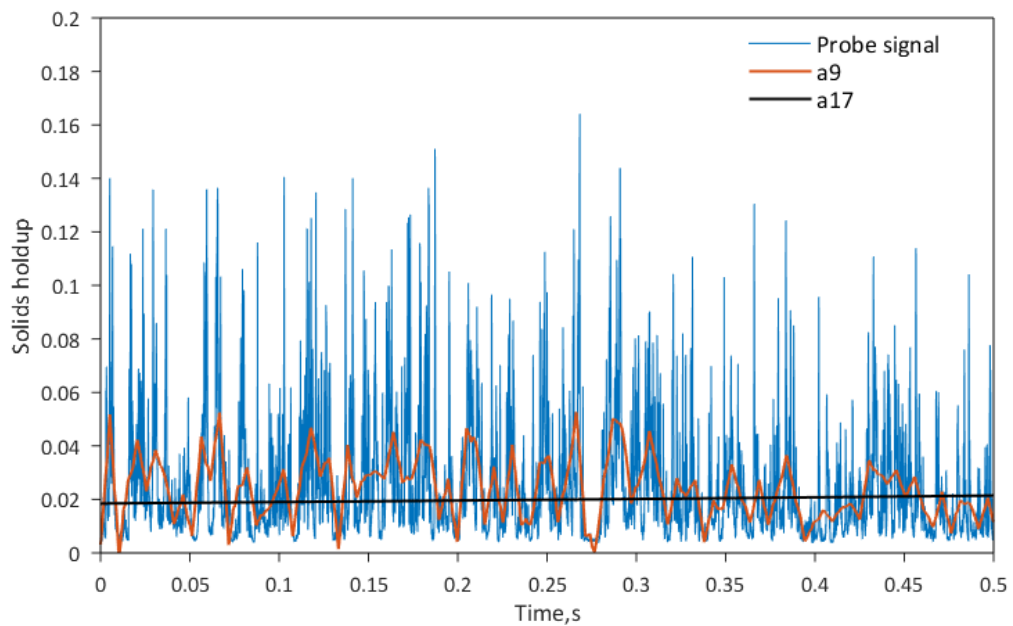


Figure 9-7 Probe signal and approximate signals (a9 and a17)

Then, a discrimination method has been proposed to analyze phase information in the CFB downer:

1. d1 and d2 correspond to the signal noise and a2, instead of the original signal, is used for further analysis.
2. Fragments in a2, whose solids holdup is higher than a9, correspond to clusters.
3. Fragments in a2, where solids holdup in a9 is above a17, correspond to crest phase.

To filter out the solids holdup fluctuating caused by later movement, the minimum size for clusters shall be 5 times particle diameter (d_p), the minimum size for crest phase shall be 2 cm, maximum solids holdup for clusters shall be at least 0.01 higher than a9, maximum solids holdup for crest phase shall be at least 0.01 higher than a17. Knowing the coordinates of clusters and crest phase, clusters within the crest phase are classified as crest clusters and other clusters are classified as trough clusters. crest clusters, trough clusters and crest phase are characterized in solids holdup, duration time, time fraction and frequency. Then, instantaneous velocity was calculated by cross-correlation of signal intervals (0.1s) and phase length was computed by multiplying duration time with instantaneous velocity. Finally, coalesced particles and dispersed particles are also characterized in solids holdup and time fraction using following equations where T_{pc} is time fraction of coalesced particles, T_{cp} is time fraction of crest phase, T_{cc} is time fraction of crest clusters, T_{tc} is time fraction of trough clusters, ε_{pc} is solids holdup of coalesced particles, ε_{ip} is solids holdup of dispersed particles, ε_{cp} is solids holdup of crest phase, ε_{cc} is solids holdup of crest clusters, ε_{tc} is solids holdup of trough clusters, ε_{ip} is solids holdup of dispersed particles, ε_m is mean solids holdup.

$$T_{pc} = T_{cp} - T_{cc} \quad \text{Equation 9-1}$$

$$T_{ip} = 1 - T_{cp} - T_{tc} \quad \text{Equation 9-2}$$

$$\varepsilon_{pc} = \frac{\varepsilon_{cp} * (T_{cc} + T_{pc}) - \varepsilon_{cc} * T_{cc}}{T_{pc}} \quad \text{Equation 9-3}$$

$$\varepsilon_{ip} = \frac{\varepsilon_m - T_{cp} * \varepsilon_{cp} - T_{tc} * \varepsilon_{tc}}{1 - T_{cp} - T_{tc}} \quad \text{Equation 9-4}$$

9.3 Results and discussion

9.3.1 Overall flow structure

The instantaneous flow structure in the fully developed region (at $H=3.26\text{m}$) was first analyzed with the radial distribution of solids holdup (see Figure 9-8). In the downer, particles accelerate in acceleration region, then particle velocity becomes steady in fully developed region. According to the previous study, $H=3.26\text{m}$ belongs to fully developed region for this downer (Wang et al., 2015a). At $G_s = 100, 300$ and $500 \text{ kg/m}^2\text{s}$, solids holdup is constant in the center, then increases and decreases near the downer wall, which agrees with previous studies (Zhang et al., 2003; Zhu et al., 1995;). Radially, solids holdup reaches its maxima around $r/R=0.7$ for $G_s = 100 \text{ kg/m}^2\text{s}$, around $r/R=0.85$ for $G_s = 300$ and $500 \text{ kg/m}^2\text{s}$. At $G_s = 700 \text{ kg/m}^2\text{s}$, solids holdup keeps increasing toward downer wall. In other words, solids holdup first increases then decreases near the downer wall at low solids circulation rate. With increasing solids circulation rate, solids holdup finally increases monotonically towards downer wall.

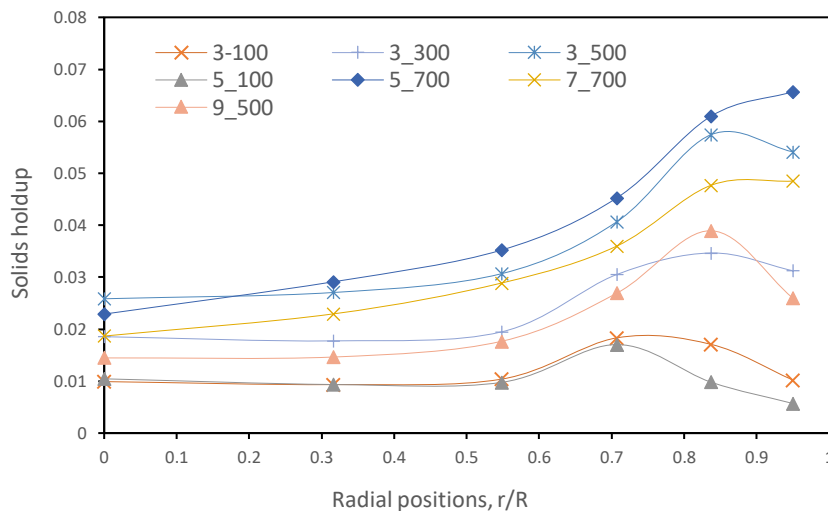


Figure 9-8 Radial distributions of solids holdup in the CFB downer

With the phase discrimination method, phase solids holdup has been extracted from probe signals. Radial distributions of phase solids holdup in low and high solids circulation rate are shown in figure 9-9. In both circumstances, crest clusters have highest

solids holdup across riser, followed by trough clusters, local-mean solids holdup, coalesced particles and dispersed particles. Moreover, phase solids holdup is found to be positively related to mean solids holdup. In terms of solids holdup, crest clusters and trough clusters are the dominant phases of aggregations.

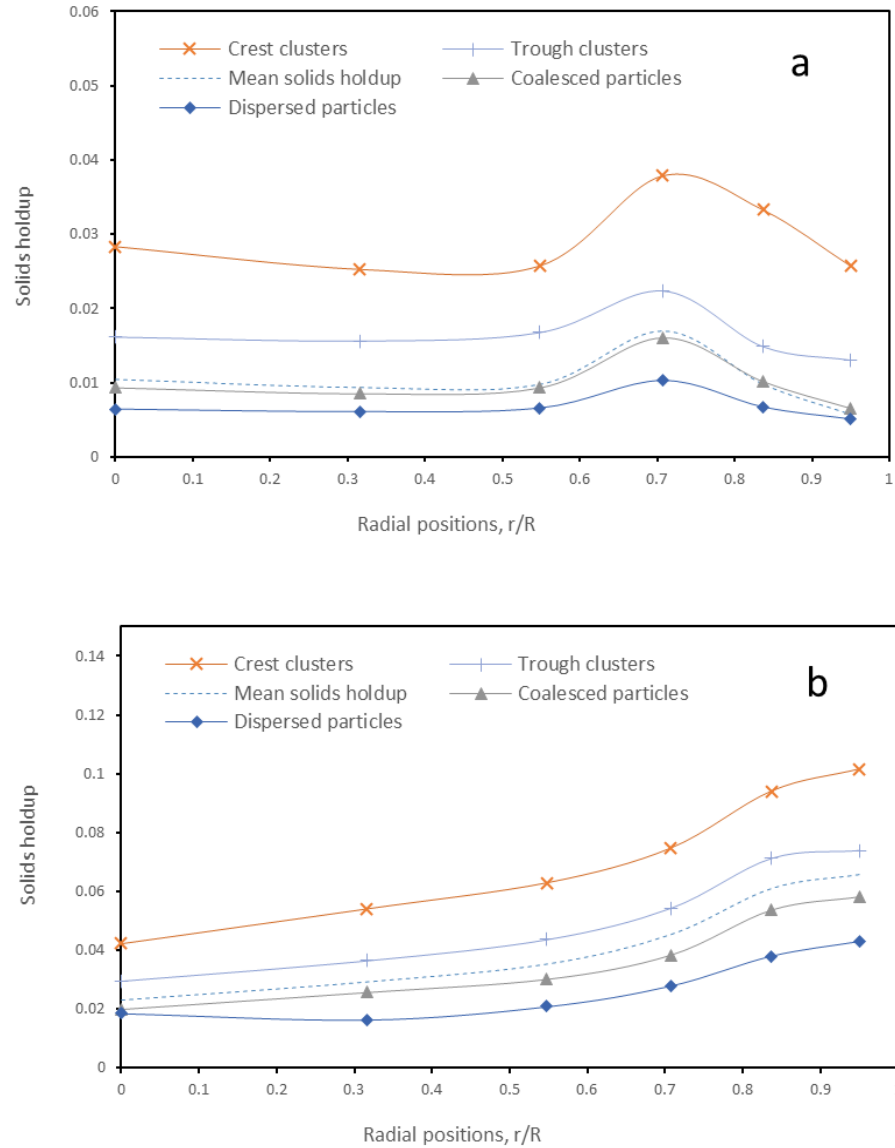


Figure 9-9 Radial distribution of phase solids holdup (a: $U_g=5$ m/s, $G_s=100$ kg/m² s; b: $U_g=5$ m/s, $G_s=700$ kg/m² s)

9.3.2 Trough clusters and crest clusters

As crest clusters and trough clusters are dominant aggregations in the CFB downer in terms of solids holdup, their properties, including solids holdup, length, frequency and time fraction, were discussed in terms of radial distribution (fully developed region, $H=3.26\text{m}$), axial distribution and statistic data in the fully developed region.

Radial distributions

Crest clusters and trough clusters share similar characteristics in radial distributions (see Figure 9-10). When the solids circulation rate is high and superficial gas velocity is low, solids holdup of crest clusters and trough clusters increases monotonically towards downer wall. When the solids circulation rate is low and superficial gas velocity is high, solids holdup of crest clusters and trough clusters is uniform in the center, but first increases then decrease near downer wall. Length of crest clusters and trough clusters is flat in the center, then increases from the center to downer wall. However, a little drop may occur in the boundary between the center region and wall region. This drop of length may relate to the shear force generated by the velocity difference in the downer center and downer wall (Wang et al., 2015b). Frequency is how many times a certain phase appears within a unit time. The frequency of crest clusters and trough clusters first increases then decreases towards downer wall. This may owe to two reasons: (1) length of crest clusters and trough clusters is higher in wall region, (2) crest clusters and trough clusters in wall region may move slower due to the friction of downer wall. Time fraction is the appearance time of certain phase divided by the measurement time and it approximately reflects the volumetric fraction occupied by a certain phase. Time fraction of crest clusters and trough clusters increases, then decreases towards downer wall. The increase may be caused by the increase of solids holdup toward downer wall. The decrease at wall may attribute to the wall frictions acted to crest clusters and trough clusters. Collectively, the radial distributions of properties were reported in detail, but further study is still needed to reveal the mechanism behind these distributions.

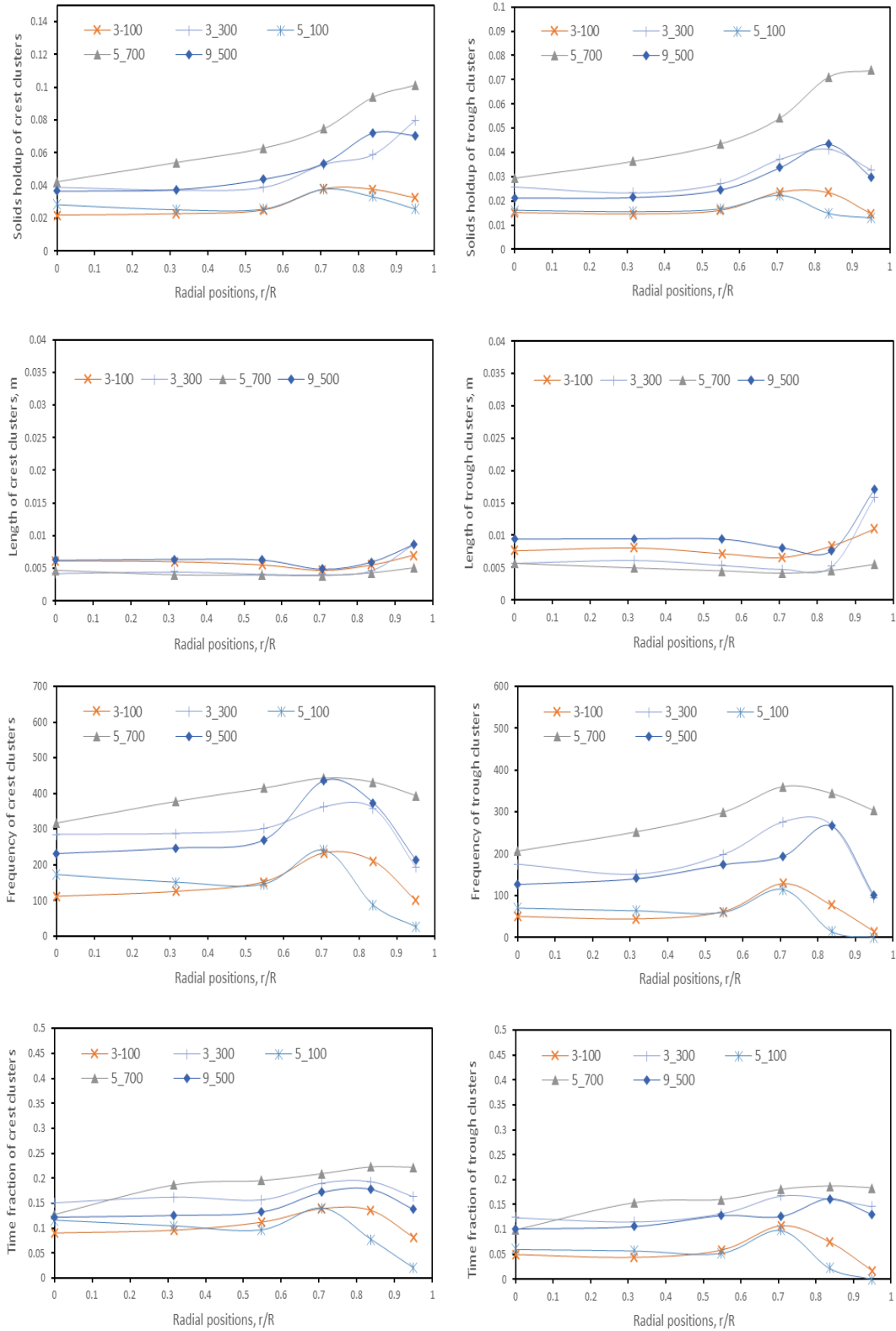


Figure 9-10 Properties of crest clusters and trough clusters versus radial positions

Axial distributions

Crest clusters and trough clusters also share similar characteristics in axial distributions (see Figure 9-11). Solids holdup of crest clusters and trough clusters is slightly lower at downer entrance. This may attribute to the vigorous gas-solid mixing near the gas distributor. After that, solids holdup of crest clusters and trough clusters remains constant along downer. Length of crest clusters and trough clusters is also uniform along downer. The frequency of crest clusters and trough clusters first increases with height, then becomes constant. This may relate with the existence of the acceleration region and fully developed region (Wang et al. 2015b). In the acceleration region, particle velocity keeps increasing, which causes the frequency of crest clusters and trough clusters to increase with height. In the fully developed region, particle velocity is steady, and frequency of crest clusters and trough clusters becomes constant. To the best of our knowledge, this is the first time that the axial distribution of aggregation properties has been reported in a downer. Crest clusters and trough clusters are in the dynamic process of formation and disintegration. This study only characterizes the statistical data in axial directions. Further study is still needed to reveal the mechanism behind these distributions.

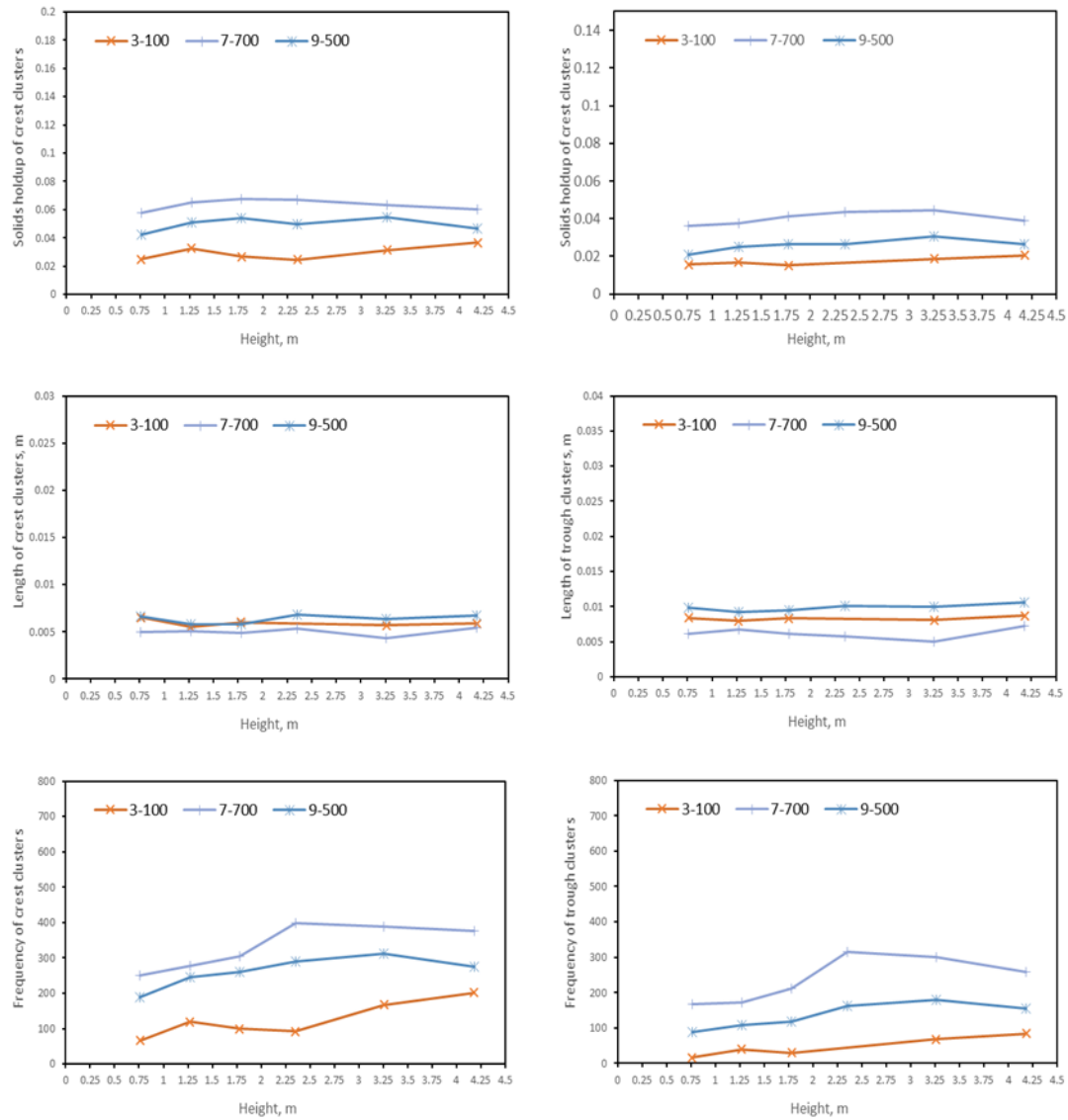


Figure 9-11 Properties of crest clusters and trough clusters versus axial positions

Statistic properties in the fully developed region

Statistical data in the fully developed region was computed to investigate how operating conditions influence crest clusters and trough clusters (see Figure 9-12). This information can also be used for the development and validation of numerical models. Comparatively, crest clusters have higher solids holdup than trough clusters. Solids holdup of crest clusters and trough clusters increases with solids circulation rate and decreases with superficial gas velocity. However, their increases with solids circulation rate is more

significant, when superficial gas velocity is low. Crest clusters have lower length than trough clusters. Length of crest clusters and trough clusters decreases with solids circulation rate, indicating that the high solids circulation rate may cause severe collision and shorten the crest clusters and trough clusters. Length of crest clusters and trough clusters is found to increase with superficial gas velocity. With the help of a high-speed camera, elongation of aggregations has also been quantitatively analyzed in the CFB riser (Chapter 6). In the downer, crest clusters and trough clusters may also be elongated by high-velocity gas. Crest clusters have a higher frequency than trough clusters. The frequency of crest clusters and trough clusters increases with solids circulation rate and decreases with superficial gas velocity. Crest clusters have higher time fraction than trough clusters. Time fraction of crest clusters and trough clusters increases with solids circulation rate and decreases with superficial gas velocity. According to signal details, crest clusters are surrounded with coalesced particles and trough clusters are surrounded with dispersed particles. Even though they share similar axial and radial distributions, they differ significantly at a variety of operating conditions in the magnitude of solids holdup, length, time fraction and frequency.

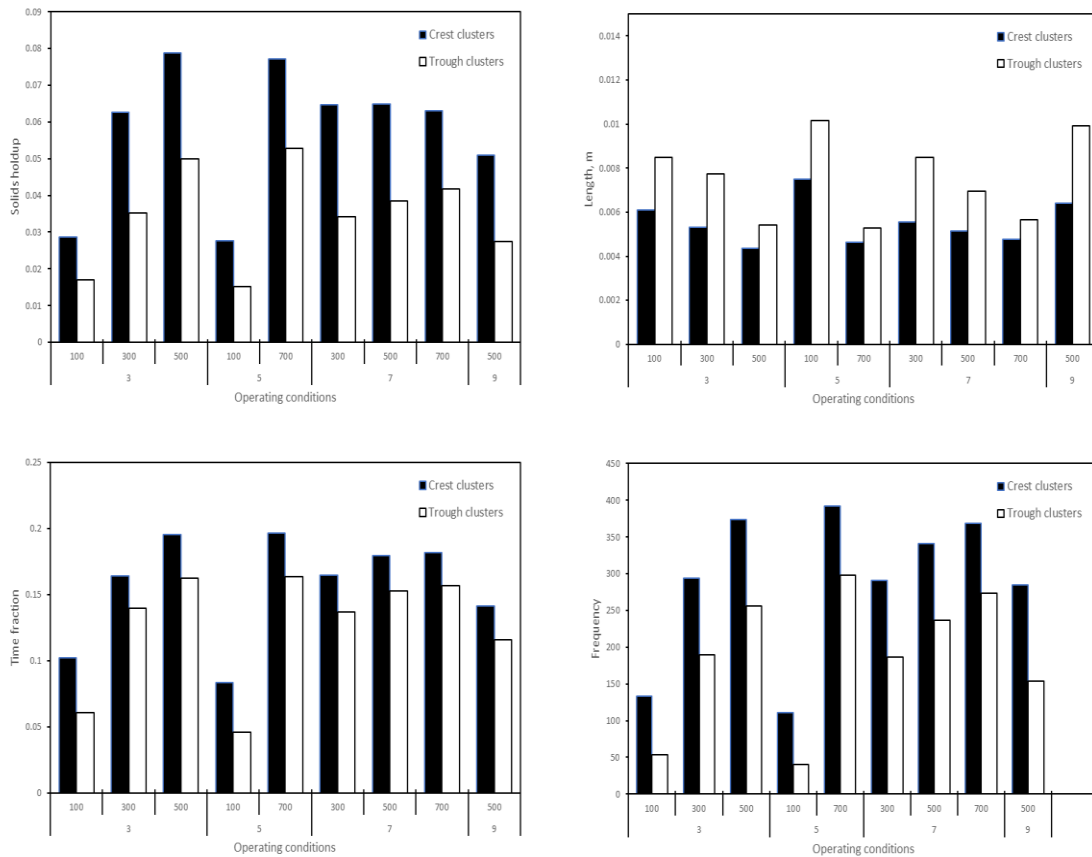


Figure 9-12 Statistic properties of crest clusters and trough clusters versus operating conditions

9.3.3 Phase comparison with CFB riser

To understand the aggregation mechanism, phase information (crest clusters, trough clusters and crest phase) in the CFB downer was compared quantitatively with CFB riser. In the downer, solids are accelerated by gas and gravity in acceleration region. After acceleration, solids move faster than gas with gravity as driving force and gas as resistance (Wang et al. 2015b). In the riser, solids always move slower than gas with gravity serves as resistance and gas as driving force (Wang et al., 2014). Gravity acts on single particles and the magnitude is regardless of particle velocity, while the force originated from flowing gas depends on the slip velocity. As the transition of flow structure has been reported to exist near riser wall at high solids circulation rate

conditions (chapter 8), the data resource of this comparison is the center region ($r/R=0, 0.316, 0.548, 0.707$) along CFB riser and downer.

When the operating conditions are the same, solids holdup in the CFB downer is significantly lower than that in the riser (Wang et al., 2015b). Comparison of crest clusters and trough clusters is conducted on the basis of mean solids holdup (see Figure 9-13 and 9-14).

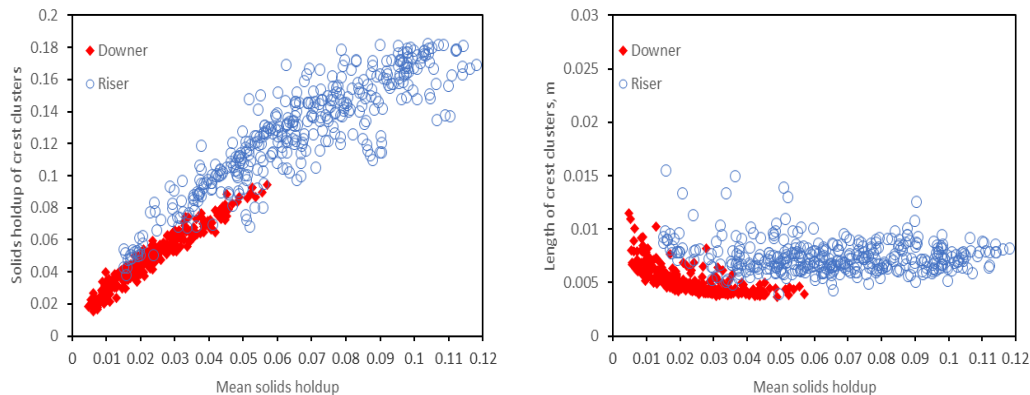


Figure 9-13 Comparison of crest clusters between riser and downer

For both riser and downer, properties of crest clusters have the same trend with mean solids holdup. Solids holdup of crest clusters increases with mean solids holdup. Length of crest clusters decreases exponentially with mean solids holdup. Comparatively, data in the riser is more scattered than that in the downer. When the mean solids holdup is similar, crest clusters in the downer has lower solids holdup and lower length than that in the riser.

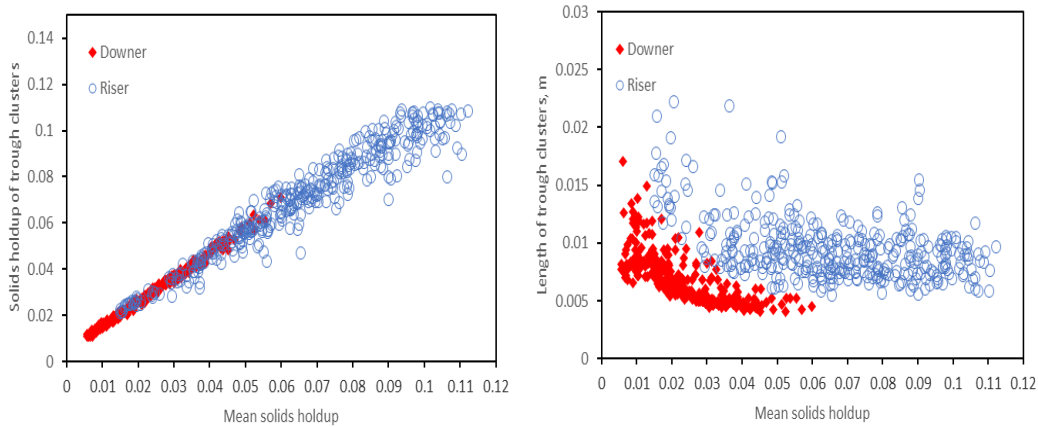


Figure 9-14 Comparison of trough clusters between riser and downer

Similar to crest clusters, properties of trough clusters in the downer and riser have the same trend with mean solids holdup. Solids holdup of trough clusters increases with mean solids holdup and length of trough clusters decreases exponentially with mean solids holdup. Comparatively, data in the downer is less scattered than that in the riser. Solids holdup of trough clusters in the downer is similar in magnitude with that in the riser. Length of trough clusters is lower than that in the riser.

Crest phase

Crest phase contains crest clusters and coalesced particles. As the crest phase is in macroscopic, its comparison is based on operating conditions (see Figure 9-15). Crest phase in the CFB downer has lower solids holdup and lower length than that in the CFB riser. In addition, the crest phase in the CFB riser is found to be more sensitive to operating conditions in the CFB riser.

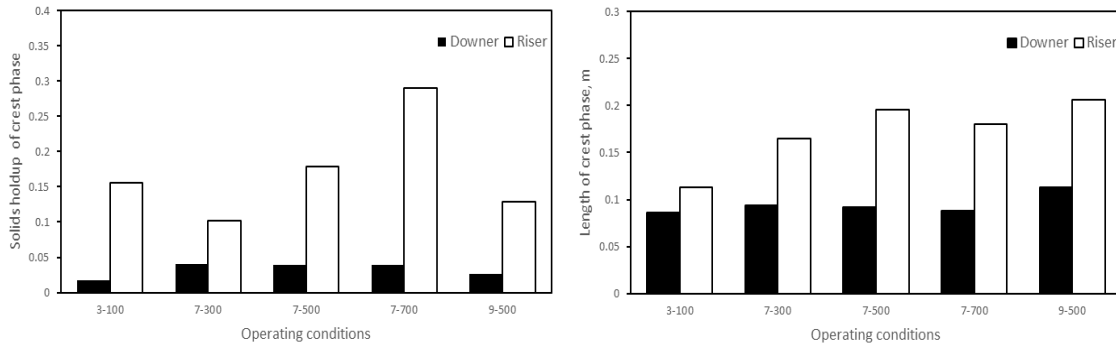


Figure 9-15 Comparison of crest phase between riser and downer

9.4 Conclusions

Gas-solids flow in the CFB downer has been characterized systematically using an optical fiber probe. In probe signals, crest clusters, coalesced particles, trough clusters and dispersed particles are identified based on solids holdup characteristics. Then, a phase discrimination method has been proposed using wavelet analysis to extract phase information. Finally, the phase has been characterized in terms of solids holdup, length, frequency and time fraction.

In perspectives of phase solids holdup, crest clusters and trough clusters are considered as the dominant aggregations. Their radial distributions in fully developed region, axial distributions along downer and statistical data in the fully developed region have been analyzed and discussed in detail. In addition, phase information in the CFB riser and downer was compared systematically in perspectives of crest clusters, trough clusters and crest phase. Collectively, this study shall contribute to (1) the understanding of particle aggregation mechanism, (2) the numerical modeling of CFB downer, (3) comparison of CFB downer with CFB riser, and (4) designing and scale-up of downer reactors.

Nomenclature

U_g is superficial gas velocity, [m/s];

G_s is solids circulation rate, [kg/m²s];

T_{pc} is time fraction of coalesced particles;

T_{cp} is time fraction of crest phase;

T_{cc} is time fraction of crest clusters;

T_{tc} is time fraction of trough clusters;

ϵ_{pc} is solids holdup of coalesced particles;

ϵ_{ip} is solids holdup of dispersed particles;

ϵ_{cp} is solids holdup of crest phase;

ϵ_{cc} is solids holdup of crest clusters;

ϵ_{tc} is solids holdup of trough clusters;

ϵ_{ip} is solids holdup of dispersed particles;

ϵ_m is mean solids holdup;

References

- Anantharaman, A., Karri, S. R., Findlay, J. G., Hrenya, C. M., Cocco, R. A., & Chew, J. W. (2016). Interpreting Differential Pressure Signals for Particle Properties and Operating Conditions in a Pilot-Scale Circulating Fluidized Bed Riser. *Industrial & Engineering Chemistry Research*, 55(31), 8659-8670.
- Bi, H. T., Zhu, J. X., Jin, Y., & Yu, Z. Q. (1993, October). Forms of particle aggregations in CFB. *In Proceedings of the Sixth Chinese Conference on Fluidization*, Wuhan, China (pp. 162-167).
- Chew, J. W., Hays, R., Findlay, J. G., Knowlton, T. M., Karri, S. R., Cocco, R. A., & Hrenya, C. M. (2012a). Cluster characteristics of Geldart Group B particles in a pilot-scale CFB riser. I. Monodisperse systems. *Chemical engineering science*, 68(1), 72-81.
- Chew, J. W., Hays, R., Findlay, J. G., Knowlton, T. M., Karri, S. R., Cocco, R. A., & Hrenya, C. M. (2012b). Cluster characteristics of Geldart group B particles in a pilot-scale CFB riser. II. Polydisperse systems. *Chemical engineering science*, 68(1), 82-93.
- Chew, J. W., Parker, D. M., Cocco, R. A., & Hrenya, C. M. (2011). Cluster characteristics of continuous size distributions and binary mixtures of Group B particles in dilute riser flow. *Chemical engineering journal*, 178, 348-358.
- Li, D., Ray, M. B., Ray, A. K., & Zhu, J. (2013). A comparative study on hydrodynamics of circulating fluidized bed riser and downer. *Powder technology*, 247, 235-259.
- Li, H., Xia, Y., Tung, Y., & Kwauk, M. (1991). Micro-visualization of clusters in a fast fluidized bed. *Powder Technology*, 66(3), 231-235.
- Lu, X., Li, S., Du, L., Yao, J., Lin, W., & Li, H. (2005). Flow structures in the downer circulating fluidized bed. *Chemical Engineering Journal*, 112(1), 23-31.
- Manyele, S. V., Zhu, J., & Zhang, H. (2003). Analysis of the microscopic flow structure of a CFB downer reactor using solids concentration signals. *International Journal of Chemical Reactor Engineering*, 1(1).

- Shi, H., Wang, Q., Xu, L., Luo, Z., & Cen, K. (2008). Visualization of clusters in a circulating fluidized bed by means of particle-imaging velocimetry (PIV) technique. *In Proceedings of the 9th International Conference on Circulating Fluidized Beds*, Hamburg, Germany (pp. 1013-1019).
- Soong, C. H., Tuzla, K., & Chen, J. C. (1994). Identification of particle clusters in circulating fluidized bed. *Circulating fluidized bed technology*, 4, 615-620.
- Tuzla, K., Sharma, A. K., Chen, J. C., Schiewe, T., Wirth, K. E., & Molerus, O. (1998). Transient dynamics of solid concentration in downer fluidized bed. *Powder Technology*, 100(2-3), 166-172.
- Wang, C., Zhu, J., Barghi, S., & Li, C. (2014). Axial and radial development of solids holdup in a high flux/density gas–solids circulating fluidized bed. *Chemical Engineering Science*, 108, 233-243.
- Wang, C., Li, C., & Zhu, J. (2015a). Axial solids flow structure in a high density gas–solids circulating fluidized bed downer. *Powder Technology*, 272, 153-164.
- Wang, C., Li, C., Zhu, J., & Barghi, S. (2015b). A comparison of flow development in high density gas - solids circulating fluidized bed downer and riser reactors. *AIChE Journal*, 61(4), 1172-1183.
- Wang, C., Zhu, J., & Barghi, S. (2015c). Performance evaluation of high density riser and downer: Experimental study using ozone decomposition. *Chemical Engineering Journal*, 262, 478-489.
- Wei, F., & Zhu, J. X. (1996). Effect of flow direction on axial solid dispersion in gas—solids cocurrent upflow and downflow systems. *The Chemical Engineering Journal and the Biochemical Engineering Journal*, 64(3), 345-352.
- Yunhau, Z., Huilin, L., Yurong, H., Ding, J., & Lijie, Y. (2006). Numerical prediction of combustion of carbon particle clusters in a circulating fluidized bed riser. *Chemical Engineering Journal*, 118(1), 1-10.

Zhang, H., Johnston, P. M., Zhu, J. X., De Lasa, H. I., & Bergougnou, M. A. (1998). A novel calibration procedure for a fiber optic solids concentration probe. *Powder Technology*, 100(2-3), 260-272.

Zhang, H., Huang, W. X., & Zhu, J. X. (2001). Gas - solids flow behavior: CFB riser vs. downer. *AIChE Journal*, 47(9), 2000-2011.

Zhang, M., Qian, Z., Yu, H., & Wei, F. (2003). The solid flow structure in a circulating fluidized bed riser/downer of 0.42-m diameter. *Powder Technology*, 129(1), 46-52.

Zhu, J. X., Yu, Z. Q., Jin, Y., Grace, J. R., & Issangya, A. (1995). Cocurrent downflow circulating fluidized bed (downer) reactors—a state of the art review. *The Canadian Journal of Chemical Engineering*, 73(5), 662-677.

CHAPTER 10

Conclusions and Recommendations

10.1 Conclusions

In this work, the instantaneous flow structure in the CFB has been comprehensively analyzed and quantitatively characterized using a high-speed camera and optical fiber probe at a wide range of operating conditions.

1. In the literature, different phases were characterized as clusters, resulting in severe discrepancy on cluster properties.
2. In the CFB, there are crest clusters, coalesced particles, trough clusters and dispersed particles. In terms of solids holdup, (1) crest clusters and trough clusters are significantly denser than coalesced particles and dispersed particles, respectively, (2) coalesced particles are denser than dispersed particles, (3) solids holdup increase around coalesced particles is much less abrupt than those around crest clusters and trough clusters (4) crest clusters have highest solids holdup, followed by trough clusters, coalesced particles and dispersed particles.
3. In macroscope, the crest phase consists of crest clusters and coalesced particles, while the trough phase contains trough clusters and dispersed particles. With the help of a high-speed camera, it has been found that the alternating appearance of the crest phase and trough phase causes significant fluctuation of solids holdup and solids circulating rate.
4. With the tracking of image blocks, the appearance of crest clusters, coalesced particles, trough clusters and dispersed particles influences instantaneous flow dynamics (particle velocity and solids flux).
5. Using the high-speed camera and optical fiber probe, an abrupt increase of solids holdup has been found to exist around crest clusters and trough clusters, evidencing phase segregation. With the determination of cluster boundary as where solids holdup has the sharpest increase, crest clusters and trough clusters are found to have irregular shapes and be elongated in CFB riser.

6. Using wavelet transform, a discrimination method has also been proposed for optical fiber probe to identify crest clusters, coalesced particles, trough clusters and dispersed particles. Phase information originated from optical fiber probe is consistent with that acquired using the high-speed camera. By comparing phases formed by FCC and glass beads, it has been found that phase properties are dependent on the type of particles.
7. In high-density riser, the instantaneous flow structure in the riser wall transits to “dense structure” which particulate phase is dominant in time fraction.
8. In high-density downer, the instantaneous flow structure is featured with “dilute structure” which is featured with crest clusters dispersed in coalesced particles and trough clusters immersed in dispersed particles. With the comparison between riser and downer, it has been found that aggregations in the CFB downer is less severe than those in the CFB riser.

In summary, this is the first time that the instantaneous flow structure has been studied comprehensively and systematically at such a wide range of operating conditions. In the literature, key cluster properties vary in an order of magnitude, owing to that existing cluster definitions characterize different phases in the CFB. With the help of an optical fiber probe and a high-speed camera, this work proposed the phase identification based on solids holdup characteristics. Then, the instantaneous flow structure has been quantified with phase characterization in larger scale risers and downer. Detailed phase information, including radial distributions, axial distributions, trends with operating conditions and so on, could contribute to (1) the prediction of CFB performances, (2) the optimization of CFB reactors, (3) the understanding of flow mechanisms in the CFB, (4) the development and validation of numerical models.

10.2 Recommendations

This study conducted a thorough analysis of the instantaneous flow structure in circulating fluidized beds. However, there are still certain fields where further research is needed.

This work is either based on one-dimensional optical fiber probe data or two-dimensional images. But, phases in the CFB are three-dimensional. Right now, the three-dimensional detective technique, in the literature, is only applicable in extremely dilute suspension. It is recommended to develop three-dimensional detective technique in order to map the solids holdup in dense suspension.

Aggregations are in the process of formation and breaking. However, the instruments in this work are not able to track how particles develop to aggregations and how aggregations become dispersed particles. Details of the above processes are crucial for the understanding of aggregation mechanism and for the analysis of gas-solids contact. It is recommended to design an online particle-tracking system.

This study conducted phase characterizations in the CFB. Investigations on how gas interacts with aggregations and what is the percentage of gas penetrating into aggregations are essential to relate aggregation properties with reactor performance. It is recommended to study the gas-particle interaction phase by phase.

Most numerical models still view fast fluidization as a system of gas and dispersed particles. Since aggregation information is discussed in detail in this work, it is suggested to develop a numerical model to incorporate aggregations as another phase.

Appendix

```

% below is an example MATLAB code to process signals acquired using optical fiber
probe.
% 2nd cluster refers to the information combing crest clusters and trough clusters.
% cluster in dilute refers to trough clusters.
% cluster in dense refers to crest clusters.
% dense phase refers to crest phase.
% dilute phase refers to trough phase.

clear all
close all
clc
path='D:\Pyramid-Tracy\UWO degree\Experiment2012(riser)\Ug3Gs100\H3\R4\';
% vector ch1 is the original signal
minimumclusterlength=5*70*10^-6;
for Ug=[3 5 7 9] % 15 20]10 100 180 180 250
    if Ug==3
        Gss=100;
    end
    if Ug==5
        Gss=200:100:400;
    end
    if Ug==7
        Gss=100:100:800 ;
    end
    if Ug==9
        Gss=100:100:800 ;
    end
    for Gs= Gss

        %
        condition='a10_a2_sort_phase_WAVELET_Shawn_TRACY_7_100.xlsx';
        %

        condition(end-7:end-5)=num2str(Gs);
        condition(end-9)=num2str(Ug);

        path(end-12)=num2str(Ug);

        path(end-9:end-7)=num2str(Gs);
        % hh=figure;
        ins_clusterlength=0;
        ins_clusterdensity=0;
    end
end

```

```

for height=1:10

    if height<10
        path(end-4)=num2str(height);
    end
    if height==10
        path(end-4:end+1)='10\R2\'
    end

    for path_i=1:6
        path(end-1) = num2str(path_i);
        % set the current work dictionary
        if exist(path)==7
            cd(path)

            path

            Edense(path_i,height)=0;

            % retrieve the effective length & frequency from cap file
            % capfile = dir('*.cap');
            % capfilename = capfile.name;
            % to retrieve effective length of the probe used, mm

            % to retrieve sampling time interval (ms) and total data points in that data file
            % [datapoints time_interval] = textread([path,capfilename], '%f %f',
1,'delimiter',';', 'headerlines', 3);
            frequency = 10^5;%*1/time_interval; % Sampling frequency (Hz)

            %set the pma files as the working object
            files = dir('*.pma');

            m=numel(files); % No. of files to open

            denselocation=[];
            cluster_in_dilute=0;

            cluster_in_dense=0;

            effective_length=1.51;
            % mean_cluster_dense
            %%

```

```

% to read data
for i=1:m
    [ch1(:,i),ch2(:,i)] = textread(files(i).name,'%d
%d','delimiter',' ','headerlines', 3);
    L=length(ch1(:,i));

    if path_i<=4

        for j=1:L

            ch1(j,i)=0.02227*(ch1(j,i)/1000)^2-0.0131*(ch1(j,i)/1000)+0.00563;
            ch2(j,i)=0.01712*(ch2(j,i)/1000)^2-
0.00533*(ch2(j,i)/1000)+0.00251;

            end
        else

            for j=1:L

                ch1(j,i)=0.02405*(ch1(j,i)/1000)^2-
0.01767*(ch1(j,i)/1000)+0.00734;
                ch2(j,i)=0.02757*(ch2(j,i)/1000)^2-
0.03945*(ch2(j,i)/1000)+0.01945;
            end

        end

    end

    %%

    % for each file the data behind 13000 is abandoned since a 10000 segment
    % is selected to calculate the velocity

    ch1mm=ch1(1:end-1,:);
    ch2nn=ch2(1:end-1,:);

    % shape the matrix as vector

    vector_ch1=ch1mm(:);
    vector_ch2=ch2nn(:);

    % mean signal solids holdup is calculated

```



```

mean_density(path_i,height)=mean(vector_ch1);
mean_std(path_i,height)=std(vector_ch1);

maxlevel=wmaxlev(size(vector_ch1),'db3');

[c,l]=wavedec(vector_ch1,maxlevel,'db3');

for scale=1:maxlevel

    d(scale,:)=wrcoef('d',c,l,'db3',scale);

    a(scale,:)=wrcoef('a',c,l,'db3',scale);

end

for scale=1:maxlevel
    Ed(scale)=sum(d(scale,:).^2);
end

Ea=sum((a(maxlevel,:)-mean(a(maxlevel,:))).^2);

Etotal=sum(Ed)+Ea;

%           plot(Ed./Etotal);
%           hold on

[~,cluster_scale(path_i,height)]=max(Ed./Etotal);
% figure
% plot(vector_ch1)

if cluster_scale(path_i,height)>=17||cluster_scale(path_i,height)<=2

    clear a d ch1 ch2 maxlevel c l vector_ch1 vector_ch2 ch1mm ch1nn m

    continue

else

```

```

for scale=cluster_scale(path_i,height):maxlevel
    Edense(path_i,height)=Edense(path_i,height)+Ed(scale);
end

Edense(path_i,height)=Edense(path_i,height)+Ea;

Edense(path_i,height)=Edense(path_i,height)/numel(vector_ch1)*frequency;

% plot(a(cluster_scale(path_i,height),:))
% hold on
% plot(a(17,:))

vector_ch11=vector_ch1;

vector_ch1=a(2,:);

vector_ch11(vector_ch1<a(10,:))=0;
%%
% the cluster number is set as 1 first for each work dictionary
clusternumber=1;
% the indices of non zero elements are recorded
peak_indice=find(vector_ch11~=0);

% the difference between adjacent elements is calculated
diffpeakwidth=diff(peak_indice);
% set initial value for peakwidth(1,path_i)and
cluster_left_boundary(1,path_i)
peakwidth(1)=1;
cluster_left_boundary(1)= peak_indice(1);

for sequence=1:length(diffpeakwidth)

    if diffpeakwidth(sequence)==1
        peakwidth(clusternumber)=peakwidth(clusternumber)+1;
    else
        cluster_right_boundary(clusternumber)=peak_indice(sequence);

cluster_density(clusternumber)=mean(vector_ch1(cluster_left_boundary(clusternumber):
cluster_right_boundary(clusternumber)));

significance(clusternumber)=max(vector_ch1(cluster_left_boundary(clusternumber):clust

```

```

er_right_boundary(cluster_number))-
a(cluster_scale(path_i,height),cluster_left_boundary(cluster_number):cluster_right_bound
ary(cluster_number))');
    cluster_number=cluster_number+1;

    cluster_left_boundary(cluster_number)=peak_indice(sequence+1);
    peakwidth(cluster_number)=1;
end

end
cluster_number=cluster_number-1;

%%

densephase_signal=a(10,:);

densephase_signal(densephase_signal<a(17,:))=0;

% the cluster number is set as 1 first for each work dictionary
dense_phasenum=1;
% the indices of non zero elements are recorded
dense_phase_indice=find(densephase_signal~=0);

% the difference between adjacent elements is calculated
dense_diffpeakwidth=diff(dense_phase_indice);
% set initial value for peakwidth(1,path_i)and
cluster_left_boundary(1,path_i)
dense_phasewidth(1)=1;
dense_phase_left_boundary(1)=dense_phase_indice(1);

for dense_sequence=1:length(dense_diffpeakwidth)

    if dense_diffpeakwidth(dense_sequence)==1

dense_phasewidth(dense_phasenum)=dense_phasewidth(dense_phasenum)+1;
        else

dense_phase_right_boundary(dense_phasenum)=dense_phase_indice(dense_sequence
);

dense_phase_density(dense_phasenum)=mean(vector_ch1(dense_phase_left_boundar
y(dense_phasenum):dense_phase_right_boundary(dense_phasenum)));

dense_significance(dense_phasenum)=max(vector_ch1(dense_phase_left_boundary(d
ense_phasenum):dense_phase_right_boundary(dense_phasenum)))-

```

```

a(maxlevel,dense_phase_left_boundary(dense_phasenumber):dense_phase_right_boundar
y(dense_phasenumber))');
    if dense_significance(dense_phasenumber)>0.01
        denselocation=[denselocation
dense_phase_left_boundary(dense_phasenumber):dense_phase_right_boundary(dense_p
hasenumber)];
    end
    dense_phasenumber=dense_phasenumber+1;

dense_phase_left_boundary(dense_phasenumber)=dense_phase_indice(dense_sequence+
1);
    dense_phasewidth(dense_phasenumber)=1;
end

end
dense_phasenumber=dense_phasenumber-1;
vector_ch1x=vector_ch1-a(cluster_scale(path_i,height,:));
[c2,l2]=wavedec(vector_ch2,maxlevel,'db3');

for scale=1:maxlevel

    d2(scale,:)=wrcoef('d',c2,l2,'db3',scale);

    a2(scale,:)=wrcoef('a',c2,l2,'db3',scale);

end

vector_ch2x=vector_ch2-a2(cluster_scale(path_i,height,:));

%%
segmentnumber=2;
N=10000;
LL=length(vector_ch1x);
for j=N:N:LL-2*N+1
    [acor,lag]=xcorr(vector_ch1x(j:j+N-1),vector_ch2x(j:j+N-1));
    [~,I] = max(acor);
    lagDiff = lag(I);
    R=corrcoef(vector_ch1x(j-N+I:j-N+I+N-1),vector_ch2x(j:j+N-1));
    RR(segmentnumber)=R(1,2);
    timeDiff = lagDiff/(frequency);

```

```

velocity(segmentnumber)=effective_length*10^-3/-timeDiff;
if abs(velocity(segmentnumber))>30||RR(segmentnumber)<0.6
    velocity(segmentnumber)=nan;
end
segmentnumber=segmentnumber+1;
end
clustervelocity(path_i,height)=mean(mean(velocity(isnan(velocity)==0)));
for jj=1:clusternumber
    segmentvelocity=floor(cluster_left_boundary(jj)/N)+1;
    if segmentvelocity>1&&segmentvelocity<segmentnumber-1

clusterlength(jj)=peakwidth(jj)*abs(velocity(segmentvelocity))/frequency;
        else
            clusterlength(jj)=nan;
        end
    end
    for jj=1:clusternumber

        if abs(clusterlength(jj))>minimumclusterlength&significance(jj)>0.01
            mark_cluster(jj)=1;
        else
            mark_cluster(jj)=0;
        end
    end
    %%
    for jj=1:dense_phasenumbr
        segmentvelocity=floor(dense_phase_left_boundary(jj)/N)+1;
        if segmentvelocity>1&&segmentvelocity<segmentnumber-1

dense_phaselength(jj)=dense_phasewidth(jj)*abs(velocity(segmentvelocity))/frequency;
            else
                dense_phaselength(jj)=nan;
            end
        end
        for jj=1:dense_phasenumbr

            if abs(dense_phaselength(jj))>0.02&dense_significance(jj)>0.01
                mark_dense_phase(jj)=1;
            else
                mark_dense_phase(jj)=0;
            end
        end
    end
    %%
    peakwidth_=peakwidth(:);
    clusterlength_=clusterlength(:);

```

```

cluster_density_=cluster_density(:);
significance_=significance(:);
%% all secondary cluster

clustersignificance(path_i,height)=mean(significance_(mark_cluster==1));
cluster_time_fraction(path_i,height)=sum(peakwidth_(mark_cluster==1))/(numel(vector_
ch1)-2*N);
realclusternumber=numel(clusterlength_(mark_cluster==1)
meanclusterfrequency(path_i,height)=realclusternumber/((numel(velocity(isnan(velocity)
==0))-2)*N/frequency);

meanclusterdensity(path_i,height)=mean(cluster_density_(mark_cluster==1));
% updated cluste density reffers to lengthweighted cluster density
updated_meanclusterdensity(path_i,height)=sum(cluster_density_(mark_cluster==1)'.*pe
akwidth(mark_cluster==1))/sum(peakwidth(mark_cluster==1));

meanclusterlength(path_i,height)=mean(clusterlength_(mark_cluster==1));

medianclusterlength(path_i,height)=median(clusterlength_(mark_cluster==1));
% ins_clusterlength=[ins_clusterlength
clusterlength_(~isnan(clusterlength_)&clusterlength_>70*5*10^-6)];
% ins_clusterdensity=[ins_clusterdensity
cluster_density_(~isnan(clusterlength_)&clusterlength_>70*5*10^-6)];

cluster_particle_percentage(path_i,height)=meanclusterdensity(path_i,height)*cluster_ti
me_fraction(path_i,height)/mean_density(path_i,height);
%% dense phase
dense_phasewidth_=dense_phasewidth(:);
dense_phaselength_=dense_phaselength(:);
dense_phase_density_=dense_phase_density(:);
dense_significance_=dense_significance(:);
for dense_sequence=1:numel(dense_phasewidth_)
    if dense_significance_(dense_phasenumbe)>0.01&
dense_phaselength_(dense_phasenumbe)>0.02
        denselocation=[denselocation
dense_phase_left_boundary(dense_phasenumbe):dense_phase_right_boundary(dense_p
hasenumbe)];
    end
end
dense_phase_time_fraction(path_i,height)=sum(dense_phasewidth_(mark_dense_phase=
=1))/(numel(vector_ch1)-2*N);
dense_realphasenumbe=numel(dense_phaselength_(mark_dense_phase==1));

dense_meanphasefrequency(path_i,height)=dense_realphasenumbe/((numel(velocity(isn
an(velocity)==0))-2)*N/frequency);
dense_meanphasedensity(path_i,height)=mean(dense_phase_density_(mark_dense_phase

```

```

==1));
updated_dense_meanphasedensity(path_i,height)=sum(dense_phase_density(mark_dense
_phase==1).*dense_phasewidth(mark_dense_phase==1))/sum(dense_phasewidth(mark_
dense_phase==1));

dense_meanphaselength(path_i,height)=mean(dense_phaselength_(mark_dense_phase==
1));
dense_medianphaselength(path_i,height)=median(dense_phaselength_(mark_dense_phas
e==1));

dense_phase_particle_percentage(path_i,height)=dense_meanphasedensity(path_i,height)
*dense_phase_time_fraction(path_i,height)/ mean_density(path_i,height);

%% cluster in dilute & cluster in dense

for dense_sequence=1:numel(dense_phasewidth_)
    if dense_significance_(dense_phasenumber)>0.01&
dense_phaselength_(dense_phasenumber)>0.02
        denselocation=[denselocation
dense_phase_left_boundary(dense_phasenumber):dense_phase_right_boundary(dense_p
hasenumber)];
    end
end
for jj=1:clusternumber
    if
abs(clusterlength_(jj))>minimumclusterlength&(isnan(clusterlength_(jj))==0&significan
ce_(jj)>0.01)
        if any(denselocation==cluster_left_boundary(jj))==1
            cluster_in_dense=cluster_in_dense+1;% [cluster_dense jj]
            mark(jj)=1;

            elseif any(denselocation==cluster_left_boundary(jj))==0
                cluster_in_dilute=cluster_in_dilute+1;% jj]
                mark(jj)=0;
            end
        end
    else
        mark(jj)=2;
    end
end
end

meandensity_cluster_indense(path_i,height)=mean(cluster_density_(mark'==1));

meandensity_cluster_indilute(path_i,height)=mean(cluster_density_(mark'==0));
updated_meandensity_cluster_indense(path_i,height)=sum(cluster_density_(mark'==1)).*
peakwidth(mark'==1))/sum(peakwidth(mark'==1));

```

```

updated_meandensity_cluster_indilute(path_i,height)=sum(cluster_density_(mark'==0)).*
peakwidth( mark'==0))/sum(peakwidth( mark'==0));

meanlength_cluster_indense(path_i,height)=mean(clusterlength_(mark'==1));

meanlength_cluster_indilute(path_i,height)=mean(clusterlength_(mark'==0));

medianlength_cluster_indense(path_i,height)=median(clusterlength_(mark'==1));

medianlength_cluster_indilute(path_i,height)=median(clusterlength_(mark'==0));
frequency_cluster_indense(path_i,height)=cluster_in_dense/((numel(velocity(isnan(velocity)
)==0))-2)*N/frequency);
frequency_cluster_indilute(path_i,height)=cluster_in_dilute/((numel(velocity(isnan(velocity)
)==0))-2)*N/frequency);
timefraction_cluster_indense(path_i,height)=sum(peakwidth_((mark'==1)))/(numel(vector
_ch1)-2*N);

timefraction_cluster_indilute(path_i,height)=sum(peakwidth_(mark'==0))/(numel(vector
_ch1)-2*N);
particlefraction_cluster_indense(path_i,height)=
timefraction_cluster_indense(path_i,height)*
meandensity_cluster_indense(path_i,height)/mean_density(path_i,height);
particlefraction_cluster_indilute(path_i,height)=timefraction_cluster_indilute(path_i,height)*
meandensity_cluster_indilute(path_i,height)/mean_density(path_i,height);
clusternumer_per_dense(path_i,height)=frequency_cluster_indense(path_i,height)/dense_
meanphasefrequency(path_i,height);
%%
TimeFraction_cloud(path_i,height)=dense_phase_time_fraction(path_i,height)-
timefraction_cluster_indense(path_i,height);

density_cloud(path_i,height)=(dense_meanphasedensity(path_i,height)*dense_phase_time_
fraction(path_i,height)-
meandensity_cluster_indense(path_i,height)*timefraction_cluster_indense(path_i,height)
)/TimeFraction_cloud(path_i,height);
TimeFraction_individualParticles(path_i,height)=1-
dense_phase_time_fraction(path_i,height)-timefraction_cluster_indilute(path_i,height);

density_individualParticles(path_i,height)=(mean_density(path_i,height)-
dense_phase_time_fraction(path_i,height)*dense_meanphasedensity(path_i,height)-
timefraction_cluster_indilute(path_i,height)*
meandensity_cluster_indilute(path_i,height))/
TimeFraction_individualParticles(path_i,height);
save myfile1 path Ug Gs path_i height condition mean_density mean_std
meanclusterdensity meanclusterlength medianclusterlength meanclusterfrequency
cluster_particle_percentage cluster_scale cluster_time_fraction ...

```



```

        dense_phase_time_fraction dense_meanphasefrequency
dense_meanphasedensity dense_meanphaselength dense_medianphaselength
dense_phase_particle_percentage ...
        meandensity_cluster_indense particlefraction_cluster_indense
particlefraction_cluster_indilute timefraction_cluster_indilute
timefraction_cluster_indense ...
        meandensity_cluster_indense meandensity_cluster_indilute
meanlength_cluster_indense meanlength_cluster_indilute medianlength_cluster_indense
...
        medianlength_cluster_indilute frequency_cluster_indense
frequency_cluster_indilute clusternumer_per_dense minimumclusterlength ...
        clustersignificance clustervelocity Edense updated_meanclusterdensity
updated_dense_meanphasedensity updated_meandensity_cluster_indense
updated_meandensity_cluster_indilute ...
        density_cloud TimeFraction_cloud density_individualParticles
TimeFraction_individualParticles;
        clear all
        load myfile1
        end
        end
        end
        end
        path='D:\Pyramid-Tracy\UWO
degree\Experiment2012(riser)\Ug3Gs100\H3\R4\';
        cd('D:\Pyramid-Tracy\UWO degree\Experiment2012(riser)\');
%% SIG secondary cluster
lateralposition=-1:0.25:1;
xlswrite(condition,{path(end-14:end)},'2ndcluster','A1')
xlswrite(condition,{'mean_density'},'2ndcluster','A2')
xlswrite(condition,mean_density,'2ndcluster','A3')
xlswrite(condition, {'mean_std'},'2ndcluster','A15')
xlswrite(condition, mean_std,'2ndcluster','A16')
xlswrite(condition, {'meanclusterdensity'},'2ndcluster','A28')
xlswrite(condition, meanclusterdensity,'2ndcluster','A29')
xlswrite(condition, {'meanclusterlength'},'2ndcluster','A41')
xlswrite(condition, meanclusterlength,'2ndcluster','42')
xlswrite(condition, {'medianclusterlength'},'2ndcluster','A54')
xlswrite(condition, medianclusterlength,'2ndcluster','A55')
xlswrite(condition,{'meanclusterfrequency'},'2ndcluster','A67')
xlswrite(condition,meanclusterfrequency,'2ndcluster','A68')
xlswrite(condition,{'cluster_particle_percentage'},'2ndcluster','A80')
xlswrite(condition,cluster_particle_percentage,'2ndcluster','A81')
xlswrite(condition,{'cluster_time_fraction'},'2ndcluster','A93')
xlswrite(condition,cluster_time_fraction,'2ndcluster','A94')
%xlswrite(condition, ins_clusterlength,' ins_clusterlength','A2')
%xlswrite(condition, ins_clusterdensity,' ins_clusterdensity','A2')

```

```

xlswrite(condition,{'cluster_scale'},'2ndcluster','A106')
xlswrite(condition,cluster_scale,'2ndcluster','A107')
xlswrite(condition,{'clusterdensity-meansignaldensity'},'2ndcluster','A119')
xlswrite(condition,meanclusterdensity'-mean_density','2ndcluster','A120')
xlswrite(condition,{'clustervelocity'},'2ndcluster','A132')
xlswrite(condition, clustervelocity,'2ndcluster','A133')
xlswrite(condition,{'clustersignificance'},'2ndcluster','A145')
xlswrite(condition, clustersignificance,'2ndcluster','A146')
%   xlswrite(condition, {'meanCLUSTERdensity'},'2ndcluster','K1')
%   xlswrite(condition, meanclusterdensity(:),'2ndcluster','K2')
%   xlswrite(condition, {'meanSIGNALdensity'},'2ndcluster','L1')
%   xlswrite(condition, mean_density(:),'2ndcluster','L2')
%% dense phase
xlswrite(condition,{'path(end-14:end)}','dense_phase','A1')
xlswrite(condition,{'mean_density'},'dense_phase','A2')
xlswrite(condition,mean_density','dense_phase','A3')
xlswrite(condition, {'mean_std'},'dense_phase','A15')
xlswrite(condition, mean_std','dense_phase','A16')
xlswrite(condition, {'meandensity_densephase'},'dense_phase','A28')
xlswrite(condition, dense_meanphasedensity','dense_phase','A29')
xlswrite(condition, {'meanlength_densephase'},'dense_phase','A41')
xlswrite(condition,dense_meanphaselength','dense_phase','A42')
xlswrite(condition, {'medianlength_densephase'},'dense_phase','A54')
xlswrite(condition, dense_medianphaselength','dense_phase','A55')
xlswrite(condition,{'meanfrequency_densephase'},'dense_phase','A67')
xlswrite(condition, dense_meanphasefrequency','dense_phase','A68')
xlswrite(condition,{'particle_percentage_densephase'},'dense_phase','A80')
xlswrite(condition,dense_phase_particle_percentage','dense_phase','A81')
xlswrite(condition,{'time_fraction_densephase'},'dense_phase','A93')
xlswrite(condition, dense_phase_time_fraction','dense_phase','A94')
xlswrite(condition,{'cluster_maxscale'},'dense_phase','A106')
xlswrite(condition,ones(11,6)*17,'dense_phase','A107')
xlswrite(condition,{'density_densephas-meansignaldensity'},'dense_phase','A119')
xlswrite(condition, dense_meanphasedensity'-mean_density','dense_phase','A120')
xlswrite(condition, {'energy_densephase_per_second'},'dense_phase','A132')
xlswrite(condition, Edense,'dense_phase','A133')
%% cluster in dense
xlswrite(condition,{'path(end-14:end)}','cluster_indense','A1')
xlswrite(condition,{'mean_density'},'cluster_indense','A2')
xlswrite(condition,mean_density','cluster_indense','A3')
xlswrite(condition, {'mean_std'},'cluster_indense','A15')
xlswrite(condition, mean_std','cluster_indense','A16')
xlswrite(condition, {'meandensity_cluster_indense'},'cluster_indense','A28')
xlswrite(condition,meandensity_cluster_indense','cluster_indense','A29')
xlswrite(condition, {'meanlength_cluster_indense'},'cluster_indense','A41')
xlswrite(condition,meanlength_cluster_indense','cluster_indense','A42')

```

```

xlswrite(condition, {'medianlength_cluster_indense'}, 'cluster_indense', 'A54')
xlswrite(condition, medianlength_cluster_indense, 'cluster_indense', 'A55')
xlswrite(condition, {'meanfrequency_cluster_indense'}, 'cluster_indense', 'A67')
xlswrite(condition, frequency_cluster_indense, 'cluster_indense', 'A68')
xlswrite(condition, {'particle_percentage_cluster_indense'}, 'cluster_indense', 'A80')
xlswrite(condition, particlefraction_cluster_indense, 'cluster_indense', 'A81')
xlswrite(condition, {'time_fraction_cluster_indense'}, 'cluster_indense', 'A93')
xlswrite(condition, timefraction_cluster_indense, 'cluster_indense', 'A94')
%xlswrite(condition, ins_clusterlength, 'ins_clusterlength', 'A2')
%xlswrite(condition, ins_clusterdensity, 'ins_clusterdensity', 'A2')
xlswrite(condition, {'clusternumer_per_dense'}, 'cluster_indense', 'A106')
xlswrite(condition, clusternumer_per_dense, 'cluster_indense', 'A107')
%    xlswrite(condition, {'meandensity_cluster_indense'}, 'cluster_indense', 'K1')
%    xlswrite(condition, meandensity_cluster_indense(:), 'cluster_indense', 'K2')
%
%    xlswrite(condition, {'meandensity_cluster_indense'}, 'cluster_indense', 'L1')
%    xlswrite(condition, mean_density(:), 'cluster_indense', 'L2')
%% cluster in dilute
xlswrite(condition, {path(end-14:end)}, 'cluster_indilute', 'A1')
xlswrite(condition, {'mean_density'}, 'cluster_indilute', 'A2')
xlswrite(condition, mean_density, 'cluster_indilute', 'A3')
xlswrite(condition, {'mean_std'}, 'cluster_indilute', 'A15')
xlswrite(condition, mean_std, 'cluster_indilute', 'A16')
xlswrite(condition, {'meandensity_cluster_indilute'}, 'cluster_indilute', 'A28')
xlswrite(condition, meandensity_cluster_indilute, 'cluster_indilute', 'A29')
xlswrite(condition, {'meanlength_cluster_indilute'}, 'cluster_indilute', 'A41')
xlswrite(condition, meanlength_cluster_indilute, 'cluster_indilute', 'A42')
xlswrite(condition, {'medianlength_cluster_indilute'}, 'cluster_indilute', 'A54')
xlswrite(condition, medianlength_cluster_indilute, 'cluster_indilute', 'A55')
xlswrite(condition, {'meanfrequency_cluster_indilute'}, 'cluster_indilute', 'A67')
xlswrite(condition, frequency_cluster_indilute, 'cluster_indilute', 'A68')
xlswrite(condition, {'particle_percentage_cluster_indilute'}, 'cluster_indilute', 'A80')
xlswrite(condition, particlefraction_cluster_indilute, 'cluster_indilute', 'A81')
xlswrite(condition, {'time_fraction_cluster_indilute'}, 'cluster_indilute', 'A93')
xlswrite(condition, timefraction_cluster_indilute, 'cluster_indilute', 'A94')
%% Phase solids holdup
xlswrite(condition, {'mean_density'}, 'Cloud_IndividualParticles', 'A2')
xlswrite(condition, mean_density, 'Cloud_IndividualParticles', 'A3')
xlswrite(condition, {'mean_std'}, 'Cloud_IndividualParticles', 'A15')
xlswrite(condition, mean_std, 'Cloud_IndividualParticles', 'A16')
xlswrite(condition, {'density_cloud'}, 'Cloud_IndividualParticles', 'A28')
xlswrite(condition, density_cloud, 'Cloud_IndividualParticles', 'A29')
    xlswrite(condition, {'density_individual
particles'}, 'Cloud_IndividualParticles', 'A41')
    xlswrite(condition, density_individualParticles, 'Cloud_IndividualParticles', 'A42')
xlswrite(condition, {'TimeFraction_cloud'}, 'Cloud_IndividualParticles', 'A54')

```

```
xlswrite(condition, TimeFraction_cloud,'Cloud_IndividualParticles','A55')

xlswrite(condition,{'TimeFraction_individualParticles'},'Cloud_IndividualParticles','A67'
)
    xlswrite(condition,
TimeFraction_individualParticles','Cloud_IndividualParticles','A68')
    % condition(end-4:end)='a.bmp';
    %saveas(hh,condition)
        save myfile2 Ug Gs path path_i height condition minimumclusterlength
    clear all
    load myfile2
end
end
```

Curriculum Vitae

Name: Xiaoyang Wei

Place of Birth Hebei, China

Post-secondary Education: Department of Chemical and Biochemical Engineering
University of Western Ontario, London, Ontario, Canada
2014-2019 Ph.D.

Department of Chemical Engineering
China University of Petroleum (East China), Qingdao, China
2009-2013 B.Sc.

Work Experience: Research Assistant and Teaching Assistant
University of Western Ontario
London, Ontario, Canada
2014-2019

Honors and Awards: Graduate Student Scholarship, Western University, Canada
2015-2019

The Second Prize Scholarship, China university of Petroleum,
China 2012